KU LEUVEN

ARENBERG DOCTORAL SCHOOL
Faculty of Engineering Science

Integration of Flexibility from Battery Storage in the Electricity Market

Jonas Engels

Supervisors:
Prof. dr. ir. G. Deconinck
Prof. dr. ir. B. J. Claessens

Dissertation presented in partial fulfilment of the requirements for the degree of Doctor of Engineering Science (PhD): Electrical Engineering

January 2020

Integration of Flexibility from Battery Storage in the Electricity Market

Jonas ENGELS

Examination committee:
Prof. dr. ir. H. Hens, chair
Prof. dr. ir. G. Deconinck, supervisor
Prof. dr. ir. B. J. Claessens, supervisor
Prof. dr. ir. J. Suykens
Prof. dr. ir. R. V. Sabariego
Prof. dr. ir. G. Strbac
(Imperial College London)
Dr. K. De Vos
(Elia System Operator, Belgium)

Dissertation presented in partial fulfilment of the requirements for the degree of Doctor of Engineering Science (PhD): Electrical Engineering

January 2020

© 2020 KU Leuven – Faculty of Engineering Science
Uitgegeven in eigen beheer, Jonas Engels, Kasteelpark Arenberg 10 box 2445, B-3001 Leuven (Belgium)

Alle rechten voorbehouden. Niets uit deze uitgave mag worden vermenigvuldigd en/of openbaar gemaakt worden door middel van druk, fotokopie, microfilm, elektronisch of op welke andere wijze ook zonder voorafgaande schriftelijke toestemming van de uitgever.

All rights reserved. No part of the publication may be reproduced in any form by print, photoprint, microfilm, electronic or any other means without written permission from the publisher.

Abstract

A growing share of intermittent renewable generation in the electric power system is increasing the need for flexibility. At the same time, decreasing battery prices are opening up new opportunities for energy storage. Battery energy storage systems can be used for multiple applications in the power system, such as storing an excess of renewable generated energy for later consumption, wholesale market arbitrage or providing ancillary services to the grid operators. Nevertheless, the return of investment in battery energy storage systems is often still perceived too low and uncertain. Selecting the right application, combining applications, and optimising the control and the size of a battery energy storage system are important steps to reduce uncertainty and increase the return on investment.

This dissertation addresses how to make optimal use of flexibility from battery energy storage in electricity markets and the power system. The thesis provides an overview of the different applications battery storage can be used for and gives a quantitative estimation of the value battery storage can bring when delivering these applications. The results show that providing reserves for frequency control, i.e. supporting the stability of the grid frequency, is one of the applications that has the highest value for a battery storage system. Although arbitraging on short-term wholesale and imbalance markets have theoretically a higher potential value, achieving this value requires a perfect hindsight knowledge of the market prices, so that the practically achievable value lies a lot lower. Finally, there can also be considerable value in battery storage installed behind the meter, providing direct services to the electricity consumer, such as storing locally generated solar energy or reducing peak consumption.

As battery storage systems have a limited energy content, they have to be operated in a different way than traditional power plants. When for instance used to provide symmetric frequency control, a battery energy storage system needs to control its state of charge to ensure the battery is never empty nor full, as this would mean the symmetric frequency control capacity is not available any

more. This thesis presents a detailed, holistic framework to optimise such a state of charge controller and determine the optimal size of a battery storage system used for frequency reserves, taking degradation and regulatory requirements into account. As a case study, the optimisation framework is applied to the German frequency containment reserve market, providing some novel, relevant insights into the economics and sizing of a battery energy storage system in this market.

Consecutively, this thesis looks at combining multiple applications simultaneously with battery storage installed behind the meter at residential and industrial consumers. The thesis presents optimised control strategies which allow the use of battery storage for the combination of frequency reserves with increasing self-consumption or with peak shaving. Stochastic optimisation is used together with robust optimisation techniques, giving a safe and tractable approximation to chance constraints, while dynamic programming is adopted to combine the longer-term objective of peak shaving with the daily decision making in the frequency reserve market. Case study results using real data show that there are indeed synergies when combining frequency reserves with increasing self-consumption or with peak shaving and the resulting controllers are able to significantly increase the value of a battery energy storage system compared to the use of the battery energy storage system for one application only.

Finally, as battery storage is often connected to the distribution grid, this dissertation discusses the impact of distribution grid constraints on the aggregated flexibility from battery storage or from other flexible assets connected to the low-voltage distribution grid. The thesis focusses on a regulatory constraint which has been put in place in Belgium to prevent congestion of the distribution grid, limiting the frequency control capacity these assets can provide. A distributed optimisation algorithm is proposed to maximise the total frequency control capacity from low-voltage grid connected flexible assets while respecting these distribution grid constraints.

Beknopte samenvatting

Het groeiende aandeel van hernieuwbare energie, die niet continu beschikbaar is, doet de nood aan flexibiliteit in het elektriciteitsnet toenemen. Tegelijkertijd ontstaan er, door de dalende kost van batterijcellen, nieuwe mogelijkheden voor de opslag van energie. In het elektriciteitsnet kunnen batterij-energieopslagsystemen gebruikt worden voor verschillende toepassingen, zoals het opslaan van een overschot aan hernieuwbare energie voor later verbruik, prijsarbitrage op de groothandelsmarkt voor elektriciteit of het leveren van ondersteunende diensten aan de netbeheerders. Desondanks wordt het rendement van een investering in batterijopslag vaak nog als te laag en onzeker ervaren. Het selecteren van de juiste toepassing, het combineren van toepassingen, het optimaliseren van de aansturing en de dimensionering van een batterijopslagsysteem zijn daarom belangrijke stappen om de onzekerheid te verminderen en het rendement van een investering in batterijopslag te vergroten.

Dit proefschrift onderzoekt hoe de flexibiliteit van batterij-energieopslagsystemen optimaal ingezet kan worden in de elektriciteitsmarkt en het elektriciteitsnet. De thesis geeft een overzicht van de verschillende toepassingen waarvoor batterijopslag gebruikt kan worden en maakt een kwantitatieve schatting van de waarde die batterijopslagsystemen kunnen hebben bij het leveren van deze toepassingen. De resultaten tonen aan dat het leveren van frequentiecontrole, het ondersteunen van de frequentiestabiliteit van het net, één van de toepassingen is die de meeste waarde kan bieden voor batterijopslag. Arbitrage op de korte-termijn groothandels- en onbalansmarkt biedt theoretisch een grotere potentiële waarde, maar omdat men de echte marktprijzen pas kent na de sluiting van de markt, ligt de praktisch haalbare waarde een stuk lager. Ten slotte kan er ook aanzienlijke waarde zitten in batterijopslag die achter de meter geïnstalleerd is en directe diensten levert aan de elektriciteitsverbruiker, zoals de opslag van lokaal gegenereerde zonne-energie of het verlagen van het piekverbruik.

Omdat batterij-energieopslagsystemen een beperkte energiecapaciteit hebben, moeten ze op een andere manier aangestuurd worden dan traditionele

energiecentrales. Indien bijvoorbeeld batterijopslag gebruikt wordt voor frequentiecontrole, moet men de laadtoestand zo regelen dat de batterij nooit volledig vol of leeg is, want dit zou betekenen dat de frequentiecontrolecapaciteit niet meer beschikbaar is. Deze thesis gaat hier dieper op in en presenteert een holistische manier om een dergelijke laadtoestandsregelaar te optimaliseren en de optimale grootte van een batterijopslagsysteem dat gebruikt wordt voor frequentiecontrolecapaciteit te bepalen, rekening houdend met degradatie en regulatoire vereisten. Het toepassen van de ontwikkelde optimalisatietechniek op de Duitse markt voor frequentiecontrole geeft enkele relevante nieuwe inzichten in de waarde en de dimensionering van batterijsystemen in deze markt.

Vervolgens wordt er in deze thesis gefocust op het leveren van meerdere toepassing tegelijkertijd door batterijopslag geïnstalleerd achter de meter, bij residentiële en industriële elektriciteitsverbruikers. De thesis presenteert geoptimaliseerde besturingsstrategieën die toelaten om batterijopslag gelijktijdig te gebruiken voor de combinatie van frequentiecontrole met de opslag van lokaal gegenereerde energie, of met het verminderen van het piekverbruik. Hiervoor wordt stochastische optimalisatie gebruikt samen met robuuste optimalisatietechnieken, die een veilige en oplosbare benadering vormen voor stochastische beperkingen in het optimalisatieprobleem, terwijl dynamisch programmeren gebruikt wordt om de dagelijkse beslissingsmomenten in de frequentiecontrolemarkt te combineren met de langere tijdschaal die nodig is bij het verminderen van het piekverbruik. Het toepassen van de ontwikkelde technieken op reële data toont dat er inderdaad synergieën bestaan bij het combineren van frequentiecontrole met de opslag van lokaal gegenereerde energie of met het verminderen van het piekverbruik door eenzelfde batterijopslagsysteem. De resultaten tonen ook dat de ontwikkelde batterijbesturingsstrategieën de waarde van een batterijopslagsysteem aanzienlijk kunnen verhogen vergeleken met het gebruik van het batterijopslagsysteem voor slechts één toepassing.

Aangezien batterijopslag meestal op het distributienet aangesloten wordt, bespreekt dit proefschrift de impact van beperkingen van het distributienet op de geaggregeerde flexibiliteit uit batterijopslag of andere bronnen van flexibiliteit verbonden met het laagspanningsnet. De focus ligt op een nieuwe regulatoire beperking die in België is ingevoerd om congestie in het distributienet te voorkomen, waardoor de frequentiecontrolecapaciteit die deze flexibiliteitsbronnen kunnen bieden wordt ingeperkt. De thesis stelt het gebuikt van een gedistribueerd optimalisatie-algoritme voor om de totale frequentiecontrolecapaciteit van flexibiliteitsbronnen aangesloten op het laagspanningsnet te maximaliseren, rekening houdend met deze distributienetbeperkingen.

Acknowledgements

During my bachelor and master studies, I never really intended to start a PhD. However, a very interesting master thesis and an unique opportunity to do a PhD in cooperation with REstore made me decide otherwise. It has been quite a ride and, although it was not always easy to combine work at REstore with academic research, it has been a unique experience and a true added value to get to know both the academic and the commercial world.

First of all, I would like to thank my academic supervisor Geert Deconinck to give me the opportunity to pursue a PhD in the first place, to always being available for guidance and discussion on both content-related and practical topics. I would also like to thank Bert Claessens, for being my industrial supervisor and mentor, for the many discussions on yet another controller, for challenging me and make me go the extra mile, but also to make sure I had the time to do research and write this PhD.

Of course, a sincere thank you to all the members of the examination committee, for sharing their very useful thoughts and insights. Prof. Hens, thank you for chairing the committee. Thank you Johan Suykens and Ruth Sabariego for being part of my supervisory committee throughout the years. Thank you Kristof De Vos and Goran Strbac for being part of the jury and for the useful remarks that have definitely made this thesis more complete and of higher quality. I must also gratefully acknowledge VLAIO for their financial support and making this project possible.

Thank you Jan-Willem, for giving me the opportunity to start this PhD at REstore. Also all the other colleagues at REstore (although I should now say CBS Belgium), the analytics team and Stef and Ruben from the research team, thank you for all the interesting discussions, sharing your practical knowledge on demand response, the energy markets and very useful coding tips. You are an exceptional team at REstore, very motivated and intelligent people, great to work with! Thank you Sylvie for always being prepared to help with all

practicalities and administrative hassle.

A big thank you to the colleagues at Electa, for the fun times we had together, the interesting discussions, for sharing your knowledge on everything related to power systems, optimisation and control. Thanks Hamada for the good times working together during the P2P SmartTest project in the first months of my PhD. Thank you also everybody from the Electa and EnergyVille secretariat, to be always available to help out, and to the technical staff of Electa and EnergyVille for all the practical knowledge and help on lab setups.

Thanks to all my family and friends, to (at least pretend to) show some interest in the work I have been doing, for all the moments to that allowed me to relax and recharge my batteries. Thanks mama and papa for the continued support and encouragements. And last but not least, thank you Saren, for keeping up with me all these years, for your unlimited support and encouragement, to bear with me in stressful times and for always being there for me.

Jonas Engels,
January 2020

Abbreviations and Acronyms

AC	Alternate Current.
ACE	Area Control Error.
ADMM	Alternating Direction Method of Multipliers.
aFRR	automatic Frequency Restoration Reserve.
BESS	Battery Energy Storage System.
BMS	Battery Management System.
BRP	Balance Responsible Party.
C-rate	Rated power divided by the rated energy content of a battery energy storage system.
CAISO	California Independent System Operator.
CE	Continental Europe.
CIM	Continous Intraday Market.
CLT	Central Limit Theorem.
CVaR	Conditional Value-at-Risk.
CWE	Central Western Europe.
DAM	Day-Ahead Market.
DC	Direct Current.
DoD	Depth of Discharge.
DR	Demand Response.
DSO	Distribution System Operator.
ENTSO-E	European Network of Transmission System Operators for Electricity.
EV	Electric Vehicle.
FCR	Frequency Containment Reserve.
FSP	Flexibility Service Provider.

HVAC	Heating, Ventilation and Air Conditioning.
iid	independent and identically distributed.
IoT	Internet of Things.
LPWAN	Low Power Wide Area Networks.
LV	Low Voltage.
mFRR	manual Frequency Restoration Reserve.
MPC	Model Predictive Control.
NGR	Non-Generator Resource.
NMC	Lithium Nickel-Manganese-Cobalt Oxide.
NPV	Net Present Value.
NRMSE	Normalized Root Mean Square Error.
PJM	PJM Interconnection LLC, a regional transmission organisation in the Northeast of the USA.
PV	Photovoltaics.
RC	Resistance-Capacitance.
REM	Regulation Energy Management.
RMS	Root Mean Square.
RoCoF	Rate of Change of Frequency.
RR	Replacement Reserve.
SAA	Sample Average Approximation.
SEI	Solid Electrolyte Interphase.
SoC	State of Charge.
SOCP	Second-Order Cone Problem.
ToU	Time of Use.
TSO	Transmission System Operator.
UK	United Kingdom.
UPS	Uninterruptable Power Supply.
USA	United States of America.
WAP	Weighted Average Price.

Terminology

Aggregator An entity in the electricity market that aggregates distributed flexibility from consumers or prosumers with demand response capabilities or storage assets.

Demand Response A change in the electricity consumption of a site to achieve a new consumption profile, e.g. decreasing a consumption profile at a time where there is not enough energy generation in the grid.

Distributed Energy Resources Small-scale energy assets, such as local PV or wind generation or storage, connected to the low- or medium-voltage distribution grid rather than to the high-voltage transmission grid.

Flexibility When used in the context of the electricity grid: the ability of an asset to reduce or increase its power consumption or production on request.

Load-Frequency Control All actions and processes, on all timelines, which allow transmission system operators to maintain the stability of the power system frequency and load balance (also shortened as *Frequency Control*).

Market Abritrage Buying/charging energy from the market at time periods with low market prices and selling/discharging this energy at time periods with high market prices.

Peak Shaving Actively reducing the peak consumption of an electricity consumer or a part of the electricity grid.

Prosumer An electricity consumer who also produces electricity locally.

Self-Consumption Direct consumption of locally generated energy without transporting this energy over the grid; storage of an excess of locally generated energy for later consumption.

Nomenclature

Variables and Parameters

C_1	Capacitance.	F
C	Battery cell capacity.	A h
C^k	Capacity at the start of year k.	Ah
ΔC^k	Capacity degradation in year k.	Ah
C_p	Heat Capacity.	J/K
COP	Coefficient of Performance.	
$cycles_{max}$	Maximum number of cycles.	
D	Linear recharge controller matrix.	
d_{ki}	Element on the k-th row and i-th column of D.	
db_p	Deadband recharge controller.	
$D_K(\Omega, \Omega_r)$	Kantorovich distance between Ω and Ω_r.	
E	Energy content.	J
$g(\cdot)$	Objective function.	
gap_{SAA}	Optimality gap due to SAA method.	
I	Current.	A
k_{IP}	Number of iterations with binary variables in ADMM.	
K_p	Proportional gain P-controller.	
m	Parameter in binomial distribution.	
o_d	Overdelivery percentage.	
$p_{i,t}$	FCR capacity of asset i at timestep t.	W
p_F	Aggregated FCR capacity.	W
p^k	Penalty in year k.	
P	Power.	W
Q	Battery cell throughput.	Ah
Q_{i_c}	Cumulative throughput after cycle i_c.	Ah
Q	Diagonal matrix of the forward deviations σ_{f_i}.	
r	FCR capacity.	W

$r_{i,t}$	FCR capacity of site i at time step t.	W
r	Radius circle.	m
R	Resistance.	Ω
R^k	Resistance at the start of year k.	Ω
R	Diagonal matrix of the backward deviations σ_{b_i}.	
rev	Discounted net reveneus.	€
s	Sample standard deviation.	
S_t^{emerg}	Grid frequency emergency state indicator.	
SoC	Battery State of Charge.	
SoC_0	SoC setpoint of recharge controller.	
t	Time.	s
Δt	Length of one time step.	s
$t_{\beta,\nu}$	β-percentile of the Student's t-distribution with ν degrees of freedom.	
T	Temperature.	K
T_{ref}	Reference Temperature.	K
$\boldsymbol{u}_i$	Scaled dual variables in ADMM.	
V	Value function.	
$\tilde{V}^{rule}$	Convex piecewise approximation of V^{rule}.	
V^{rule}	Value function using the rule-based controller.	
V^{bat}	Battery cell terminal voltage.	V
V^{C_1}	Voltage over capacitor C_1.	V
V_{cutoff}	Battery cell cut-off voltage when charging.	V
V_{nom}	Nominal voltage.	V
V_{OC}	Open-circuit voltage.	V
W	Whitening transformation matrix.	
$\boldsymbol{x}_i = (x_i^0, x_i^1)$	Geographical coordinates of an asset.	
x_j^b	Breakpoints of piecewise function.	
z	Binary variable.	
z_β	Z-score of the standard normal distribution evaluated at β.	
α	Parameter to define relative error of ADMM.	
$\alpha_{cap}, \alpha_{res}$	Capacity and resistance calendar ageing factors.	
α_j, β_j	Coefficients of piecewise linear function.	
β	Confidence bound.	
β_{cap}, β_{res}	Capacity and resistance cycle ageing factors.	
γ	Discount rate.	
Δ	Difference.	
ϵ	Probability of constraint violation.	
η	Efficiency.	

$\eta_{coulomb}$	Coulombic of Faraday efficiency.	
λ	Dual variable.	
$\pi(\cdot)$	Control policy.	
ρ	Parameter in binomial distribution.	
ρ_c	Augmented Lagragian parameter for the circle constraints.	
ρ_F	Augmented Lagragian parameter for the FCP constraint.	
σ_f, σ_b	Forward and backward deviations.	
$\Sigma_{\boldsymbol{x}}$	Covariance matrix of $\boldsymbol{x}$.	
$\Phi(z)$	Cumulative density function of the standard normal distribution.	
ω	A scenario from Ω.	
$\mathfrak{b}(m; \rho, n)$	Cumulative binomial probability function with parameters n and ρ, evaluated at m.	

Grid Frequency Variables

$f(t)$	Grid frequency.	
f_{nom}	Nominal Grid frequency.	
Δf	Relative grid frequency deviation.	
Δf_{max}	Frequency deviation at which maximum FCR capacity r need to be activated.	
Δf_k	Discretized relative grid frequency deviation, corrected for battery effiency losses.	
Δf_k^0	Discretized relative grid frequency deviation, not corrected for battery effiency losses.	
Δf_{db}	Frequency deadband in which no FCR reaction is required.	
$\boldsymbol{\Delta f}_d$	Gid frequency deviation sample of one day.	
$\boldsymbol{\Delta f}_y$	Gid frequency deviation sample of one year.	
$\tilde{\boldsymbol{f}}$	Whitened frequency deviation profile with zero mean.	
$\boldsymbol{f^r}$	Generated frequency deviation samples.	

Costs

c_{cell}	Cost of a battery cell.	€
c_{cons}	Consumed electricity unit cost.	€/kWh
c_{elec}	Electricity unit cost.	€/kWh
c_{FCR}, c^{FCR}	FCR unit price.	€/MW
c_{inj}	Injected electricity unit price.	€/kWh
c_{peak}	Demand charge or peak power charge.	€/MW
c_p	Weighting factor of penalty.	
c_k^{DAM}	Day-ahead market price at time step k.	€/MWh
$\tilde{c}_k^{DAM}$	Predicted day-ahead market price at time step k.	€/MWh

$c(\boldsymbol{\omega}, \boldsymbol{\omega}')$	Cost function for scenario reduction.	
$\tilde{c}(\boldsymbol{\omega}, \boldsymbol{\omega}')$	New proposed cost function for scenario reduction.	
$c_i(\boldsymbol{p}_i)$	Local cost function to provide FCR capacity $\boldsymbol{p}_i$.	€
C^{elec}	Total electricity cost.	€

Descriptive Indices

av	Average.
bat	Battery.
BESS	Battery Energy Storage System.
c	Charging.
cal	Calendar.
ctrl	Control.
cyc	Cycle.
d	Discharging.
dem	Demand.
FCR	Frequency containment reserve.
grid	Grid.
init	Initialisation.
inv	Inverter.
max	Maximum.
min	Minimum.
nom	Nominal.
peak	Peak.
prod	Production.
prof	Net consumption profile.
ps	Peak Shaving.
rated	Rated.
rc	Recharge.
req	Required.
sc	Self-consimption.
thr	Threshold.
f	Variables in the local optimisation in ADMM.
g_s	Variables in circle constraint s optimisation in ADMM.
h	Variables in the FSP optimisation in ADMM.

Valued Indices

d	Day d.
i	General index.
(i)	Index of a sorted set.
i_c	Cycle index.

j_r	Reduced scenario index.
k	Discrete timestep, $k = 1, \ldots, n_t$.
k	Year k, $k = 1, \ldots, n_k$ (in Chapter 3.
k	Iteration numer (in Chapter 6.
t	Time step.
$t_{recharge}$	Time step recharge controller.
t_{lead}	Lead time recharge controller.
t_{set}	Time step to set recharge controller.
v	Consumption profile sample index.
v_r	Reduced consumption profile sample index.
w	Frequency profile sample index.
w_r	Reduced frequency profile sample index.

Sets

$\mathcal{C}_s$	Set of points i that belong to circle constraint s.
$\mathcal{D}$	Set of frequency deviation profile samples of one day.
$\mathcal{F}$	Uncertainty set.
$\mathcal{I}$	Set containing all assets or points i.
$\mathcal{P}$	Set of frequency deviation profiles for penalty checking.
$\mathcal{S}$	Set containing all circle constraint sets $\mathcal{C}_s$.
$\mathcal{X}$	Constraining set of x.
$\mathcal{Y}$	Set of frequency deviation profile samples of one year $\boldsymbol{\Delta f}_y$.
Ω, Ω_r	Original and reduced set of scenarios $\boldsymbol{\omega}$.

Counts

n_c	Number of samples for constraint violation.
n_{cells}	Number of cells in the BESS.
n_{check}	Number of iterations before checking for penalties.
n_{cyc}	Number of cycles.
n_d	Number of days.
n_{eval}	Number of samples for evaluation.
n_L	Number of samples to calculate lower bound on the SAA.
n_R	Number of generated frequency samples.
n_s	Number of industrial sites.
n_{sc}	Number of scenarios.
n_{sc_r}	Number of reduced scenarios.
n_t	Number of time steps.
$n_{t,d}$	Number of time steps in one day.
$n_{t,y}$	Number of time steps in one year.
$n_{\mathcal{T}}$	Number of time steps in a bidding period.

n_U	Number of samples to calculate upper bound on the SAA.
n_v	Number of consumption profile samples.
n_{v_r}	Number of reduced consumption profile samples.
n_w	Number of frequency profile samples.
n_{w_r}	Number of reduced frequency profile samples.
$n_{\mathcal{X}}$	Cardinality of set $\mathcal{X}$.

Notation

$\boldsymbol{x}$	A bold symbols: a vector with elements x_i: $\boldsymbol{x} = (x_0, x_1, \ldots, x_{n_x})^T$.
$\hat{\cdot}$	Optimised value.
$\bar{\cdot}$	Sample mean.
$\lvert\cdot\rvert$	Absolute value or cardinalty of a Set.
$\lfloor\cdot\rfloor$	The floor function.
$[\cdot]^+$	$\equiv$ $\max(\cdot, 0)$, the ramp function, element-wise on vectors.
$\mathrm{E}[\cdot]$	Expected value operator.
$\mathrm{E}[\cdot]^+$	$\equiv$ $\mathrm{E}[\max(\cdot, 0)]$, the expected value of the ramp function.
$f(\cdot)$	General function.
I_{n_t}	Identity matrix of size n_t.
$std[\cdot]$	Standard deviation.
$sign(x)$	Sign function, returning 1 if $x \geq 0$ and -1 otherwise.
$diag(\boldsymbol{x})$	Diagonal matrix of $\boldsymbol{x}$.
$max(\boldsymbol{x})$	$\equiv$ $\max_k(x_k)$, the maximum element of the vector $\boldsymbol{x}$.
$\Pr\{x > 0\})$	Probability that $x > 0$.
$\mathbb{1}\{x > x_0\}$	Indicator function, returning 1 if the value between brackets is true and 0 otherwise.

Contents

Abstract i

Beknopte samenvatting iii

Abbreviations and Acronyms viii

Terminology ix

Nomenclature xvi

Contents xvii

List of Figures xxiii

List of Tables xxvii

1 Introduction 1

1.1 Context and Motivation 1

1.2 Road Towards This Thesis 3

1.3 Research Questions, Challenges and Scope 5

1.4 Outline and Contributions 6

2 Battery Storage in Electricity Markets 9

2.1 Introduction 9
2.2 Overview of Battery Energy Storage Applications 10
2.3 Description and Value Estimation of Battery Energy Storage Applications 13
2.3.1 Frequency Containment Reserve (FCR) 14
2.3.2 Automatic Frequency Restoration Reserve (aFRR) . . . 17
2.3.3 Manual Frequency Restoration Reserve (mFRR) 21
2.3.4 Replacement Reserve (RR) 23
2.3.5 Inertia 24
2.3.6 Black Start 25
2.3.7 Voltage Control 26
2.3.8 Congestion Management & Network Investment Deferral 27
2.3.9 Day-Ahead Market Arbitrage 28
2.3.10 Intraday Market Arbitrage 32
2.3.11 Imbalance Price Arbitrage & Portfolio Balancing 33
2.3.12 Increasing Self-Consumption 36
2.3.13 Peak Shaving 38
2.3.14 Time of Use Bill Management 40
2.3.15 Power Quality Improvements 41
2.3.16 Uninterruptible Power Supply 42
2.4 Quantitative Comparison of the Applications 42
2.5 Conclusion 46

3 Battery Storage Used for Frequency Reserves 49

3.1 Introduction 50
3.1.1 Frequency Containment Reserve 51
3.1.2 Related Works and Contributions 51
3.2 BESS Model and FCR Controller 53

3.2.1 Battery Cell Model 54
3.2.2 Degradation Model 56
3.2.3 From a Battery Cell Model to a BESS Model 58
3.2.4 FCR Controller 62
3.3 Optimisation Framework 64
3.3.1 Expected Value Approximation 66
3.3.2 Chance Constraint Approximation 69
3.3.3 Optimisation Algorithm 70
3.3.4 Total Revenues and Costs 73
3.4 Case Study: BESSs in German FCR 73
3.4.1 Data and Regulatory Requirements 74
3.4.2 Optimisation Setup 77
3.4.3 Results and Discussion 78
3.5 Conclusions 83

4 Combining Self-Consumption and Frequency Control Applications with a Battery 85

4.1 Introduction 86
4.2 Background and Related Work 88
4.2.1 Background on Frequency Control 88
4.2.2 Related Work 89
4.3 Problem formulation 91
4.4 Primary Frequency Control 92
4.4.1 Recharging Policy 93
4.4.2 Battery Efficiency 93
4.4.3 Chance-Constraints and Robust Optimisation 94
4.4.4 Equivalent State Feedback Policy 96
4.5 Self-Consumption 97

4.5.1 Self-Consumption Policy 97
4.5.2 Stochastic Optimisation 98
4.5.3 Scenario Reduction 100
4.5.4 Evaluation of the Solution Quality 101
4.6 Simulation and Results 101
4.6.1 Primary Frequency Control 102
4.6.2 Combination with Self-Consumption 106
4.7 Conclusion 107

5 Combining Frequency Control and Peak Shaving with Battery Storage Systems 111

5.1 Introduction 112
5.1.1 Frequency Control with a BESS 113
5.1.2 Peak Shaving 113
5.1.3 Related Literature 114
5.2 Optimisation and Control Framework 114
5.2.1 Frequency Control Framework 115
5.2.2 Combining Peak Shaving and Frequency Control 118
5.2.3 Stochastic Optimisation 119
5.2.4 Non-Anticipative Peak Shaving Controller 122
5.2.5 Dynamic Programming Framework 123
5.3 Aggregating Multiple Sites 126
5.4 Simulation and Results 127
5.4.1 Combining Peak Shaving and Frequency Control 128
5.4.2 Dynamic Programming Framework 128
5.4.3 Monthly Costs and Revenues 132
5.5 Conclusion 133

6 Impact of Distribution Grid Constraints on Low-Voltage Grid Connected Flexibility 135

6.1 Introduction 136

6.2 FCR with Low-Voltage Connected Assets in Belgium 138

6.2.1 A Distributed Optimization Framework for the FSP . . 139

6.3 Construction of Circle Constraints 141

6.4 Distributed Optimization of a Pool of Assets 145

6.4.1 Central Optimization Problem 145

6.4.2 Distributed Optimization 147

6.5 Case Study: Distributed Assets in Breda 153

6.5.1 Impact of Circle Constraints on Usable FCR Capacity . 154

6.5.2 Performance of the Distributed Optimization Algorithm 155

6.6 Conclusion 160

7 General Conclusions and Future Work 161

7.1 Answers to the Research Questions 162

7.2 General Conclusions 165

7.3 Future Work 168

A Rainflow Counting Algorithm 171

Bibliography 173

Curriculum Vitae 195

List of Publications 197

List of Figures

1.1 Relationship between the various optimisations and controllers presented in this thesis. 8

2.1 Load-frequency control services as defined by ENTSO-E. 12

2.2 FCR prices and revenues 16

2.3 Activation energy and payments in the Germany aFRR market 19

2.4 Activation energy and payments in the Germany mFRR market 22

2.5 Revenues of a battery in the day-ahead market 31

2.6 Revenues of a battery in the intraday market 33

2.7 Revenues of a battery in the imbalance market 35

2.8 Value of a battery used for self-consumption 37

2.9 Value of a battery used for peak shaving 39

2.10 Value of a battery used for time of use bill management 41

2.11 Comparison of the value of different battery applications 43

3.1 Overview of the components used in modelling a battery energy storage system. 54

3.2 First-order RC model of a battery cell. 54

3.3 Open-circuit voltage curve and pulse power test of a battery cell. 56

3.4 One-way efficiency of an inverter. 59

3.5 Available energy and efficiency when charging and discharging at constant power. 61

3.6 Example of a recharge controller function. 63

3.7 Example of the grid power of a battery delivering primary frequency control. 64

3.8 Relative error of the sample average approximation with frequency samples of one day. 67

3.9 Optimality gap due to the sample average approximation. . . . 68

3.10 Historical and forecasted FCR price in Germany 77

3.11 Revenues of a BESS providing FCR in the German market . . 80

3.12 Capacity degradation of a BESS delivering FCR 82

4.1 Energy content and recharging power of a battery performing frequency control optimised using robust optimisation. 103

4.2 Maximum probability of constraint violation with the equivalent state feedback controller resulting from the robust optimisation. 104

4.3 Primary frequency control capacity in function of the C-rate of the battery, using robust optimisation. 105

4.4 Energy content and battery power for self-consumption. 106

4.5 Revenues when combining frequency control and self-consumption. 108

5.1 Optimisation and control framework for combining peak shaving with frequency control 115

5.2 Effect of scenario reduction techniques to decrease the optimality gap in stochastic optimisation 121

5.3 Example of the value function in the dynamic programming framework 125

5.4 Example of peak shaving boundaries and power while aggregating frequency control with two batteries at two sites 129

5.5 Change of the value function and optimal frequency control capacity during one month 130

5.6 Peak shaving example of a battery while performing frequency control 131

6.1 Proposed distributed optimisation architecture. 140

6.2 Illustration of the two unique circles with a radius r passing through two points. 142

6.3 Example of circles with more than 10 assets in the city of Breda. 145

6.4 Usable proportion of total available FCR capacity per neighbourhood in the city of Breda. 153

6.5 Usable proportion of total available FCR capacity in the city centre, a residential and rural neighbourhood neighbourhood. . 154

6.6 Objective value and primal residuals when using the proposed distribution optimisation algorithm. 156

6.7 Optimality gap versus iterations with the proposed distribution optimisation algorithm. 158

6.8 Optimisation time needed with the centralised solver and with the distribution optimisation algorithm. 159

List of Tables

2.1 Overview of the potential services battery storage could provide. 11

3.1 Parameters of the first-order RC battery cell model. 55

3.2 Elements making up the cost of electricity for a grid-connected stand-alone battery in Germany. 76

3.3 Net present value of batteries in German FCR market 79

3.4 Payback period of a 1.6 MWh/1.6 MW BESS in the German FCR Market. 83

5.1 Expected monthly costs and revenues of aggregating frequency control by two batteries while performing peak shaving 132

6.1 Optimality gap and objective value with a central solver and with the proposed distribution optimisation algorithm. 159

Chapter 1

Introduction

1.1 Context and Motivation

Providing an answer to climate change has repeatedly been identified as one of the biggest challenges of the twenty-first century [1, 2]. In the Paris Agreement, signed in April 2016, 195 state members of the United Nations agreed on the common goal to keep the increase in global temperature due to climate change well below 2 °C above pre-industrial levels, and pursue effort to limit the increase to 1.5 °C [3]. To achieve this goal, a rapid reduction of global greenhouse gas emissions, amongst which CO_2 is the most prominent, is required.

The energy sector is one of the largest emitters of greenhouse gasses [4], and therefore one of the principal sectors which will have to transform towards near-zero greenhouse gas emissions. A widespread electrification of not only the energy sector, but also of the transport sector, together with a decarbonisation of electricity production, will be part of the solution needed to reach the goal of the Paris Agreement [5].

In this context, the European Union has set itself the target to reduce greenhouse gas emissions with 40 %, increase renewable energy to a share of 32 % of final energy consumption and improve energy efficiency with at least 32.5 % by 2030 [6], and has a long-term vision for a climate-neutral economy by 2050 [7].

Apart from the objective of coming to a sustainable and climate-neutral energy provision, achieving security of supply and affordability of energy for the end user are of major concern to policy makers. These three goals have been the main motivation for imposing new policies, which have initiated a large-scale

transformation of the energy and power sector.

Besides, the advent of new technological developments are generating new opportunities for end users in the electricity markets. Traditionally, the electricity sector has operated in a top-down fashion, with producers generating electricity in large power stations and transporting the electricity over the power grid towards the end-consumer. Decreasing prices of distributed energy resources however, have enabled the end-consumer to generate their own energy and become an active participant in the market. Likewise, demand response aggregators are coming up with new business models, facilitating the use of demand side flexibility in electricity markets,[1] allowing the previously passive end user to take up a more active role in the electricity market.

Opportunities for Battery Energy Storage

In this changing energy landscape, a lot of opportunities are emerging for energy storage in general and for battery energy storage systems (BESSs) specifically. An increasing share of intermittent renewable generation, such as solar and wind, increases the need for flexibility in the electricity grid, as total production and total consumption need to be balanced at every moment in time. In addition, an increase of renewable generation leads to a reduction of rotational inertia in the grid, as most of these renewable resources are connected through a power electronics based converter [9]. To ensure the stability of the grid, a reduction of rotational inertia increases the need for fast-responding flexible assets which can limit frequency deviations and may even provide virtual inertia to the grid. On the other hand, due to their zero marginal cost of producing energy, renewable energy resources are pushing the assets that traditionally provide flexibility and inertia, such as gas-fired power plants, out of the market [10]. Besides, these traditional flexible assets are not carbon neutral and therefore other ways of balancing the grid will be needed. Battery energy storage is a promising alternative and a likely part of the solution, as it provides fast-responding flexibility which can help to stabilise and balance the grid and store renewable energy [11].

Apart from grid balancing, battery energy storage can provide a range of other services to different stakeholders, such as increasing self-consumption (storing the excess of locally generated energy for later consumption), wholesale market arbitrage or grid congestion management. Despite the fact that the cost of battery storage, and specifically the cost of Li-ion battery storage, has been decreasing faster than expected [12], the return of investment in battery storage

[1] Note that also other parties, such as a supplier or a grid operator, can take up the role of an aggregator and facilitate the use of demand response flexibility [8].

projects is often perceived too low and uncertain [13]. Therefore, being able to accurately estimate the value of battery storage used for different application and optimise the control and sizing is crucial to reduce uncertainty and increase the return on investment.

One way to increase the return on investment is to use a battery storage system to provide multiple applications simultaneously. Besides, this can reduce the uncertainty on the revenues as the value of one application can act as a hedge against a reduction in value of another application. Previous work indicates that when battery storage installed behind the meter, i.e. at the customer's premises, can provide the largest amount of services and shows the largest potential for combining applications [14]. In this position, battery storage cannot only provide services directly to the customer, but could potentially also offer services to grid operators or energy suppliers.

However, control of battery storage to provide multiple services is not straightforward, as one has to ensure that using the battery for one service does not jeopardize the use of the battery for the other services. Such a controller will have to perform a continuous trade-off between the value of the multiple services that can be provided, maximising the total value for the owner of the battery system.

Within this context, this thesis focusses on the use of battery energy storage systems in electricity markets. The thesis provides a general overview of the services battery storage can provide and identifies which services can create the most value. In addition, the focus is on the optimised control of behind-the-meter battery storage systems to provide one or a combination of these services, in an attempt to increase the value of the battery storage. Finally, this thesis looks at the impact of distribution grid constraints on flexibility from low-voltage grid connected battery storage systems.

1.2 Road Towards This Thesis

The usage of BESSs in the electricity grid and electricity markets has since long been a key topic of academic research, but has recently also attracted attention from industry. New, innovative business models and decreasing battery prices have fuelled the interest from not only traditional energy utilities, but also energy consumers and new players in the energy markets, such as demand response aggregators. Many of these organisation are asking the question if and how BESSs can be valuable to them. With their experience in this topic, academic institutions can help the industry in answering this question, advancing BESSs in electricity grids from a theoretical option to a commercially viable product.

It is on this crossroad of academic research and commercial application that this thesis was made possible. More specifically, the research project which led to this thesis is the result of a cooperation between industry and academics, between REstore (now Centrica Business Solutions Belgium), a demand response aggregator, and the energy research group Electa[2] at KU Leuven and EnergyVille.

At the start of this research, the core business of REstore was the aggregation of automatic demand response from flexible industrial processes. However, given the developments of battery storage, REstore expected BESSs to provide significant value for them as an aggregator and for their industrial clients when installed at their site. Besides, REstore was interested to develop residential demand response (DR) applications and believed residential battery storage would be a key enabler for the residential DR market. However, at the time experience with battery storage was limited and there were questions around the optimal sizing and control, and around which applications that can provide the most value for both the aggregator and the owner of the battery storage system.

KU Leuven on the other hand had already extensive experience with research on demand response, battery storage, smart grids and electricity markets. In this regard, the research presented in this thesis has benefited from both the knowledge and expertise at KU Leuven and the experience of being present as an aggregator in the electricity markets from REstore.

A major focus of this thesis is the use of battery storage for primary frequency control or frequency containment reserve (FCR), possibly in combination with other applications. As shown in Chapter 2, this is due to the high value of FCR for BESSs compared to other services, but also because it was, and to some extent still is, one of the most important demand response applications for REstore.

This focus did not only lead to the academic work presented in this thesis, but also enabled REstore to put a first commercial BESS system, a 18 MW Tesla Powerpack at the Terhills site,[3] in the Belgian FCR market.

[2]Electa is the research group of electrical energy and robust control of industrial systems within the Departement of Electrical Engineering (ESAT) at KU Leuven.

[3]https://www.terhills.com/news/large-scale-european-battery-project-offers-sustainable-alternative-to-stabilize-power-grid/

1.3 Research Questions, Challenges and Scope

This thesis addresses how to make optimal use of flexibility from battery storage systems in electricity markets and the power grid. The thesis is written from the perspective of a BESS owner or operator who tries to maximise value from the battery, rather than from a grid operator who tries to operate the grid in a safe and secure way or a policy maker who tries to maximise social welfare. This perspective allows us to adopt a pragmatic view on battery storage operation: observing the state of the market and the imposed regulations, the BESS operator uses a battery for those applications that bring the most value. Assuming the markets work in a correct way, this also means that the flexibility and storage capability of the battery system will be used where it is the most needed and thereby contributes to maximise social welfare.

The main research questions answered in this thesis are:

1. For which applications can battery storage systems be used in today's market conditions?
   (a) Which of these applications are relevant for third party battery owners and operators?
   (b) What is the value of a battery in each of these applications and which application can be expected to deliver the most value?
2. What is the value of a battery storage system delivering frequency control reserves?
   (a) How to optimise the battery control over its lifetime, while taking the details of battery dynamics and degradation into account?
   (b) What is the optimal size of a battery delivering frequency control?
3. How can a battery storage system combine multiple applications?
   (a) How to design a controller that optimally combines multiple applications?
   (b) Does the value of the battery storage increases by combining multiple applications?
4. What is the impact of distribution grid constraints on flexibility from battery storage?

To limit the scope, the focus of the thesis is on the Central Western Europe (CWE) electricity markets. Where specific numbers or a regulatory framework is

used, we have taken Germany as a case study, since there is already a relatively large amount of battery energy storage installed in Germany and its electricity market is relatively mature with regard to participation of non-conventional energy resources [15, 16]. Besides, the German electricity and ancillary services markets are highly integrated with neighbouring countries, so that the results can assumed to be representative for the entire CWE region.

When mentioning battery storage, we have implicitly assumed Li-ion battery storage, as Li-ion is currently the most widely used battery technology for battery energy storage [17]. However, most of the the battery models used in the thesis can easily be parametrised to represent other types of battery storage, so that the optimisation methods and controllers presented in this thesis are generic towards other types of battery storage systems.

Where possible, real data has been used. All frequency data is actual measured frequency data with a granularity of one second. The industrial consumption profiles used in Chapters 2 and 5 were provided by REstore. The locational data of the grid connection points used in Chapter 6 is publicly available data from Enexis.

1.4 Outline and Contributions

Each of the following chapters of this thesis attempts to provide an answer to one of the research questions presented above: Chapter 2 studies research question 1, Chapter 3 deals with research question 2, while Chapters 4 and 5 treat research question 3, and Chapter 6 addresses research question 4.

Chapters 3, 4 and 6 of this thesis each consist of a published peer-reviewed journal paper. Chapter 3 is published in Applied Energy, while Chapters 4, 5 and 6 are published in IEEE Transactions on Smart Grid. The paper-based chapters all contain the author's version of the final accepted paper. Changes resulting from the publishing process, such as editing, corrections, structural formatting, and other quality control mechanisms may not be reflected in the version displayed in this dissertation. Small changes have been made to the nomenclature so that it is consistent across the chapters.

The main contributions of the chapters of this thesis can be summarised as follows:

Chapter 2 – Battery Storage in Electricity Markets – gives an descriptive overview of the different services battery storage can provide, and, where possible, gives a quantitative estimation of the value of a BESS providing these services. By comparing the value of the different services, the chapter

shows that FCR is the application which brings the highest value for BESSs. One of the main contributions of this chapter are the insights provided by the quantitative comparison of the different services that can be provided by battery storage.

Chapter 3 – Battery Storage Used for Frequency Reserves – performs an in-depth techno-economic analysis of a BESS providing FCR. The main contributions of the chapter include the presented holistic framework for the investment analysis, sizing and optimal control design of a BESS providing frequency reserves, while complying with regulatory requirements. The chapter presents a novel, data-driven stochastic optimisation algorithm. A case study applying the method to the German market gives new insights in the economics of BESSs providing FCR.

Chapter 4 – Combining Self-Consumption and Frequency Control Applications with a Battery – focusses on the control of a behind-the-meter BESS used for both self-consumption and FCR simultaneously. The chapter presents a novel, optimised controller using stochastic and robust optimisation techniques, maximising the expected profit from combining self-consumption and FCR applications.

Chapter 5 – Combining Self-Consumption and Peak Shaving with Battery Storage Systems – extends the optimisation framework proposed in Chapter 4 to allow a BESS to deliver the combination of FCR and peak shaving. The method is extended using dynamic programming to link the daily decision making in FCR with the longer-term peak shaving objective. The method also allows to aggregate frequency control capacity over multiple BESSs installed at different sites while performing peak shaving.

Chapter 6 – Impact of Distribution Grid Constraints on Low-Voltage Grid Connected Flexibility – analysis the impact of distribution grid constraints on the FCR capacity that can be provided by flexible assets connected to the low-voltage distribution grid. More specifically, the chapter deals with a regulation that has been put in place in Belgium in 2018, imposing specific constraints on low-voltage grid connected assets providing FCR, in order to prevent congestion in the distribution grid.

Figure 1.1 gives an overview of the various optimisations and BESS controllers presented in this thesis and how they relate to each other. Chapter 3 presents a global optimisation of an FCR controller and discusses the optimal sizing of a BESS operated with an optimised controller in the German FCR market. Chapter 4 presents a stochastic and robust optimisation method to optimise a controller that is able to combine self-consumption with frequency control. Chapter 5 extends this method to also combine peak shaving with frequency

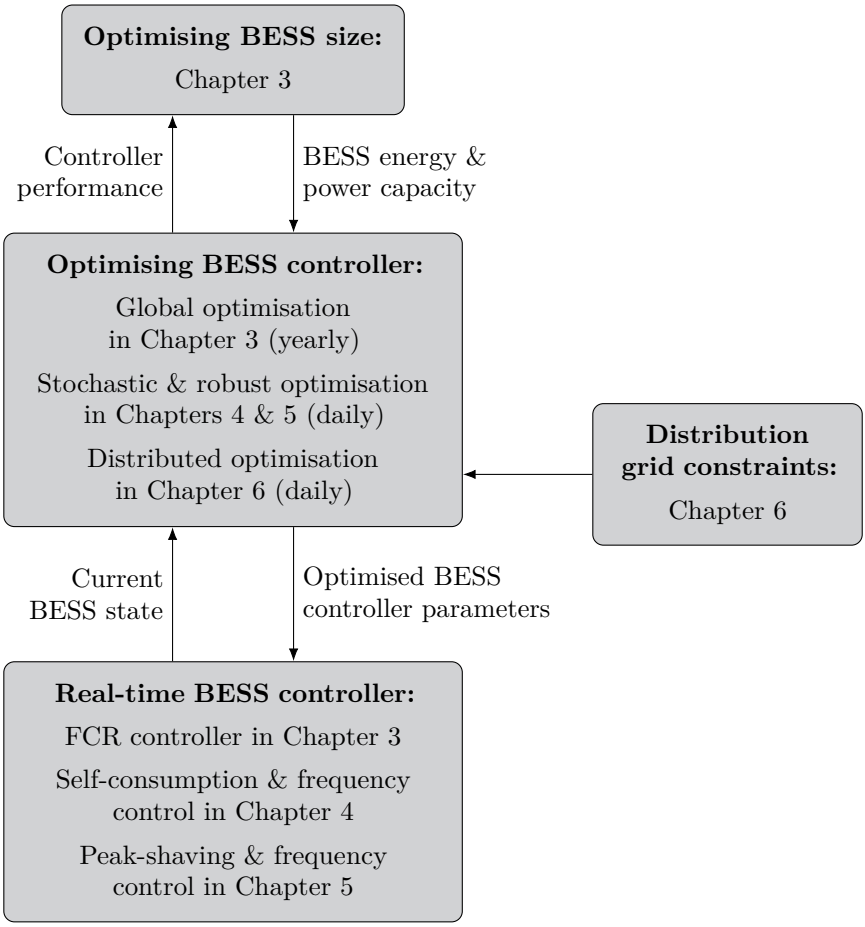

Figure 1.1: Relationship between the various optimisations and controllers presented in this thesis.

control. The optimisations take the current state of the BESS into account to optimise and update the controller parameters on a daily basis (Chapters 4 & Chapter 5) and on a yearly basis (Chapter 3). Chapter 6 presents a distributed optimisation to take distribution grid constraints into account.

Chapter 2

Battery Storage in Electricity Markets

2.1 Introduction

Stationary BESSs can be used for a large number of different applications in the electrical power grid. As each application has specific requirements and creates a different value to a different party, this chapter gives a high-level overview of the different applications of a BESS in the European power grid and electricity markets.

The chapter starts with classifying the applications into three groups: ancillary services, wholesale electricity market applications and consumer applications. Then, each of the individual applications is described in more detail and, where possible, a quantitative estimation of the value of the application provided by a BESS is performed. Finally, the value estimations of the different applications are compared. The results of this analysis motivates the selection of the applications that are studied in more detail in the following chapters. To limit the scope of the chapter, the value estimation is performed for Germany as a case study.

2.2 Overview of Battery Energy Storage Applications

There are multiple applications for BESSs in the electricity markets and power grid and the definition of the applications can vary from one country to another. In general, one can divide most of these applications into one of the three following categories, depending for which player in the electricity market the application creates value.

- **Ancillary services:** services provided to the grid operators – the transmission system operator (TSO) or the distribution system operator (DSO) – for the operation of the transmission or distribution grid.
- **Wholesale electricity market applications:** providing market arbitrage by storing energy when electricity prices are low and selling when prices are high. Usually, the energy supplier benefits from these applications, although larger consumers might have direct exposure to these markets and can therefore also benefit from these applications.
- **Consumer applications:** applications where the electricity consumer (which can be a residential, commercial or industrial consumer) benefits directly from using a BESS, such as peak-shaving or storing excess photovoltaic (PV) generation for later consumption.

The specific details of a particular application depends highly on the structure of the market, which varies from one regulatory region to another. There are not only large differences between the electricity markets in e.g. Europe and North America [18], but also between different European regions the markets vary significantly [19]. However, in Europe, TSOs are working towards more integrated European electricity markets with unified products [20] by implementing the regulations from the European Commission on the electricity transmission system operation (SO GL) [21] and electricity balancing (EB) [22].

As the focus of this thesis is on European wholesale electricity and ancillary services markets, rather than North American markets, we will follow the terminology used by the European network of transmission system operators for electricity (ENTSO-E) [23] as closely as possible.

The applications which a BESS can provide depend on the location of the BESS in the grid: a large, utility-scale BESS connected directly to the transmission grid will be able to provide ancillary services to the TSO, but not to the DSO or to the consumer. A BESS installed *behind the meter*, i.e. at the consumer's premises, can provide consumer applications, but cannot access

wholesale electricity and ancillary services markets, unless provided via a third party.[1]

Application	Creates value for	Stand-alone	Behind the meter
Frequency containment reserve (FCR) Automatic frequency restoration reserve (aFRR) Manual frequency restoration reserve (mFRR) Replacement reserve (RR) Synthetic Inertia Black start	TSO	Yes	Indirect*
Voltage control Congestion management & network investment deferral	TSO or DSO	Yes	Indirect*
Day-ahead market arbitrage Intraday market arbitrage Imbalance price arbitrage & portfolio balancing	Producer/supplier, large consumers	Yes	Indirect*
Self-consumption Peak shaving Time of use bill management Power quality improvements Uninterruptible power supply (UPS)	Consumer/ prosumer	No	Yes

* A third party will be needed to enable behind-the-meter BESSs to participate in these markets.

Table 2.1: Non-exhaustive overview of the potential services battery storage could provide, the parties they can create value for and if the service can be delivered from a battery installed behind the meter or stand-alone.

[1] Very large consumers sometimes act as their own electricity supplier and therefore do not need a third party to provide them access to the wholesale market.

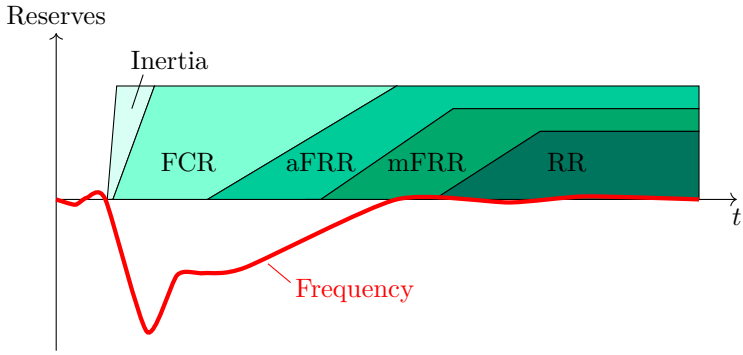

Figure 2.1: Load-frequency control services as defined by ENTSO-E [24].

Table 2.1 gives an overview of the most important applications a BESS can be used for, organised according to the three categories defined above. The table also shows if the application can be provided by a stand-alone BESS, or by a BESS installed behind the meter.

First the ancillary services are listed. The traditional ancillary services for load-frequency control: frequency containment reserve FCR, automatic frequency restoration reserve (aFRR), manual frequency restoration reserve (mFRR) and replacement reserve (RR), are used by the TSO to maintain the balance between generation and demand in the grid on various timescales. Figure 2.1 shows the order in which the load-frequency control services are activated to restore the balance in the grid after a frequency deviation occurs. Inertia is automatically provided by synchronous generators, and therefore not actively procured by TSOs, but BESSs could also provide synthetic inertia to the grid. Black start capability is used by the TSO to be able to recover the electric grid after a shutdown. The other ancillary services listen in Table 2.1: voltage control, congestion management and network investment deferral, can be used by both the TSO and the DSO, although a BESS can only be used by the DSO when the BESS is connected to the distribution grid.

After the ancillary services, the table lists the applications in the wholesale electricity market, including portfolio balancing and imbalance price arbitrage. Finally, the most important consumer applications are given. As mentioned before, only BESSs installed behind the meter, at the consumer's premises, can provide these applications.

2.3 Description and Value Estimation of Battery Energy Storage Applications

Each of the following subsections discusses one of the applications listed in Table 2.1 in more detail. Each subsection first describes the application and then performs a quantitative estimation of the revenues a BESS can obtain by delivering the application, when possible.

An accurate, fully detailed analysis of the value of a certain application can quickly become very complex as a lot of elements, such as battery degradation, control strategy and forecasts of stochastic variables have to be taken into account. As the purpose of this chapter is to provide a high-level overview and comparison of the applications, such a detailed estimation is considered out of scope. The value estimations presented here will therefore be limited to a high-level assessment without consideration of all the detailed costs and battery degradation. Nevertheless, we always provide a value estimation without any hindsight assumptions, as this can result in an unrealistically high estimation of the value. Estimating the value of applications that require an in-depth case-by-case analysis, such as network investment deferral or UPS, will therefore also be considered out of scope for this chapter.

To be able to compare the value of the different applications, the value will be estimated for a 1 C BESS, with the C-rate defined as the rated power capacity divided by the rated energy capacity: C-rate $= P_{rated}/E_{rated}$. A 1 MWh, 1 C BESS will thus have a rated power capacity of 1 MW. We will assume the BESS has a round trip efficiency of $\eta = 90\,\%$, with the charging efficiency equal to the discharging efficiency $\eta^c = \eta^d = \sqrt{0.9}$. Where applicable, we estimate the value of a BESS at 500 equivalent cycles per year, as using more cycles would result in a too fast degradation. The number of equivalent cycles can be calculated as follows [25]:

$$cycles = \frac{\eta^c \sum_{k=1}^{n_t} P_k^c \Delta t}{E_{rated}}, \tag{2.1}$$

with η^c the charging efficiency, P_k^c the battery charging power at time step k and Δt the number of time steps per hour.

Finally, to limit the scope of the chapter, the value estimation will be performed for Germany only.

2.3.1 Frequency Containment Reserve (FCR)

Description

Frequency containment reserve (also referred to as primary frequency control) is traditionally the fastest actively procured reserve used to maintain the active power balance between generation and consumption in the electrical grid. Any deviation of the power balance between generation and consumption will result in a deviation of the grid frequency f from the nominal frequency f_{nom} ($f_{nom} = 50\,\text{Hz}$ in Europe). If there is more consumption than generation in the grid, the frequency of the grid will decrease due to fact that the synchronous generators, which generate the grid frequency, will start to slow down. If, on the other hand, there is more generation than consumption, the frequency of the grid will increase as the synchronous generators will start to speed up. The total rotational inertia of the synchronous generators in the grid determines the rate at which the frequency of the grid will change in response to a change in the power balance. If the grid frequency increases or decreases too much, the generators will disconnect, the grid becomes unstable and might eventually collapse. Therefore, it is of uttermost importance that the balance between generation and consumption is kept stable at any moment in time.

When a frequency deviation occurs, the FCR will be automatically triggered to counteract the mismatch in generation and consumption and stabilise the frequency to a steady state value, as shown in Figure 2.1. The other reserves, described below, will then ensure the grid frequency returns to its nominal value. From a system control perspective, FCR acts as proportional (P) controller, i.e. adjusting the power output proportionally to the frequency deviation, stabilising the frequency deviation to a steady state value. The other reserves (and specifically aFFR) then act as an integral control, where the power output is adjusted proportionally to the integral of the grid frequency deviation, which is on its turn proportional to the system imbalance. Together they make up a PI-controller, controlling the frequency of the grid towards its nominal value at all times. As the grid frequency is equal across an entire AC-connected electricity grid, the total required FCR capacity of the interconnected Continental Europe (CE) transmission grid is shared by all TSOs operating a part of this grid.

In many European countries, the TSO procures its required amount of FCR capacity in a public auction or tender in which tertiary parties, such as BESS operators, can offer a certain amount of FCR capacity at a certain price. The TSOs of Austria, Belgium, France, Germany, the Netherlands and Switzerland acquire their required FCR capacity through a common tender on the *Regelleistung* platform [26], thereby creating one large FCR market with a high liquidity. On the Regelleistung platform, one can bid a symmetric FCR

capacity r at a capacity price c_{FCR}. When accepted, the FCR capacity r should be available symmetrically (i.e. both for power increase and power decrease) during the entire contracted period. During this period, one has to adjust the power for FCR $P^{FCR}(t)$ continuously, so that the FCR power is proportional to the relative grid frequency deviations $\Delta f(t) = (f(t) - f_{nom})/\Delta f_{max}$ and the entire FCR capacity r is reached when $|f(t) - f_{nom}|$ reaches a predefined maximum value Δf_{max} (200 mHz in the CE synchronous region). There is also a small deadband Δf_{db} in which no FCR reaction is required:

$$P^{FCR}(t) = r\Delta f(t) = r \begin{cases} \left[\frac{f(t)-f_{nom}}{\Delta f_{max}}, 0\right] & \text{if } -\Delta f_{db} \leq \frac{f(t)-f_{nom}}{\Delta f_{max}} \leq 0, \\ \left[0, \frac{f(t)-f_{nom}}{\Delta f_{max}}\right] & \text{if } 0 \leq \frac{f(t)-f_{nom}}{\Delta f_{max}} \leq \Delta f_{db}, \\ \frac{f(t)-f_{nom}}{\Delta f_{max}} & \text{otherwise.} \end{cases}$$

Failure to meet these requirements will results in penalties charged by the TSO which can cancel out all revenues made from FCR or can, in case delivery is consistently insufficient, even lead to exclusion from further participation in the market [27].

As a BESS has a limited energy content, ensuring the FCR capacity r is available during the entire contracted period is not straightforward. A BESS can become empty or full due to efficiency losses or the frequency signal which has a non-zero energy content over short time periods. If a BESS is empty or full, it cannot discharge or charge any more and no longer provide a symmetric FCR service. To avoid this, a State of Charge (SoC) management strategy or *recharge controller* is needed that controls the SoC of the BESS so it is never empty nor full while providing FCR. Managing the SoC can be done by offsetting the FCR delivery with the recharge power, creating a non-zero *baseline* against which the BESS provides the required FCR capacity. A certain power capacity P^{rc}_{max} for recharging, will have to be reserved for this, which cannot be used for FCR at the same time. The FCR capacity r will thus be limited by the maximum power capacity of the battery P_{max}, minus the recharge power capacity [28]:

$$r \leq P_{max} - P^{rc}_{max}. \tag{2.2}$$

Value Estimation

It is clear from (2.2) that the recharge controller will have to be designed carefully, as more power capacity for recharging P^{rc}_{max} will mean that less FCR capacity r can be sold to the TSO, while on the other hand the power capacity for recharging P^{rc}_{max} should be sufficient to ensure the SoC of the BESS is never empty nor full.

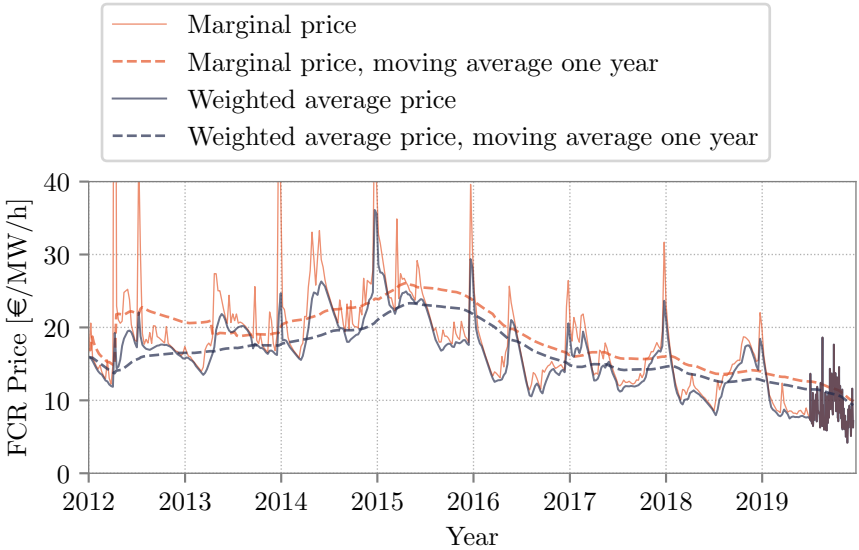

(a) Historic FCR price evolution on the international bidding platform Regelleistung [26].

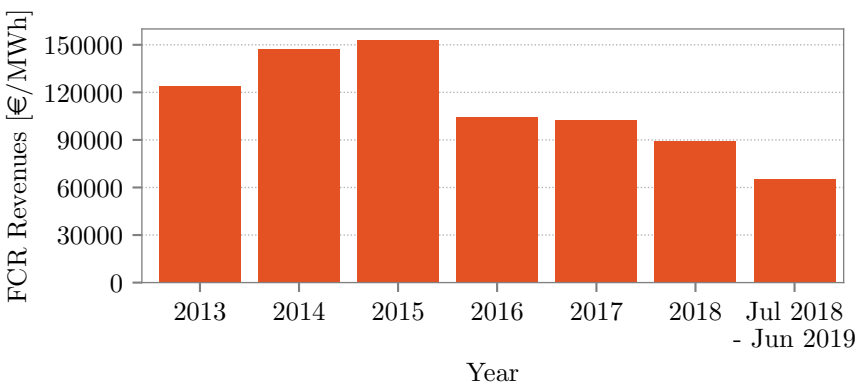

(b) Yearly revenues of a 1 C BESS following (2.3) and assuming the weighted average price shown above.

Figure 2.2: FCR price evolution and value estimation of a 1 C BESS participating in the international FCR market organised on Regelleistung.

A detailed analysis of the design of the recharge controller and how to determine r and P^{rc}_{max} is out of scope of this paragraph, but will be discussed in more detail in Chapters 3 and 4.

Here, we will limit ourselves to the regulatory requirements currently applicable in Germany, which states that the power reserved for SoC management has to be least a quarter of the FCR capacity [29]:

$$P_{max}^{rc} \geq 0.25r \Leftrightarrow r \leq 0.8P_{max}. \tag{2.3}$$

Figure 2.2a shows the evolution of the historic FCR price c_{FCR} on the Regelleistung bidding platform. As the FCR tenders were organised as a pay-as-bid market until the 1st of July 2019, the figure shows both the marginal price as the weighted average price (WAP) of all accepted bids, as well as the yearly moving average of both. It is clear from the figure that FCR prices have been decreasing, from a maximum yearly moving average WAP of 23.3 €/MW/h by May 2015 to 11.5 €/MW/h by July 2019, a trend which can partially be explained by the introduction of BESSs in the FCR market [30].

Figure 2.2b shows the yearly revenues per MWh a 1 C BESS could have obtained on Regelleistung given the historical weighted average FCR prices of Figure 2.2a and using the maximum FCR capacity from (2.3):

$$\begin{aligned} value_{FCR} &= \frac{r \cdot c_{FCR} \cdot 24 \cdot 365}{E_{rated}} \\ &= \frac{0.8P_{rated} \cdot c_{FCR} \cdot 24 \cdot 365}{E_{rated}} \\ &= 0.8c_{FCR} \cdot 24 \cdot 365, \end{aligned}$$

for a battery with a C-rate $= P_{rated}/E_{rated} = 1$. Due to the decrease in FCR market prices, the yearly revenues have decreased from above 150 000 €/MWh in 2015 to 80 500 €/MWh between July 2018 and June 2019.

2.3.2 Automatic Frequency Restoration Reserve (aFRR)

Description

The automatic frequency restoration reserve (or secondary frequency control), is used to restore the frequency to the nominal value after a frequency deviation has been stabilised by the FCR. Where FCR acts as a proportional controller, aFRR acts as an integral controller to grid frequency deviations. As indicated in Figure 2.1, the required response is slower and the duration of activation longer than for FCR. In North America, *frequency regulation* is a service comparable to aFRR, as it serves the same purpose from a high-level grid operating perspective [31].

Using aFRR, each TSO tries to reduce its area control error (ACE), which is the difference between the scheduled and the measured power balance within the control area of the TSO, corrected for the effect of a frequency bias. This reserve is activated in an automatic way by sending a continuous activation signal to the assets participating in aFRR. These assets should react automatically within the required reaction time.

In many European countries, aFRR is procured in public aFRR tenders. However, contrary to the FCR tenders, aFRR markets have often only been open for traditional power plants. It is only recently that aFRR markets have been starting to open up for non-conventional assets such as BESSs. For instance in Germany, where the TSOs have published some first guidelines on providing aFRR with BESSs [32] or in Belgium, where the TSO has conducted pilot projects on aFRR with decentralised flexibility resources [33] and foresees to open up the market for all technologies in 2020.

Usually, aFRR is procured in an asymmetric way, with separate tenders for positive and negative reserves. Apart from a capacity payment for reserving the power capacity, assets in aFRR also get paid an activation payment when they are activated.

Value Estimation

Since the required maximum duration of activation of aFRR is longer than for FCR, a BESS will need to have a larger energy content per unit of aFRR capacity to be able to sustain these long activations. As current aFFR markets are dominated by traditional power plants, which are not energy constrained, most aFRR markets do not specify any minimum energy requirements and it is implicitly assumed any participating asset can deliver the aFRR capacity for the entire bidding period [34].

In Germany, aFRR is tendered daily in 4-hourly blocks [26]. For energy constrained assets to participate in aFRR, there is the explicit requirement to have an energy capacity large enough to deliver at least one hour of the marketable aFRR capacity. Besides, the assets have to be able to deliver the service continuously for four hours. However, it is allowed to use energy management measures, such as buying and selling on the intraday market for recharging and SoC management [32].

To estimate the value of a BESS in aFRR, we assume the BESS participates in the aFRR market continuously, and therefore needs a recharge power that is able to completely compensate for the aFRR capacity sold on the market. In this way, the BESS can be activated at full power for an unlimited amount

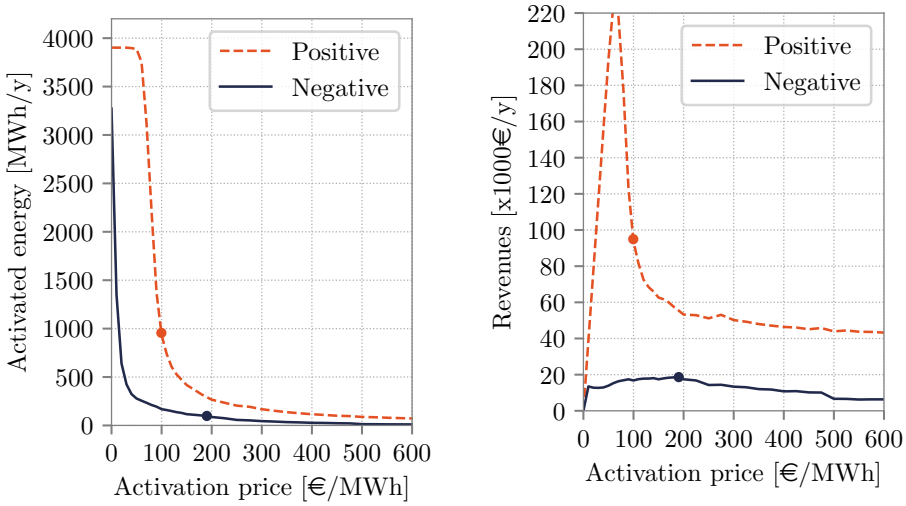

(a) Activated energy per year in function of the activation price for 1MW aFRR capacity in the German market.

(b) Revenues per year from activation payments in function of the activation price for 1MW aFRR capacity in the German market.

Figure 2.3: The highest revenues from activation payments in aFRR can be found at a lower activation price, when the asset is activated a lot. At higher activation prices, the assets gets activated less with reduced revenues as a consequence [26]. The dots correspond to the activation prices used here for the value estimation.

of time, as it can compensate for the required aFRR capacity by executing transactions on the intraday market. This means that a 1 MWh, 1 C BESS can only sell 0.5 MW aFRR capacity in the market, albeit in a symmetrical way.

As explained above, an asset in aFRR gets paid a remuneration for the capacity made available and a remuneration when the assets is activated. In this analysis, we use the market prices from the German aFRR market platform *Regelleistung* [26], from July 2018, the start of the daily bidding.[2] The weighted average capacity price during this period is 1.78/ €MW/h for positive aFRR and 0.76 €/MW/h for negative aFRR.

The remuneration for activation is dependent on the total energy the asset has

[2] We did however exclude the period between October 15, 2018 and July 31, 2019, as during this period the clearing mechanism of aFRR capacity included the activation bid prices, while currently the aFRR capacity market is cleared using only the capacity bid prices.

to deliver. In the German aFRR market, the assets are activated in merit order, activating the ones with the cheapest activation price first. The number of activations will therefore depend on the activation price of the bid. Figure 2.3 shows the historical activated energy and corresponding revenues in function of the activation price in the German aFRR market, for both positive and negative reserves. From Figure 2.3b, it can be seen that the activation payments can be very high, especially for positive aFRR. However, this comes with a high amount of energy that needs to be delivered (Figure 2.3a). If a BESS would need to deliver this energy, this would result in a very fast degradation of the BESS.

Here, we limit the BESS to 500 cycles per year. As we assume a 1 C BESS can only deliver 0.5 MW of aFRR capacity per MWh of energy capacity, this corresponds to a maximum energy throughput of $\eta^c \cdot 500/0.5 = 1024\,\text{MWh}$ throughput per MWh of energy capacity, following (2.1). Dividing this throughput optimally between positive and negative aFRR, one obtains the activation prices and corresponding activation revenues indicated by the red and black dots in Figure 2.3:

$$value_{aFRR,act,pos} \approx 94\,900\,\text{EUR/MW}$$

$$value_{aFRR,act,neg} \approx 18\,600\,\text{EUR/MW}$$

As the activation revenues from positive aFRR are generally much higher than for negative, it is beneficial to devote almost all energy throughput to positive aFRR.

Putting everything together, the revenues of a 1 MWh, 1 C BESS with 500 cycles in the German aFRR market can be estimated by adding up the positive and negative capacity payments and the activation payments:

$$\begin{aligned} value_{aFRR,cap} &= 0.5\,\text{MW/MWh} \cdot (1.78\,€\text{/MW/h} + 0.76\,€\text{/MW/h}) \cdot 24 \cdot 365 \\ &= 11\,125\,€\text{/y}, \\ value_{aFRR,act} &= 0.5\,\text{MW/MWh} \cdot (94\,900\,€\text{/MW/y} + 18\,600\,€\text{/MW/y}) \\ &= 56\,750\,€\text{/y}, \\ value_{aFRR} &= value_{aFRR,cap} + value_{aFRR,act} = 67\,875\,€\text{/y}. \end{aligned}$$

2.3.3 Manual Frequency Restoration Reserve (mFRR)

Description

The manual frequency restoration reserve (or tertiary frequency control) serves the same purpose as aFRR, with the difference that these reserves are manually activated instead of automatically. The mFRR will only be activated when a severe imbalance occurs which cannot be restored using aFRR alone. The number of activations of mFRR will therefore be less than the number of activations in aFRR, which is called upon almost continuously. One has more time to react and ramp up to full power in mFRR than in aFRR, so that slower assets are also able to provide mFRR.

Comparably to aFRR, mFRR is procured in an asymmetric way, with separate tenders for positive and negative reserves. Assets in mFRR also get paid a capacity payment for reserving the power capacity, and an activation payment when they are activated.

Due to its manual activation procedure, mFRR has been one of the first ancillary services for which TSOs have been contracting demand response flexibility. Today, mFRR is procured in different products, with features designed for a specific type of flexibility. For instance, the German TSOs procures mFRR via their standard mFRR product (Minutenreserveleistung), but has also a specific mFRR product for interruptible loads. Similarly, Elia, the Belgian TSO, has an 'R3-flex' product with some features that are attractive for demand response assets, e.g. a maximum number of activations per month, next to an 'R3-standard' product product.[3]

Value Estimation

Comparably to aFRR, the duration of activation for an asset in mFRR is longer than for FCR and a BESS participating in mFRR will need to have an energy content large enough to provide the maximum duration of activation.

The energy requirements for mFRR in the German markets are the same as for aFRR: there is an explicit requirement to have an energy capacity large enough to deliver the marketable mFRR capacity for at least one hour. The assets also have to be able to deliver the service continuously for the entire bidding period

[3] As a part of the ongoing harmonisation of ancillary service products on an European level, Elia foresees to phase out the distinction between the R3-standard and the R3-flex product in the near future.

of four hours, but this can be achieved with the help of energy management measures.

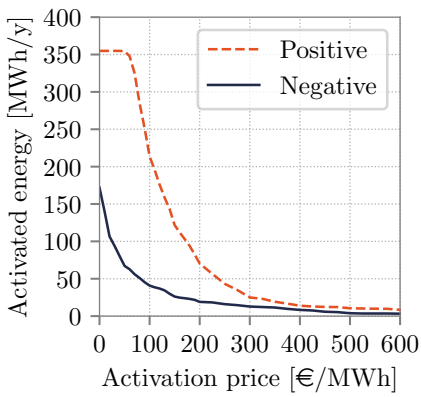

(a) Activated energy per year in function of the activation price for 1MW mFRR capacity in the German market.

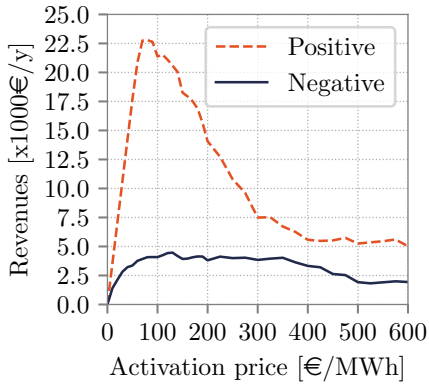

(b) Revenues per year from activation payments in function of the activation price for 1MW mFRR capacity in the German market.

Figure 2.4: As mFRR is much less called upon than aFRR, the activated energy in mFRR is a lot lower, with lower activation payments as a consequence [26].

To compute the marketable mFRR capacity of a BESS, we use the same assumptions as for aFRR, meaning that a 1 MWh, 1 C BESS can only sell 0.5 MW of symmetric mFRR capacity in the market. With the recent historical weighted average capacity prices around 0.27 €/MW/h for positive mFRR and around 0.45 €/MW/h for negative mFRR [26], the total capacity payments for a 1 MWh, 1 C BESS amount up to 6300 € over one year.

Assets in mFRR are activated in merit order. Figure 2.4 shows the historical activated energy and corresponding revenues in function of the activation price in the German mFRR market, for both positive and negative mFRR.

Comparing Figure 2.4a to Figure 2.3a shows that the activated energy in mFRR is a lot lower than in aFRR. Degradation due to a high amount of cycles will therefore not be an issue in mFRR, contrary to aFRR, hence we assume a BESS is able to capture the maximum activation revenues shown in Figure 2.4b:

$$value_{mFRR,act,pos} \approx 22\,800\,\text{EUR/MW},$$

$$value_{mFRR,act,neg} \approx 4500\,\text{EUR/MW}.$$

Nevertheless, the reduced activated energy means that these activation payments are much lower than for aFRR.

Combining capacity and activation payments, the revenues of a 1 MWh, 1 C BESS in the German mFRR market can be estimated to be around 16 800 € over one year:

$$\begin{aligned} value_{mFRR,cap} &= 0.5\,\mathrm{MW/MWh} \cdot (0.27\,€/\mathrm{MW/h} \quad + 0.45\,€/\mathrm{MW/h}) \cdot 24 \cdot 365 \\ &= 3153\,€/\mathrm{y}, \\ value_{mFRR,act} &= 0.5\,\mathrm{MW/MWh} \cdot (22\,800\,€/\mathrm{MW/y} + 4500\,€/\mathrm{MW/y}) \\ &= 13\,650\,€/\mathrm{y}, \\ value_{mFRR} &= value_{mFRR,cap} + value_{mFRR,act} = 16\,803\,€/\mathrm{y}. \end{aligned}$$

2.3.4 Replacement Reserve (RR)

Description

Replacement reserves are used to free up the automatic and manual frequency restoration reserves so that these are ready to support an additional imbalance event. The replacement reserves are thus only used in case the imbalance event lasts considerably longer than usual and are therefore rarely activated. Activating replacement reserves is a manual process, comparable to mFRR. Not all European TSOs are actively procuring RR [35], as it is not strictly required by the system operation guideline (SO GL) regulation of the European Commission [21]. TSOs that do not actively procure RR instead use mFRR capacity to function both as frequency restoration reserve and as replacement reserve.

Value Estimation

The product characteristics of the replacement reserve products of the TSOs that actively procure replacement reserves are very comparable to the product characteristics of the mFRR products, but usually with a longer time to ramp up to full capacity.

The German TSOs do not actively procure RR, but instead use mFRR capacity to function both as manual restoration reserves and as replacement reserves. To estimate the value of a BESS delivering RR in this chapter, we will therefore use

data from RTE, the French TSO, who does procure both mFRR and RR. The prices for the RR capacity procured by RTE in 2019 where around 63 % of the prices of the mFRR capacity procured by RTE. As an hypothetical estimation of the value of RR on the Germany market, we will therefore assume the revenues of delivering RR are 63 % of the revenues of mFRR:

$$value_{RR} = 0.63 value_{mFRR} = 10\,586\,€/\text{y}.$$

2.3.5 Inertia

Description

Inertia in the electrical grid is the resistance of the power system against sudden frequency changes, which would lead to stability issues. Traditionally, the inertia in the electrical grid originates from the rotational inertia that is an inherent mechanical property of synchronous generators and motors. When a power imbalance occurs, the rotational inertia of these machines prevent the grid frequency to change instantaneously, by momentarily compensating for the power imbalance, and thereby limiting the rate of change of frequency (RoCoF).

As the share of asynchronous generation increases, which is the case with an increase of PV and wind generation as they are connected to the grid via power electronics based inverters, the share of synchronous generators and therefore the inertia in the grid decreases. This on its turn increases the RoCoF and reduces the stability of the grid [36].

However, with the correct control methods, it is possible for some assets that have a power electrics based interface with the grid, like BESSs, to mimic the inertial response of synchronous generators, providing *synthetic inertia* to the grid [37]. As the inertial response of a synchronous machine is a power change proportional to the RoCoF, an asset providing a certain amount of synthetic inertia H_{syn} should also adjust its power proportional to the RoCoF [38]:

$$\Delta P_{inertia}(t) = -H_{syn} \frac{df(t)}{dt} ft.$$

The synthetic inertia should not be confused with fast frequency response products. The purpose of synthetic inertia is to mimic the inertial response of synchronous machines, adjusting the power output proportionally to the RoCoF. With fast frequency response products on the other hand, one has to responde to frequency deviations rather than to the RoCoF [38]. In this regard, fast frequency response products are similar to traditional FCR products, however with a faster required response time. In power systems with reduced inertia,

fast frequency response products help to reduce the frequency deviations better than traditional FCR, but will not help to reduce the RoCoF of the system.

Value Estimation

Currently, synthetic inertia is not actively procured by European TSOs as the inertia of the grid is still provided by synchronous machines. However, it is recognised that in systems with a larger share of renewable energy generation there will be a need for synthetic inertia in the future [39]. Estimating the value of a BESS procured to deliver synthetic inertia therefore requires a more in-depth analysis of a potential synthetic inertia market and is considered out of scope for this chapter.

2.3.6 Black Start

Description

Traditional electricity generation units are not able to start up completely by themselves, but need external power which they normally obtain from the electricity grid. However, in case of a partial or total shut down or *black out* of the grid, it is not possible for a generator to obtain the necessary start-up power from the grid. To be able to restore the grid in such a situation, some generation units have to be capable to start without relying on external power.

Black start is the capability of production units to start up without relying on the external power grid. This can for instance be achieved by having the required power delivered by a smaller, auxiliary diesel or gas-fired generator. When a black out occurs, the production units with black start capability are able to re-energise parts of the grid, enabling other production units without black start capability to also start up and so gradually recover the grid.

The TSO procures black start capabilities from selected production units, which get paid to recover the investment costs needed to equip a production unit with black start capabilities. As the technical requirements for the black start service are rather stringent, the black start service is currently only being procured from traditional power plants. Nevertheless, there are some TSOs investigating the use of non-conventional energy resources for black start services, with Imperial Irrigation District, a utility from southern California, having demonstrated an emergency black start with a BESS [40].

Value Estimation

Since black start provision by a BESS is still in an early demonstration phase, there are no commercial examples of third party BESSs providing black start capabilities to a TSO yet. Besides, the TSO procures black start capabilities from traditional production units usually through tenders in which the offer is evaluated on a technical and economical perspective in a case-by-case analysis, rather than through a liquid market.

The commercial value of a BESS providing black start services can therefore not be estimated without performing an in-depth analysis, which is considered out of scope for this chapter.

2.3.7 Voltage Control

Description

Both the TSO and the DSO have to ensure the voltage of the grid remains within a predefined tolerance band around the nominal voltage of the grid. Contrary to the frequency, the voltage is not equal over the grid, but varies with the location in the grid. Therefore, the amount of voltage control capability required by the system operator depends on the location in the grid.

In the high voltage grid, operated by the TSO, voltage control can be achieved by adjusting the reactive power consumption or injection of an asset directly connected to the point in the grid where the voltage has to be controlled. In the low voltage grid, operated by the DSO, voltage control can be achieved by adjusting both active and reactive power of an asset, although reactive power will have less effect and incur more active power losses than in the high voltage grid.

BESSs can provide voltage control services, as they are connected via an inverter which can be controlled to inject or consume both active and reactive power into and from the grid.

Value Estimation

As the purchase of voltage control services by the grid operators varies with location, a real liquid market for voltage control does not exist. The use of active voltage control by DSOs is still in a demonstration stage with various

pilot projects being carried out around the world, but a mature commercial market for voltage control in the distribution grid does not yet exist.

Similarly to the black start service, estimating a quantitative value for voltage control delivery by a BESS is considered out of scope for this chapter.

2.3.8 Congestion Management & Network Investment Deferral

Description

Congestion in the grid occurs when the transfer of active power over the grid exceeds the transfer capability of the grid [41]. When congestion occurs on a part of the grid, the grid operator has two options: to limit the active power transfer or to increase the transfer capacity of the grid. The first option has an impact on the users of the grid, as they need to adjust their power consumption, while the second option involves a severe long-term investment from the grid operator.

Typically, the periods for which congestion occurs are limited in time and investing in an increase of grid capacity to cover only these few moments is not cost effective. A BESS could then be used to manage active power at the congestion point during these moments, ensuring the power throughput stays below the transfer capability and deferring or even eliminating completely the need for investments to upgrade the grid. Congestion management can be used by both TSOs and DSOs, depending on which part of the grid the congestion occurs and the BESS is connected to. Active congestion management performed by the TSOs within its control area is sometimes also referred to as *redispatch* [42].

Value Estimation

Comparably to voltage control, the value of congestion management depends on the geographical location of the BESS in the grid. A BESS which is not connected to the congested part of the grid cannot reduce the congestion in the congested part of the grid. Previous work in the literature has estimated that the use of BESSs for congestion management and network investment deferral can reduce the total cost of the DSO by 28 % [43] and therefore would present a positive business case, although the value depends highly on the degree of congestion of the network. In these use cases however, the BESS is owned and operated by the DSO as being part of the grid.

Another option to avoid congestion in a part of the grid would be for a grid operator to buy flexibility on that specific location from third party flexibility providers through local energy markets and local flexibility markets. However, such market places are still a topic of active research [44], with ongoing pilot projects to demonstrate the effectiveness of such markets [45]. Besides, concerns on the possibility of strategic bidding and locational market power that can occur with market-based congestion management results in some actors advocating against market-based congestion management [46].

Since market-based congestion management is currently still under discussion, estimation the value requires an in-depth study, taking assumption on the possible market design, the product features, the grid topology and the costs of other assets, amongst others. As this is beyond the scope of this chapter, we will exclude the value of congestion management from the comparison with the other services.

2.3.9 Day-Ahead Market Arbitrage

Description

On the day-ahead market (DAM), producers, suppliers and large consumers can trade energy for the next day. Typically, the energy is traded in hourly blocks (or half hourly blocks in the UK). Producers place offer bids, consisting of a certain capacity at a certain price for a specific hour the next day while suppliers place demand bids. All bids have to submitted before market closing time, after which the market clearing algorithm calculates the accepted bids and prices for each hour of the next day.

Historically, the DAMs in Europe have been cleared by placing the offer and demand bids in merit order with the intersection of the offer and demand curves determining the clearing price. In the current European DAMs the concept of merit order still exists, however, the implementation of the flow-based market coupling has significantly increased complexity of the market clearing algorithm [47].

BESSs can provide DAM arbitrage as they are able to store energy, charging at times when the day-ahead price is low and discharging at times when the day-ahead price is high. For this application, the BESS needs to have access to the DAM, which can be provided by a supplier or a balance responsible party (BRP). Often, large consumers which are directly connected to the transmission grid also have access to the DAM, and would therefore also be able to use a BESS for DAM arbitrage.

Recently, the products in some European DAMs have been expanded to include more advanced products, such as *linked block orders*, *exclusive block orders* and *loop blocks* [48, 49]. Loop blocks are especially interesting for BESSs, as they allow to couple the sale of a volume of energy at a certain time period with the purchase of a volume of energy at another point in time. This avoids the risk of selling a volume of energy with the BESS without having the possibility to charge the BESS first.

Value Estimation

To estimate the value of a BESS in the day-ahead market, we propose a simple optimisation problem, minimising the cost of charging and discharging against the DAM prices $c_k^{DAM}, k = 1, \ldots, n_t$, thereby maximising DAM arbitrage profits. When the DAM bids have to be placed, the cleared prices are not yet known. Therefore, we will assume here the BESS has access to a prediction of the DAM prices $\tilde{c}_k^{DAM}$, and optimises its (dis)charging schedule against these predicted prices $\tilde{c}_k^{DAM}$.

Let $0 \leq P_k^c$ and $P_k^d \leq 0$ be the battery charging and discharging power respectively, at time step k, with duration Δt. The optimisation problem can then be formulated as follows:

$$\min \quad \sum_{k=1}^{n_t} \tilde{c}_k^{DAM}(P_k^c + P_k^d)\Delta t \tag{2.4a}$$

$$\text{s.t.} \quad 0 \leq P_k^c \leq P_{max}^{bat}, \qquad k = 1, \ldots, n_t, \tag{2.4b}$$

$$P_{min}^{bat} \leq P_k^d \leq 0, \qquad k = 1, \ldots, n_t, \tag{2.4c}$$

$$0 = P_k^c P_k^d, \qquad k = 1, \ldots, n_t, \tag{2.4d}$$

$$E_{min}^{bat} \leq E_k \leq E_{max}^{bat}, \qquad k = 1, \ldots, n_t, \tag{2.4e}$$

$$E_{k+1} = E_k + (\eta^c P_k^c + \frac{1}{\eta^d} P_k^d)\Delta t, \quad k = 1, \ldots, n_t, \tag{2.4f}$$

$$\eta^c \sum_{k=1}^{n_t} P_k^c \leq cycles_{max} \frac{365 \cdot 24}{n_t \Delta t}. \tag{2.4g}$$

Constraints (2.4b) and (2.4c) limit the charging and discharging power to the maximum $P_{max}^{bat} = P_{rated}^{bat}$ and minimum $P_{min}^{bat} = -P_{rated}^{bat}$ power of the battery, respectively. Constraint (2.4d) is an integer constraint, denoting that the battery

cannot charge and discharge at the same time. Constraint (2.4e) limits the energy content of the battery to the maximum $E^{bat}_{max} = E^{bat}_{rated}$ and minimum $E^{bat}_{min} = 0$ energy content, while constraint (2.4f) relates the battery power to the battery energy content, taking into account a constant battery charging η^c and discharging η^d efficiency. Finally, constraint (2.4g) limits the amount of equivalent cycles over one year, using (2.1).

After solving (2.4) with the predicted prices $\tilde{c}^{DAM}_k$, the resulting value of the BESS in the DAM can be calculated by multiplying the battery charging and discharging power schedule with the actual day-ahead prices c^{DAM}_k:

$$value_{DAM} = \sum_{k=1}^{n_t} c^{DAM}_k (P^c_k + P^d_k)\Delta t. \tag{2.5}$$

For this analysis, we used the DAM prices of Germany from January 2016 to July 2019 [50]. As the German DAM is traded in blocks of one hour, $\Delta t = 1\,\mathrm{h}$. In reality, one has to place a DAM bid every day and therefore the problem (2.4) should be executed daily. Constraint (2.4g) may then be overly conservative, as on days with highly volatile prices and it would be beneficial to run more cycles, and compensate for this on days with less price volatility by running less cycles. In this analysis however, we run (2.4) over the entire horizon of DAM prices (from January 2016 to July 2019), and scale $value_{DAM}$ from (2.5) to represent the value over one year.

We assume one is able to predict the DAM prices c^{DAM}_k with an additive error ϵ^{DAM} which follows a normal distribution with zero bias and standard deviation σ_{DAM}:

$$\tilde{c}^{DAM}_k = c^{DAM}_k + \epsilon^{DAM}, \quad \epsilon^{DAM} \sim \mathcal{N}(0, \sigma^2_{DAM})\,. \tag{2.6}$$

Figure 2.5 shows the average value $value_{DAM}$ of a 1 MW, 1 MWh BESS in the German DAM over one year, in function of the normalized root mean square error (NRMSE) of the predicted DAM prices $\tilde{c}^{DAM}_k$ (in this case here $NRMSE = \sigma_{DAM}/\overline{c^{DAM}}$). A NRMSE of 0 corresponds to the perfect hindsight value, where one is able to predict the future prices perfectly. From the figure, it can be clearly seen that with a higher error on the predicted prices, a lower value on the DAM can be achieved.

The figure shows the curve for multiple maximum cycles per year $cycles_{max}/y$. It can be easily understood that with a maximum of 300 cycles per year the value of the BESS is less than with a maximum of 500 cycles per year, although the difference between the two curves decreases with an increased prediction error. However, it is interesting to note that at a maximum of 1000 cycles per year, the value of the BESS is only higher when the error on the predicted prices

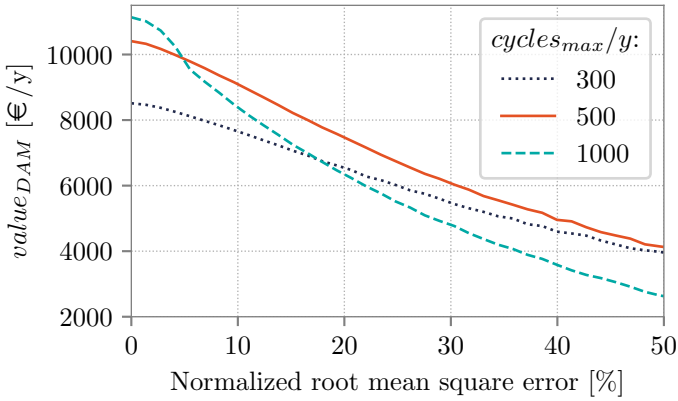

Figure 2.5: Average value of a 1 MW, 1 MWh BESS on the Germany DAM per year, in function of the NRMSE of the predicted DAM prices, and for a maximum of 300, 500 and 1000 cycles per year.

is low. When the predicted prices have a higher error, it is actually beneficial to limit the maximum amount of cycles to 500, even if the BESS can support up to a 1000 cycles. This can be explained by the fact that with a high number of cycles, when solving (2.4) with the predicted prices, the BESS will try to leverage all arbitraging possibilities on the predicted prices, also when this will only result in a small expected profit. When the actual prices are then different from the predicted prices, this small expected profit can quickly become a loss. It is therefore beneficial to limit the amount of cycles, as the BESS will then only perform arbitrage when the expected profit of a cycle is large enough. A more accurate, but also more involved way of achieving this would be to take the uncertainty on the predicted prices into account in the optimisation problem.

Current state-of-the-art day-ahead market forecasters using artificial neural networks are able to obtain a NRMSE of around 22 % [51], corresponding to a value of 7100 €/y in Figure 2.5.

Usage of more the advanced products when bidding in the day ahead market, such as the loop blocks mentioned above, will allow one to reduce the risk on trading with losses, and therefore will increase the value on the day ahead market when the prices are uncertain. A detailed analysis of advanced trading strategies leveraging the capabilities of these product is out of scope of this chapter, however, it is clear that this value can never be more than the perfect hindsight value corresponding to a NRMSE of 0 in Figure 2.5.

2.3.10 Intraday Market Arbitrage

Description

After the day-ahead market is closed, it is still possible to buy and sell energy on the continous intraday market (CIM), which is cleared on a continuous basis, rather than only at closure [52]. This means that once a buy bid can be matched to a sell offer, both bids are cleared before market closure. The cleared market price of a specific energy block can therefore vary as long as the market is open for trading that energy block.

Depending on the country, the CIM allows to trade in blocks of 1 hour, 30 minutes or 15 minutes and closes between 1 hour and 5 minutes before delivery. Recently, the CIM of various countries in Europe have been linked to create a cross-border intraday market with implicit continuous allocation of cross-border transmission capacity [53].

Similarly to the DAM, a BESS can perform arbitrage on the CIM, by charging when intraday prices are low and discharging when intraday prices are high. Besides, a BESS could also provide arbitraging between the DAM and the CIM, for instance by buying a volume of energy on an hour with high day-ahead prices, and selling this energy back when prices on the CIM are lower on a later time period.

Value Estimation

In the German CIM, energy is traded in hourly and a quarter-hourly blocks, which can be traded up to 5 minutes before the delivery period in the same TSO area [54].

The highest and lowest price traded and a weighted average trade price are publicly available [55] for the hourly and quarter-hourly blocks of the German CIM. One can obtain the most value when performing arbitrage on the highest and lowest traded prices. However, it is very unlikely one is always able to trade at these prices because it requires perfect hindsight knowledge of all bids placed in the market.

As using the highest and lowest traded prices results in the maximum achievable value of a BESS performing CIM arbitrage, we use these prices to calculate an upper bound. To calculate a lower bound, we use the weighted average trade prices, assuming one is definitely able to trade at the weighted average trade prices.

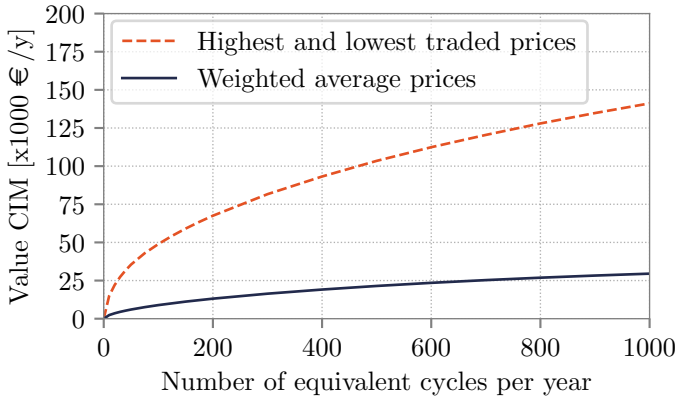

Figure 2.6: Value of a 1 MW, 1 MWh BESS performing arbitrage on the Germany CIM over one year, in function of the average number of cycles. The maximum achievable value is given using the highest and lowest traded prices, while using the weighted average trade prices gives a lower bound on the value.

Figure 2.6 shows the value of a 1 MW, 1 MWh BESS performing arbitrage on the quarter-hourly German CIM for one year in function of the number of cycles. The value is calculated using (2.4), but with the highest (for discharging) and lowest (for charging), or weighted average CIM prices, instead of the day-ahead prices. There is large difference between the maximum achievable value using the highest and lowest traded prices, and arbitraging using the weighted average prices. A good trading algorithm can therefore be expected to create considerably more value than the lower bound of Figure 2.6, but it can be assumed that the value corresponding to the highest and lowest traded prices will never be achieved in practice.

2.3.11 Imbalance Price Arbitrage & Portfolio Balancing

Description

The imbalance of a BRP is equal to the difference between the sum of all its produced energy, including purchases on future, day-ahead and intraday markets, and the sum of all consumed energy, including all sales on future, day-ahead and intraday markets. If a BRP has an imbalance during a settlement period, the TSO will charge the BRP an imbalance price. These imbalance

prices vary per settlement period and depend on the amount of imbalance in the system and the amount of reserves the TSO had to activate to maintain the balance in its control area. In some TSO control areas, the imbalance price for a positive imbalance is different from the imbalance price for a negative imbalance, although there is a trend on European level to work with a single imbalance price.

A BRP can use a BESS for portfolio balancing, minimising its exposure to these imbalance prices by charging the BESS when the portfolio of the BRP has a positive imbalance and discharging when the portfolio has a negative imbalance. In this way, the BESS will try to balance the portfolio of the BRP in such a way that imbalance is minimised, avoiding possible high imbalance charges.

As the imbalance prices vary over time, one can also use a BESS to perform imbalance price arbitrage, by charging the BESS when imbalance prices are low and discharging when imbalance prices are high.[4]

An additional difficulty of performing arbitrage on imbalance prices is that the imbalance prices for a settlement period are only calculated by the TSOs after the settlement period. A BRP that wants to perform imbalance price arbitrage will therefore have to predict the imbalance prices of both the future and the current settlement periods using the available data at that moment in time.[5]

Value Estimation

Both portfolio balancing and arbitraging are ways to create value with a BESS on the imbalance prices. The objective of portfolio balancing is not to maximise revenues, but rather to minimise the risk of having to pay high imbalance costs. When performing arbitrage however, the objective is clearly to maximise revenues by minimising imbalance costs (although it would be possible to take a risk metric into account here as well). Therefore, to compare the value of a BESS arbitraging on imbalance prices with the other applications, we focus on imbalance price arbitrage rather than portfolio balancing.

Most TSOs, such as the Belgian TSO Elia or the British TSO National Grid, publish a first non-validated estimation of the imbalance price of a settlement period during the current or the next settlement period. In Germany however, the imbalance prices are only published once a month, 20 workdays after the

[4] In some countries there exists a balancing obligation, meaning that the BRP is not allowed to make its portfolio go in imbalance on purpose. However, when the imbalance caused by a BRP helps to reduce the general imbalance in the system, this is often tolerated.

[5] Some TSOs such as Elia now publish non-validated estimations of the current imbalance price in real time.

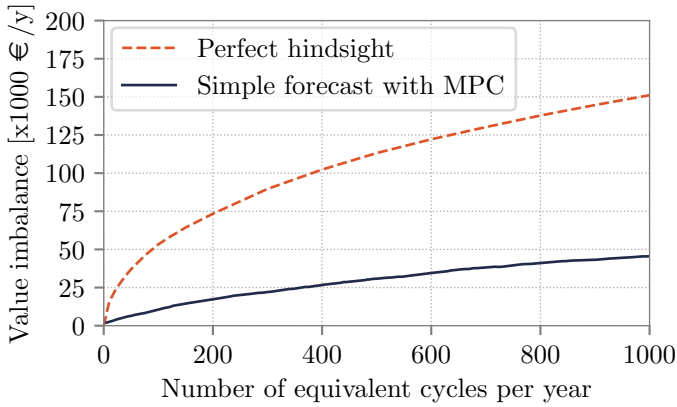

Figure 2.7: Value of a 1 MW, 1 MWh BESS performing arbitrage on the German imbalance prices over one year, in function of the average number of cycles. The maximum value is given using the perfect hindsight prices while a lower bound is given by the MPC with a simple imbalance price forecaster.

end of the month in which they occur. This makes it harder to predict future imbalance prices, as no short-term historical data is available.

It is clear that with a better forecast of the imbalance prices, higher revenues can be obtained. The theoretically maximum achievable revenues can be calculated by using the actual imbalance prices in (2.4). To obtain a lower bound on the imbalance revenues, we created a simple forecast of the imbalance prices, using a linear regression with L1 regularization from a set of available data points that can be correlated to the actual German imbalance price.

For the regression we used information from the day-ahead and intraday markets, the marginal prices of the activated aFRR and mFRR reserves, the activated aFRR and mFRR volumes and the ACE of the last settlement price period. We ran the regression model for the current and the future 20 quarters. For the control of the battery, we used a model predictive control (MPC) approach [56], where we run the optimisation (2.4) with the 21 forecasted imbalance prices, and only execute the first upcoming quarter hour of the battery power resulting from the optimisation. For the next quarter hour, we generate a new forecast using the latest available information, and repeat the process for every consecutive quarter hour. We use two years of data for training the regression and evaluate the performance on the imbalance prices of 2018.

The value of a 1 MW, 1 MWh BESS performing arbitrage on the German

imbalance prices of 2018 is shown in Figure 2.7 in function of the maximum number of cycles per year. The figure gives an upper bound on the value of the BESS using the perfect hindsight imbalance price information, and a lower bound using the MPC with the linear regression as a simple imbalance price forecaster.

As with the CIM, the maximum value in the German imbalance market is pretty high, however, in practice this value is unachievable as one does not know the imbalance prices upfront. Nevertheless, a good imbalance price forecaster in combination with a good control algorithm should be able to create considerably more value than the lower bound shown in Figure 2.7.

2.3.12 Increasing Self-Consumption

Description

When an electricity consumer has locally installed electricity generation such as PV, the consumer is also referred to as a *prosumer*. Depending on the tariff, the energy exported to the grid will be measured separately from the energy imported from the grid. Due to grid costs, taxes and levies, the electricity price paid for the imported energy is usually higher than the electricity price the prosumer receives for the exported energy. It is therefore beneficial for the prosumer to consume the generated electricity locally instead of exporting the energy to the grid. However, not all locally generated electricity can always be consumed directly. This is for instance the case with residential PV, where most of the electricity is generated during the day but most of the residential electricity consumption occurs in the evening and in the morning.

Using a BESS, a prosumer can store the excess generated production for later consumption which would otherwise be exported to the grid. In this way, the prosumer increases the self-consumption of the locally generated energy, and saves the difference between the import and export electricity price per unit of electrical energy stored in the BESS. As this application aims to adjust the prosumers' metered imported and exported energy, this application can only be provided by a BESS installed behind-the-meter, i.e. at the prosumers' premises.

Value Estimation

The value of a BESS increasing self-consumption depends on the actual consumption profile of the prosumer, the production profile of the locally

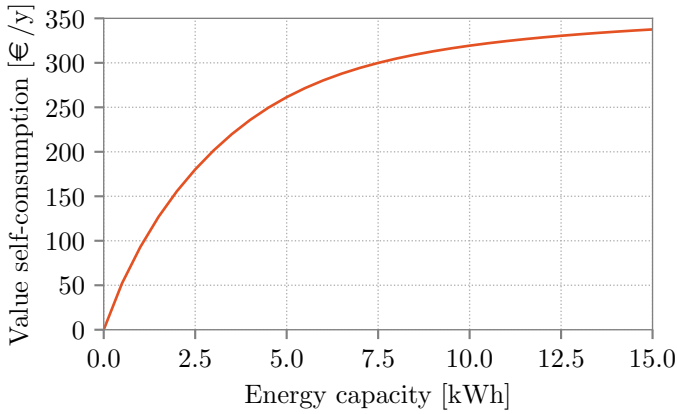

Figure 2.8: Value of a residential 1 C BESS performing self-consumption in function of the energy capacity of the BESS.

installed generation asset and the difference between the import and export prices.

As the electricity import price of residential consumers is usually higher than the import price of large commercial or industrial consumers, self-consumption is an application with a high potential for residential electricity prosumers, which usually have rooftop PV.

To estimate the value of self-consumption for residential prosumers with PV, we run a Monte Carlo simulation with multiple residential consumption profiles, generated using the model from [57], and PV production profiles generated from the model presented in [58]. The consumption profiles are scaled so that, on average, they consume 3500 kWh/y, while the PV profiles are scaled to represent a system of 4.0 kWp.

We use the average import price for households in Germany of 30.43 c€/kWh [59] and the latest German feed-in tariff for residential PV systems of 10.18 c€/kWh [60].

Figure 2.8 shows the average value due to a decrease in electricity costs of a residential 1 C BESS used for self-consumption of rooftop PV. The graph shows the value of the BESS in function of the energy capacity. The larger energy capacity of the BESS, the higher the value, as the BESS can store more generated PV energy. However, saturation of the value occurs for larger BESS, meaning that the value per kWh of energy capacity actually reduces with larger BESS. Commercially available residential BESS have a size between

5.0 kWh and 13.0 kWh, which gives a value between 250 and 340 €/y, or between 52 €/kWh/y to 25 €/kWh/y, according to Figure 2.8.

2.3.13 Peak Shaving

Description

Grid tariffs charged to commercial and industrial electricity consumers consist not only of an energy component (in €/kWh), but also of a peak demand charge c_{peak} (in €/kW), proportional to the highest measured consumption peak over a certain time period, usually a month or a year [61]. With this tariff structure, a BESS can reduce network costs by discharging at the moments when the site is consuming its maximum power and charging when the site is consuming less, thereby reducing the site's metered peak consumption, and therefore also reduce the charged grid fees.

Beside a proportional peak demand charge, often, a large reduction on total grid fees is given to large consumers who have a very flat profile, expressed by the *profile duration* (equal to the total energy consumption divided by the maximum consumption peak). For example in Germany, if the profile duration of a consumption site is above 7000 h, the site can get a reductions up to 80 % of the total grid fees [62]. Also in France, similar reductions are give to large electricity consumers [63]. A BESS installed at such a site can help the site to increase its profile duration by reducing the maximum consumption peak, so that the site reaches the threshold needed to obtain the reduction.

Value Estimation

As demand charges are usually charged to larger industrial or commercial consumers but not to residential consumers, we simulate a BESS performing peak shaving on 64 industrial consumption profiles, varying from large, industrial sites such as metal melters to smaller wood pulp processing companies and cold stores.

We employ a simple, rule base BESS control strategy for peak shaving: optimise a threshold value based on historical data, have the BESS discharge when the consumption profile goes above this threshold value, and charge otherwise. This is an effective controller which can easily be employed in real life, however, it is not an optimal controller, as an optimal peak shaving controller will know at which moment exactly the consumption peak occurs and only then starts

to discharge. However, such an optimal controller requires perfect hindsight knowledge of the consumption profile which is not available in practice.

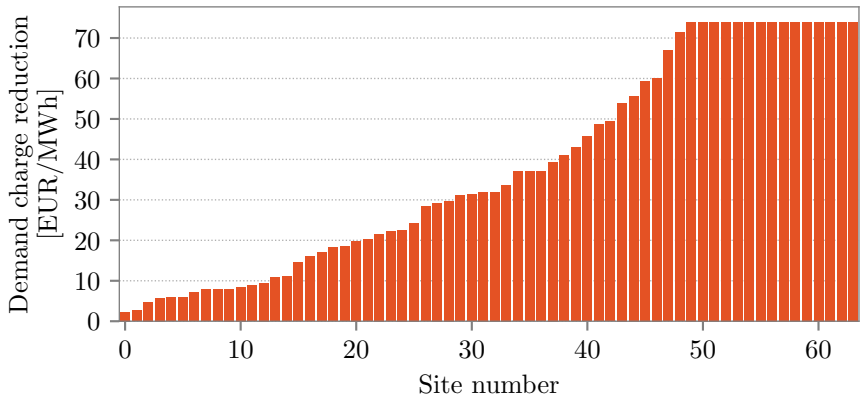

Figure 2.9: Value created of energy capacity of a 1 C BESS when performing peak shaving on 64 industrial and commercial consumption profiles. The power capacity of the BESS is chosen to be 10 % of the peak power of the consumption profile.

In Germany, the grid tariffs of large consumers have a demand charge component proportional to the maximum power consumption peak per month or per year. The exact value of the demand charge depends on the distribution grid the site is connected to. Here, we use the demand charges of *Westnetz*, a large DSO in the west of Germany, which charges a demand charge of 74.27 €/kW/y on the maximum power peak over one year [64].

Figure 2.9 shows the value due to a reduction in demand charges per MWh of a 1 C BESS, for the 64 industrial sites. As the size of the profiles varied a lot, we dimensioned the size of a BESS at a consumption site so that it equals 10 % of maximum site power.

From the figure, it is clear that there is a large difference in the value of a BESS for peak shaving amongst the various sites. For some sites, the BESS is able to reduce the peak power significantly, and therefore create considerable value. For other sites, the BESS can only reduce the peak power slightly and therefore does not create much value.

2.3.14 Time of Use Bill Management

Description

Smaller industrial, commercial and residential consumers usually have a flat rate or a time of use (ToU) electricity tariff [65]. With ToU tariffs, the electricity price is higher during specific, predefined hours of the day. The objective of the ToU tariffs is to shift electricity demand to hours where there is typically less consumption or wholesale prices are lower. Examples are peak/off-peak tariffs such as the economy 7 tariff in the UK or typical day/night tariffs which offers consumers a lower price during the night.

A BESS performing ToU bill management provides direct value to the consumer, by discharging the BESS when there is consumption during peak hours, and charging the BESS during off-peak hours. This service can only be provided by a BESS installed behind the meter. As the tariffs and peak/off-peak hours are known before hand, there is no need for price forecasting, simplifying the control of the BESS significantly.

Value Estimation

One of the most occurring time of use tariffs is the day and night tariff for residential consumers. In this scheme, the consumers are charged less during the night and in the weekends than during the day. A BESS can then simply charge during the night hours and discharge during the day hours to reduce the electricity costs of the consumer.

In Germany, a day and night tariff scheme exists, however, the difference between the day and the night tariff has been decreasing during the latest years. To estimate the value of a BESS in the day and night tariff, we assume an electricity costs of 30 c€/kWh during the day and 25 c€/kWh during the night periods. In Germany, the day periods typically run from 6h00 to 22h00 on weekdays.

To estimate the value of a BESS arbitraging between day and night tariffs, we perform a Monte Carlo simulation with residential demand profiles, generated in the same way as described in Section 2.3.12.

Figure 2.10 shows the value due to a reduction in energy costs when charging a BESS during the night tariff and discharging while consuming during the day tariff, in function of the energy capacity of the BESS. Because the small difference between day and night tariff (5 c€/kWh), the value of the BESS in arbitraging between the day and night tariff is rather low.

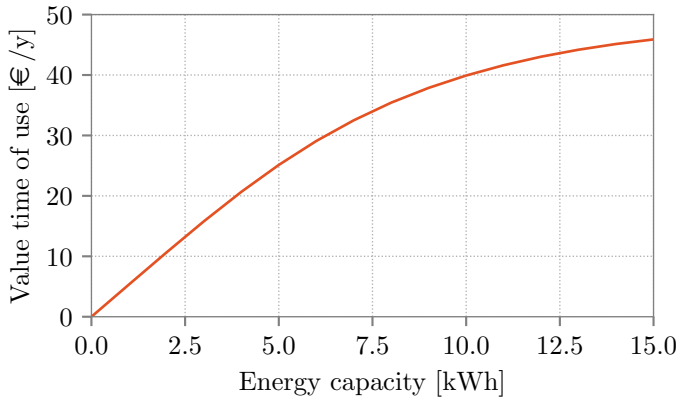

Figure 2.10: Value of a residential 1 C BESS charging during the night tariff and discharging when consuming during the day tariff.

2.3.15 Power Quality Improvements

Description

Power quality is an overarching concept to denote the quality of the voltage and current waveforms. A good power quality means a steady power supply, a steady frequency and root mean square (RMS) voltage and the absence of transients, harmonics, voltage dips or phase imbalances.

Sometimes, highly sensitive loads such as special production processes require a power quality which is higher than the power quality from the grid, and therefore need measures to increase power quality. At places with a weaker grid the power quality might be too low, and measures are needed to increase power quality.

As a BESS is connect to the grid via an inverter, it can to increase power quality [66, 67] by performing phase balancing [68], absorbing harmonics or performing voltage control, for instance.

Value Estimation

A BESS can be used for power quality improvements due to the presence of an inverter, rather than the ability to actually store energy, power quality

improvements can usually be added on top of other services. The value of providing power quality improvement however is very dependent on the specific case, and should be analysed on a case-by-case basis. Estimation the value of a BESS for power quality improvements is therefore considered out of scope of this chapter.

2.3.16 Uninterruptible Power Supply

Description

An uninterruptable power supply (UPS) is used to provide emergency power in case of failure from the main power supply. Depending on the amount of time needed to overcome a possible power failure, a UPS can consist, amongst others, out of a super capacitor, a BESS, a diesel generator, or a combination of these.

A BESS is used as a UPS to provide power during very short interruptions to interruptions of a couple of hours. For longer durations, diesels generators are normally used.

Value Estimation

A UPS is used for emergency situations only. Using a BESS to serve as a UPS is thus an application to mitigate risk rather than an application to create pure value by decreasing costs or obtaining revenues. It is thus not straightforward to put a general value on a BESS used as a UPS which can be compared to the value of the other applications described in this chapter. Therefore, we will also consider this out of scope of this chapter.

2.4 Quantitative Comparison of the Applications

The previous section describes the most important applications of battery energy storage systems, following the classification of Table 2.1. Where possible, the previous section also provides a quantitative estimation of the value of the application in the German market. These value estimations are combined in Figure 2.11, per MWh of usable energy capacity of a 1 C BESS and a maximum of 500 equivalent cycles per year.

In the figure, the red bars corresponding to the CIM and imbalance market applications, where the value depends highly on the accuracy of the price

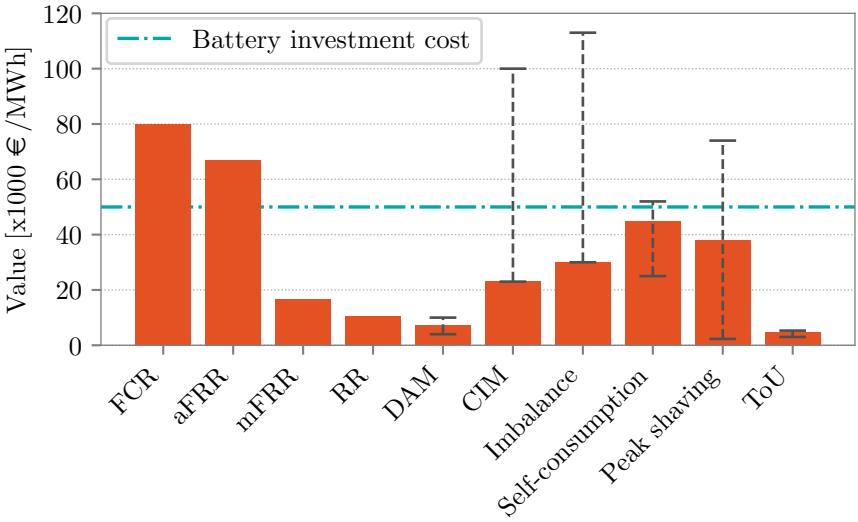

Figure 2.11: Estimation of the value per year of a 1 C BESS in Germany used for different applications, per MWh and with a maximum of 500 cycles per year, as derived in Section 2.3. The dash-dotted line gives the yearly cost of a BESS with a lifetime of 10 years at a price of 500 €/kWh as an indicative reference of profitability.

forecaster, show the lower bound on the value, derived using simple price forecasters, while the top of the error bars show the maximum achievable value if one had perfect hindsight knowledge. As stated in Section 2.3, this maximum value is not achievable in practice, but with good price forecasters, one should be able to outperform the lower bound. The red bar corresponding to the DAM application shows the value of a price forecaster with a NRMSE of 22 %, which is achievable by current day-ahead price forecasters [51], while the error bars give the maximum and minimum value from Figure 2.5.

For the residential self-consumption and ToU applications, for which the value depends highly on the size of the BESS, the red bars correspond to a BESS of 6 kWh, while the error bars denote the value range of BESSs between 5 kWh and 15 kWh. For the peak shaving application, the red bar is the average value for all 64 industrial sites analysed in Section 2.3.13, while the error bars give the minimum and maximum value of the 64 sites.

Finally, the red bars for the ancillary services applications (FCR, aFRR, mFRR and RR) correspond to the value as derived before.

The figure shows that, although there is a high theoretical value in the CIM and imbalance market, FCR is the application which has probably the highest achievable value in practice, despite falling prices in FCR markets. The total value of aFRR is also considerably high, due to the high amount of activation payments one is able to obtain when setting the right activation price. The value of mFRR and RR is much lower due to the higher energy capacity requirements and lower market prices of these applications. It is important to note that the cost of recharging is not incorporated in this value estimation, and this cost is expected to be higher for aFRR than for FCR due to the longer duration of activations in aFRR.

With regard to the behind-the-meter consumer applications, both self-consumption and peak shaving can create considerable value, but the value depends highly on the size of the BESS, the specific consumption profile, and the electricity tariff of the consumer.

Finally, as an indicative reference for the profitability of a BESS, the dashed line in the figure gives the yearly revenues needed to pay the investment back in a BESS over 10 years, at an investment cost of 500 €/kWh. It can be seen that both FCR and aFRR can be profitably applications, as well as peak shaving, and self-consumption, although the latter only barely and in a few cases. Intraday and imbalance market arbitrage can also be profitable if one is able to obtain more value than our proposed lower bound by developing better price forecasts and trading strategies.

Aggregation

Aggregating BESSs in a pool with other flexible assets that are not limited in energy content but might have other constraints such as a maximum number of activations or a limited ramp up speed, can help to achieve the energy capacity requirements of the ancillary services used for load-frequency control (FCR, aFRR, mFRR and RR) and therefore has the potential to increase the total power capacity that can be offered in the market.

However, these additional assets also need to be compensated for their capabilities, representing additional costs that need to be taken into account. These costs can be the actual cost of activating such assets, for instance when this represents additional consumption of fuel, or opportunity costs these assets can obtain when using their flexibility stand-alone for other ancillary services or electricity markets.

When aggregating a BESS with assets that have a slower reaction time, increasing the power capacity that can be offered in the load-frequency control

market is not straightforward. One has to make sure the offered capacity can always be activated, even if the other asset is used to recharge the BESS. For example when aggregating a BESS for use in the FCR market with a slower asset that can only ramp up to 20 % of its capacity in 30 seconds, one can only increase the total FCR capacity with 20 % of the capacity of the slower asset, otherwise the FCR capacity cannot always be delivered in time. Nevertheless, such slower assets can be used effectively to decrease the recharging costs or to reduce the amount of cycles and therefore the degradation of BESS.

Assets that are faster but limited in number of activations do not have this issue and can be used to help the BESS manage its SoC in case of rare but long activations that would for which the BESS would otherwise not have enough energy content.

Future Outlook

A further increase of intermittent renewable generation will not only lead to a reduction of the inertia of the grid, but it is generally expected that it will also lead to an increased volatility on the wholesale energy market prices [69, 70]. An increase in price volatility would result in increased profits for BESSs performing arbitrage on these markets, improving the business case for BESSs in short-term wholesale markets.

As stated before, an increase of renewable generation will also lead to a decrease of rotational inertia in the grid. To compensate for this, faster FCR (fast frequency response), or even synthetic inertia will need to be procured by the TSOs. As traditional power plants are unable to provided such fast response, the prices of these fast frequency response products will be set by fast flexible energy resources such as BESSs. It is hard to predict if these prices will be higher or lower compared to the current FCR price, as these prices should be high enough to pay back the investments in BESSs, but a low marginal costs of providing frequency reserves with BESSs can easily put a downward pressure on the prices from the moment when there is too much capacity in the market.

It is likely that, when local energy and flexibility markets will be implemented in practice, voltage control and congestion management will become important revenue streams for BESSs, especially if they are situated in the specific locations in the grid that face a high congestion.

Finally, other resources of flexibility can present considerable competition to BESSs in all of the applications mentioned above. Important examples of such resources are demand response flexibility and electric vehicles (EVs). Demand response from industrial loads is already today an important source of flexibility.

However, certain limitations, for instance on reaction time, availability or number of activations, make that stand-alone demand response can only be used for a limited number of applications and can actually be complementary with BESSs when aggregated together, as elaborated above.

With increasing sales of EVs, they will represent an important source of flexibility in the electric grid. Despite that their flexibility originates from batteries, they do have other constraints that stationary BESSs do not have. Electric vehicles need to be charged at a certain time when the owner of the EV wants to leave, and vehicle to grid applications, where the battery of the EV is discharged into the grid, reduces the lifetime of the battery cells and is therefore not always desired. Nevertheless, aggregating power from EVs that are charging will represent considerable amount of flexibility and can therefore be used for wholesale market arbitraging or to provide ancillary services (albeit asymmetrically in case vehicle to grid is not allowed).

2.5 Conclusion

In this chapter we have given an overview of the possible applications of battery energy storage systems in the European power grid and electricity markets. We have classified the applications into three main groups, according to whom the application creates value: ancillary services that create value for the grid operators, wholesale electricity market applications for the suppliers and consumer applications for the electricity consumers.

We have given a general description of each of the applications, and where possible tried to obtain a quantitative estimation of the value of the applications, per MWh of a 1 C BESS in the German market. The analysis shows that there is a lot of theoretical value in the short-term wholesale electricity market applications (arbitraging on the intraday and imbalance markets). However, the practically achievable value lies a lot lower as one does not have perfect hindsight of the actual prices.

Taking this into account, two ancillary services for load-frequency control: FCR and aFRR can provide the most value in practice, and are able to pay back the investment in a BESS at an investment cost of 500 €/kWh. Of these two ancillary services, FCR can still provide more value than aFRR, despite decreasing FCR market prices in the past years. On the consumer side, self-consumption and peak shaving are two applications which can also provide considerable value, depending on the actual size of the BESS and the specific consumption profile. Yet, these applications alone are unlikely to pay back for the investment into a BESS.

The analysis performed in this chapter looks at the use of a BESS for one application only. However, if a BESS is able to combine multiple applications, it might be possible to increase the total value created by the BESS, combining the value streams of the respective applications. Control of a BESS providing multiple applications is a lot more complex, as the different objectives, which are often conflicting, have to be delivered by one BESS.

The following chapter will perform an in-depth study on the delivery of FCR with a BESS, as we have seen this is the application which can provide the most value. We will then develop control strategies to combine FCR with self-consumption in Chapter 4, and with peak shaving in Chapter 5, the two services which create the most value behind the meter.

Chapter 3

Battery Storage Used for Frequency Reserves

Techno-Economic Analysis and Optimal Control of Battery Storage for Frequency Control Services, Applied to the German Market

Jonas Engels, Bert Claessens and Geert Deconinck

Published in Applied Energy, vol. 242, pp. 1036-1049, May 2019

The first author is the main author of the article. The contributions of the first author include the literature review, the development of the model and the optimisation framework, the execution and analysis of the case study, and the writing of the article.

Abstract:

Optimal investment in battery energy storage systems, taking into account degradation, sizing and control, is crucial for the deployment of battery storage, of which providing frequency control is one of the major applications. In this paper, we present a holistic, data-driven framework to determine the optimal investment, size and controller of a battery storage system providing

frequency control. We optimised the controller towards minimum degradation and electricity costs over its lifetime, while ensuring the delivery of frequency control services compliant with regulatory requirements. We adopted a detailed battery model, considering the dynamics and degradation when exposed to actual frequency data. Further, we used a stochastic optimisation objective while constraining the probability on unavailability to deliver the frequency control service. Through a thorough analysis, we were able to decrease the amount of data needed and thereby decrease the execution time while keeping the approximation error within limits. Using the proposed framework, we performed a techno-economic analysis of a battery providing 1 MW capacity in the German primary frequency control market. Results showed that a battery rated at 1.6 MW, 1.6 MWh has the highest net present value, yet this configuration is only profitable if costs are low enough or in case future frequency control prices do not decline too much. It transpires that calendar ageing drives battery degradation, whereas cycle ageing has less impact.

3.1 Introduction

Lithium-ion BESSs are being installed around the world at an increasing rate. An important application of BESSs is to provide frequency control or frequency regulation services. In multiple markets around the world, such as the market operated by PJM, in the United Kingdom (UK) or other energy markets in Europe, it is possible for third-party BESS operators to sell frequency control capacity to the TSO.

In future power systems, increased penetration of renewable generation and reduced inertia of large synchronous generators are expected to increase the need for fast frequency control reserves [71]. To mitigate this, battery energy storage systems are expected to play an important role as they are able to reduce volatility of the frequency of the grid, as has been shown in [72], due to their rapid response time which cannot be matched by conventional generation assets.

Optimal investment, sizing and control are crucial for the deployment of BESSs to provide the required frequency control services. However, performing a correct techno-economic analysis of a BESS is challenging, as there are a large number of non-linearities, parameters and uncertainties that need to be considered. Examples of these include the nonlinear dynamics and degradation of a battery cell, parameters of the control strategy (which is specific to each market) and uncertainties in the activation profile. In this paper, we present an optimisation

framework that considers these elements in detail, while still being able to compute in a reasonable amount of time. The framework determines the control strategy that minimises degradation while ensuring a delivery of the service compliant with the requirements of the TSO. Further, the framework allows to perform a techno-economic analysis, to calculate the investment case of a BESS over its lifetime and to determine its optimal size.

3.1.1 Frequency Containment Reserve

In general, frequency control is divided into three distinct services: primary, secondary and tertiary frequency control. In this paper, we will focus on the primary frequency control service, or FCR, as defined by ENTSO-E [24], as it requires the fastest reaction time and least amount of energy content, making it very appropriate for a BESS. However, the framework presented in this paper can also be applied to secondary and tertiary frequency control services.

When providing FCR with an asset, the asset has to regulate its power output proportional to the deviation of the grid frequency from the nominal frequency (50 Hz in Europe). The maximum contracted reserve capacity should be activated when this frequency deviation reaches a predefined maximum value (200 mHz in the Continental Europe (CE) synchronous region) and within a predefined time interval (30 s in the CE region).

When having sold FCR capacity to the TSO in European FCR markets, one is required to deliver the service continuously during the contracted period. This is a problem for energy-constrained assets such as a BESS, because when a BESS is completely charged or discharged, it can no longer provide a symmetric service and faces penalties that are usually high (and can lead to exclusion from the market). Therefore, an appropriate SoC controller or *recharge controller* has to be in place, which maintains the SoC of the BESS within limits, ensuring the contracted FCR capacity is always available to be activated.

Note that this penalty mechanism as such does not exist in pay-for-performance frequency regulation markets in the United States of America (USA), where one is paid according to a performance metric rather than penalised in case one does not deliver properly. Hence, the design requirements of the recharge controller in these pay-for-performance markets will also be different.

3.1.2 Related Works and Contributions

In the literature, quite a number of studies have been conducted on the use of a BESS for frequency control services, concentrating on different parts of the

problem and using models with various degrees of detail. However, to the best of our knowledge, there is currently no work consolidating all elements with sufficient detail into one model.

The main focus of the work in [73–79] is on the operational control strategy, including the recharge controller, of a BESS providing frequency control. This control strategy should be designed carefully, as it has an important impact on the required energy content and on the lifetime of the BESS, as shown in [73, 74, 80]. Specifically, in [80], it was shown that it is important for the short-term operational control strategy to consider the long-term degradation for maximal revenues over the lifetime of the BESS, a conclusion that was also made in [72].

Rule-based recharge controllers, of which the parameters can be tuned, were proposed in [73–75, 81, 82] to provide FCR services to the German market. More complex optimisation frameworks were proposed in [76], [77] and [78], albeit applied only to pay-for-performance frequency regulation markets. Dynamic programming was used in [76] and [77], but the results were operational control strategies that are computationally demanding and not feasible to calculate over the entire lifetime of the BESS, which is needed for investment analysis. In [78], a control strategy that considers a more complex degradation model was optimised using a subgradient method. It was shown that a simple, rule-based controller can achieve a constant worst-case optimality gap with regard to a perfect-hindsight solution in pay-for-performance regulation markets.

A BESS is combined with a power-to-heat system to provide FCR services to the German market using a rule-based control strategy in [81]. The combination of a BESS with a wind power plant to provide frequency control services was investigated in [83], where they conducted an economic optimisation to determine the optimal size of the BESS.

A techno-economic analysis of a BESS performing frequency control with Li-ion battery cells was performed in [84] for the German market, in [82] for the UK market and in [85] for the US market (Texas) but with a vanadium redox flow battery. Battery degradation was considered in both [82] and [84], but not in [85]. The operational control strategy was optimised in [82] via a grid search and in [85] using a nonlinear solver, but not in [84].

In [73–78, 81–84], a simple, linear charge-counting battery model with constant efficiencies, energy and power capacities was used. In [80], the efficiency losses were not considered. Only in [79] and [85] dynamic battery cell models were used, and it was argued that it is necessary to use accurate battery models when performing economic assessments. This was confirmed in [86], where they showed how the efficiency varies with the (dis)charging power when providing

frequency control.

In each of these previous works, the focus was on a specific part of the problem: some works focussed on the design of the controller, but did not (or only to a limited extent) consider the dynamics or the degradation of the BESS or the stochastic nature of the FCR signal. Other works focussed on the battery model or on the degradation of the BESS, but did not optimise the controller. In other works, a techno-economic analysis was performed, but without a dynamic battery model or an optimised controller. Hence, there is a clear need for a holistic approach, that allows conducting a complete techno-economic assessment of a BESS providing FCR using detailed models and an optimised FCR controller while considering the stochasticity in a correct way.

Therefore, in this work, we consolidated the results of previous works and appended to them the following contributions:

- We present an all-encompassing framework for the investment analysis, sizing and control design of a BESS providing frequency control, featuring a dynamic BESS model, a semi-empirical degradation model and an optimised FCR controller that complies with current regulatory requirements.
- We propose a stochastic, data-driven optimisation algorithm that uses detailed historical frequency data and that allows constraining the probability on unavailability to a small value with high confidence.
- We apply the framework to the German FCR market and analyse the results, which provides new insights into the economics and sizing of a BESS in this market.

The remainder of the paper is organised as follows: Section 3.2 elaborates the used models and the FCR controller. Section 3.3 presents the proposed optimisation algorithm. In Section 3.4, we discuss the application of the optimisation framework to the German FCR market and present the analysis of the results. Finally, the paper is concluded in Section 3.5.

3.2 BESS Model and FCR Controller

In this section, we elaborate the different parts of the BESS model and the FCR controller that we use in the optimisation. Figure 3.1 gives an overview of all models used and their interaction. All parts in this figure will be discussed in this section one by one, except for the optimiser, which is discussed in Section 3.3.

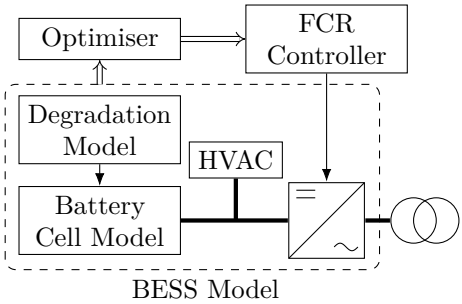

Figure 3.1: Overview of the different models used in this study and their interaction.

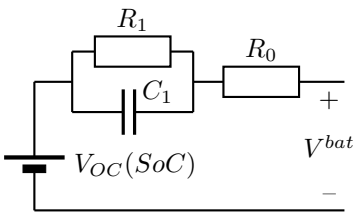

Figure 3.2: First-order RC model of a battery cell.

3.2.1 Battery Cell Model

Various types of battery cell models exist, each with its own level of detail and computational complexity. The most detailed cell models are the electrochemical models, such as the dualfoil model [87], which try to capture in detail the various electrochemical processes that occur in the cells. These are typically the most accurate cell models, but require a large number of parameters and are computationally very demanding. Alternative analytical models, such as the kinetic battery model (KiBaM), are discussed in [88].

Lumped battery cell models or equivalent circuit battery cell models are often used because they require only a limited number of parameters, which provides a lower risk of overfitting compared to more complex models, while still attaining a good accuracy. Among the equivalent circuit models, resistance-capacitance (RC) models of various orders are popular because of their simplicity and familiarity to the electrical engineering community. In [89], Hu et al. made a comparison of 12 distinct equivalent circuit models for Li-ion battery cells. They showed that, of the 12 equivalent circuit models, the first-order RC model, shown in Figure 3.2, had the best performance, both on training and on unseen

validation datasets. More specifically, as shown in [79], when providing frequency control, a purely resistive-based battery cell model already produces good results, with the main differences between the model and the measurements due to the absence of a capacitive element in the model.

As a compromise between accuracy and model complexity, we have used a first-order RC model in our BESS model, minimising the chances of overfitting. This RC model allows to capture the dynamics of the battery cells accurately, such as the variation in charging and discharging efficiencies with the current [90], which is neglected in simpler bi-linear battery models.

The parameters to be determined in this model are the ohmic resistances R_0 and R_1, the capacitance C_1 and the open circuit voltage $V_{OC}(SoC)$ as a function of the state of charge. In this study, we modelled the Sanyo UR18650E battery cell [91], a commercially available lithium-ion Nickel-Manganese-Cobalt (NMC) cell with a graphite anode, which is one of the most common Li-ion cell chemistries in commercial grid storage battery systems. We used the results of Schmalstieg et al. [92, 93], who created a detailed degradation model of this specific battery cell and provided enough information to determine the required parameters of the first-order RC model.

Figure 3.3a shows the open-circuit voltage curve $V_{OC}(SoC)$ of the cell. We determined the remaining parameters from the battery cell voltage response to a pulse power test, shown in 3.3b, using a least squares fit. The voltage response of the fitted RC model is also shown in 3.3b. Table 3.1 summarises the values of the fitted parameters of the RC model, together with some other key parameters of the battery cell. The cut-off voltage when charging $V_{cutoff,charge}$ and discharging $V_{cutoff,discharge}$, which are the cell terminal voltages at which (dis)charging is stopped, was obtained from the Sanyo UR18650E datasheet [91]. The heat capacity C_p of the cell, needed for the heating, ventilation and air conditioning (HVAC) model, was retrieved from [94].

Parameter	Value	Parameter	Value
Nominal capacity C	2.05 Ah	$V_{cutoff,charge}$	4.2 V
Nominal resistance R_0	0.0334 Ω	$V_{cutoff,discharge}$	2.75 V
Nominal resistance R_1	0.0114 Ω	Nominal voltage V_{nom}	3.6 V
Nominal capacitance C_1	1867.0 F	Heat capacity C_p	40.05 J/K
Coulombic efficiency $\eta_{coulomb}$	99 %	Rated energy capacity E_{rated}	7.38 Wh

Table 3.1: Parameters of the first-order RC model, fitted on the pulse power test profile as shown in Figure 3.3b

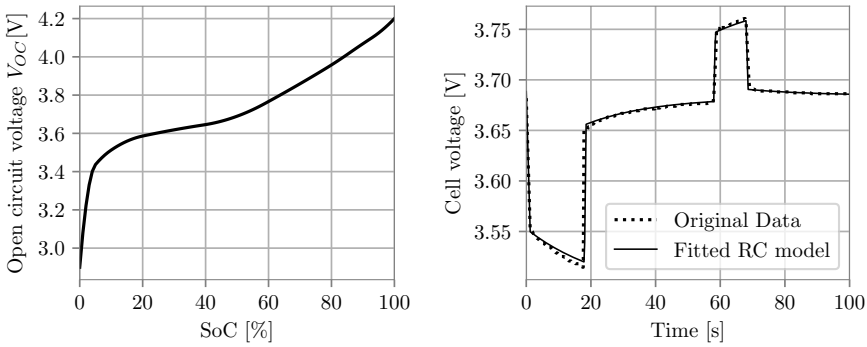

(a) Open-circuit voltage curve V_{OC}

(b) Pulse power test and fitted RC model response

Figure 3.3: (a) Open-circuit voltage curve in the function of the SoC of the considered Li-ion NMC battery cell and (b) pulse power test and least-squares fit of the first-order RC model response, both from [92].

3.2.2 Degradation Model

Accurately quantifying the ageing or degradation of battery cells is important because degradation represents a capital loss of the battery investment costs. Unfortunately, degradation of battery cells is complex and not always well understood. Degradation originates from the interaction of various processes, complicating the identification of the root causes. Vetter et al. [95] gave a detailed qualitative overview of the various degradation processes in Li-ion batteries. Formation of the solid electrolyte interphase (SEI) on the anode is considered one of the most important sources of degradation. The SEI is a protective layer between the electrolyte and the anode, formed by decomposition of the electrolyte and accompanied by the irreversible consumption of lithium ions and a rise in impedance.

Generally, battery degradation can be attributed to two factors: calendar ageing due to storage over time and cycle ageing due to repetitively charging and discharging of the battery cells. Barré et al. [96] identified five different types of battery ageing models, ranging from detailed electrochemical models, such as extensions of the dualfoil model [97] and [98], to general statistical models.

Empirical degradation models are often used due to their lower computational complexity. These models result from experiments in which ageing of the cells is observed when these are exposed to various stress factors. For instance, a cell is stored at a certain SoC level or cycled with a certain depth of discharge

(DoD) and the degradation is checked periodically. A mathematical function, such as a polynomial or an exponential, is then used to describe the relationship between the applied stress factors and the observed degradation.

In their work [92], [93], Schmalstieg et al. described the ageing of the Sanyo UR18650E battery cell in detail. They described both capacity degradation and resistance growth when the cells were stored at various SoC levels and temperatures (calendar ageing), and when the cells were cycled around different SoC levels at various depths of discharge (cycle ageing). This results in an empirical model that correlates the SoC level and temperature during storage to the calendar capacity degradation and resistance growth with a $t^{0.75}$ time dependency, and the DoD and average SoC during cycling with the throughput Q (in ampere hour) as follows:

$$C = 1 - \alpha_{cap}(SoC_{av}^{cal}, T)t^{0.75} - \beta_{cap}(SoC_{av}^{cyc}, DoD)\sqrt{Q}, \tag{3.1a}$$

$$R = 1 + \alpha_{res}(SoC_{av}^{cal}, T)t^{0.75} + \beta_{res}(SoC_{av}^{cyc}, DoD)Q. \tag{3.1b}$$

Here, $\alpha_{cap}(SoC_{av}^{cal}, T)$ and $\alpha_{res}(SoC_{av}^{cal}, T)$ are the calendar ageing factors of capacity degradation and resistance growth, respectively, which are a function of the average state of charge during storage SoC_{av}^{cal} and the temperature T at which the cell is stored. The cycle ageing factors $\beta_{cap}(SoC_{av}^{cyc}, DoD)$ and $\beta_{res}(SoC_{av}^{cyc}, DoD)$ on the other hand, are a function of the average state of charge SoC_{av}^{cyc} during the cycle and the depth of discharge (in percent) DoD. The capacity degradation due to cycling has a square root dependency on the throughput Q, whereas the resistance growth shows a linear dependency on Q.

When performing frequency control the battery is cycled according to a stochastic profile rather than cycled repetitively with a constant depth of discharge. This makes the extraction of clearly defined cycles from the SoC profile not straightforward. Therefore, we employed a *rainflow* counting algorithm [99], originating from material fatigue stress analysis to determine the cycles when materials are subject to an arbitrary load profile, but is also often used for cycle life assessment of batteries (e.g. in [78], [100] and [101]). The rainflow counting algorithm takes as input the state of charge profile over time $\boldsymbol{SoC} \in \mathbb{R}^{n_t}$, with n_t being the number of time steps. We adapted the original algorithm slightly to return, besides the DoD of a cycle, also the average state of charge of a cycle and the cumulative throughput Q_{i_c} after each cycle $i_c = 1, \ldots, n_{cyc}$. The algorithm that implements the $Rainflow(\boldsymbol{SoC})$ function is detailed in Appendix A:

$$\boldsymbol{SoC}_{av}^{cyc}, \boldsymbol{DoD}, \boldsymbol{Q} = Rainflow(\boldsymbol{SoC}), \tag{3.2}$$

where $\boldsymbol{SoC}_{av}^{cyc}, \boldsymbol{DoD}, \boldsymbol{Q} \in \mathbb{R}^{n_{cyc}}$, with n_{cyc} being the number of cycles detected by the rainflow counting algorithm. We can calculate the capacity degradation

after each cycle i_c by integrating (3.1a) over the throughput Q as follows:

$$C_{i_c}^{cyc} = C_{i_c-1}^{cyc} - \int_{Q_{i_c-1}}^{Q_{i_c}} \frac{\partial \beta_{cap}(SoC_{av,i_c}^{cyc}, DoD_{i_c})\sqrt{Q}}{\partial Q} dQ$$
$$= C_{i_c-1}^{cyc} - \beta_{cap}(SoC_{av,i_c}^{cyc}, DoD_{i_c}) \cdot (\sqrt{Q_{i_c}} - \sqrt{Q_{i_c-1}}). \quad (3.3)$$

An analogue reasoning is followed for the resistance growth due to cycling. To model calendar ageing, we determine the SoC_{av}^{cal} in α_{cap} and α_{res} from (3.1) to be the average SoC of the entire profile $\boldsymbol{SoC}$.

In the remainder of the paper, we simulate the model for various operational years $k = 1, \ldots, n_k$ and use the index k to denote the remaining capacity of the cell at the start of year k by C^k and the resistances by R_0^k and R_1^k.

3.2.3 From a Battery Cell Model to a BESS Model

With the dynamic and degradation model of the battery cell determined, this section elaborates on how we used the cell model to simulate the behaviour of an entire BESS containing n_{cells} cells. We did not model a battery management system (BMS), as we assumed that the BMS succeeds in balancing the cells in the battery pack perfectly and consumes a negligible amount of power. We also assumed that variations in cell characteristics are averaged out, allowing to simulate only one cell in detail, namely, the average cell, thereby drastically decreasing the simulation time. It is then straightforward to extrapolate the simulated power and SoC of the average cell proportionally to the required number of cells in the BESS.

Two other elements of the battery pack that cannot be neglected are the direct current (DC)/alternate current (AC) inverter and the HVAC system.

Inverter Model

Typically, the time constant of an inverter and its control system is an order smaller than the time constant needed for FCR. Therefore, we assumed that the inverter does not influence the dynamics of the BESS and can deliver any power required within one simulation time step, as long as this is possible within the capacity limits of the battery cell and the inverter.

The efficiency of an inverter is typically high, except at low power levels. Nevertheless, this can have considerable impact when performing frequency control, as the required power is often low and rarely reaches its maximum.

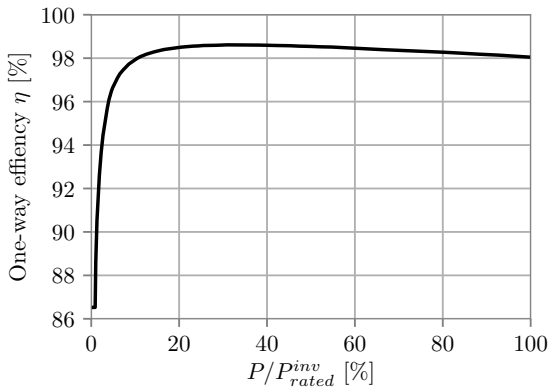

Figure 3.4: One-way efficiency of the inverter in function of its operating power relative to the rated power of the inverter P^{inv}_{rated}, based on the SMA STP60-10 model [102].

We modelled the efficiency of the inverter using the efficiency curve shown in Figure 3.4, taken from a commercial three-phase inverter (the SMA STP60-10 [102]) which can be configured to deliver up to 2.5 MW of power. We assumed the same efficiency curve for both consuming from and injecting into the grid. As the inverter is the gateway between the battery cells and the grid, the rated power of the inverter also determines the maximum power of the BESS: $P^{inv}_{rated} = P^{BESS}_{max}$.

HVAC Model

To determine the power consumption of the HVAC system, we employed a first-order thermal model of the battery cell, following [103]. From the first-order RC model of Figure 3.3, the Joule losses in the resistances R^k_0 and R^k_1 are dissipated as heat, thereby increasing the temperature of the cell T. This temperature is controlled by the HVAC system towards the reference temperature $T_{ref} = 25\,°\mathrm{C}$. The thermal model of a system with n_{cells} battery cells is governed by the following equation:

$$T_{t+1} = T_t + \frac{(R^k_0 + R^k_1){I_t}^2 n_{cells} - COP \cdot P^{HVAC}_t}{C_p n_{cells}} \Delta t, \tag{3.4}$$

with C_p being the heat capacity of the cell; I_t, the current in one cell at time step t; COP, the coefficient of performance, which we assumed to be $COP = 2.5$;

and P_t^{HVAC}, the instantaneous power of the HVAC system. The Joule losses are equal to $(R_0^k + R_1^k){I_t}^2 n_{cells}$ and $COP \cdot P_t^{HVAC}$ is the amount of heat removed by the HVAC system. To prevent an unrealistically high HVAC power, we limited the power P_t^{HVAC} to 2 % of the maximum power of the battery pack P_{max}^{BESS}.

BESS Model

Putting together the cell model, the HVAC model and the inverter model, one obtains the following discretised model, which describes the dynamics of a BESS consisting of n_{cells} battery cells required to deliver a certain power to

$$P_t^{bat} = \eta_{inv}(P_t^{grid}) \max(P_t^{grid}, 0) + \frac{1}{\eta_{inv}(P_t^{grid})} \min(P_t^{grid}, 0) - P_t^{HVAC}, \tag{3.4a}$$

$$I_t = \frac{1}{2R_0^k}\Bigg(- V_{OC}(SoC_t) - V_t^{C_1} + \sqrt{\left(V_{OC}(SoC_t) + V_t^{C_1}\right)^2 + 4R_0^k P_t^{bat}/n_{cells}}\Bigg) \tag{3.4b}$$

$$V_{t+1}^{C_1} = V_t^{C_1} e^{\Delta t/(R_1^k C_1)} + (1 - e^{\Delta t/(R_1^k C_1)}) R_1^k I_t, \tag{3.4c}$$

$$SoC_{t+1} = SoC_t + \eta_{coulomb} \max(I_t, 0)\frac{\Delta t}{C^k} + \frac{1}{\eta_{coulomb}} \min(I_t, 0)\frac{\Delta t}{C^k}. \tag{3.4d}$$

The first equation calculates the required battery cell power P_t^{bat} from the requested grid power P_t^{grid} and the HVAC power P_t^{HVAC}, which results from (3.4), while considering the inverter efficiency $\eta_{inv}(P_t^{grid})$, which is dependent on P_t^{grid} according to Figure 3.4. Here, $P_t^{grid} > 0$ when consuming from the grid and $P_t^{grid} < 0$ when injecting into the grid and $P_t^{bat} > 0$ when charging and $P_t^{bat} < 0$ when discharging the battery cells.

Equation (3.4b) translates the battery power divided by the number of cells P_t^{bat}/n_{cells} into the battery cell current I_t, considering the voltage drop over the resistance R_0^k and capacitor $V_t^{C_1}$. Equation (3.4c) represents the discretised dynamics of the parallel RC circuit C_1, R_1^k, whereas Equation (3.4d) represents the dynamics of the SoC of the battery, with C^k being the remaining capacity of the battery, $\eta_{coulomb}$ the coulombic efficiency and Δt the duration of one time step. The BESS stops charging and discharging when the terminal voltage

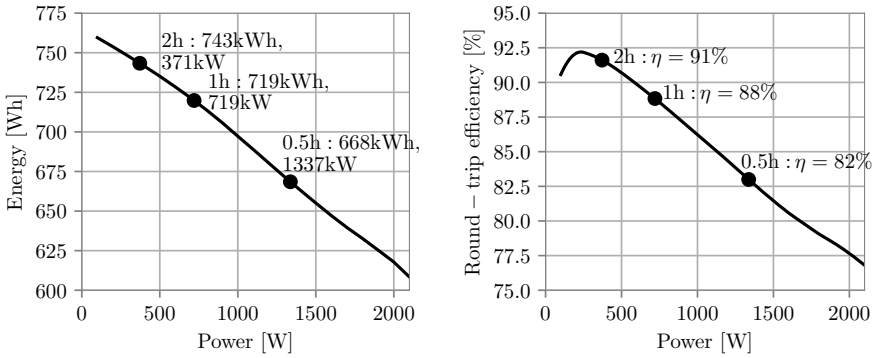

(a) Available energy content when charging and discharging at constant power.

(b) Round-trip efficiency η when charging and discharging at constant power

Figure 3.5: (a) Available energy and (b) round-trip efficiency η when charging and discharging at constant power until the cut-off voltage is reached, using the BESS model with 100 battery cells, inverter rated at 2100 W and a 42 W HVAC system.

$V_t^{bat} = V_{OC}(SoC_t) + V_t^{C_1} + R_0^k I_t$ reaches $V_{cutoff,discharge}$ and $V_{cutoff,charge}$, respectively.

Energy and Power Capacity of a BESS

The capacity of a battery cell is usually expressed in ampere hour (Ah), whereas the energy capacity of a commercial BESS is usually expressed in kilowatt hour (kWh). Although the energy content of the cell is rated at 7.35 Wh, the actual energy that can be charged or discharged is dependent on the (dis)charging current. A higher current will induce greater losses in the resistive elements and thus provide less usable energy. Moreover, the voltage drop over the resistive elements will mean that the cutoff voltage $V_{cutoff,discharge}$ will be reached earlier and discharging will stop before the SoC reaches 0 %. An analogue reasoning holds when charging the battery cell.

This effect is quantified in Figure 3.5a, which shows the available energy capacity of the simulated BESS system containing $n_{cells} = 100$ battery cells, an inverter rated at $P_{rated}^{inv} = 2100$ W and a 42 W HVAC system when charging at constant power until the terminal voltage V^{bat} reaches $V_{cutoff,charge}$ and subsequently discharging at constant power until V^{bat} reaches $V_{cutoff,discharge}$. As can be seen in the figure, the available energy capacity of the BESS decreases with an increase in power, due to an increase in losses, and reaches the cut-off

voltages earlier. Figure 3.5b shows the round-trip efficiency of the same BESS in the function of the (dis)charging power, in line with the experimental results from [86]. Because of an increase in resistive losses in the battery cells, the round-trip efficiency of the BESS decreases with an increase in power. However, at low power, the efficiency of the BESS decreases as well. This decrease is due to the low efficiency of the inverter at low power rates (as shown in Figure 3.4) rather than to efficiency losses in the battery cells themselves. At higher power rates, the efficiency of the inverter has less impact as it is rather high and nearly constant.

Finally, in battery cells, the rate-capacity effect [104] (also described by Peukert's law [105]) also limits the available capacity of the cell when discharged at higher currents. We did not explicitly model the rate-capacity effect, as it has been shown that it does not hold when operating the cell at variable currents [106], which is the case when performing frequency control services.

3.2.4 FCR Controller

When providing frequency containment reserves, one has to adjust its power for FCR proportionally to the relative deviation of the frequency of the grid from the nominal frequency: $P_t^{FCR} = r\Delta f_t = r(f_t - f_{nom})/\Delta f_{max}$, so that the contracted FCR capacity r is reached at a maximum predefined frequency deviation Δf_{max}.

As explained in Section 3.1.1, a recharge controller $\pi(SoC)$ that controls the SoC is necessary when participating in FCR markets with energy-constrained assets. In the literature, different versions of such recharge controllers have been proposed, ranging from simple rule-based controllers in [73], [74], [75], [82], [107] and [108], to moving average filters in [109], [110] and linear state-feedback controllers optimised using robust optimisation in [111].

In this study, we adopted a simple, discretised P-controller $f(\cdot)$ with a deadband db_p and a proportional gain K_p that controls the SoC back to a setpoint SoC_0, shown in Figure 3.6. The output of the proportional error is discretised in steps of 100 kW, kept constant for a time period $t_{recharge}$ and determined upfront with a lead time t_{lead} to be compliant with the requirements of the German FCR market (see Section 3.4.1): $P_t^{rc} = f(SoC_{t_{set}})$, with $t_{set} = \lfloor t/t_{recharge} \rfloor t_{recharge} - t_{lead}$. As the recharge power cannot be used as FCR capacity at the same time, the maximum recharge power P_{max}^{rc} is limited to the maximum power of the battery minus the FCR capacity: $|P_t^{rc}| \leq P_{max}^{rc} \leq P_{max}^{BESS} - r$.

Besides specifically reserving recharge power, we also implemented overdelivery

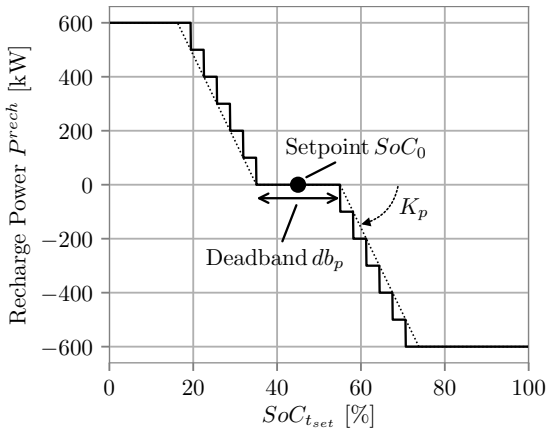

Figure 3.6: Example of a possible recharge controller function $P_t^{rc} = f(SoC_{t_{set}})$ of a 1.6 MW/1.6 MWh BESS delivering $r = 1$ MW of FCR capacity, with $K_p = 2, SoC_0 = 0.45$ and $db_p = 0.2$. The dotted line represents a linear P-controller, whereas the black line is the version discretised to multiples of 100 kW, as implemented in this study.

as a way to recharge the battery. When overdelivering, the BESS delivers more power than required (in absolute value). In our controller, we perform overdelivery only when this is beneficial to get the SoC back to the setpoint:

$$P_t^{od} = \begin{cases} o_d r \Delta f_t & \text{if } sign(SoC_t - SoC_0) = -sign(\Delta f_t), \\ 0 & \text{otherwise,} \end{cases} \tag{3.5}$$

with o_d being the percentage of overdelivery. The total power at the grid P_t^{grid} is then the sum of the power for FCR $P_t^{FCR} = r\Delta f_t$, the recharging power P_t^{rc} and the power for overdelivery P_t^{od}, for every time step t :

$$P_t^{grid} = r\Delta f_t + P_t^{rc} + P_t^{od}, \tag{3.6}$$

which is limited by the maximum power $|P_t^{grid}| \leq P_{max}^{BESS}$ of the BESS. This controller can be seen as an extension of the rule-based controllers proposed in [73], [74], [75], [82], [107] and [108], and as a special case of the ones in [109], [110] and [111].

Figure 3.7 shows an example of the grid power P_t^{grid} of a battery delivering $r = 1$ MW of FCR capacity, according to (3.6). The figure also shows the

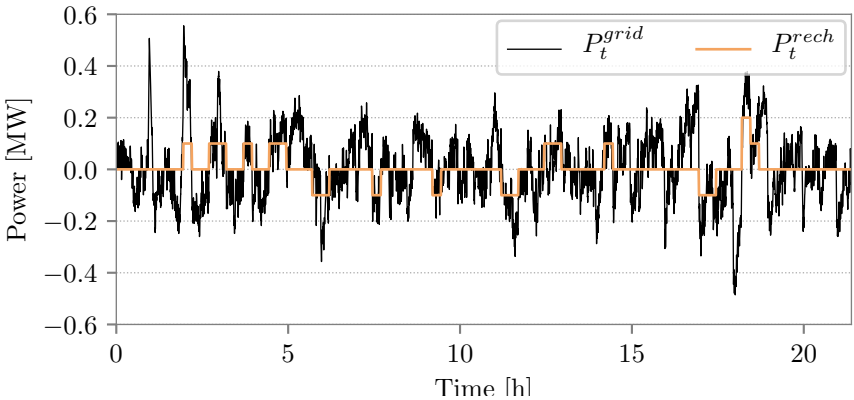

Figure 3.7: Example of the grid power P_t^{grid} and recharge power P_t^{rc} of a 1.6 MW/1.6 MWh BESS delivering $r = 1$ MW of FCR capacity, with the recharge controller from Figure 3.6.

corresponding recharge power P_t^{rc} according to the recharge controller from Figure 3.6.

3.3 Optimisation Framework

The FCR controller of the BESS discussed in the previous section has four parameters (i.e., the deadband db_p, the setpoint SoC_0, the proportional gain K_p and the amount of overdelivery o_d), which can be chosen independently. These parameters determine how the battery will be used, how fast it degrades and how much the electricity costs will be. For instance, increasing the deadband db_p reduces the throughput but increases the width of the SoC distribution and, thus, the DoD of the cycles, whereas increasing the overdelivery parameter o_d increases the throughput but reduces the probability on penalties due to unavailability of the BESS.

To determine the value of these parameters, we defined the following optimisation problem, which maximises the revenues from providing r FCR capacity taking into the electricity costs C_{elec}^k and the degradation ΔC^k, while constraining the

probability on penalties p^k:

$$\min_{\boldsymbol{x} \in \mathcal{X}} \quad -\mathrm{E}[c^k_{FCR}]r + \mathrm{E}[C^k_{elec}(\boldsymbol{x}, \boldsymbol{\Delta f})] + \frac{\mathrm{E}[\Delta C^k(\boldsymbol{x}, \boldsymbol{\Delta f})]}{100\,\% - 80\,\%} c_{cell}, \quad (3.7a)$$

$$\text{s.t.} \quad \Pr\{p^k(\boldsymbol{x}, \boldsymbol{\Delta f}) > 0\} \leq \epsilon^{req}, \quad (3.7b)$$

with $\boldsymbol{x} = (K_p, SoC_0, o_d, db_p) \in \mathcal{X}$ being the decision variables constrained to the admissible set $\mathcal{X} \subset \mathbb{R}^4$ and $\boldsymbol{\Delta f} = (\Delta f^0, \Delta f^1, \ldots, \Delta f^{n_{t,y}})$ being the stochastic frequency deviation of length $n_{t,y} = 365 \times 24 \times 3600/\Delta t$, covering one year. As the frequency of the grid and, thus ,the required battery power are unknown upfront, a probabilistic approach is required. The optimisation is to be executed each year $k = 1, \ldots, n_k$ the BESS is operational in FCR, allowing the adjustment of the controller parameters as the battery degrades, for instance, decreasing the deadband db_p when less energy capacity is remaining.

The objective function is a compromise between three factors: the revenues from delivering FCR with a capacity r at an expected price $\mathrm{E}[c^k_{FCR}]$, the electricity costs C^k_{elec} and the degradation of the battery ΔC^k. Whereas the first two are easily expressed in monetary value, we assign a value to the last one, which is equal to the cost of replacing the battery cells c_{cell} times the incremental degradation $\Delta C^k = C^k - C^{k+1}$ from (3.1a), divided by $(100\,\% - 80\,\%)$, as the battery's end of life is assumed to be reached when $C = 80\,\%$. We employ the expected value operator $\mathrm{E}[\cdot]$ over the electricity costs and the degradation as both are dependent on the actual frequency deviation profile $\boldsymbol{\Delta f}$, which is stochastic by nature. The optimisation is constrained by a chance constraint (3.7b), forcing the probability of incurring penalties $p^k(\boldsymbol{x}, \boldsymbol{\Delta f})$ to be less than or equal to ϵ^{req}. The functions are indexed with k to denote their dependence on the remaining battery capacity C^k and resistances R^k_0, R^k_1 at the start of year k.

It is interesting to note that the optimisation problem (3.7) is part of the family of dynamic programming problems [112]. Indeed, (3.7) is actually a policy search over the policies parametrised by $\boldsymbol{x}$, with the last term of (3.7a) being a heuristic approximation of the value function $V(C^{k+1})$ of the next state C^{k+1}.

In the next subsections, we will elaborate first on how we approximate the expected value operators in the objective function, then on how we deal with the chance constraint on the penalty and, finally, on the global optimisation algorithm we employ to solve (3.7).

3.3.1 Expected Value Approximation

The objective function (3.7a) consists of the sum of three expected value operators. The first one, the expected FCR price $\mathrm{E}[c^k_{FCR}]$ during year k, is independent of the decision variables $\boldsymbol{x}$ and can thus be evaluated before the start of the optimisation routine.

The second and third expected value operators, however, do depend on the decision variables $\boldsymbol{x}$ and will thus have to be approximated when evaluated during optimisation. A general approach is to use a sample average approximation (SAA) [113] of the expected value by taking the empirical mean over independent and identically distributed (iid) samples of the stochastic variable, i.e. the frequency deviation profile $\boldsymbol{\Delta f}$. Let $\boldsymbol{\Delta f}_y \in \mathcal{Y} \subset \mathbb{R}^{n_{t,y}}$ be a frequency deviation profile sample with the length of one year, with $|\mathcal{Y}| = n_{\mathcal{Y}}$, then:

$$\mathrm{E}[C^k_{elec}(\boldsymbol{x}, \boldsymbol{\Delta f})] \approx \frac{1}{n_{\mathcal{Y}}} \sum_{\boldsymbol{\Delta f}_y \in \mathcal{Y}} C^k_{elec}(\boldsymbol{x}, \boldsymbol{\Delta f}_y), \tag{3.8a}$$

$$\mathrm{E}[\Delta C^k(\boldsymbol{x}, \boldsymbol{\Delta f})] \approx \frac{1}{n_{\mathcal{Y}}} \sum_{\boldsymbol{\Delta f}_y \in \mathcal{Y}} \left(\Delta C^{cal,k}(\boldsymbol{x}, \boldsymbol{\Delta f}_y) + \Delta C^{cyc,k}(\boldsymbol{x}, \boldsymbol{\Delta f}_y)\right). \tag{3.8b}$$

Following (3.1a), the incremental degradation of the battery ΔC^k in (3.8b) has been written down directly as the sum of calendar degradation $\Delta C^{cal,k}$ and cycle degradation $\Delta C^{cyc,k}$.

SAA Using Frequency Samples of One Day

Problem (3.7) optimises one year of operation of the BESS and thus needs various frequency samples of one year $\boldsymbol{\Delta f}_y \in \mathbb{R}^{n_{t,y}}$ for an accurate SAA (3.8). As simulating multiple samples of one year of frequency data generally takes too long to employ during each step of an optimisation algorithm, we used $n_{\mathcal{D}}$ iid frequency samples of one day $\boldsymbol{\Delta f}_d \in \mathcal{D} \subset \mathbb{R}^{n_{t,d}}, n_{t,d} = n_{t,y}/365$ instead of one year in (3.8) during the optimisation. The electricity costs of one year in (3.8a) can then be retrieved by linear extrapolation of the electricity costs of one day: $C^k_{elec}(\boldsymbol{x}, \boldsymbol{\Delta f}_y) \approx 365 C^k_{elec}(\boldsymbol{x}, \boldsymbol{\Delta f}_d)$.

However, simple linear extrapolation does not work in (3.8b) as the degradation ΔC^k is a nonlinear function of $\boldsymbol{\Delta f}$. Therefore, we approximated ΔC^k as follows. Concatenate all samples of one day $\boldsymbol{\Delta f}^i_d \in \mathcal{D}$ into $\boldsymbol{\Delta f}_{\mathcal{D}} = (\boldsymbol{\Delta f}^1_d, \boldsymbol{\Delta f}^2_d, \ldots, \boldsymbol{\Delta f}^{n_{\mathcal{D}}}_d) \in \mathbb{R}^{n_{\mathcal{D}} n_{t,d}}$ and simulate the BESS model (3.5) to receive the corresponding $\boldsymbol{SoC}_{\mathcal{D}} \in \mathbb{R}^{n_{\mathcal{D}} n_{t,d}}$. Using the rainflow counting algorithm (3.2), one receives the corresponding $SoC^{cyc}_{av,i_c}, DoD_{i_c}, Q_{i_c} = Rainflow(\boldsymbol{SoC}_{\mathcal{D}})$

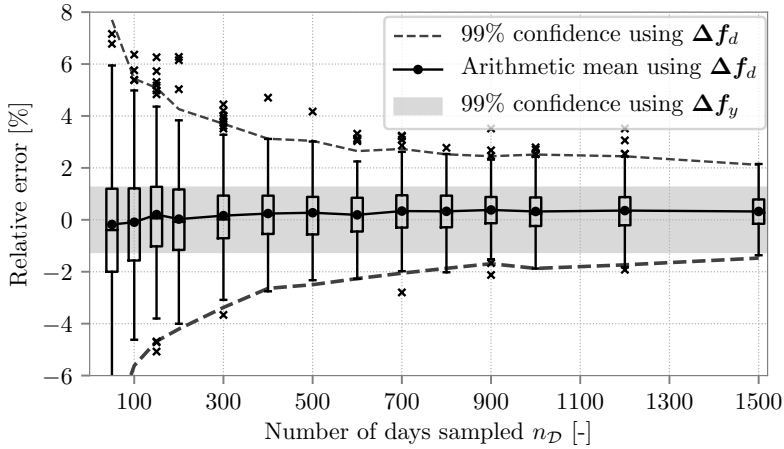

Figure 3.8: Boxplot of the relative error when approximating the SAA of (3.7a) with frequency samples of one day $\boldsymbol{\Delta f}_d$ and using (3.9), compared to the SAA using frequency samples of one year $\boldsymbol{\Delta f}_y$. The 99 % confidence intervals of the error using samples of one day $\boldsymbol{\Delta f}_d$ and of the SAA using samples of one year $\boldsymbol{\Delta f}_d$ are shown.

of each cycle $i_c = 1, \ldots, n_{cyc}$. As this accounts for only $n_{\mathcal{D}}$ days out of the 365 in a complete year, we obtained an approximation of the degradation due to cycling by scaling the throughput with $365/n_{\mathcal{D}}$. To approximate the calendar ageing, we used the empirical mean over $\boldsymbol{SoC}_{\mathcal{D}}$ as SoC_{av}^{cal} in (3.1a):

$$\begin{aligned}
\mathrm{E}[\Delta C^{cyc,k}(\boldsymbol{x}, \boldsymbol{\Delta f})] &\approx \Delta C_{\mathcal{D}}^{cyc,k}(\boldsymbol{x}, \boldsymbol{\Delta f}_{\mathcal{D}}) \\
&= -\sum_{i_c=1}^{n_{cyc}} \beta_{cap}(SoC_{av,i_c}^{cyc}, DoD_{i_c}) \cdot \left(\sqrt{\frac{365}{n_{\mathcal{D}}} Q_{i_c}} - \sqrt{\frac{365}{n_{\mathcal{D}}} Q_{i_c-1}} \right), \qquad (3.9a) \\
\mathrm{E}[\Delta C^{cal,k}(\boldsymbol{x}, \boldsymbol{\Delta f})] &\approx \Delta C_{\mathcal{D}}^{cal,k}(\boldsymbol{x}, \boldsymbol{\Delta f}_{\mathcal{D}}) \\
&= -\alpha_{cap}(\overline{\boldsymbol{SoC}_{\mathcal{D}}}, T) \left((365(k+1))^{0.75} - (365k)^{0.75} \right). \qquad (3.9b)
\end{aligned}$$

To illustrate the quality of this approximation, Figure 3.8 shows a boxplot of the relative error of the SAA in (3.7a) using samples of one day $\boldsymbol{\Delta f}_d$ as explained in the paragraph above, compared to the SAA in (3.7a) using samples of one year $\boldsymbol{\Delta f}_y$, for various numbers of samples of one day $n_{\mathcal{D}}$. One can see that the SAA using $\boldsymbol{\Delta f}_d$ converges towards the expected value of the SAA using

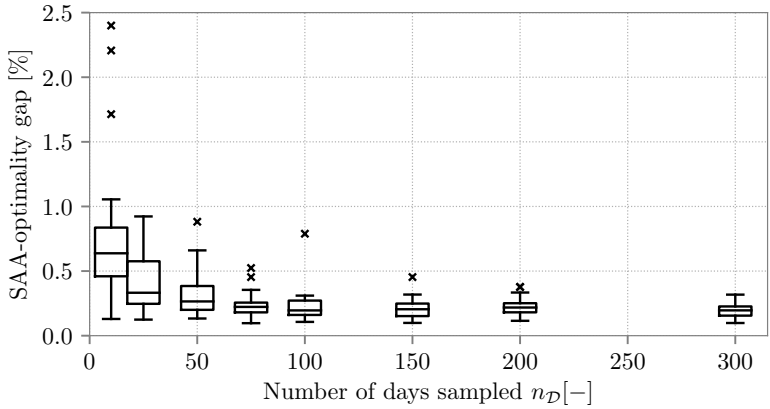

Figure 3.9: Boxplot of the 99 %-confidence optimality gap due to the SAA approximation of (3.7) for various sample sizes $n_{\mathcal{D}}$ used in the optimisation. For each sample size, the problem was solved 25 times with different sample sets $\mathcal{D}$.

$\boldsymbol{\Delta f}_y$, for $n_{\mathcal{D}} \to \infty$. The expected value of the SAA using $\boldsymbol{\Delta f}_d$ has a negligible bias of around 0.3 %. The figure also shows the 99 % Monte Carlo confidence intervals of the expected value when using samples of one day and when using four samples of one year of frequency data, which equals $4 \times 365 = 1460$ samples of one day.

Evaluation of SAA Solution Quality

To estimate the amount of samples $n_{\mathcal{D}}$ needed, we evaluated the SAA quality of a candidate solution $\hat{\boldsymbol{x}}$ obtained by the optimisation algorithm presented further, for various sample sizes $n_{\mathcal{D}}$. To evaluate the SAA quality of $\hat{\boldsymbol{x}}$, we used the approach of Mak et al. [114]. Let $g(\boldsymbol{x}, \boldsymbol{\Delta f}_y)$ be the value of objective function (3.7a) evaluated at $\boldsymbol{x}$ with frequency sample $\boldsymbol{\Delta f}_y$ and define

$$G^i_{n_{\mathcal{Y}}} = \frac{1}{n_{\mathcal{Y}}} \sum_{\boldsymbol{\Delta f}_y \in \mathcal{Y}^i} g(\hat{\boldsymbol{x}}, \boldsymbol{\Delta f}_y) - \min_{\boldsymbol{x} \in \mathcal{X}} \frac{1}{n_{\mathcal{Y}}} \sum_{\boldsymbol{\Delta f}_y \in \mathcal{Y}^i} g(\boldsymbol{x}, \boldsymbol{\Delta f}_y), \tag{3.10}$$

with $\mathcal{Y}^i, |\mathcal{Y}^i| = n_{\mathcal{Y}}$ being a set of iid frequency samples of one year, then $\mathrm{E}[G_{n_{\mathcal{Y}}}] \geq gap_{SAA}(\hat{\boldsymbol{x}})$ is the optimality gap due to the SAA method at $\hat{\boldsymbol{x}}$. Therefore, by sampling n_g batches $\mathcal{Y}^0, \ldots, \mathcal{Y}^{n_g}$ and calculating $G^i_{n_{\mathcal{Y}}}, i = 1, \ldots, n_g$, we can obtain a $100(1-\beta)\%$ confidence bound on the SAA optimality gap from $1/n_g \sum_i^{n_g} G^i_{n_{\mathcal{Y}}} + s(G_{n_{\mathcal{Y}}}) t_{\beta, n_g - 1}/\sqrt{n_g}$, with $t_{\beta, n_g - 1}$ being the β-

percentile of the Student's t-distribution with $n_g - 1$ degrees of freedom and $s(G_{n_\mathcal{Y}})$ being the sample standard deviation of $G^i_{n_\mathcal{Y}}$.

Figure 3.9 shows this 99 %-confidence SAA optimality gap for various sample sizes $n_\mathcal{D}$ used in the optimisation routine. The resulting solutions $\hat{\boldsymbol{x}}$ were evaluated using (3.10) with $n_\mathcal{Y} = 3$, i.e. sampling three years out of the four years of available data with replacement, and $n_g = 20$. For each sample size $n_\mathcal{D}$, the optimisation was performed 25 times to obtain a view on the statistics of the SAA optimisation gap. As can be seen in the figure, the SAA optimality gap decreased quickly to be $< 1\,\%$ and followed a $1/n_\mathcal{D}$ trend, which is as expected when using an SAA.

Note that the actual optimality gap at $\hat{\boldsymbol{x}}$ consists of two parts: the optimality gap due to the SAA $gap_{SAA}(\hat{\boldsymbol{x}})$ discussed here and an optimality gap due to the heuristic optimisation algorithm elaborated in Section 3.3.3, whose global optimality cannot be proven.

3.3.2 Chance Constraint Approximation

The optimisation problem (3.7) is constrained by a chance constraint (3.7b), which limits the probability of penalties due to bad delivery of the frequency control service to be below a threshold ϵ^{req}. Generally, chance constraints are dealt with by one of the following two methods: The first method is to use an analytical reformulation of (3.7b), which is not possible in our case owing to the unavailability of a closed mathematical form of the BESS model. Moreover, a realistic stochastic model of $\boldsymbol{\Delta f}$ using analytical distributions is difficult to set up as it concerns a very high-dimensional multivariate stochastic variable.

A second method is to use Monte Carlo sampling to approximate the value of the probability of (3.7b). Scenario methods [115] provide explicit bounds on the number of samples one needs to constrain. However, these are only valid for convex optimisation problems. Statistical learning theory [116, 117] is applicable to non-convex control design; however, it requires a very large number of samples [118] and the method uses the Vapnik–Chervonenkis (VC) dimension [119], which is very difficult to compute for general functions and can be infinite.

As neither method is practically applicable to our model, the most we can do is to perform an a posteriori evaluation of a candidate solution $\hat{\boldsymbol{x}}$ in (3.7b) using the classical Monte Carlo approach as follows. Consider n_c iid frequency samples $\boldsymbol{\Delta f}^i$, and let $m = \sum_i^{n_c} \mathbb{1}\{p^k(\hat{\boldsymbol{x}}, \boldsymbol{\Delta f}^i) > 0\}$ be the total number of constraint violations, i.e. the number of times a frequency sample induces a penalty. A $100(1-\beta)\%$ confidence upper bound to the probability of (3.7b) is

then given by [120]:

$$\Pr\{p^k(\hat{\boldsymbol{x}}, \boldsymbol{\Delta f}) > 0\} \leq \sup_{\rho \in [0,1]} \{\rho : \mathfrak{b}(m; \rho, n_c) \geq \beta\} \leq \epsilon^{req}, \tag{3.11}$$

with $\mathfrak{b}(m; \rho, n_c)$ being the cumulative binomial probability function with parameters n_c and ρ, evaluated at m. As $\mathfrak{b}(m; \rho, n_c)$ is continuous and monotonically decreasing in $\rho \in (0, 1)$, the supremum $\sup_{\rho \in [0,1]}$ can easily be calculated by, e.g. a line search along ρ.

Expression (3.11) also defines the maximum number of samples with a penalty m_{max} one can allow to ensure that (3.7b) is true with a confidence of $100(1-\beta)\%$. For instance, if one requires $\epsilon^{req} \leq \rho \leq 0.005, \beta = 0.001$, and one uses $n_c = 10000$ samples, then $m \leq m_{max} = 29$.

3.3.3 Optimisation Algorithm

Even with the approximations explained above, the optimisation problem (3.7) is non-convex and a closed mathematical form of (3.7) is not readily available, resulting in an intractable problem. However, given a parameter vector $\boldsymbol{x}$ and a frequency sample $\boldsymbol{\Delta f}^i$, one can simulate the BESS model (3.5) with the FCR controller (3.6) and calculate the corresponding degradation using (3.1) and penalties p^k quite efficiently. This allowed us to employ a global optimisation algorithm that only requires function evaluations to find an approximate solution, without, however, providing any optimality guarantees.

To solve (3.7), we propose the use of the differential evolution algorithm [121], which belongs to the family of genetic algorithms. This has the advantage of being gradient free, which is required as the objective and constraints are non-differentiable. Although other gradient-free global optimisation algorithms can also be applied, we found that the differential evolution converges relatively fast and consistent towards a good suboptimal solution.

As constraints cannot be enforced directly in these types of global optimisation algorithms, we incorporated the constraint (3.7b) into the objective with an if-condition, returning a term proportional to the maximum penalty of a frequency dataset used for penalty checking $\mathcal{P} \subset \mathbb{R}^{n_{t,d}}, |\mathcal{P}| = n_{\mathcal{P}}$, if there is indeed a penalty detected in this frequency set. The optimisation objective can then be

written down as

$$g^k(\boldsymbol{x}, \mathcal{D}, \mathcal{P}) = \begin{cases} -\operatorname{E}[c^k_{FCR}]r \\ \qquad + \dfrac{365}{n_{\mathcal{D}}} \displaystyle\sum_{\boldsymbol{\Delta f}_d \in \mathcal{D}} C^k_{elec}(\boldsymbol{x}, \boldsymbol{\Delta f}_d) & \text{if } \max\limits_{\boldsymbol{\Delta f} \in \mathcal{P}} p^k(\boldsymbol{x}, \boldsymbol{\Delta f}) \leq 0 \\ \qquad + \dfrac{(3.9a) + (3.9b)}{100\,\% - 80\,\%} c_{cell} \\ c_p \max\limits_{\boldsymbol{\Delta f} \in \mathcal{P}} p^k(\boldsymbol{x}, \boldsymbol{\Delta f}) & \text{otherwise,} \end{cases} \tag{3.12}$$

with c_p being a weighting factor.

The optimisation objective thus depends on two sets of frequency samples: $\mathcal{D}, \mathcal{P} \subset \mathbb{R}^{n_{t,d}}$; the former consists of iid samples for the SAA of (3.7a), whereas the latter is a set of samples used to check the violation of the penalty constraint. From Figure 3.9, we can observe that selecting $n_{\mathcal{D}} = 50$ results in an SAA optimality gap of $< 1\%$. The set $\mathcal{P}$ can be thought of as a *worst-case* frequency dataset containing extreme samples that the BESS should be able to provide without incurring penalties. This set will be generated during the optimisation algorithm, which is shown in Algorithm 1.

Steps 8 to 15 in Algorithm 1 show the procedure used to create set $\mathcal{P}$: for a given point $\boldsymbol{x}_i$, draw n_c iid samples and calculate the upper bound on constraint violation using (3.11). If this upper bound is higher than the required ϵ^{req}, one cannot ensure that (3.7b) is satisfied with confidence β for the current most optimal point $\boldsymbol{x}_i$. We know from (3.11) that there can be maximum m_{max} samples with a penalty $p^k > 0$ given n_c. Thus, in steps 11 and 12, we add the $\Delta f_d^{(j^*)}$ sample that gives the j^*th-largest penalty, with $j^* = n_c - m_{max}$, to $\mathcal{P}$ as this is the sample with the largest penalty of all samples that are actually not allowed to have a penalty at all. If the upper bound (3.11) is smaller than or equal to ϵ^{req}, the optimisation continues with the same $\mathcal{P}$ as before and one is guaranteed that (3.7b) is satisfied with confidence $100(1-\beta)\%$ at $\boldsymbol{x}_i$.

As evaluating the penalty p^k on n_c samples is computationally expensive owing to the large number of samples required for small ϵ^{req}, we only check this after n_{check} iterations. If no penalties are found, n_{check} is updated according to an exponential update rule in step 15.

In step 7, the differential evolution performs one optimisation step, in which it updates each member of its population and returns the population member with the lowest objective value $g^k(x, \mathcal{D}, \mathcal{P})$. In this study, we used a population size of 60 members, chose the best member to be mutated and used a binomial crossover scheme. The differential evolution stops if the standard deviation of

Algorithm 1 Optimisation algorithm

1: $C^0 \leftarrow C^{init}, R_0^0 \leftarrow R_0^{init}, R_1^0 \leftarrow R_1^{init}, k \leftarrow 0.$
2: $\mathcal{D} \leftarrow \{\boldsymbol{\Delta f}_d^1, \ldots, \boldsymbol{\Delta f}_d^{n_\mathcal{D}}\}$ iid frequency samples.
3: **while** $C^k \geq 0.8C^{init}$ **and** $\epsilon^{k-1} \leq \epsilon^{req}$, **do**
4: $\quad i \leftarrow 0, \boldsymbol{x}_i \leftarrow \boldsymbol{x}^{init}, \mathcal{P} \leftarrow \emptyset, n_{check} \leftarrow n_{check}^{init}.$
5: $\quad$ **while** $not(StoppingCriterion)$, **do**
6: $\quad\quad i \leftarrow i + 1.$
7: $\quad\quad \boldsymbol{x}_i \leftarrow DifferentialEvolutionStep$ with $g^k(\boldsymbol{x}, \mathcal{D}, \mathcal{P})$, according to [121].
8: $\quad\quad$ **if** $i = n_{check}$ **then**
9: $\quad\quad\quad m \leftarrow \sum_j^{n_c} \mathbb{1}\{p^k(\boldsymbol{x}_i, \boldsymbol{\Delta f}_d^j) > 0\}$, with $\boldsymbol{\Delta f}_d^1, \ldots, \boldsymbol{\Delta f}_d^{n_c} \in \mathbb{R}^{n_{t,d}}$ drawn iid.
10: $\quad\quad\quad$ **if** $\sup_{\rho \in [0,1]}\{\rho : \mathfrak{b}(m; \rho, n_c) \geq \beta\} > \epsilon^{req}$ **then**
11: $\quad\quad\quad\quad$ Sort $\boldsymbol{\Delta f}_d^j$, so that $p^k(x_i, \boldsymbol{\Delta f}_d^{(1)}) \leq p^k(\boldsymbol{x}_i, \boldsymbol{\Delta f}_d^{(2)}) \leq \ldots \leq p^k(x_i, \boldsymbol{\Delta f}_d^{(n_c)})$.
12: $\quad\quad\quad\quad \mathcal{P} \leftarrow \mathcal{P} \cup \boldsymbol{\Delta f}_d^{(j^*)}$, with $j^* = n_c - m_{max}$.
13: $\quad\quad\quad\quad n_{check} \leftarrow n_{check}^{init}.$
14: $\quad\quad\quad$ **else**
15: $\quad\quad\quad\quad n_{check} \leftarrow n_{check} + n_{check}/2.$
16: $\quad \epsilon^k \leftarrow \sup_{\rho \in [0,1]}\{\rho : \mathfrak{b}(m'; \rho, n_c') \geq \beta\}$, with $n_c' > n_c$.
17: $\quad$ Get $\boldsymbol{SoC}_y$ by simulating the BESS model (3.5),(3.6) with $\boldsymbol{x}_i, \forall \boldsymbol{\Delta f}_y \in \mathcal{Y}$.
18: $\quad C^{k+1} \leftarrow \overline{C^{k+1}}, R_0^{k+1} \leftarrow \overline{R_0^{k+1}}, R_1^{k+1} \leftarrow \overline{R_1^{k+1}}$, using (3.1)–(3.3) with $\boldsymbol{SoC}_y, \forall y = 1 \ldots n_\mathcal{Y}$.
19: $\quad k \leftarrow k + 1.$
20: $k_{max} \leftarrow k - 1.$

the objective values of the population is smaller than $5 \cdot 10^{-4}$ times the mean of the objective values of the population.

When converged to an optimal value $\hat{\boldsymbol{x}}$, we check the actual probability on a penalty in step 16 on a broader set $n_c' > n_c$ of iid samples and calculate the empirical mean of the capacity degradation $\overline{C^{k+1}}$ and resistance growth $\overline{R_0^{k+1}}, \overline{R_1^{k+1}}$ over all available years in the dataset $\mathcal{Y}$, which serves as the capacity and resistance for year $k+1$. The algorithm stops when the battery capacity reaches 80 % of its initial capacity or when it is unable to provide the service, with the probability on a penalty being smaller than required (i.e. $\epsilon^k > \epsilon^{req}$).

3.3.4 Total Revenues and Costs

Algorithm 1, gives a solution to optimisation problem (3.7) for each year k the BESS is able to deliver FCR services. To then calculate the total expected revenues and costs of the BESS over its lifetime, we use the resulting optimised control variables $\hat{\boldsymbol{x}}^k$ and expected capacity degradation $\overline{C^{k+1}}$ of the optimisation routine defined by Algorithm 1. The expected electricity costs of year k can then be estimated by taking the empirical mean over all frequency samples of one year $\hat{c}^k_{elec} = \overline{C^k_{elec}(\hat{\boldsymbol{x}}^k, \boldsymbol{\Delta f}_y)}$. The FCR revenues of year k are simply the product of r and $\mathrm{E}[c^k_{FCR}]$, except for the last year $k_{max} - 1$. To evaluate the proportion of year $k_{max} - 1$ the battery is still able to provide the service, we perform a linear interpolation. The total discounted net revenues of the BESS can then be calculated as

$$rev = \sum_{k=1}^{k_{max}} \frac{\mathrm{E}[c^k_{FCR}]r - \hat{c}^k_{elec}}{(1+\gamma)^k} \cdot \max\left(\min\left(\frac{0.8 - C^{k-1}}{C^k - C^{k-1}}, \frac{\epsilon^{req} - \epsilon^{k-1}}{\epsilon^k - \epsilon^{k-1}}, 1\right), 0\right), \tag{3.13}$$

with k_{max} as determined by step 20 of the optimisation algorithm and γ being an appropriate discount rate. As long as the battery is not degraded in year k ($C^k > 0.8$), and is able to provide the FCR services with a probability on a penalty smaller than required ($\epsilon^k > \epsilon^{req}$), the second term in the equation will equal to one and the FCR revenues of the entire year are taken into account. If this is not the case, the minimum in the second term is taken between the linear interpolation of the degradation and the linear interpolation of the ϵ^{req} metric in case both occur during the same year k.

3.4 Case Study: BESSs in German FCR

In this section, we discuss the application of the proposed optimisation algorithm to the German FCR market, which is currently the largest FCR market in Europe and has a considerable amount of BESS capacity participating. In Germany, FCR is auctioned through the common platform *Regelleistung* [26] shared by the four German TSOs (TenneT, Amprion, 50Hertz and TransnetBW). Starting from 2012, TSOs of neighbouring countries have been coupling their primary frequency control markets to the Regelleistung platform, which currently manages the joint tendering of FCR volume for the German, Swiss, Austrian, Belgian, French and Dutch TSOs.

On Regelleistung, each week, a week-ahead auction[1] is organised, where the bids are placed in merit order and the market clears on the price of the bid, where

[1] As from 1 July 2019, the Regelleistung FCR market changed to a daily auctioning.

the cumulative sum of the bid volumes equals the tendering volume, subject to certain cross-border constraints. The market is a pay-as-bid market,[2] which means that each selected participant is awarded its bid price rather than the marginal clearing price. However, the bidcurves are generally relatively flat, meaning that participants are fairly good in forecasting the marginal price.

In the case study, we applied all relevant regulations as they are currently imposed. We used real, measured frequency data from the CE region together with the detailed BESS model elaborated in Section 3.2 to obtain results that are practically relevant in real applications.

3.4.1 Data and Regulatory Requirements

Regulation in Germany on battery storage in frequency control reserve is one of the most detailed of the entire ENTSO-E region. Specific requirements for batteries are given in [28, 29] and will be discussed shortly in the following paragraph.

BESS in German FCR

When providing FCR in Germany, one is restricted to the degrees of freedom described in [28]. The maximum frequency deviation at which all FCR power should be active is $\Delta f_{max} = 200\,\text{mHz}$ and should be reached after 30 s. There is a 10 mHz deadband in which no delivery is required.

Overdelivery is allowed, but only up to 20 %, limiting the parameter $o_d \in [0.0, 0.2]$. Recharging the battery is allowed by reserving BESS power capacity that cannot be sold as FCR power. One also has to compensate the recharging power with other assets or by buying/selling the power on the intraday markets. The latter option presents the additional constraints that the recharging power should be constant for 15 minutes, corresponding to the intraday trading blocks, and be decided upon with a lead time of at least 5 min, as the German intraday market closes 5 minutes before delivery. Moreover, as the granularity on the intraday market is 100 kW, the recharge power has to be constrained to multiples of 100 kW [54].

[2] At the time of writing this paper, the FCR market on Regelleistung was still a pay-as-bid market. However, this has changed as from 1 July 2019, where the market has changed to a marginal pricing or pay-as-cleared

When providing FCR with any energy-constrained asset in Germany, one has to comply with the *30-minutes criterion* [29].[3] This criterion states that, except in emergency states, the battery should always reserve enough energy to be able to provide 30 minutes of FCR power in both the positive and the negative direction. An emergency state is reached if $|\Delta f| > 200\,\text{mHz}$, $|\Delta f| > 100\,\text{mHz}$ for longer than 5 minutes or $|\Delta f| > 50\,\text{mHz}$ for longer than 15 minutes. This also implies that, in case $10\,\text{mHz} < |\Delta f| \leq 50\,\text{mHz}$, the battery should be able to deliver for an infinite amount of time. This is only possible if the recharge power is able to compensate for the required delivery, resulting in the additional requirement that $P^{rc}_{max} \geq 0.25r$, the power sold as FCR capacity, or $r \leq 0.80P^{BESS}_{max}$.

When prequalifying the battery to participate in the Germany FCR market, one has to perform a *Doppelhöckertest* [29], which is used to determine the available energy capacity of the battery at the FCR power r one wants to prequalify. The test starts at full SoC and consists of two times a discharge period of 15 minutes at the FCR power r followed by a rest period of 15 minutes. After this, the BESS has to discharge further at FCR power r until the battery is empty. The total discharged energy is used to monitor the 30-minutes criterion defined above.

Electricity Costs

BESSs in Germany are exempt from many grid costs and other levies that typically apply to the regular consumer. An overview of all elements making up cost of the electricity is given in Table 3.2. The battery is exempted from network charges and electricity tax, and pays the EEG (Renewable Energy Resources Act) and KWK (combined heat and power) levies only on the losses incurred in the BESS. We assumed that the battery buys and sells its recharge power on the intraday market, whereas the remaining energy is settled on the imbalance price. All other costs and levies only have to be paid on the energy consumed from the grid. We assumed electricity costs rise with inflation.

FCR Price

Figure 3.10 shows the yearly averaged historical FCR prices published on the Regelleistung platform [26]. The figure shows both the yearly averaged marginal

[3] At the time of writing the paper, the 30-minutes criterion was still in place. On 15 May 2019 however, the Germany regulator changed this to a 15-minutes criterion, in line with European legislations. The principle stays the same, but delivery in emergency states is only required for 15 minutes instead of 30 minutes as before. This means less energy capacity is required from the BESS to deliver a same amount of FCR capacity.

Cost Element	Amount	Applicable	Regulation and Law
Recharge power	Intraday market	Applicable	[28]
FCR power	Imbalance market	Applicable	–
Network charges	–	Exempted	EnWG §118 Abs. 6 [122]
Electricity tax	2.05 c€/kWh	Exempted	StromStG §5 Abs. 4 [123]
EEG levy	6.88 c€/kWh	Exempted except for losses	EEG §61k [124]
KWK levy	0.4438 c€/kWh	Exempted except for losses	KWKG §27b [125]
StromNEV §19-Levy	0.370 c€/kWh	Applicable	StromNEV §19 [62]
Concession Fee	0.11-2.39 c€/kWh	Applicable	KAV §1-2 [126]
Offshore liability levy	0.037 c€/kWh	Applicable	EnWG §17(f) [122]
Interruptible load levy	0.011 c€/kWh	Applicable	AblaV §1 [127]

Table 3.2: Elements making up the cost of electricity for a grid-connected stand-alone battery in Germany.

price and the weighted average accepted bid price (WAP). As the FCR volume auctioned on the Regelleistung platform is much larger than that of a single regular-sized BESS, we assume the BESS operates as a price-taker in the FCR market. We assume a bidding strategy that is able to capture the WAP rather than the marginal price. In the literature, the FCR price of the German market is forecasted to decrease in the coming years, mainly due to an increase of BESSs in the market that can provide the service at lower costs [84]. Various predictions can be found, varying from a value of 1630 €/MW/week [30] to below 1000 €/MW/week [84, 128] in 2035. We adopted two exponentially decreasing scenarios, a moderate and a low scenario, both shown in Figure 3.10, which correspond to the forecasts from [30, 84, 128].

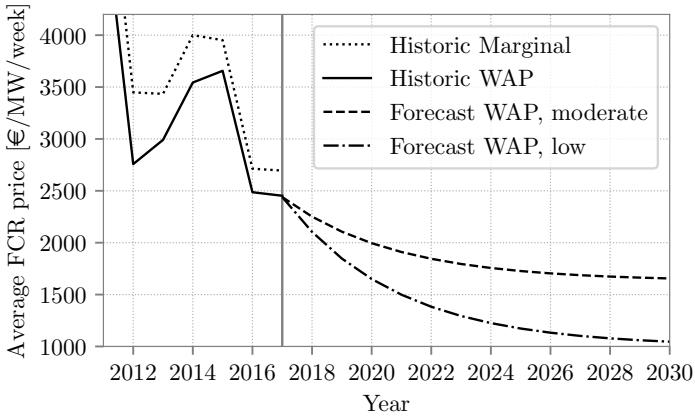

Figure 3.10: Historical marginal and weighted average price (WAP) in the German FCR market averaged per year [26]. As from 2017, a moderate and a low WAP forecast scenario are shown (nominal value).

3.4.2 Optimisation Setup

In optimizing and evaluating the model, we used four years (2014-2017) of frequency, intraday and imbalance market data ($n_{\mathcal{Y}} = 4$). We split these data into samples of one day, starting from each quarter hour in the dataset, which resulted in 140 256 samples of one day. We discretised the model with a time step $\Delta t = 10\,\text{s}$. The parameters of the battery cell are as given in Table 3.1. To determine the number of cells of a BESS with a certain rated energy capacity E_{rated}^{BESS}, we used the rated energy capacity of one cell E_{rated}, given in Table 3.1, which is equal to the nominal capacity C times the nominal voltage V_{nom}. Although the actual energy capacity varies with the rated power of the BESS, as explained in Section 3.2.3, this approach accounts for an easy one-to-one relation of energy capacity to the number of cells, rather than relying on more complex relationships. For example, a BESS rated at $E_{rated}^{BESS} = 1\,\text{MWh}$ would then contain $1\,000\,000\,\text{Wh}/7.38\,\text{Wh} = 135\,501$ cells.

This also means that, when executing the *Doppelhöckertest* [29], which is used to determine the energy boundaries for the 30-minutes criterion, the actual energy discharged will differ from the rated energy capacity E_{rated}^{BESS}. Therefore, in our model, we simulated the Doppelhöckertest to determine the maximum and minimum state of charge boundaries $SoC_{30min}^{max,k}$ and $SoC_{30min}^{min,k}$, and used

these to determine the penalty metric p^k:

$$p^k = \frac{1}{n_t} \sum_{t}^{n_t} \left(\mathbb{1}\{SoC_t > SoC_{30min}^{max,k}\} + \mathbb{1}\{SoC_t < SoC_{30min}^{min,k}\} \right) S_t^{emerg}, \quad (3.14)$$

where S_t^{emerg} is 0 if t is in an emergency state and 1 otherwise, and n_t denotes the number of time steps in the sample. The dependency of $SoC_{30min}^{max,k}$ and $SoC_{30min}^{min,k}$ on the year k is due to the degradation in capacity C^k and growth of resistances R_0^k, R_1^k, which also changes the actual energy capacity one can discharge during the Doppelhöckertest. Furthermore, we require $\epsilon^{req} = 0.005$ and $\beta = 0.001$, giving a very small probability on penalties. To achieve this, we set $n_c = 10000$ and $n_c' = 50000$. Finally, we have chosen $n_{\mathcal{D}} = 50$, which gives a good compromise between SAA error and number of samples (see Figure 3.9).

With this configuration, Algorithm 1 needs, on average, 202 iterations per year k, which takes around 24 minutes when run on a 2.83 GHz Intel Core 2 Quad Processor (Q9550) with 10 GB of RAM. To speed up the execution time, one can run the algorithm in parallel for different battery configurations.

3.4.3 Results and Discussion

The goal is to determine the optimal BESS power and energy capacity to provide $r = 1$ MW of FCR capacity, the minimum bid size on Regelleistung, during its lifetime. For another bid size that is a multiple of 1 MW, the results can be scaled proportionally.

To determine the optimal BESS sizing, we ran the optimisation algorithm repeatedly for a BESS with a rated energy capacity varying between 1.0 MWh and 2.5 MWh, and with a varying C-rate. The C-rate is defined as the rated power divided by the rated energy capacity: C-rate $= P_{max}^{BESS}/E_{rated}^{BESS}$. The results are shown in Figure 3.11 for C-rates of 0.6 C, 0.7 C, 1.0 C and 1.5 C.

Figure 3.11a shows the total revenues minus the electricity costs in the FCR market according to (3.13), with $\gamma = 1.7\,\%$ to adjust for inflation [129], over the operational lifetime of the BESS, using the FCR prices of the moderate scenario of Figure 3.10, whereas Figure 3.11b shows the total inflation-adjusted net revenues using the low scenario. The figure also shows a couple of lines indicating the potential cost of a BESS, so that the net present value (NPV), which equals the discounted net revenues (3.13) minus the investment costs: $NPV = rev - cost_{BESS}$, can be read on the y-axis by taking the difference between the revenue and the cost lines. Table 3.3 shows the NPV with the moderate FCR price scenario for the various BESS energy capacities, C-rates and battery costs $cost_{BESS}$. As can be seen in the table and in Figure 3.11, a

C-rate	Rated Energy Capacity E_{rated}^{BESS} [MWh]															
	1.0	1.1	1.2	1.3	1.4	1.5	1.6	1.7	1.8	1.9	2.0	2.1	2.2	2.3	2.4	2.5
500 €/kWh																
0.6 C	-500	-550	-600	-650	-700	-750	-800	-850	-900	-950	-1000	39	8	-26	-61	-98
0.7 C	-500	-550	-600	-650	-700	-750	-800	-850	119	91	65	36	-1	-30	-63	-102
1.0 C	-500	-550	-600	-636	-361	-117	161	144	113	92	60	30	0	-36	-75	-113
1.5 C	-500	-550	-600	-636	-354	-61	158	131	108	84	52	22	-12	-49	-82	-118
400 €/kWh																
0.6 C	-400	-440	-480	-520	-560	-600	-640	-680	-720	-760	-800	249	228	204	179	152
0.7 C	-400	-440	-480	-520	-560	-600	-640	-680	299	281	265	246	219	200	177	148
1.0 C	-400	-440	-480	-506	-221	33	321	314	293	282	260	240	220	194	165	137
1.5 C	-400	-440	-480	-506	-214	89	318	301	288	274	252	232	208	181	158	132
300 €/kWh																
0.6 C	-300	-330	-360	-390	-420	-450	-480	-510	-540	-570	-600	459	448	434	419	402
0.7 C	-300	-330	-360	-390	-420	-450	-480	-510	479	471	465	456	439	430	417	398
1.0 C	-300	-330	-360	-376	-81	183	481	484	473	472	460	450	440	424	405	387
1.5 C	-300	-330	-360	-376	-74	239	478	471	468	464	452	442	428	411	398	382

Table 3.3: Net present value in $\times 1000$ € at a discount rate $\gamma = 1.7\,\%$ equal to the expected inflation [129] over the lifetime of a BESS providing FCR services to the German market, using the moderate FCR price scenario of Figure 3.10, for a BESS cost $cost_{BESS}$ of 500 €/kWh, 400 €/kWh and 300 €/kWh.

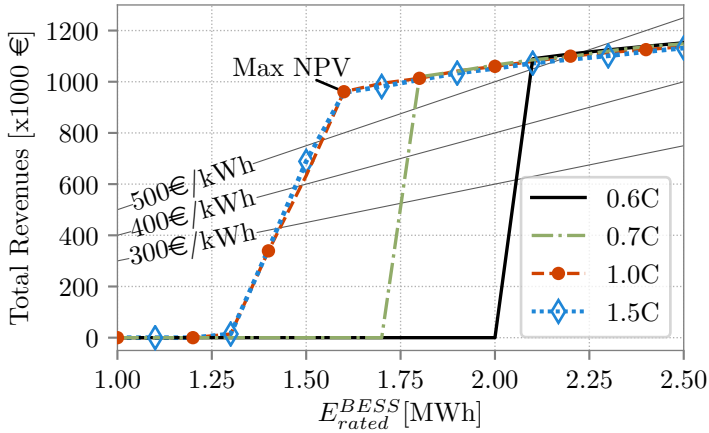

(a) Moderate German FCR price scenario.

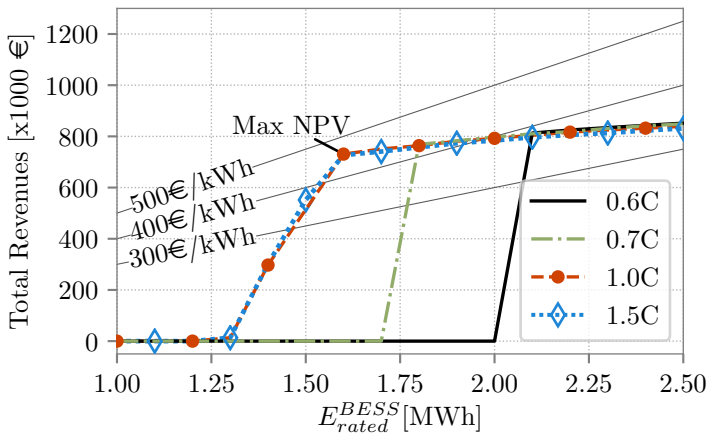

(b) Low German FCR price scenario.

Figure 3.11: Total revenues over the lifetime of a BESS providing FCR services to the German market minus the electricity costs (3.13), optimised according to Algorithm 1, in the function of the rated energy capacity E_{rated}^{BESS} and the C-rate. Indicative lines of battery costs in euro per kilowatt hour (/ €kWh) are also plotted. Revenues were adjusted for the expected inflation, assumed at $\gamma = 1.7\,\%$ [129]. The point with the highest NPV, at an energy capacity of 1.6 MWh and C-rate ≥ 1.0 C, is denoted on both figures by "Max NPV".

1.6 MWh battery with a power rating higher than 1.6 MW results in the highest NPV[4] and would thus be the optimal BESS sizing for the German FCR market (only at a cost of 300 €/kWh, the 1.7 MWh/1.0 C battery has a slightly higher NPV and would be the better choice).

Figure 3.11 shows that a BESS with a lower C-rate (0.7 C and 0.6 C) can only obtain revenues by participating in the German FCR market with a relatively high rated energy capacity. This is due to the requirement that $P_{max}^{BESS} \geq 1.25r \geq 1.25$ MW. For a 0.6 C BESS, this means a minimum energy capacity of 2.09 MWh is needed.

For a BESS with a higher C-rate (1.0 C and 1.5 C), one needs at least 1.3 MWh to be able to participate with a 1 MW FCR capacity in the German market. This is due to the 30-minutes criterion, which obliges to reserve at least 1 MWh of energy capacity for emergency states. A battery with a rated energy capacity of 1.6 MWh has much larger revenues and NPV than those of a battery rated at 1.5 MWh, whose revenues are already much higher than those of a battery rated at 1.4 MWh and 1.3 MWh. This occurs because, in this part of the graph (between 1.3 MWh and 1.6 MWh, C-rate $\geq$ 1.0 C), the revenues of a BESS are limited by the years the BESS can provide the FCR service without violating the penalty constraint (3.11). In this range, a BESS with a larger energy capacity will be able to satisfy the penalty constraint for a longer period of time and therefore obtain more revenues.

A battery with an energy capacity larger than 1.6 MWh will also see larger revenues; however, the slope of the increase in revenues with larger energy capacity is smaller than the slope between 1.3 MWh and 1.6 MWh. In this part of the graph, the operational lifetime of the BESS in the FCR market is not limited by the penalty constraint, but rather by the end-of-life criterion ($C = 80\,\%$). The BESS will be able to provide FCR while respecting (3.11) its entire lifetime until it is degraded completely. The degradation curve of three 1.0 C batteries is shown in Figure 3.12. As can be seen in the figure, a larger energy capacity reduces degradation, as the DoD of the cycles will be smaller and, therefore, extends the lifetime of the BESS. However, the additional revenues do not outweigh the costs of installing additional energy capacity, resulting in a lower NPV with additional energy capacity, as can be seen in Table 3.3. It is also interesting to note that, in this part of the graph, the

[4]This value is calculated complying with the 30-minutes criterion, which was active at the time of writing the paper. As from 15 May 2019, this has been changed to a 15-minutes criterion. Applying the 15-minutes criterion to Figure 3.11 would result in a shift of the 1.0 C and 1.5 C lines to the left, with the 1.0 C line going to 0 at an energy capacity $<$ 1.25 MWh due to the requirement that the recharge power has to be able to compensate a 50 mHz activation. This will mean that a BESS with a higher C-rate will and a lower energy capacity than a 1.0 C, 1.6 MWh BESS will have an high NPV that what is depicted here.

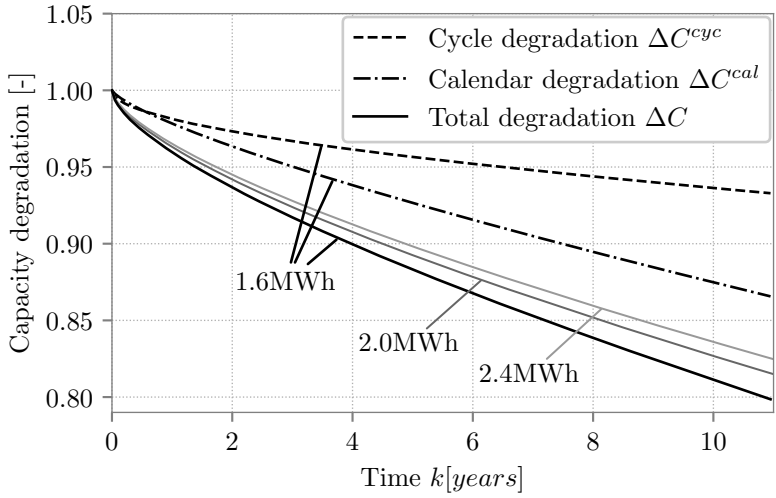

Figure 3.12: Total capacity degradation of a 1.0 C BESS with a rated energy capacity of 1.6 MWh, 2.0 MWh and 2.4 MWh delivering $r = 1$ MW of FCR power in Germany. The calendar degradation ΔC^{cal} and the degradation due to cycling ΔC^{cyc} of the 1.6 MWh/1.6 MW BESS are also shown.

power capacity has almost no impact on the total revenues. This occurs because the BESS has to provide 1 MW of FCR capacity and a BESS with a power capacity of 1.6 MW has enough recharging power to provide the FCR service over its entire lifetime. A larger power capacity only results in a larger available recharging power, which is already sufficient to provide the FCR service, with no impact on the total revenues.

The point at 1.6 MWh (denoted in Figure 3.11 with "Max NPV") is where the two parts with the different slopes meet, which explains why this point has the highest NPV: a BESS with 1.6 MWh and a C-rate $\geq$ 1.0 C has the smallest amount of energy capacity that is able to provide the FCR while respecting the penalty constraint (3.11) until it is degraded to its end-of-life criterion. The payback period of a BESS with this configuration is shown in Table 3.4, for the different costs $costs_{BESS}$ and for the moderate and low Germany FCR price scenarios.

The electricity costs of a BESS are very low (in the moderate scenario, between 0.94 % and 2.97 % of total FCR revenues, or between 135 € and 2575 € per year), as BESSs are exempted from many of the electricity cost elements in Germany (see Table 3.2). Therefore, the total net revenues are governed by the revenues of selling the FCR capacity on the market. As degradation is the main

	FCR price scenario	
$cost_{BESS}$	Moderate	Low
500 €/kWh	7.1 years	–
400 €/kWh	5.3 years	7.3 years
300 €/kWh	3.6 years	4.7 years

Table 3.4: Payback period of a 1.6 MWh/1.6 MW BESS.

limitation to the amount of time a BESS can participate in the FCR market, it is interesting to take a closer look at the calendar and cycle degradation of a 1.6 MWh/1.6 MW BESS, both shown in Figure 3.12. The BESS reaches its end-of-life criterion ($C = 80\,\%$) after 10.8 years of service. As can be seen in the figure, most of the degradation is actually due to calendar degradation. Although there are plenty of cycles, these often have a low DoD and, thus, have a limited effect on the total degradation.

3.5 Conclusions

In this paper, we have proposed a holistic, data-driven optimisation framework for the investment analysis, sizing and control design of a battery energy storage system participating in frequency control markets. To control the state of charge of a battery storage system performing frequency control, we used a parametrised recharge controller compliant with regulatory requirements, which we optimised to minimise degradation over the lifetime of the battery storage system using real frequency data.

As the required activation profile when providing frequency control is stochastic, we formulated a probabilistic optimisation problem that allows the probability of being unavailable to be constrained to a small value with high confidence. We solved the problem by adopting a global evolutionary optimisation algorithm that only requires function evaluations, which allows the use of a battery energy storage model of which a closed mathematical form is not directly available, but can only be simulated. This approach allowed us to use a battery energy storage model that is more detailed than usually seen in the literature, featuring a dynamic RC battery cell model, a semi-empirical degradation model, an inverter model and an HVAC model.

Finally, we performed a techno-economic analysis of a battery in the German primary frequency control (frequency containment reserve) market, using the proposed framework. We considered all relevant regulations and used real

frequency data, so that the results are applicable to a real case. We found that a battery storage system rated at 1.6 MW/1.6 MWh provides the highest net present value and can deliver 1.0 MW of frequency control capacity for 10.8 years, after which it is degraded to 80 %, which is the end-of-life criterion. Most of the observed degradation was due to calendar degradation, as the cycles performed in frequency control had a limited depth of discharge.

It is worth mentioning that the developed optimisation framework can easily be applied to other countries by incorporating the regulations specific to that country. Interesting future work would be to apply the developed framework to various countries and compare the impact of different regulations on the investment case of the battery system.

Although all models used in the framework are each separately validated by experiments, validating the combination of all models on a battery system providing frequency control would also be relevant future work. Other future work may consist of extending the dynamic program (3.7) to incorporate a broader class of policies, different approximations of the value function or more decisions such as buying additional battery cells for the battery system or using the battery for other services could increase the total value of the battery system. Finally, it would also be interesting to investigate the combination of frequency control with other revenue streams, such as day-ahead or imbalance market arbitraging.

Chapter 4

Combining Self-Consumption and Frequency Control Applications with a Battery

---

Combined Stochastic Optimization of Frequency Control and Self-Consumption with a Battery

Jonas Engels, Bert Claessens and Geert Deconinck

Published in IEEE Transactions on Smart Grid, vol. 10, no. 2, pp. 1971-1981, March 2019.

The first author is the main author of the article. The contributions of the first author include the literature review, the development of the optimisation problem, the analysis of the simulation results, and the writing of the article.

©2019 IEEE. Reprinted, with permission.

Abstract:

Optimally combining frequency control with self-consumption can increase revenues from battery storage systems installed behind the meter. This

work presents an optimised control strategy that allows a battery to be used simultaneously for self-consumption and primary frequency control. Therein, it addresses two stochastic problems: the delivery of primary frequency control with a battery and the use of the battery for self-consumption.

We propose a linear recharging policy to regulate the state of charge of the battery while providing primary frequency control. Formulating this as a chance-constrained problem, we can ensure that the risk of battery constraint violations stays below a predefined probability. We use robust optimisation as a safe approximation to the chance-constraints, which allows to make the risk of constraint violation arbitrarily low, while keeping the problem tractable and offering maximum reserve capacity. Simulations with real frequency measurements prove the effectiveness of the designed recharging strategy.

We adopt a rule-based policy for self-consumption, which is optimised using stochastic programming. This policy allows to reserve more energy and power of the battery on moments when expected consumption or production is higher, while using other moments for recharging from primary frequency control. We show that optimally combining the two services significantly increases value from batteries.

4.1 Introduction

Battery energy storage systems installed behind the meter have been increasingly popular at both residential and industrial consumers. This trend is mostly driven by decreasing prices, technological advancements and regulatory incentives. Increasing self-consumption from local generation by storing excess electricity generation for later use, is one of the major applications for installing behind-the-meter battery storage systems. For instance, in 2016, up to 46% of installed PV systems smaller than 30 kWp were equipped with a battery storage system in Germany [130].

In many cases however, the cost of a BESS remains high and the return on investment from solely self-consumption is too low [131]. Adding supplementary services to be delivered by the same BESS can lead to additional revenue streams and increase the return on investment.

A service for which BESSs are deemed to be very appropriate is primary frequency control [132] (also referred to as frequency containment reserve (FCR) or frequency response) due to their fast ramp rate [76]. Besides, frequency control has been identified as one of the highest value services for BESSs [133].

Complementary between primary frequency control and self-consumption can be expected, as primary frequency control is a service where power capacity is offered, while revenues from self-consumption are more driven by energy capacity.

When participating in primary frequency control, one has to regulate his power consumption or injection to react proportionally on deviations of the grid frequency from the nominal frequency. The maximum contracted reserve capacity has to be activated when the frequency deviation is at a maximum, predefined value and within a predefined time limit. In the continental Europe (CE) synchronous area, this maximum is at a deviation of 200 mHz and has to be reached within 30s [24].

In liberalised ancillary services markets, the TSO buys reserve capacity for frequency control from tertiary parties, who get paid for the power capacity they sell. In this work, we assume an end-consumer is able to offer this service to the TSO, possibly through an intermediary, for example an aggregator.

When participating in primary frequency control, an asset has to be able to deliver the contracted power and follow the frequency signal during the entire contracted period. If the asset fails to do so, it is unavailable to provide the frequency control service and faces penalties charged by the TSO. As these penalties are usually high and the TSO expects an optimal service, in this work, we to constrain the risk of unavailability when delivering primary frequency control.

Being continuously available can be an issue when using energy-constrained assets such as a BESS. Over limited time periods, the frequency signal has a non-zero energy content and after having provided the service for a while, a BESS can be empty or full. In addition, efficiency losses in battery systems decrease their energy content or SoC when being charged and discharged continuously. Therefore, a controller, or *recharging strategy*, has to be in place to control the SoC to be within limits, ensuring that the reserve capacity remains available during the contracted period.

Different strategies can be used: overdelivery (i.e. delivering more power than required), utilizing the deadband of the frequency signal (typically 10 or 20 mHz) to recharge or using a specific recharge controller that offsets the frequency control power for recharging. A comparison of these methods is made in [134], in which they conclude that overdelivery and deadband utilisation alone is not sufficient to maintain the SoC within limits and an additional recharge controller is unavoidable. However, when using part of the BESS power for recharging, this part cannot be sold as a reserve capacity at the same time. One will thus have to optimise one's battery asset, maximizing the reserve capacity while

minimizing the risk of unavailability.

The same is true when using the battery for the combination of frequency control and self-consumption. The BESS power used for self-consumption cannot be sold as reserve capacity for frequency control. One faces a trade-off between the two objectives which we incorporate into our optimisation model. We see that complementarity between the two services occurs and show in a case study that optimally combining both services increases revenues from the BESS by 25% compared to offering solely frequency control.

The remainder of the paper is organised as follows: in section 4.2, related literature is reviewed and the main contributions of this paper are identified. The general problem treated in this paper is formulated in section 4.3. As it concerns a highly intractable problem, we treat the problem of providing solely frequency control first in section 4.4. In section 4.5, the objective of self-consumption is added, using a rule-based controller, optimised through stochastic optimisation. With the mathematical framework defined, section 4.6 presents some simulations and results. Finally the paper is concluded and some suggestions for future work are given.

4.2 Background and Related Work

4.2.1 Background on Frequency Control

While in Europe, liberalised markets exist for primary frequency control, this is not the case in North America, where primary frequency control is traditionally delivered by generator governors or frequency responsive loads and is imposed as a requirement on large generators while no compensation is given for this service [31].

Markets do exist for regulation services, which is part of secondary frequency control, allowing third parties to offer their resources as regulation capacity. Here, the asset has to follow a centrally dispatched signal to correct for the ACE of the respective control area. Compensation is not only based on offered capacity, but also on actual performance, rewarding assets that are able to perform better in following the regulation signal. Moreover, the California Independent System Operator (CAISO) has implemented a program for non-generator resources (NGRs) with regulation energy management (REM) allowing for NGRs with limited energy content such as battery storage systems to competitively bid into the regulation market [135]. PJM has implemented a high pass filter over its regulation signal in order to remove most of the energy content, making it more suitable for energy constrained resources such as BESSs [136].

In the European context, some research has been conducted to create zero-mean frequency control signal [137], but so far this has not been commercially implemented by any TSO.

While the approach presented in this paper can be applied to any type of frequency or regulation signal, the focus is on primary frequency control as defined by European TSOs, as they impose the strictest rules by requiring a 100 % availability and near perfect delivery.

4.2.2 Related Work

From previous work on the provision of primary frequency control with a BESS, we identify two distinct approaches. A first approach is to design a heuristic recharging strategy with simulations over historical frequency data for empirical optimisation of the heuristic. For instance, Oudalev et al. [107] design a rule-based recharge controller that acts when the SoC leaves the range (SoC_{max}, SoC_{min}). They use auxiliary resistors to consume additional power when the battery cannot provide enough, which we want to avoid in this work. The heuristic recharging strategy presented in [109] is based on the moving average of the frequency signal, corrected for efficiency losses. The goal is to create a power profile with zero-mean, so that the battery does not get charged or discharged over time. A variant on this strategy is presented in [110] and evaluated to give a higher return on investment when compared to the strategies from [107, 109]. A rule-based control policy for fast energy storage unit in combination with a slower unit that is able to capture the energy content of the regulating signal is presented in [138]. While these heuristic strategies give good results, they do not ensure any form of optimality.

A second approach tries to overcome this by using more formal methods that can ensure optimality within the adopted framework. For instance, in [139], a fuzzy control logic is used for primary frequency control and energy arbitrage in the Italian energy market. Zhang et al. [76] use dynamic programming to calculate an optimal recharging policy, recharging only when the frequency is in the deadband. Dynamic programming is also used for combining energy arbitrage and frequency regulation in the PJM regulatory zone [77]. However, both papers assume the reserve capacity a given parameter and are not able to optimise over this capacity itself.

The combination of primary frequency control provision and minimisation of PV and load curtailment by a battery storage system is considered in [140], where a MPC is proposed to compute the allocation of the storage system for the two objectives. Although they model uncertainty in PV and consumption forecasts, they do not take this into account in the MPC controller. Combination of

self-consumption and primary frequency control is studied in [141], however they use a heuristic controller that is only able to provide primary frequency control through pooling with a combined heat and power plant. Peak shaving and frequency regulation are combined in [142]. By using the fast regulation signal from PJM, they are able to avoid the issue of limited energy content when offering frequency control services, which we want to overcome in this paper.

Using BESSs connected to the distribution grid for frequency control might cause voltage problems or jeopardise the reliability of the distribution grid, when several BESSs are connected to the same feeder [143]. A potential solution can be a local voltage droop controller, which is shown to be effective in to avoid distribution grid constraint violations while having very limited impact on the performance of the service to be delivered [144]. In the remainder of this paper however, we will assume that the BESS providing frequency control are sufficiently dispersed over various feeders and do not endanger the reliability of the distribution grid.

Finally, it is worth mentioning that lately, there has been some commercial interest in the combination of self-consumption and frequency control with residential battery storage systems in Germany. More specifically, both companies *Caterva* [145] and *Sonnen* [146] have presented a concept to combine self-consumption from PV with frequency control with a residential battery storage system. In both cases, the company acts as the intermediary party, operating a part of the storage systems for frequency control and offering the aggregated frequency control capacity to the TSO.

In this paper, we complement previous work by elaborating a controller that co-optimises self-consumption, the reserve capacity and a recharge controller for primary frequency control. The main contributions can be summarised as follows:

- We propose an optimised controller to maximise reserve capacity, which is able to provide more reserve capacity compared to the heuristic methods proposed in the literature.
- Building further on the work of Vrettos et al. [147], we extend their robust optimisation approach towards a BESS application, and propose a new uncertainty set that provides explicit probability guarantees on battery constraint violation when providing frequency control.
- By co-optimizing self-consumption and frequency control, our approach is able to obtain more value than by using the BESS completely for only one of the objectives.

4.3 Problem formulation

We consider a simple, discrete battery model subject to a stochastic demand and production profile $\boldsymbol{P}_{prof} = \boldsymbol{P}_{dem} - \boldsymbol{P}_{prod}$ and normalised frequency deviations $\boldsymbol{\Delta f}$. We model the BESS with constant charging and discharging efficiencies η^c, η^d. The battery has an effectively usable energy capacity in the range (E_{min}, E_{max}) in which it is assumed to be able to provide the power range (P_{min}, P_{max}).

The price for electricity injection into the grid is assumed smaller than the price for electricity consumption $c_{inj} < c_{cons}$, as this is imperative to make self-consumption financially interesting. The price for primary frequency control c_{FCR} is assumed to be known, while the capacity r is a variable to be optimised.

The objective of the problem is to minimise expected electricity consumption costs and maximise profits from primary frequency control, while keeping the BESS within its energy and power constraints. This results in following stochastic optimisation program:

$$\min \quad \mathrm{E}[(c_{cons}[\boldsymbol{P}_{grid}]^+ - c_{inj}[-\boldsymbol{P}_{grid}]^+)\Delta t] - c_{FCR} r \tag{4.1a}$$

$$\text{s.t.} \quad \boldsymbol{P}_{grid} = \boldsymbol{P}_{prof} + \boldsymbol{P}_{bat}, \tag{4.1b}$$

$$\boldsymbol{P}_{bat} = \boldsymbol{P}_{ctrl} + r\boldsymbol{\Delta f}, \tag{4.1c}$$

$$E_{min} \leq \boldsymbol{E}_{bat} \leq E_{max}, \tag{4.1d}$$

$$P_{min} + r \leq \boldsymbol{P}_{ctrl} \leq P_{max} - r, \tag{4.1e}$$

$$E_{k+1}^{bat} = E_k^{bat} + (\eta^c [P_k^{bat}]^+ - \frac{1}{\eta^d}[-P_k^{bat}]^+)\Delta t. \tag{4.1f}$$

Here, $\mathrm{E}[\cdot]$ denotes the expected value operator and $[\cdot]^+ \equiv \max(\cdot, 0)$, operating element-wise on vectors. The power vector $\boldsymbol{P}_{grid}$ is the power that is actually put on the grid, consisting of the battery power $\boldsymbol{P}_{bat}$ and the demand profile $\boldsymbol{P}_{prof}$. The BESS power consist of two parts. One part is due to the frequency control and thus equal to the capacity times the frequency deviations $r\boldsymbol{\Delta f}$. A second part $\boldsymbol{P}_{ctrl}$ is dedicated to control the battery state of charge when providing frequency control, while optimizing the self-consumption. Self-discharge losses, not incorporated here, can be added by subtracting them from the energy equation (4.1d).

To account correctly for the energy content of the battery (4.1d), we assume that all power values are kept constant over one time step Δt. However, this is not possible when providing primary frequency control, as the BESS typically

has to react within seconds to the real frequency control signal. Therefore, we define the discrete normalised frequency deviations Δf_k as the average value over one time step:

$$\Delta f_k = \frac{1}{\Delta t} \int_{(k-1)\Delta t}^{k\Delta t} \frac{(f(t) - f_{nom})}{\Delta f_{max}} dt,$$

with $f(t)$ the real frequency, f_{nom} the nominal value and Δf_{max} the maximum frequency deviation on which on a has to react (for instance 200 mHz in the CE region). To ensure that the instantaneous reserve capacity r is always available, we have added it explicitly to the hard power constraints in (4.1e).

As both the power profile $\boldsymbol{P}_{prof}$ and the frequency deviations $\boldsymbol{\Delta f}$ are stochastic variables that are gradually revealed over time, problem (4.1) is a multi-stage stochastic program. This means that the "here and now" decision of the control power $\boldsymbol{P}_{ctrl}$ can be relaxed to a "wait and see" decision and depend on the past realisations of the power profile and frequency deviations $P_k^{ctrl} = \pi^k(P_1^{prof}, \ldots, P_k^{prof}, \Delta f_1, \ldots, \Delta f_k)$ [120]. This is not true for the frequency control capacity r, as this value should be contracted with the TSO before the actual delivery takes place and one is not allowed to change this capacity during the delivery period.

Problem (4.1) is a multi-stage non-linear stochastic program, which quickly becomes computationally intractable. To simplify, we propose to split the control power into two separate parts: a part for self consumption $\boldsymbol{P}_{sc}$ and a part for recharging after frequency control activations $\boldsymbol{P}_{rc}$. Each is then depending on only one source of uncertainty:

$$\boldsymbol{P}_{ctrl} = \boldsymbol{P}_{sc}(\boldsymbol{P}_{prof}) + \boldsymbol{P}_{rc}(\boldsymbol{\Delta f})$$

We can now look at (4.1) as the combination of two distinct sub-problems: providing frequency control with a BESS and optimizing self-consumption. These sub-problems can then be put together, according to (4.1), for joint optimisation, which is expected to yield a better solution than the simple addition of the two objectives.

4.4 Primary Frequency Control

In this section we will try to approximately solve problem (4.1), without the objective of self consumption (i.e. $\boldsymbol{P}_{prof} = 0$). The focus will be on the determination of the maximum frequency capacity r the BESS can provided and the recharging policy $\boldsymbol{P}_{rc}(\boldsymbol{\Delta f})$ needed to keep the risk of unavailability as low as possible.

4.4.1 Recharging Policy

The goal is to design a controller that ensures that the energy constraints (4.1d) are not violated when providing frequency control. The typical control problem is to design a control policy which is a function of the current and past states of the system, here $P_k^{bat,rc} = \pi^k(E_1^{bat}, \ldots, E_k^{bat})$. To come to a problem that can be solved efficiently, we will restrict ourselves to a linear policy. When writing this policy as an linear policy on the *disturbance* $\boldsymbol{\Delta f}$ instead of the state, the problem becomes tractable [148]. The restriction to a disturbance feedback policy is not a limitation as it has been shown that a linear policy on the disturbance is as at least as general as an linear state feedback policy [149]. We can thus write the recharging policy as:

$$P_k^{rc} = \sum_{i=1}^{k-1} d_{ki} \Delta f_i, \quad \boldsymbol{P}_{rc} = D \boldsymbol{\Delta f}, \tag{4.2}$$

with d_{ki} the coefficients of the recharge strategy, contained in the lower triangular matrix $D \in \mathbb{R}^{n_t \times n_t}$ with zeros on the diagonal. Note that we only sum up to $k-1$ in (4.2) so that there is no interference of the recharging power with the instantaneous frequency deviation $\Delta f(t)$.

One can interpret this recharging policy as a filter applied to the frequency control signal that creates a zero-mean signal, comparable to [109, 110]. In this case, the recharge policy represents a change in the baseline on which the battery will perform the required frequency control activations.

An aggregator can also pool the BESS together with another flexibility resource that is able to compensate for the recharging policy [150]. Together they are able to follow the frequency signal exactly.

4.4.2 Battery Efficiency

Using the linear recharging policy (4.2), problem (4.1) results in a mixed-integer stochastic program, which is known for its high computational complexity [151]. Therefore, we will use a heuristic approximation to turn (4.1) into a linear stochastic program. The integer variables in (4.1) arise purely because of the efficiencies η^c, η^d. By assuming an ideal battery and setting $\eta^c = \eta^d = 1$ in (4.1f), the integer variables are removed and (4.1) becomes a linear problem.

As setting $\eta^c = \eta^d = 1$ can be quite a coarse approximation, we instead apply the efficiencies to the frequency deviations:

$$\Delta f_k = \frac{1}{\Delta t} \int_{(k-1)\Delta t}^{k\Delta t} \Big(\eta^c \Big[\frac{\Delta f(t)}{\Delta f_{max}} \Big]^+ - \frac{1}{\eta^d} \Big[- \frac{\Delta f(t)}{\Delta f_{max}} \Big]^+ \Big) dt, \tag{4.3}$$

which is exact if $\text{sign}(\Delta f_k) = \text{sign}(P_k^{bat,rc})$. By transforming the resulting disturbance feedback policy to an equivalent state feedback policy, it is possible to react appropriately to the impact of the efficiency. Detailed simulations with real frequency data presented in section 4.6 demonstrate the validity of this approximation.

4.4.3 Chance-Constraints and Robust Optimisation

When applying the linear recharging policy from (4.2), the power and energy content of the BESS are fully determined by the frequency deviations. The frequency deviation vector $\boldsymbol{\Delta f}$ is a multivariate stochastic variable in $\mathbb{R}^{n_t}$. This means that constraints (4.1d), (4.1e) are actually probabilistic constraints, or so-called chance-constraints [152], and one has to constrain the probability of violation to be at maximum $\epsilon \in (0, 1)$:

$$\Pr\{\boldsymbol{a_i}^T \boldsymbol{\Delta f} \leq b_i\} \geq 1 - \epsilon, \qquad i = 1, \ldots, n_c. \tag{4.4}$$

Here, $n_c = 4n_t$ is the total number of constraints in (4.1d), (4.1e) and $(\boldsymbol{a_i}, b_i)$ are defined to represent one constraint of (4.1d), (4.1e).

As breaching these constraints means that the frequency control service cannot be delivered, we want to make sure that the risk that this happens is as small as possible. Therefore, the goal is to get ϵ on the order of 10^{-4} or 10^{-5}.

Several approaches to solve a chance-constrained problem exist. A popular approach is to use Monte Carlo sampling to approximate the real value of the probability in (4.4). Explicit bounds on the number of samples are given in [115, 153] and are on the order of $O(n_\delta/\epsilon)$, with n_δ the dimension of the uncertainty. This would lead to a sample size on the order of 10^6 for $\epsilon = 10^{-4}$, which is not feasible if one considers a horizon of one day or more as we intend in this paper. Generating additional samples would require complete knowledge of the multivariate distribution of $\mathbf{\Delta f}$, which is never completely possible when working with observed data.

Analytic reformulation of (4.4) into a second-order cone constraint is possible if one assumes a Gaussian distribution [154], which is not the case when considering $\boldsymbol{\Delta f}$.

One can also use a safe, convex approximation of (4.4). The conditional value-at-risk (CVaR) [155] is typically used as it is the tightest convex approximation to (4.4):

$$\text{CVaR}_i^{1-\epsilon}(\boldsymbol{a_i}^T \boldsymbol{\Delta f} - b_i) \equiv \min_\beta \left\{ \beta + \frac{1}{\epsilon} \text{E}[\boldsymbol{a_i}^T \boldsymbol{\Delta f} - b_i - \beta]^+ \right\} \leq 0, \tag{4.5}$$

where $\mathrm{E}[\cdot]^+ \equiv \mathrm{E}[\max(\cdot, 0)]$. Despite its convexity, the CVaR risk measure is difficult to evaluate as the evaluation of $E[\cdot]^+$ requires multidimensional integration over the $\max(\cdot, 0)$ operator. A sample average approximation of (4.5) requires complete knowledge of the multivariate distribution and a large amount of samples to be accurate at small ϵ [120].

Finally, the paradigm of robust optimisation [148] can be used to construct safe, tractable approximations to chance-constraints. The concept is to design an uncertainty set $\mathcal{F}$ of frequency deviations $\boldsymbol{\Delta f} \in \mathcal{F}$, against which the constraint has to be satisfied at all times:

$$\boldsymbol{a_i}^T \boldsymbol{\Delta f} \leq b_i, \quad \forall \boldsymbol{\Delta f} \in \mathcal{F}, \qquad i = 1, \ldots, n_c.$$

This is equivalent to following worst-case formation:

$$\max_{\boldsymbol{\Delta f} \in \mathcal{F}} \boldsymbol{a_i}^T \boldsymbol{\Delta f} \leq b_i, \qquad i = 1, \ldots, n_c. \tag{4.6}$$

By correct design of $\mathcal{F}$, the solution of (4.6) can ensure that the probability in (4.4) is bigger than or equal to the $(1 - \epsilon)$ required, while retaining a tractable problem.

Different uncertainty sets are proposed in literature (see e.g. [148, 156, 157]) of which their robust counterparts are shown to be upper bounds on the CVaR measure (4.5) [158]. Clearly, one is looking for the uncertainty set that provides the tightest upper bound. The robust counterparts of five types of tractable uncertainty sets are compared to the actual value of the CVaR measure in [159] and it is shown that for small ϵ, the uncertainty set based on forward and backward deviations provides the tightest bound to (4.5). Furthermore, the robust counterpart is second-order cone representable and thus efficiently solvable by commercial solvers.

Unfortunately, the probability guarantee is only applicable to independent variables with zero mean, which is not the case when considering $\boldsymbol{\Delta f}$. However, by applying a whitening transformation [160], one can obtain independent variables with zero mean:

$$\tilde{\boldsymbol{f}} = W(\boldsymbol{\Delta f} - \overline{\boldsymbol{\Delta f}}), \tag{4.7}$$

where $\overline{\boldsymbol{\Delta f}}$ is the mean of $\boldsymbol{\Delta f}$, and $W^T W = \Sigma_{\boldsymbol{\Delta f}}^{-1}$ the Cholensky decomposition of the inverse of the covariance matrix $\Sigma_{\boldsymbol{\Delta f}}$ of $\boldsymbol{\Delta f}$.

The forward and backward deviations allow to include distributional asymmetry in the uncertainty set. They are defined for the stochastic variable $\tilde{f}_i$ as:

$$\sigma_{fi}(\tilde{f}_i) = \sup_{\theta>0} \sqrt{2 \ln \mathrm{E}[\exp(\theta \tilde{f}_i)]/\theta^2},$$

$$\sigma_{bi}(\tilde{f}_i) = \sup_{\theta>0} \sqrt{2 \ln \mathrm{E}[\exp(-\theta \tilde{f}_i)]/\theta^2},$$

with $\theta \in \mathbb{R}$. The superior over θ can be found by applying a line search and approximating the expected value by its empirical average over the sampled data. Define also $Q = \mathrm{diag}(\sigma_{f1}, \ldots, \sigma_{fn_t})$ and $R = \mathrm{diag}(\sigma_{b1}, \ldots, \sigma_{bn_t})$. The uncertainty set $\mathcal{F}_\epsilon$ becomes then:

$$\mathcal{F}_\epsilon = \{\mathbf{f} : \exists \boldsymbol{\beta}, \boldsymbol{\theta} \in \mathbb{R}_+^{n_t}, \mathbf{f} = \boldsymbol{\beta} - \boldsymbol{\theta},$$
$$\|Q^{-1}\boldsymbol{\beta} + R^{-1}\boldsymbol{\theta}\|_2 \leq \sqrt{-2 \ln \epsilon}\}$$

Following [158] and using (4.7) to obtain independent variables $\tilde{\boldsymbol{f}}$ from $\boldsymbol{\Delta f}$, the $\mathrm{CVaR}^{1-\epsilon}$ in (4.5) is bounded by the worst-case of the constraint over the uncertainty set $\mathcal{F}_\epsilon$:

$$\mathrm{CVaR}_i^{1-\epsilon} \leq \boldsymbol{a_i}^T \overline{\boldsymbol{\Delta f}} + \max_{\tilde{\boldsymbol{f}} \in \mathcal{F}_\epsilon} \boldsymbol{a_i}^T W^{-1} \tilde{\boldsymbol{f}} - b_i \leq 0.$$

Finally, this can be reformulated as a second-order cone constraint [159]:

$$\boldsymbol{a_i}^T \overline{\boldsymbol{\Delta f}} + \sqrt{-2 \ln \epsilon} \|\boldsymbol{u_i}\|_2 \leq b_i, \qquad i = 1, \ldots, n_c, \tag{4.8}$$

where $\boldsymbol{u_i} = \max(Q\boldsymbol{a_i}^T W^{-1}, -R\boldsymbol{a_i}^T W^{-1})$, with the maximum taken element-wise. Note that ϵ in (4.8) is under the logarithm, so that small values can easily be used.

4.4.4 Equivalent State Feedback Policy

The recharging strategy of (4.2) is a disturbance feedback policy calculated with the efficiencies incorporated in the frequency signal (4.3) and not in the battery model. This policy will therefore not be directly usable on a real battery system. However, by reformulating the policy as an equivalent state feedback policy it becomes practically usable. As efficiency losses are included in the state of charge of the battery, a state feedback policy can react on efficiency losses appropriately.

Following [149], an equivalent state feedback policy can be calculated as:

$$\boldsymbol{P_{rc}} = (I_{n_t} + \frac{1}{r}D)^{-1}\frac{1}{r}D\boldsymbol{\Delta E_{bat}}, \tag{4.9}$$

with $\Delta E_k^{bat} = \left(E_k^{bat} - E_{k-1}^{bat}\right)/\Delta t$. In this form, the recharge power depends linearly on the past states, rather than on the past disturbances.

4.5 Self-Consumption

In this section we will add the second part of the problem (4.1), i.e. finding a policy $\boldsymbol{P}_{sc}(\boldsymbol{P}_{prof})$ that allows to optimise self-consumption, while keeping in mind that a part of the battery has to be reserved for providing the primary frequency control.

4.5.1 Self-Consumption Policy

The objective of self-consumption is to minimise the expected value of the total cost of electricity for the end-consumer. When facing constant consumption and production prices, a simple, rule-based control policy has proven to be very effective for this objective. The basic concept is to charge when there is more production than consumption and the battery is not full, and to discharge when there is more consumption than production and the battery is not empty.

To ensure sufficient energy and power of the BESS remains available for frequency control, we adapt the energy and power limits between which the battery can perform self-consumption to be smaller than the actual limits of the battery ($E_{max,k}^{sc} \leq E_{max}, E_{min,k}^{sc} \geq E_{min}$) and ($P_{max,k}^{sc} \leq P_{max}, P_{min,k}^{sc} \geq P_{min}$). By making these limits dependent on the time k, they can be shaped towards the expected amount of generation or consumption. The control policy for self-consumption becomes then:

$$P_k^{sc} = \begin{cases} \min(-P_k^{prof}, P_{max,k}^{sc}), & \text{if} \begin{cases} P_k^{prof} < 0, \\ E_k^{sc} \quad < E_{max,k}^{sc}, \end{cases} \\ \max(-P_k^{prof}, P_{min,k}^{sc}), & \text{if} \begin{cases} P_k^{prof} > 0, \\ E_k^{sc} \quad > E_{min,k}^{sc}, \end{cases} \\ 0, & \text{otherwise.} \end{cases} \tag{4.10}$$

This policy allows one to capture the most value from self-consumption while ensuring the capacity needed to deliver the frequency control is always available.

Notice that, when using this policy in combination with the frequency control policy described previously, one is actually dividing the battery into two virtual batteries with varying energy and power capacities: one for self-consumption and one for frequency control. Therefore, an estimation of the energy content of the virtual battery for self-consumption E^{sc} should be available. This can be obtained by integrating P^{sc}, taking into account efficiency losses and other non-linearities as much as possible. Alternatively, one can keep track of the energy content due to frequency control E^{FCR} by integrating the corresponding power set-points $P^{rc} + r\Delta f$ and subtracting it from the measured state of charge: $E^{sc} = E^{bat} - E^{FCR}$.

4.5.2 Stochastic Optimisation

Optimizing the self-consumption is a stochastic program in which the objective contains the expected value of the consumption and injection power vector:

$$\min \quad \mathrm{E}[(c_{cons}\boldsymbol{P}_{cons} + c_{inj}\boldsymbol{P}_{inj})\Delta t]. \tag{4.11}$$

A closed-form of this expected value is not readily available. Therefore, we will approximate the expected value by the SAA [120]. By using various scenarios $j = 1, \ldots, n_{sc}$ of the profile $\boldsymbol{P}^{j}_{prof}$, the empirical average of the objective will approximate the true expected value (4.11).

By splitting the power for self-consumption into a part for charging and a part for discharging $\boldsymbol{P}_{sc} = \boldsymbol{P}_{sc,c} + \boldsymbol{P}_{sc,d}$, the efficiency can be accounted for correctly. As long as $c_{cons} > c_{inj}$, there is a cost for consuming energy and an optimal solution will always set $P^{sc,c}_k \cdot P^{sc,d}_k = 0, \forall k$.

Together with the constraints imposed by the rule-based charging policy in (4.10), one gets a linear program that can be solved efficiently:

$$
\begin{aligned}
\min \quad & \frac{1}{n_{sc}} \sum_{j=1}^{n_{sc}} (c_{cons} \boldsymbol{P}_{cons}^{j} \Delta t + c_{inj} \boldsymbol{P}_{inj}^{j} \Delta t) \quad , \\
\text{s.t.} \quad & \boldsymbol{P}_{cons}^{j} + \boldsymbol{P}_{inj}^{j} = \boldsymbol{P}_{prof}^{j} + \boldsymbol{P}_{sc,c}^{j} + \boldsymbol{P}_{sc,d}^{j}, \\
& 0 \leq \boldsymbol{P}_{sc,c}^{j}, \boldsymbol{P}_{cons}^{j}, \\
& \boldsymbol{P}_{sc,d}^{j}, \boldsymbol{P}_{inj}^{j} \leq 0, \\
& \boldsymbol{E}_{min}^{sc} \leq \boldsymbol{E}_{sc}^{j} \leq \boldsymbol{E}_{max}^{sc}, \\
& \boldsymbol{P}_{sc,c}^{j} \leq \boldsymbol{P}_{max}^{sc}, \\
& \boldsymbol{P}_{min}^{sc} \leq \boldsymbol{P}_{sc,d}^{j}, \\
& E_{min} \leq \boldsymbol{E}_{min}^{sc} \leq \boldsymbol{E}_{max}^{sc} \leq E_{max}, \\
& P_{min} \leq \boldsymbol{P}_{min}^{sc} \leq \boldsymbol{P}_{max}^{sc} \leq P_{max}, \\
& E_{k+1,j}^{sc} = E_{k,j}^{sc} + (\eta^{c} P_{k,j}^{sc,c} + \frac{1}{\eta^{d}} P_{k,j}^{sc,d}) \Delta t,
\end{aligned}
\tag{4.12}
$$

for all $j = 1, \ldots, n_{sc}$ and $k = 1, \ldots, n_t$. Here, we assume the scenarios or samples $\boldsymbol{P}_{prof}^{j}$ are independent and identically distributed (iid). sampled with different probability distributions can be used by adding appropriate weights to each sample.

This problem can be combined with the chance-constrained problem of section 4.4 for providing frequency control, by adjusting the limits on energy content and BESS power in b_i of (4.8) to $(E_{max} - \boldsymbol{E}_{max}^{sc}, \boldsymbol{E}_{min}^{sc} - E_{min})$ and $(P_{max} - \boldsymbol{P}_{max}^{sc}, P_{min} - \boldsymbol{P}_{min}^{sc})$. The complete second-order cone program, combining

frequency control and self-consumption (4.12) becomes then:

$$
\begin{aligned}
\min \quad & \frac{1}{n_{sc}} \sum_{j=1}^{n_{sc}} (c_{cons} \boldsymbol{P}_{cons}^{j} \Delta t + c_{inj} \boldsymbol{P}_{inj}^{j} \Delta t) - c_{FCR} r \\
\text{s.t.} \quad & \boldsymbol{P}_{cons}^{j} + \boldsymbol{P}_{inj}^{j} = \boldsymbol{P}_{prof}^{j} + \boldsymbol{P}_{sc,c}^{j} + \boldsymbol{P}_{sc,d}^{j}, \\
& 0 \leq \boldsymbol{P}_{sc,c}^{j}, \boldsymbol{P}_{cons}^{j}, \\
& \boldsymbol{P}_{sc,d}^{j}, \boldsymbol{P}_{inj}^{j} \leq 0, \\
& \boldsymbol{E}_{min}^{sc} \leq \boldsymbol{E}_{sc}^{j} \leq \boldsymbol{E}_{max}^{sc}, \\
& \boldsymbol{P}_{sc,c}^{j} \leq \boldsymbol{P}_{max}^{sc}, \\
& \boldsymbol{P}_{min}^{sc} \leq \boldsymbol{P}_{sc,d}^{j}, \\
& E_{min} \leq \boldsymbol{E}_{min}^{sc} \leq \boldsymbol{E}_{max}^{sc} \leq E_{max}, \\
& P_{min} \leq \boldsymbol{P}_{min}^{sc} \leq \boldsymbol{P}_{max}^{sc} \leq P_{max}, \\
& E_{k+1,j}^{sc} = E_{k,j}^{sc} + (\eta^{c} P_{k,j}^{sc,c} + \frac{1}{\eta^{d}} P_{k,j}^{sc,d}) \Delta t, \\
& \sqrt{-2 \ln \epsilon} \|\boldsymbol{u_i}\|_2 \leq b_i - \boldsymbol{a_i}^T \overline{\boldsymbol{\Delta f}}, \\
& Q \boldsymbol{a_i}^T W^{-1} \leq \boldsymbol{u_i}, \\
& -R \boldsymbol{a_i}^T W^{-1} \leq \boldsymbol{u_i},
\end{aligned}
$$

for all $j = 1, \ldots, n_{sc}$, $k = 1, \ldots, n_t$ and $i = 1, \ldots n_c$. If we define constraint matrix $A = [D^T | -D^T | (D + rI_{n_t})^T G^T | -(D + rI_{n_t})^T G^T]^T$, with G a lower triangular matrix with Δt as elements, and vector $\boldsymbol{b} = [P_{max} - \boldsymbol{P}_{max}^{sc}{}^T - r | P_{min} - \boldsymbol{P}_{min}^{sc}{}^T + r | E_{max} - \boldsymbol{E}_{max}^{sc}{}^T | \boldsymbol{E}_{min}^{sc}{}^T - E_{min}]^T$, then $\boldsymbol{a_i}^T$ is the i-th row of A and b_i the i-th element of $\boldsymbol{b}$.

4.5.3 Scenario Reduction

Although the objective of the SAA problem (4.12) converges to the true value (4.11) for $n_{sc} \to \infty$, the rate of convergence is on the order of $O_p(n_{sc}^{-1/2})$ [120]. A considerably large number of samples will thus be needed for sufficient accuracy. To limit the size of the problem and keep it tractable,

scenario reduction techniques can be applied. We will use the backward scenario reduction of single scenarios of Dupačová et al. [161] based on the Kantorovich distance, since it has shown the best performance in our case.

4.5.4 Evaluation of the Solution Quality

As the objective of the SAA problem (4.12) is an approximation to the true objective value (4.11), it would be instructive to have an estimation on how close the approximation is to the true value. Mak et al. [114] provide a statistical method for calculating an upper and lower bound to the true objective value and the optimality gap of the SAA problem.

Let $\hat{x}$ be the optimal variables of the SAA problem, and $\boldsymbol{P}^j_{prof}, \quad j = 1, ..., n_U$ iid profile samples, possibly different from the ones used in the SAA problem. Define $g(\hat{x}, \boldsymbol{P}^j_{prof})$ as the objective of (4.12) evaluated at $\hat{x}$ with $\boldsymbol{P}^j_{prof}$. An approximate $100(1-\beta)\%$ confidence upper bound follows from the central limit theorem (CLT) on the average $\bar{g}_{n_U} = 1/n_U \sum_{j=1}^{n_U} g(\hat{x}, \boldsymbol{P}^j_{prof})$ of the n_U samples.

An $100(1-\beta)\%$ confidence lower bound can be estimated by solving the SAA problem (4.12) to optimality n_L times: $\hat{g}^1_{n_{sc}}, \ldots, \hat{g}^{n_L}_{n_{sc}}$. The average $\bar{g}_{n_L} = 1/n_L \sum_{i=1}^{n_L} \hat{g}^i_{n_{sc}}$ of the samples $\hat{g}^i_{n_{sc}}$ follows a t-distribution with $n_L - 1$ degrees of freedom. Finally, an $100(1-2\beta)\%$ confidence upper bound to the optimality gap at $\hat{x}$ can be expressed as:

$$gap_{SAA}(\hat{x}) = \bar{g}_{n_U} - \bar{g}_{n_L} + z_\beta \frac{s_{n_U}}{\sqrt{n_U}} + t_{\beta, n_L - 1} \frac{s_{n_L}}{\sqrt{n_L}}, \tag{4.13}$$

with $z_\beta = \Phi^{-1}(1-\beta)$, where $\Phi(z)$ is the cumulative density function of the standard normal distribution. Here, s_{n_U} is the sample standard deviation of the n_U upper bound objective values $g(\hat{x}, \boldsymbol{P}^j_{prof})$, $t_{\beta, n_L - 1}$ the β-critical value of the t-distribution with $n_L - 1$ degrees of freedom and s_{n_L} the standard deviation of the lower bound samples $\hat{g}^i_{n_{sc}}$.

4.6 Simulation and Results

In this section we will present simulations and results of the mathematical program defined above. With the presented framework, we are able to draw some interesting conclusions about batteries providing frequency control and self-consumption. We will focus first on the robust optimisation framework for frequency control only and then add the stochastic optimisation for self-consumption.

In the simulations we consider a time horizon of one day, discretised in time steps of 15 minutes, so $n_t = 96$. A time horizon of one day is motivated by the daily cyclicality of consumption and PV production profiles. The time step of 15 minutes seems appropriate for the recharging policy when providing frequency control, as the regulations set by ENTSO-E state that a frequency deviation should be resolved within 15 minutes in the CE-region [24]. The charging and discharging efficiencies are chosen to be $\eta^c = \eta^d = \sqrt{0.90}$, corresponding to a round trip efficiency of 90%.

All optimisations are performed using the YALMIP [162] toolbox with Gurobi 7.0.2 [163] in MATLAB.

4.6.1 Primary Frequency Control

To assess the performance of primary frequency control, we use locally measured frequency data in the CE synchronous region with a resolution of 1 second over a period of three years (2014 - 2016). Missing data points are linearly interpolated up to 60 seconds. Days with remaining missing data points are removed from the data set, retaining 1091 complete days or samples. To test the performance of the approach on out-of-sample data points, we select 70% of this data set randomly as training data, used to calculate σ_{fi} and σ_{bi}, leaving 30% for validation. The maximum frequency deviation on which the battery has to react Δf_{max} in (4.3) is set to 200 mHz as required in the CE synchronous region [24].

Robust Optimisation

Consider a residential battery configuration of 10 kWh and 7 kW, with an initial charge of 5 kWh. Running the robust optimisation as elaborated in section 4.4.3, with the chance of violating the battery constraints $\epsilon = 10^{-4}$, gives a maximum reserve capacity of 6.37 kW. According to (4.1e) only 0.63 kW is to be used for recharging. This reserve capacity is somewhat higher than what we found in literature, e.g. [109] gives a maximum reserve capacity of 4.66 kW for the same battery configuration.

Figure 4.1 shows the corresponding energy and recharging power profiles for each frequency profile in the dataset. One can see that for both the training and the validation data, the energy content and recharging power stay well below the limits. Having chosen a small value of ϵ this makes sense, as the battery should be able to withstand more extreme frequency profiles that are not presented in the data sets. Using the uncertainty set $\mathcal{F}_\epsilon$ in (4.6), it is

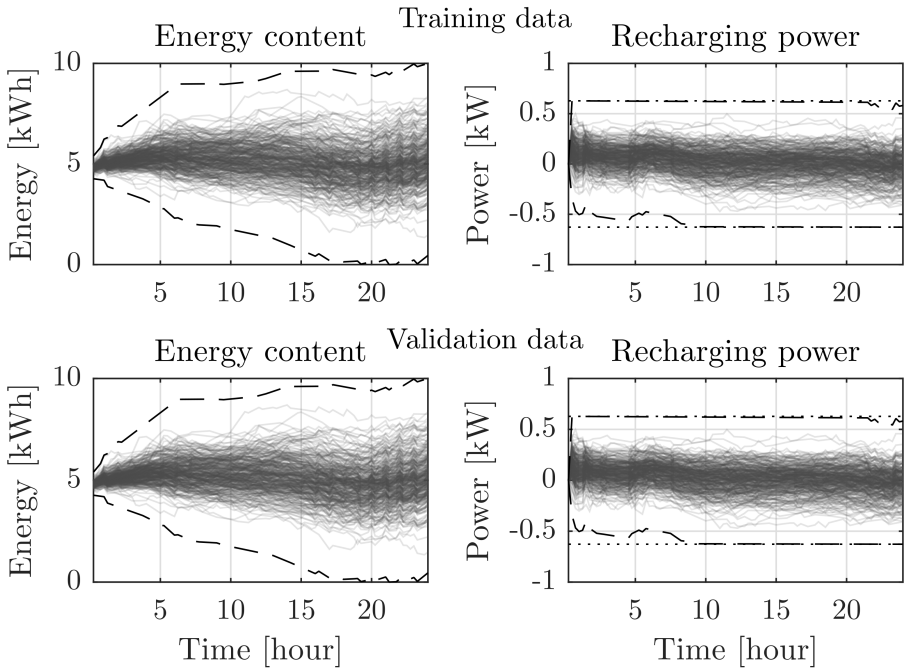

Figure 4.1: Energy content and recharging power of the battery, for the frequency data in the training set (top) and the validation set (bottom), discretised according to (4.3) The dashed lines show the maximum and minimum cases, according to (4.6). The dotted lines show the maximum and minimum recharging power that is allowed, following (4.1e). Each line represents a frequency sample of one day.

possible to calculate the maximum and minimum energy content and recharging power of the battery, shown by the dashed lines. One can see that they do not breach but do approach the boundary conditions of the battery, as expected.

Equivalent State Feedback

The results presented in figure 4.1 use an ideal battery model without losses but with the efficiencies η included into the frequency disturbances, as in (4.3). To evaluate the performance of the state feedback controller of (4.9) we have calculated the maximum probability of constraint violation:

$$\max_i \Pr\{\mathbf{a_i}\boldsymbol{\Delta}\mathbf{f} > b_i\} \tag{4.14}$$

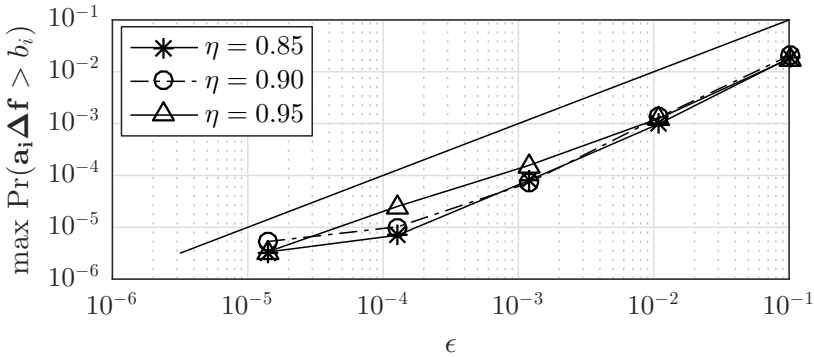

Figure 4.2: Maximum probability of constraint violation with the equivalent state feedback controller (4.9), for various values of ϵ and round trip efficiencies η, calculated with $n_R = 10^6$ samples. The solid black line denotes the maximum allowed probability.

with the state feedback controller on a battery with a round-trip efficiency $\eta < 1$ for various values of ϵ and η as follows.

To obtain the frequency signal Δf_k^o that is not corrected for efficiency losses, we use (4.3) with $\eta^c = \eta^d = 1$. By then applying the whitening transformation (4.7) on $\boldsymbol{\Delta f^o}$, we obtain independent variables with zero mean $\tilde{f}_k^o$, from which we can generate new frequency samples $\boldsymbol{\Delta f^r}$ by resampling $\tilde{f}_k^o$ with replacement n_R times and applying the inverse of the whitening transformation. Using the state feedback controller (4.9) with $\boldsymbol{\Delta f^r}$ gives then a Monte Carlo estimate of (4.14) with n_R samples.

Figure 4.2 shows the resulting 99% confidence upper bound (calculated according to p.217 in [120]) of the maximum probability of constraint violation (4.14) for various values of ϵ and η with $n_R = 10^6$ Monte Carlo samples. One can see that the actual probabilities stay well below the maximum allowed ϵ, for all evaluated values of ϵ while the effect of η is minimal.

Maximum Reserve Capacity

When offering primary frequency control, it is the reserve capacity r that is creating value for the BESS. Using the BESS solely for frequency control, the reserve capacity depends on the (C-rate) of the BESS, defined as the maximum power divided by the maximum energy content, and the energy capacity of the BESS.

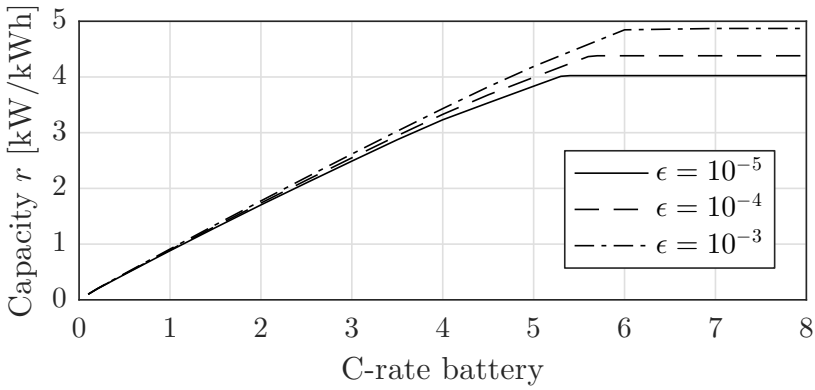

Figure 4.3: Primary frequency control capacity r per kWh of battery capacity in function of the C-rate of the battery, for various values of ϵ and a round trip efficiency $\eta = 90\%$.

Figure 4.3 shows the maximum reserve capacity r per kWh in function of the C-rate, for various values of ϵ. As one can see, the relative reserve capacity is a concave function of the C-rate. Increasing the C-rate of a battery while keeping the energy content constant will thus increase the reserve capacity one can offer with this battery. This is an interesting result, as the main cost driver for batteries is the energy content, rather than the maximum power capacity.

The reserve capacity increases with the C-rate up to a maximum point, at which it is limited solely by the energy content of the battery. Increasing the maximum power of the battery beyond this point will not have any effect on the reserve capacity one can offer. The recharge policy is at its maximum, immediately compensating for the effect of the past frequency deviation. An increase in battery power will not have an effect any more on the recharge policy, thus not be able to increase the reserve capacity.

As could be expected, increasing the probability of battery constraint violation ϵ also increases the amount of reserve capacity one can offer with the same battery. However, this also means an increased risk of unavailability and penalties. If the battery is part of a pool of an aggregator, a higher ϵ can be chosen if the pool can be used as back-up when the BESS constraints are reached.

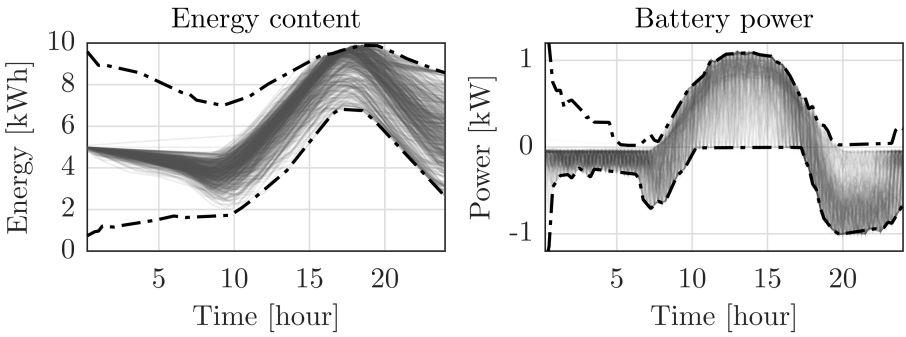

Figure 4.4: Energy content and battery power for self-consumption of 500 scenarios. The dashed black lines denote the limits $(\boldsymbol{E}^{sc}_{min}, \boldsymbol{E}^{sc}_{max})$ and $(\boldsymbol{P}^{sc}_{min}, \boldsymbol{P}^{sc}_{max})$ from the rule-based charging policy.

4.6.2 Combination with Self-Consumption

To asses the performance for the combination of frequency control and self-consumption we consider the same battery configuration as before. Residential demand profiles are generated from the CREST demand model [57] for a weekday in March. PV profiles are generated from the model presented in [58] and scaled to represent a PV system of 4.0 kWp. We assume $c_{FCR} = 14.71$ €/MW/h, which was the average price for primary frequency control on Regelleistung in 2016 [26], $c_{cons} = 28.73$ c€/kWh, corresponding to the average consumption price in Germany in 2016 [164], and $c_{inj} = 12.20$ c€/kWh, the current Germany feed-in tariff for residential PV [165].

Selection of Number of Scenarios

Calculating the optimality gap using (4.13) with $n_U = 10^5, n_L = 10$ and $\beta = 0.005$ for various numbers of scenarios n_{sc}, we find that overall, the optimality gap decreases rapidly to a small value ($\leq 3\%$ if $n_{sc} \geq 250$) and as from about 1000 scenarios, the optimality gap can be expected to be less than 1%.

When using the scenario reduction method from section 4.5.3, an optimality gap smaller than 1% can be reached from about 500 reduced scenarios.

Self-Consumption and Frequency Control

Combining primary frequency control with self-consumption with 500 scenarios from the scenario reduction gives an optimal reserve capacity of 5.65 kW. The remaining power (1.35 kW) is used for maximizing self-consumption and recharging for frequency control. Figure 4.4 shows the BESS energy and power profiles for self-consumption of 500 scenarios. The dashed black lines denote the limits $(\boldsymbol{E}^{sc}_{min}, \boldsymbol{E}^{sc}_{max})$ and $(\boldsymbol{P}^{sc}_{min}, \boldsymbol{P}^{sc}_{max})$ from the rule-based charging policy (4.10).

At moments when production is expected to be high, during noon, the controller reserves power and energy in the battery to charge for the self-consumption objective, which can be discharged at times when expected consumption is higher, mainly in the evening. Less power is reserved during the night, as less consumption is expected at these times.

The expected value of self-consumption during this day is 0.81 €, while from frequency control with $r = 5.65$ kW capacity at 14.71 €/MW/h, revenues are 2.00 €. In total, this gives a value of 2.81 €. When using the BESS only for self-consumption, the expected value is only 0.94 €. When using the BESS only for frequency control, the reserve capacity is a bit higher: $r = 6.37$ kW, and total revenues are 2.25 €. The revenues of the combined optimisation are thus more about 3 times higher compared to the case of only self-consumption and 25 % higher compared to solely frequency control.[1]

Figure 4.5 shows the total revenues and the break-down into a part from self-consumption and a part from frequency control, for varying R1 prices. A trade-off between frequency control and self-consumption is clearly visible, as with increasing reserve capacity prices a larger part of the battery is reserved for frequency control and consequently, revenues from self-consumption decrease.

4.7 Conclusion

In this paper, we have presented a framework for stochastic co-optimisation of primary frequency control and self-consumption with a battery energy storage

[1] At the time of writing this paper, in 2017, the FCR prices where around 14.71 €/MW/h. Current FCR prices have decreased to 11.5 €/MWh and using the BESS only for frequency control would result in 1.76 € of revenues. Rerunning the optimisation with this lower FCR price, gives and optimal FCR capacity of 5.58 kW with 1.54 € of FCR revenues and 0.83 € of revenues from self-consumption revenues. Together, this gives a total of 2.38 €, which is 35 % higher compared to only doing frequency control, and 2.5 times the value of only doing self-consumption. This analysis shows how combining these applications can be used as an effective hedge against changing market prices

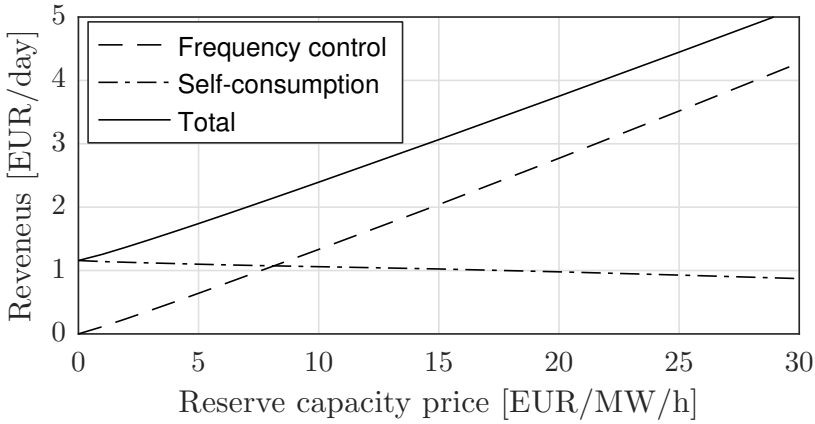

Figure 4.5: Revenues from combined frequency control and self-consumption in function of the reserve capacity price for the simulated day in March.

system.

Using robust optimisation as a safe, tractable approximation to chance-constraints, we have design a linear recharging strategy that allows one to make the risk of unavailability arbitrarily small, while keeping the problem efficiently solvable. Simulations with real frequency data show the performance of the recharging controller when converted to an equivalent state feedback controller.

We have adopted a rule-based controlled to maximizing self-consumption, which allows to reserve more energy and battery power on moments when expected consumption or production is higher, while using other moments for recharging from primary frequency control. A sample average approximation is used to estimate the expected value of self-consumption and perform the trade-off between self-consumption and primary frequency control.

We have performed a case study on a residential battery system. The results show that there is a clear complementary in combining frequency control with self-consumption. Our co-optimisation adds 25% of value compared to the use for frequency control alone, while increasing value times 3 when compared to self-consumption alone.

Interesting future work is to look into non-linear recharging policies for frequency control, e.g. by direct policy search. Incorporating a more accurate battery model, where efficiencies and power limits can be dependent on the state of charge will represent reality better. One could also incorporate the costs

of energy when providing frequency control into the model in a stochastic manner, in analogy to the way we treated self-consumption. While this paper only considers self-consumption and frequency control, other services, such as peak shaving, time of use tariff optimisation or voltage control could also be incorporate into the optimisation model. Finally, validation of the battery control strategies on a real battery system should be performed.

Chapter 5

Combining Frequency Control and Peak Shaving with Battery Storage Systems

---

Optimal Combination of Frequency Control and Peak Shaving with Battery Storage Systems

Jonas Engels, Bert Claessens and Geert Deconinck

Published in IEEE Transactions on Smart Grid (Early Access), December 2019

The first author is the main author of the article. The contributions of the first author include the literature review, the development of the optimisation problem, the analysis of the simulation results, and the writing of the article.

©2019 IEEE. Reprinted, with permission.

Abstract:

Combining revenue streams by providing multiple services with battery storage systems increases profitability and enhances the investment case. In this work,

we present a novel optimisation and control framework that enables a storage system to optimally combine the provision of primary frequency control services with peak shaving of a consumption profile.

We adopt a dynamic programming framework to connect the daily bidding in frequency control markets with the longer term peak shaving objective: reducing the maximum consumption peak over an entire billing period. The framework also allows to aggregate frequency control capacity of multiple batteries installed at different sites, creating synergies when the consumption profile peaks occur on different times.

Using a case study of two batteries at two industrial sites, we show that the presented approach increases net profit of the batteries significantly compared to using the batteries for only peak shaving or frequency control.

5.1 Introduction

Battery energy storage systems installed behind the meter at the consumer's premises can be used for a variety of different services [166]. Often, the purpose of such a BESS is to decrease the energy costs of the consumer by optimising the charging schedule of the BESS towards their energy tariff. In case the consumer faces peak demand charges, usually a part of grid tariffs, performing peak shaving with the BESS, i.e. reducing the consumer's power consumption peak, is an effective way to decrease energy costs [167].

A BESS installed behind the meter can also be used to provide ancillary services, such as frequency control, to the TSO. Especially primary frequency control (of frequency containment reserves) and frequency regulation services are seen to be a good match for a BESS, as the service provides a relatively high remuneration [133], requires only a short duration of activation and a fast response, all of which a BESS can provide without problems [76].

By using the BESS for both energy tariff optimisation and frequency control service, one can combine both revenue streams, increase profitability and build a stronger business case for the investment in the BESS. However, having a BESS providing both services concurrently is not straightforward from a control and optimisation perspective. One faces a trade-off, as using the BESS more for frequency control will decrease its peak shaving potential, which can be optimised.

5.1.1 Frequency Control with a BESS

The focus of this paper will be on primary frequency control services or frequency containment reserves, as defined by ENTSO-E [24], as it are mainly FCR markets that have been opening up for third parties in Europe. Nevertheless, the presented methodology could also be applied to other types of frequency control and frequency regulation.

When participating in FCR, one sells a certain amount of symmetric FCR capacity r to the TSO which has to be available during the entire contracted period. In FCR, one has to adjust its power P^{FCR} proportionally to deviations of the grid frequency $f(t)$ from the nominal grid frequency f_{nom} (50 Hz in Europe), so that the sold FCR capacity r is reached when the frequency deviation is at a predefined maximum Δf_{max} (= 200 mHz in the Continental Europe synchronous region): $P^{FCR}(t) = r\Delta f(t) = r(f(t) - f_{nom})/\Delta f_{max}$. In line with the recent changes in the German FCR market *Regelleistung* [26, 168], we assume a daily bidding process with daily auctions.

When delivering FCR with a BESS for a while, the battery can become full or empty at which point it is unable to provide the symmetric FCR service any further. Therefore, a SoC control strategy, or *recharge* controller, which manages the SoC to ensure the BESS can delivery the FCR capacity for the entire contract period, is necessary [134].

5.1.2 Peak Shaving

Grid tariffs for commercial and industrial consumers usually consist of an energy charge (in €/kWh) and a demand charge c_{peak} (in €/kW), where the latter is a charge proportional to the highest metered consumption peak during the billing period [61]. Such demand charges are typically used to recover the capacity-based costs of the network infrastructure, and are foreseen to become increasingly important with a growing share of distributed generation [169]. With this tariff structure, a BESS can reduce network costs by discharging at the moments when the site is consuming its maximum power and charging when the site is consuming less, thereby reducing the site's metered consumption peak.

In practice, the highest metered consumption corresponds to the highest n-minute averaged power of the site, as usually energy meters with an n-minute resolution are used for settlement. In this work, we consider demand charges proportional to the maximum quarter-hourly average power over one month, corresponding the German network tariff structure [170].

5.1.3 Related Literature

Work in [171–174] shows the ability and estimates the value of BESSs performing peak shaving. Other work [107, 110, 175] has been devoted to BESSs providing frequency control services and the design of a recharge controller.

Few authors however have looked at the combination of both services. Braeuer et al. [176] perform a high-level economic analysis of BESSs combining peak shaving with frequency control. A similar approach is followed in [177], but with the peak shaving objective formulated as a hard network constraint, rather than implicitly through a demand charge. Both papers indicate a significant added value in combining both services, however they assume perfect hindsight of the stochastic variables and do not develop a controller able to deliver the combination of services in day-to-day operation.

This work fills this gap by presenting an operational control framework that enables a BESS to successfully combine peak shaving with frequency control services. The presented method extends our previous work on frequency control with BESSs [111], by adding the peak shaving objective using dynamic programming and a customised stochastic optimisation objective. The main contributions of this paper are:

- A novel stochastic optimisation and control framework that is able to optimally combine frequency control with peak shaving objectives using a BESS.
- A methodology which can be applied to efficiently aggregate frequency control capacity of multiple BESSs at different sites.
- A case study of two real industrial sites which shows that the presented approach increases value of the BESS compared to using the BESS for only a single objective.

5.2 Optimisation and Control Framework

In this section, we describe the optimisation and control framework to combine peak shaving and frequency control with a BESS at a particular site, of which Figure 5.1 shows a schematic overview. In an FCR market with daily auctions, one has to decide every day d on the FCR capacity r_d one wants to sell. In the proposed framework, we make this decision through a stochastic optimisation problem (5.13). The results of this optimisation are then used in the real-time

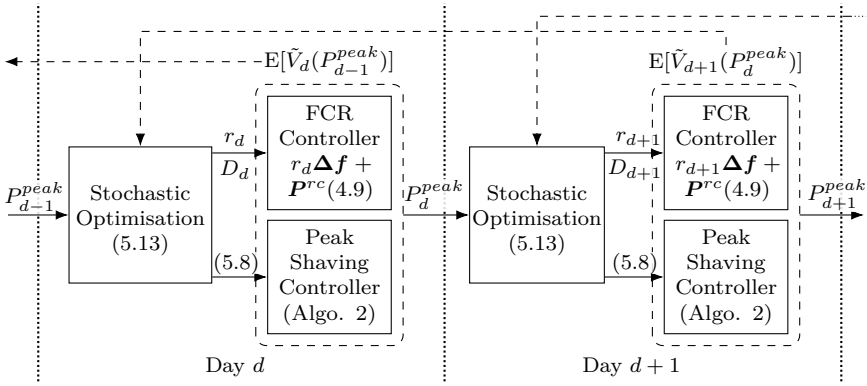

Figure 5.1: Overview of the dynamic programming-based optimisation and control framework to combine peak shaving and frequency control with a BESS.

FCR and peak shaving controllers. The observed peak power P_d^{peak} at the end of day d is used in the optimisation of the next day $d+1$.

We start this section by describing the optimisation and control of a BESS for frequency control only during one day. Subsequently, we explain how we add the peak shaving objective in the optimisation problem and propose a real-time peak shaving controller. Finally, we elaborate how we extend the peak shaving objective from one day towards the required timescale of one month using dynamic programming and value function approximations $\tilde{V}_{d+1}(P_d^{peak})$.

We employ a BESS model with constant charging and discharging efficiencies η^c, η^d, discretised with time step Δt:

$$E_{min} \leq E_k^{bat} \leq E_{max}, \quad P_{min} \leq P_k^{bat} \leq P_{max}, \tag{5.1a}$$

$$E_{k+1}^{bat} = E_k^{bat} + (\eta^c [P_k^{bat}]^+ - \frac{1}{\eta^d}[-P_k^{bat}]^+)\Delta t, \tag{5.1b}$$

where P_k^{bat}, E_k^{bat} are the power and energy content of the BESS at time step k respectively.

5.2.1 Frequency Control Framework

The frequency control framework we use in this paper is an extension of the robust optimisation presented in our previous work [111], which we will shortly summarise here. For detailed information, the reader is referred to the original paper.

The goal here is to define both the amount of frequency control capacity r the BESS can provide during one day and the power of the recharge controller $\boldsymbol{P}^{rc} \in \mathbb{R}^{n_t}$ that ensures the BESS stays within its SoC boundaries when delivering the FCR service. As the frequency deviation profile $\boldsymbol{\Delta f} \in \mathbb{R}^{n_t}$ is inherently stochastic, the energy $\boldsymbol{E}^{bat}$ and recharge power $\boldsymbol{P}^{rc}(\boldsymbol{\Delta f})$, which are dependent on the frequency profile, are also stochastic. The optimisation, maximising revenues from providing frequency control capacity r at a price c^{FCR}, can then be formulated as a chance-constrained problem:

$$\min \quad -c^{FCR} r \tag{5.2a}$$

$$\text{s.t.} \quad \boldsymbol{P}^{bat} = \boldsymbol{P}^{rc} + r\boldsymbol{\Delta f}, \tag{5.2b}$$

$$1 - \epsilon \leq \Pr\{E_{min} \leq \boldsymbol{E}^{bat}\}, \tag{5.2c}$$

$$1 - \epsilon \leq \Pr\{\boldsymbol{E}^{bat} \leq E_{max}\}, \tag{5.2d}$$

$$1 - \epsilon \leq \Pr\{P_{min} + r \leq \boldsymbol{P}^{rc}\}, \tag{5.2e}$$

$$1 - \epsilon \leq \Pr\{\boldsymbol{P}^{rc} \leq P_{max} - r\}, \tag{5.2f}$$

$$E_{k+1}^{bat} = E_k^{bat} + (\eta^c [P_k^{bat}]^+ - \frac{1}{\eta^d}[-P_k^{bat}]^+)\Delta t. \tag{5.2g}$$

We solve (5.2) using robust optimisation [148], as it generates a safe approximation to (5.2c)-(5.2f) while allowing to make ϵ arbitrary small and retaining a tractable and efficiently solvable second-order cone problem (SOCP). To achieve this, a couple of reformulations are needed.

Battery Efficiency

To avoid the integer variables resulting from the $[\cdot]^+$ operators in (5.2g), we set the efficiencies in the constraint (5.2g) itself to $\eta^c = \eta^d = 1$. In turn, we incorporate the efficiencies into the frequency deviations when discretising them:

$$\Delta f_k = \frac{1}{\Delta t} \int_{(k-1)\Delta t}^{k\Delta t} \Big(\eta^c \big[\Delta f(t)\big]^+ - \frac{1}{\eta^d} \big[-\Delta f(t)\big]^+ \Big) dt. \tag{5.3}$$

In our previous work [111], we showed that this approximation does not lead to violations of the constraints when $\eta^c, \eta^d < 1$.

Recharge Controller

The recharge power $\boldsymbol{P}_{rc}$ in (5.2) has to ensure the probabilities of (5.2c)-(5.2f) are satisfied. As the frequency deviations $\boldsymbol{\Delta f}$ are gradually revealed over time, we can have $\boldsymbol{P}_{rc}$ be dependent on the n_{rc} past frequency deviations: $P_k^{rc} = \pi^k(\Delta f_{[k-n_{rc}]^+}, \ldots, \Delta f_{k-1})$, with π^k a policy at time step k. As an optimisation over functions π^k is generally intractable, we limit ourselves to a linear policy:

$$P_k^{rc} = \sum_{i=[k-n_{rc}]^+}^{k-1} d_{ki}\Delta f_i, \quad \boldsymbol{P}^{rc} = D\boldsymbol{\Delta f}, \tag{5.4}$$

with d_{ki} the coefficients of the recharge strategy, contained in the lower triangular matrix $D \in \mathbb{R}^{n_t \times n_t}$.

As this recharging policy will be calculated with the efficiencies incorporated in the frequency signal (5.3) and not in the battery model itself, the policy will not be directly applicable to a real battery system with $\eta^c, \eta^d < 1$. However, following [149], such a linear disturbance feedback policy can be transformed into an equivalent state-feedback policy:

$$\boldsymbol{P^{rc}} = (I_{n_t} + \frac{1}{r}D)^{-1}\frac{1}{r}D\boldsymbol{\Delta E^{bat}}, \tag{5.5}$$

with $\Delta E_k^{bat} = (E_k^{bat} - E_{k-1}^{bat})/\Delta t$. In this form, the recharge power reacts on the past states, which include the effect of the actual efficiency losses and other non-linearities of the BESS.

Robust Reformulation

With the adaptations described above, we can use robust optimisation to create a safe approximation of the chance constraints (5.2c)-(5.2f). The idea is to design an uncertainty set of frequency deviations $\boldsymbol{\Delta f} \in \mathcal{F}_\epsilon$, against which each of the constraints (5.2c)-(5.2f) have to be satisfied at all times:

$$\max_{\boldsymbol{\Delta f} \in \mathcal{F}_\epsilon} \boldsymbol{a_i}^T \boldsymbol{\Delta f} \leq b_i, \qquad i = 1, \ldots, n_c, \tag{5.6}$$

with $(\boldsymbol{a_i}, b_i)$ defined to represent one constraint and $n_c = 4n_t$ the total number of constraints in (5.2c)-(5.2f).

Chen et al. show in [159] that an asymmetric uncertainty set based on forward $\sigma_{f_k}(\Delta f_k)$ and backward $\sigma_{b_k}(\Delta f_k)$ deviations, which can be estimated from samples of Δf_k, provides the tightest bound for small ϵ. With

$Q = \text{diag}(\sigma_{f1}, \ldots, \sigma_{fn_t})$ and $R = \text{diag}(\sigma_{b1}, \ldots, \sigma_{bn_t})$, we can reformulate the constraints (5.6) into the following second-order cone constraints:

$$\boldsymbol{a_i}^T \overline{\boldsymbol{\Delta f}} + \sqrt{-2\ln\epsilon}\|\boldsymbol{u_i}\|_2 \leq b_i, \qquad i = 1, \ldots, n_c, \tag{5.7}$$

where $\boldsymbol{u_i} = \max(Q\boldsymbol{a_i}^T W^{-1}, -R\boldsymbol{a_i}^T W^{-1})$, with the maximum taken element-wise and $W^T W = \Sigma_{\boldsymbol{\Delta f}}^{-1}$ the Cholensky decomposition of the inverse of the covariance matrix $\Sigma_{\boldsymbol{\Delta f}}$ of $\boldsymbol{\Delta f}$. We refer to our previous work [111] or Section 4.4.3 for the details on the derivation of (5.7).

With these reformulations, (5.2) becomes a tractable second-order cone problem, which can be readily solved by various commercial and non-commercial solvers.

5.2.2 Combining Peak Shaving and Frequency Control

When adding the peak shaving objective to the optimisation (5.2), one has to ensure the chance constraints (5.2c)-(5.2f) are still satisfied. To achieve this, we split the BESS into two virtual batteries: one for peak shaving and one for frequency control. By constraining the virtual battery for frequency control to (5.7), it is ensured (5.2c)-(5.2f) are satisfied. Besides, by intelligently shaping virtual battery boundaries, one can obtain synergies. For instance, one can reserve less recharge power and hence more power for peak shaving at the moments when consumption peaks are expected, and compensate for this at the moments where consumption is expected to be low.

For a specific FCR capacity r and recharge policy D, equation (5.6) allows to calculate the minimum and maximum power $(\boldsymbol{P}_{min}^{FCR}, \boldsymbol{P}_{max}^{FCR})$ and energy $(\boldsymbol{E}_{min}^{FCR}, \boldsymbol{E}_{max}^{FCR})$ capacity needed to perform frequency control at any time step k. The remaining power and energy capacity of the BESS can then be used to perform peak shaving:

$$\boldsymbol{P}_{min}^{ps} = P_{min} - \boldsymbol{P}_{min}^{FCR}, \quad \boldsymbol{P}_{max}^{ps} = P_{max} - \boldsymbol{P}_{max}^{FCR}, \tag{5.8a}$$

$$\boldsymbol{E}_{min}^{ps} = E_{min} - \boldsymbol{E}_{min}^{FCR}, \quad \boldsymbol{E}_{max}^{ps} = E_{max} - \boldsymbol{E}_{max}^{FCR}. \tag{5.8b}$$

Let $\boldsymbol{P}^{ps}$ and $\boldsymbol{E}^{ps}$ be the power and energy profile of the part of the BESS used for peak shaving and $\boldsymbol{P}^{prof}$ the consumption profile of the site. The combined optimisation, maximising frequency control revenues and minimising the expected maximum power consumption of the site, can then be formulated

as:

$$\min \quad \mathrm{E}[c^{peak}P^{peak} + C^{elec}] - c^{FCR}r, \tag{5.9a}$$

$$\text{s.t.} \quad P^{peak} = \max(P_0^{grid}, \ldots, P_{n_t}^{grid}), \tag{5.9b}$$

$$\boldsymbol{P}^{grid} = \boldsymbol{P}^{prof} + \boldsymbol{P}^{ps} + (D + rI_{n_t})\boldsymbol{\Delta f}, \tag{5.9c}$$

$$C^{elec} = c_{elec}\left(\boldsymbol{P}^{ps} + (D + rI_{n_t})\,\boldsymbol{\Delta f}\right)\Delta t, \tag{5.9d}$$

$$P_{min} \leq \boldsymbol{P}_{min}^{ps} \leq \boldsymbol{P}^{ps} \leq \boldsymbol{P}_{max}^{ps} \leq P_{max}, \tag{5.9e}$$

$$E_{min} \leq \boldsymbol{E}_{min}^{ps} \leq \boldsymbol{E}^{ps} \leq \boldsymbol{E}_{max}^{ps} \leq E_{max}, \tag{5.9f}$$

$$(5.1\text{b}),\ (5.7),\ (5.8), \tag{5.9g}$$

with c_{elec} the per unit energy cost.

5.2.3 Stochastic Optimisation

The expected value operator in the objective (5.9a) depends on the stochastic consumption profile $\boldsymbol{P}^{prof}$ and frequency deviation profile $\boldsymbol{\Delta f}$ and thus concerns an n_t-dimensional integration, which is intractable in practice. To approximate the expected value operator, one can use a SAA [120] by taking the empirical mean over iid samples or *scenarios* of the stochastic variables. With $\boldsymbol{P}_j^{prof}$, $\boldsymbol{\Delta f}_j$ the j-th iid consumption profile and frequency deviation sample respectively, $j = 1, \ldots, n_{sc}$, and $p_j = 1/n_{sc}$ the probability of scenario j, one can approximate the expected value operator as follows:

$$\mathrm{E}[-P^{peak} + C^{elec}] \approx \sum_{j=1}^{n_{sc}} p_j \left(c^{peak}P_j^{peak} + C_j^{elec}\right), \tag{5.10a}$$

where:

$$P_j^{peak} = \max\left(\boldsymbol{P}_j^{prof} + \boldsymbol{P}_j^{ps} + (D + rI_{n_t})\,\boldsymbol{\Delta f}_j\right), \tag{5.10b}$$

$$C_j^{elec} = c_{elec}\left(\boldsymbol{P}_j^{ps} + (D + rI_{n_t})\,\boldsymbol{\Delta f}_j\right)\Delta t. \tag{5.10c}$$

Interference Peak Shaving and Frequency Control

In case a positive frequency control power is required ($\Delta f_{k,j} > 0$) when the consumption of the site is high, this could increase the peak consumption P^{peak}

of the site. Using (5.10) in the optimisation problem (5.9) would then result in a peak shaving power $P_{k,j}^{ps}$ which completely compensates for the frequency control power: $P_{k,j}^{ps} = -r\Delta f_{k,j}$. This means that in practice, no frequency control power has been delivered to the grid.

To prevent this interference in the optimisation, the peak shaving power $\boldsymbol{P}_j^{ps}$ should be independent of the required frequency control power $r\boldsymbol{\Delta f}_j$. We achieve this by sampling the frequency profile $\boldsymbol{\Delta f}$ separately from the consumption profile $\boldsymbol{P}^{prof}$ and have each peak shaving power scenario $\boldsymbol{P}_j^{ps}$ dealing with all frequency deviation samples. Let $v = 1, \ldots, n_v$ and $w = 1, \ldots, n_w$ be the index of the consumption profile samples $\boldsymbol{P}_v^{prof}$ and frequency deviation samples $\boldsymbol{\Delta f}_w$, respectively, then:

$$P_j^{peak} = \max\left(\boldsymbol{P}_v^{prof} + \boldsymbol{P}_v^{ps} + (D + rI_{n_t})\,\boldsymbol{\Delta f}_w\right), \tag{5.11a}$$

$$C_j^{elec} = c_{elec}\left(\boldsymbol{P}_v^{ps} + (D + rI_{n_t})\,\boldsymbol{\Delta f}_w\right), \tag{5.11b}$$

$$p_j = p_v^{prof} p_w^{\Delta f}, \tag{5.11c}$$

$$j := vn_w + w, \quad v = 1, \ldots, n_v, \quad w = 1, \ldots, n_w.$$

Here, $j = 1, \ldots n_{sc}$, with $n_{sc} = n_w n_v$, is the index used in the SAA objective (5.10a), p_v^{prof} the probability of the consumption profile scenario w and $p_w^{\Delta f}$ the probability of the frequency deviation scenario v. With this approach, each battery peak shaving power scenario $\boldsymbol{P}_v^{ps}$ is able to reduce the peak of the corresponding consumption profile $\boldsymbol{P}_v^{prof}$, but also has to deal with all frequency deviation profiles $\boldsymbol{\Delta f}_w$ in the optimisation.

Scenario Reduction

As the SAA objective (5.10a) converges to the true value with a rate of $O(1/n_{sc})$ [120], a high number of scenarios are needed to reach an acceptable accuracy. To reduce the number of scenarios and increase computational efficiency, we employ the *fast forward selection* algorithm presented by Heitsch and Römisch [178]. The original fast forwards selection algorithm is a heuristic to minimise the Kantorovich distance $D_K(\Omega, \Omega_r)$ between an original set of scenarios Ω and a new, reduced set of scenarios $\Omega_r \subset \Omega$:

$$D_K(\Omega, \Omega_r) = \sum_{\boldsymbol{\omega} \in \Omega \setminus \Omega_r} p_{\boldsymbol{\omega}} \min_{\boldsymbol{\omega}' \in \Omega_r} c(\boldsymbol{\omega}, \boldsymbol{\omega}'), \tag{5.12}$$

with $p_{\boldsymbol{\omega}}$ the probability of scenario $\boldsymbol{\omega}$ and the cost function $c(\boldsymbol{\omega}, \boldsymbol{\omega}') = \|\boldsymbol{\omega} - \boldsymbol{\omega}'\|_2$ [179].

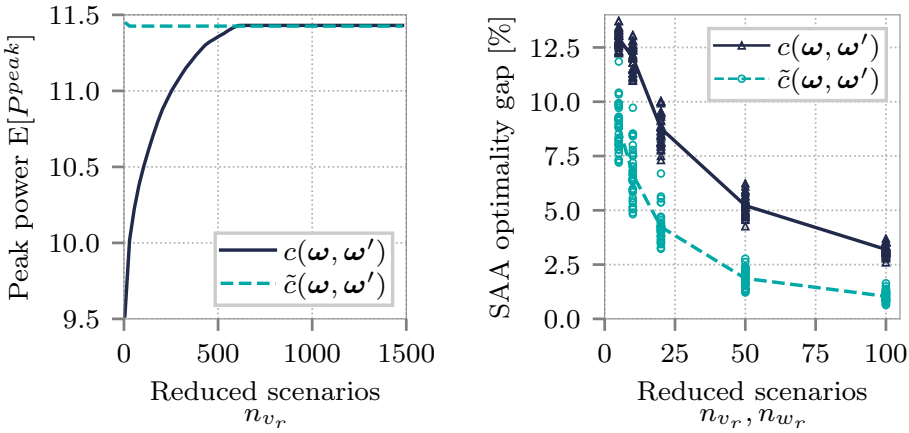

(a) E[P^{peak}] of the reduced set of consumption profile samples.

(b) SAA optimality gap when solving problem (5.9) with $n_{v_r} = n_{w_r}$.

Figure 5.2: (a) When reducing 1500 idd consumption profile samples to n_{v_r} scenarios, the generic cost function $c(\boldsymbol{\omega}, \boldsymbol{\omega}')$ introduces a significant bias in E[P^{peak}] which the proposed cost function $\tilde{c}(\boldsymbol{\omega}, \boldsymbol{\omega}')$ is able to eliminate. (b) The proposed cost function $\tilde{c}(\boldsymbol{\omega}, \boldsymbol{\omega}')$ also reduces the SAA optimality gap when solving problem (5.9) with $n_{v_r} = n_{w_r}$ reduced scenarios.

Figure 5.2a shows the expected peak power E[P_{peak}] during one day when reducing the number of scenarios using the generic cost function $c(\boldsymbol{\omega}, \boldsymbol{\omega}')$ in the fast forward selection algorithm. As one can see, the method introduces a significant bias when reducing to less than 600 scenarios. It has been noted previously in the literature [180] that using a cost function that is better able to capture the effect of adding a scenario on the objective of the problem can improve performance. As our objective function (5.10a) involves the maximum value of a scenario, we propose the following cost function in (5.12):

$$\tilde{c}(\boldsymbol{\omega}, \boldsymbol{\omega}') = |\max(\boldsymbol{\omega}) - \max(\boldsymbol{\omega}')| \,.$$

As the dashed line in Figure 5.2a shows, this new cost function is able to eliminate the bias on E[P_{peak}] almost completely.

To prevent the interference between peak shaving and frequency control objectives discussed above, we separately sample the consumption profiles $\boldsymbol{P}_v^{prof}$ and frequency deviations $\boldsymbol{\Delta f}_w$ and reduce them to $\boldsymbol{P}_{v_r}^{prof}$ with probability p_{v_r}, $v_r = 1, \ldots, n_{v_r}$ and $\boldsymbol{\Delta f}_{w_r}$ with probability p_{w_r}, $w_r = 1, \ldots, n_{w_r}$, respectively. We then combine the reduced scenarios as in (5.11), so that in total $n_{sc_r} = n_{v_r} n_{w_r}$ and $p_{j_r} = p_{v_r} p_{w_r}$ in (5.10a).

Finally, Figure 5.2b shows the optimality gap of (5.10) due to the SAA, calculated according to [114], when reducing 1500 iid consumption and frequency deviation samples to n_{v_r} and n_{w_r} scenarios. The proposed cost function $\tilde{c}(\boldsymbol{\omega}, \boldsymbol{\omega'})$ decreases the SAA optimality gap with around 50 % for a same number of reduced scenarios, increasing computational efficiency.

5.2.4 Non-Anticipative Peak Shaving Controller

When solving the stochastic optimisation problem (5.9) as described in the paragraphs above, one actually solves a two-stage stochastic problem. In a first stage, one decides on the FCR capacity r, the recharge policy D and the peak shaving boundaries $(\boldsymbol{E}^{ps}_{min}, \boldsymbol{E}^{ps}_{max}, \boldsymbol{P}^{ps}_{min}, \boldsymbol{P}^{ps}_{max})$. In the second stage, one optimises the peak shaving power $\boldsymbol{P}^{ps}_{v_r}$ with complete (perfect hindsight) knowledge of the consumption profile $\boldsymbol{P}^{prof}_{v_r}$. In reality however, the consumption profile is only gradually revealed over time. Hence, the second stage solution is not usable in practice and a non-anticipative, potentially suboptimal, peak shaving control algorithm will be required.

Examples of such controllers vary from simple, rule-based controllers [171] to model predictive control [172] and more complex dynamic programming methods [174]. The optimisation and control framework proposed in this paper allows the use of any of these control algorithms. However, to limit the scope of this paper we restrict ourselves to a rather simple, parametrised rule-based peak shaving policy.

Algorithm 2 shows the proposed rule-based peak shaving controller. The controller discharges the battery every time k the grid power $\hat{P}^{grid}_k$ surpasses a threshold P_{thr} and recharges the battery every time $\hat{P}^{grid}_k$ goes below this threshold.

The battery power due to the frequency control $(D + rI_{n_t})\boldsymbol{\Delta f}$ can induce additional power peaks, which we want to avoid as much as possible without hampering the actual FCR delivery. Therefore, in step 5, we compute a statistic of the FCR power to be delivered: the average FCR power $\overline{P^{FCR}_k}$ plus a factor z_σ times the standard deviation of the FCR power $s^{P_{FCR}}_k$, which we add to the consumption profile P^{prof}_k to obtain a modified grid power profile $\hat{P}^{grid}_k$, which is compared with the threshold P_{thr} in step 6.

Steps 8 and 10 ensure that $\boldsymbol{P}^{ps}, \boldsymbol{E}^{ps}$ stay within the peak shaving boundaries $(\boldsymbol{E}^{ps}_{min}, \boldsymbol{E}^{ps}_{max}), (\boldsymbol{P}^{ps}_{min}, \boldsymbol{P}^{ps}_{max})$. Finally, step 13 updates the threshold P_{thr} if the battery was unable to keep the modified grid power $\hat{P}^{grid}_k$ below the threshold P_{thr}.

Algorithm 2 Rule-based peak shaving controller

Parameters: P_{thr}^{init}, z_σ.
Input: $r, D, \boldsymbol{E}_{max}^{ps}, \boldsymbol{E}_{min}^{ps}, \boldsymbol{P}_{max}^{ps}, \boldsymbol{P}_{min}^{ps}$.

$P_{thr} \leftarrow P_{thr}^{init}$.
$\overline{\boldsymbol{P}^{FCR}} \leftarrow (D + rI_{n_t})\overline{\boldsymbol{\Delta f}}$.
$\boldsymbol{s}^{P^{FCR}} \leftarrow std\big[(D + rI_{n_t})\boldsymbol{\Delta f}\big]$.
for each time step $k = 1 \dots n_t$ **do**
  $\hat{P}_k^{grid} \leftarrow P_k^{prof} + \overline{P_k^{FCR}} + z_\sigma s_k^{P_{FCR}}$.
  $P_k^{ps} \leftarrow P_{thr} - \hat{P}_k^{grid}$.
  if $P_k^{ps} < 0$ **then** ▷ Discharge Battery
    $P_k^{ps} \leftarrow \max(P_k^{ps}, P_{min,k}^{ps}, \eta_d(E_{min,k+1}^{ps} - E_k^{ps})\Delta t)$,
  else ▷ Charge Battery
    $P_k^{ps} \leftarrow \min(P_k^{ps}, P_{max,k}^{ps}, \frac{1}{\eta_c}(E_{max,k+1}^{ps} - E_k^{ps})\Delta t)$.
  $E_{k+1}^{ps} \leftarrow E_{k+1}^{ps} + \eta_c \left[P_k^{ps}\right]^+ - \frac{1}{\eta_d}\left[-P_k^{ps}\right]^+$.
  if $\hat{P}_k^{grid} + P_k^{ps} > P_{thr}$ **then** ▷ Threshold Surpassed
    $P_{thr} \leftarrow \hat{P}_k^{grid} + P_k^{ps}$.

Algorithm 2 has two parameters that can be freely chosen: P_{thr}^{init} and z_σ, which and be used to adapt the controller to a specific configuration. For a particular value of these parameters, the performance of the controller can be evaluated by simulating the controller for a large number of iid consumption and frequency samples $n_{eval} \gg n_{sc}$, calculating the objective (5.10a) and taking the empirical average over all scenarios. To find the optimum values $\hat{P}_{thr}^{init}, \hat{z}_\sigma$, we then use a simple grid search.

5.2.5 Dynamic Programming Framework

The optimisation (5.9) considered so far deals with the daily decision making required in the FCR market. However, peak demand charges look at the highest peak over an entire billing period, here one month. To deal with these different time scales, we adopt a dynamic programming framework. Starting at the end of the month, we calculate the value of the objective $V_d(P_{d-1}^{peak})$ for each day $d = 1, \dots, n_d$ of the month in function of the peak power P_{d-1}^{peak} observed until

the end of the previous day $d-1$. The daily optimisation becomes then:

$$V_d(P_{d-1}^{peak}) = \min \ \mathrm{E}[V_{d+1}(P_d^{peak}) + C_d^{elec}] - c_d^{FCR} r_d, \tag{5.13a}$$

$$\text{s.t.} \quad P_d^{peak} = \max(P_{0,d}^{grid}, \ldots, P_{n_t,d}^{grid}, P_{d-1}^{peak}), \tag{5.13b}$$

$$\boldsymbol{P}_d^{grid} = \boldsymbol{P}_d^{prof} + \boldsymbol{P}_d^{ps} + (D_d + r_d I_{n_t}) \boldsymbol{\Delta f}_d, \tag{5.13c}$$

$$\text{(5.9e) - (5.9g)}, \tag{5.13d}$$

and C_d^{elec} as in (5.10c). The peak power P_d^{peak} after day d is the maximum of $\boldsymbol{P}_d^{grid}$, the grid power of day d, and P_{d-1}^{peak}. The expected value operator in (5.13a) can be approximated using the SAA (5.10) and the scenario reduction techniques explained in section 5.2.3. The final value function V_{n_d+1} used in the objective of day n_d, the last day of the billing period is:

$$V_{n_d+1}(P_{n_d}^{peak}) = c_{peak} P_{n_d}^{peak}. \tag{5.14}$$

With the final value function V_{n_d+1} defined, we can calculate $V_d(P_{d-1}^{peak})$ for each day d by solving (5.13) recursively. However, this value function would assume the perfect hindsight solution of the second stage peak shaving problem (see section 5.2.4) and not take into account the suboptimality of a practical, non-anticipative controller. Therefore, when solving (5.13), we will instead use V_{d+1}^{rule}, the value of the objective (5.13a) at day $d+1$ evaluated using the rule-based peak shaving controller of Algorithm 2.

All elements of the dynamic programming control scheme are combined in Figure 5.1. At the start of day d, the peak power P_{d-1}^{peak} is known and used as an input into the stochastic optimisation (5.13), which uses $\tilde{V}_{d+1}^{rule}(P_d^{peak})$, a convex approximation of the value function of the next day, evaluated with the rule-based controller. Solving (5.13) gives the FCR capacity r_d and recharge controller D_d, used in the FCR recharge controller (5.5), and the peak shaving boundaries ($\boldsymbol{E}_{min,d}^{ps}, \boldsymbol{E}_{max,d}^{ps}, \boldsymbol{P}_{min,d}^{ps}, \boldsymbol{P}_{max,d}^{ps}$) from (5.8) used in the peak shaving controller of Algorithm 2.

Value Function Approximation

To solve (5.13) efficiently, we need a representation of the value function $V_{d+1}^{rule}(P_d^{peak})$ that does not jeopardise the tractability of the optimisation problem. As the minimisation in (5.13) is convex, the value function V_{d+1} is a convex function of P_d^{peak}. However, the value function $V_{d+1}^{rule}(P_d^{peak})$ is not necessarily convex, as shown in Figure 5.3, owing to the non-convex peak shaving controller from Algorithm 2.

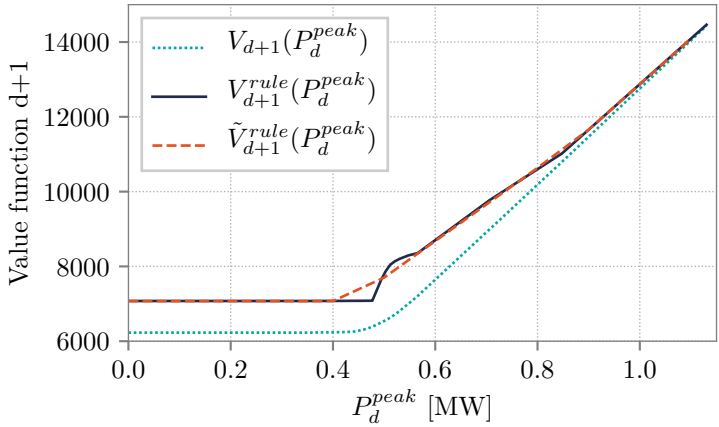

Figure 5.3: Example of $V_{d+1}(P_d^{peak})$, the value function of the optimisation (5.13), $V_{d+1}^{rule}(P_d^{peak})$, the value function with the rule-based controller, and $\tilde{V}_{d+1}^{rule}(P_d^{peak})$, the convex piecewise linear approximation hereof.

Therefore, we approximate V_{d+1}^{rule} by a convex piecewise linear function $\tilde{V}_{d+1}^{rule}(P_d^{peak})$, by a least-squares fit over the range $[0, \max(\boldsymbol{P}_{prob})]$:

$$\tilde{V}_{rule}^{d+1}(P_d^{peak}) = \max_j \left(\hat{\alpha}_j P_d^{peak} + \hat{\beta}_j\right), \tag{5.15}$$

where:

$$\hat{\alpha}_j, \hat{\beta}_j = \underset{\alpha_j, \beta_j}{\arg\min} \sum_i^{n_i} \left(y_i - V_{d+1}^{rule}(x_i)\right)^2, \tag{5.16a}$$

$$\text{s.t.} \quad y_i = \alpha_j x_i + \beta_j, \quad \forall i : x_j^b \leq x_i \leq x_{j+1}^b,$$

$$\alpha_j x_{j+1}^b + \beta_j = \alpha_{j+1} x_j^b + \beta_{j+1}, \tag{5.16b}$$

$$\alpha_j \leq \alpha_{j+1}, \quad \forall j = 1 \ldots, n_j, \tag{5.16c}$$

with n_j the number of pieces in the piecewise linear approximation, separated by the breakpoints x_j^b. Equation (5.16b) ensure the resulting piecewise function is continuous on the breakpoints x_j^b, while (5.16c) ensures convexity. The points $x_i, i = 1, \ldots, n_i$ on which the interpolation is performed are equally spread over the entire interpolation range $[0, \max(\boldsymbol{P}_{prob})]$. An example of $\tilde{V}_{rule}^{d+1}$ is also shown in Figure 5.3. To reduce the number of pieces n_j and thereby the constraints in (5.13), one can prune the pieces of which α_j and β_j are approximately equal.

5.3 Aggregating Multiple Sites

When multiple batteries are installed at different sites of which the shape of the consumption profiles are complementary, there can be added value in aggregating their frequency control capacity. For example, if one site has a high consumption peak in the morning and another site in the afternoon, the battery at the first site can do peak shaving in the morning while the battery at the second site delivers the frequency control capacity, and vice versa in the evening.

The framework for peak shaving and frequency control proposed in section 5.2 can easily be extended to incorporate multiple sites. As peak tariffs are charged to each site separately, the peak shaving objective for multiple sites is simply the sum of the peak shaving objectives of the individual sites: $\min \sum_i^{n_s} c_{peak} P_i^{peak} + C_i^{elec}$, with n_s the number of sites. With regard to frequency control, the aggregated FCR capacity r can be split into n_s FCR capacity vectors $\boldsymbol{r}_i = (r_{1,i}, \ldots, r_{n_t,i})^T$, $i = 1, \ldots, n_s$, so that the local FCR capacity can vary over time. Each site will also have its individual recharging controller D_i. Finally, the individual FCR capacities have to add up to the aggregated FCR capacity r at every time step k:

$$r = \sum_i^{n_s} r_{k,i}, \quad \forall k = 1, \ldots, n_t. \tag{5.17}$$

The dynamic programming-based control scheme of Figure 5.1 can also be used for multiple site. Because the problem is linked by (5.17), the value function of day d is a function of $P_{i,d-1}^{peak}, i = 1, \ldots, n_s$, the peak power after day $d-1$ of

every site i. The stochastic optimisation of (5.13) becomes then:

$$
\begin{aligned}
&V_d(P^{peak}_{0,d-1}, \dots, P^{peak}_{n_s,d-1}) \\
&\quad = \min \ \mathrm{E}[\tilde{V}^{rule}_{d+1}(P^{peak}_{0,d}, \dots P^{peak}_{n_s,d}) + \sum_{i=1}^{n_s} C^{elec}_{i,d}] - c^{FCR}_d r_d, \\
&\quad \text{s.t.} \quad P^{peak}_{i,d} \geq P^{prof}_{k,i,d} + P^{ps}_{k,i,d} + \sum_{l}^{k-1} d^{i,d}_{kl} \Delta f_l + r_{k,i,d} \Delta f_k, \\
&\qquad\qquad k = 1, \dots, n_k, \quad i = 1, \dots, n_s, \qquad (5.18) \\
&\quad P^{peak}_{i,d} \geq P^{peak}_{i,d-1}, \quad i = 1, \dots, n_s, \\
&\quad r_d = \sum_{i=1}^{n_s} r_{k,i,d}, \quad k = 1, \dots, n_k, \\
&\quad \text{(5.9e) - (5.9g)}, \quad i = 1, \dots, n_s,
\end{aligned}
$$

As the dimension of the state $(P^{peak}_{0,d-1}, \dots, P^{peak}_{n_s,d-1})$ of the dynamic program (5.18) is equal to the number of sites to be aggregated, the computational effort needed to solve the dynamic program increases with the number of sites considered [181]. This can partly be mitigated by solving (5.18) for multiple states in parallel. More efficient sampling of the value function, using Latin hypercube sampling [182] or orthogonal arrays [183] can further reduce the required computational effort when aggregating a larger number of sites, and interesting future work consists of analysing which of these methods show the best performance for the proposed problem.

5.4 Simulation and Results

In this section we present a case study, applying the previously presented methodology to two 1 MW, 1 MWh batteries at two industrial sites: a pumping station (site 1) and a cold store (site 2), to perform peak shaving at the sites while delivering an aggregated FCR capacity. We use real consumption data from actual industrial sites and real grid frequency measurements from the CE synchronous area. The 5th and 95th percentiles of the consumption profiles are depicted by the grey shades in Figures 5.4c and 5.4d. The average profiles are also shown. The profiles are somewhat complementary: site 1 has a high

peak around 7am and some lower peaks in the day while site 2 has the highest consumption overnight.

We assume the efficiencies at $\eta^c = \eta^d = \sqrt{90\,\%}$. We discretise each day into time steps of 15 minutes, so $\Delta t = 900\,\mathrm{s}$ and $n_t = 96$. In the second-order cone constraint (5.7), we set $\epsilon = 5 \cdot 10^{-3}$ and calculate σ_{f_k} and σ_{b_k} using four year of CE frequency data. In the stochastic optimisation (5.13), we draw 1500 iid scenarios which we reduce to $n_{v_r} = n_{w_r} = 50$ to obtain an SAA optimality gap $< 2.5\,\%$, following Figure 5.2b. We set $c^{FCR} = 12\,€/\mathrm{MW/h}, c_{peak} = 13\,000\,€/\mathrm{MW_{peak}/month}$ and $c^{elec} = 45\,€/\mathrm{MWh}$.

5.4.1 Combining Peak Shaving and Frequency Control

Figure 5.4 shows how the stochastic optimisation (5.18) succeeds in aggregating FCR capacity of the two batteries while performing peak shaving at the two sites. The two coloured areas in Figures 5.4a and 5.4b represent the FCR capacity of the sites $\boldsymbol{r}_i$, which add up to form a constant aggregated FCR capacity $r = 0.88\,\mathrm{MW}$. However, at times when consumption at site 1 is expected to be high, mainly during the day, this battery delivers less FCR capacity and has more power for peak shaving available while at site 2, which has a higher consumption at night, one can see the opposite behaviour.

The coloured lines in Figures 5.4a and 5.4b show the actual peak shaving power scenarios $\boldsymbol{P}_i^{ps}$ for different daily consumption profiles $\boldsymbol{P}_i^{prof}$ when using the rule-based peak shaving controller of Algorithm 2. The effect of this peak shaving power on the original profiles is depicted by the coloured profiles of Figures 5.4c and 5.4d. It is clear that the peak shaving power of the battery at site 1 is able to decrease the peak consumption. At site 2 it is more difficult to reduce the peak, as the energy content needed during to shave the peak in the first hours of the day can be more than the energy content of the battery. This explains the peak of the 95th percentile around 5am-6am. Nevertheless, the averaged profile with peak shaving is lower during these hours, indicating that in many scenarios the consumption power can still be reduced.

5.4.2 Dynamic Programming Framework

We will now look at the evolution of the decision making over time in the dynamic programming scheme. Figure 5.5a shows the evolution of the value function of the dynamic program (5.18) applied to the two sites, from the last day to the first day of the month. The figure shows this evolution for various values of $P_{i,d-1}^{peak}$, the sum of the maximum power observed so far at the two

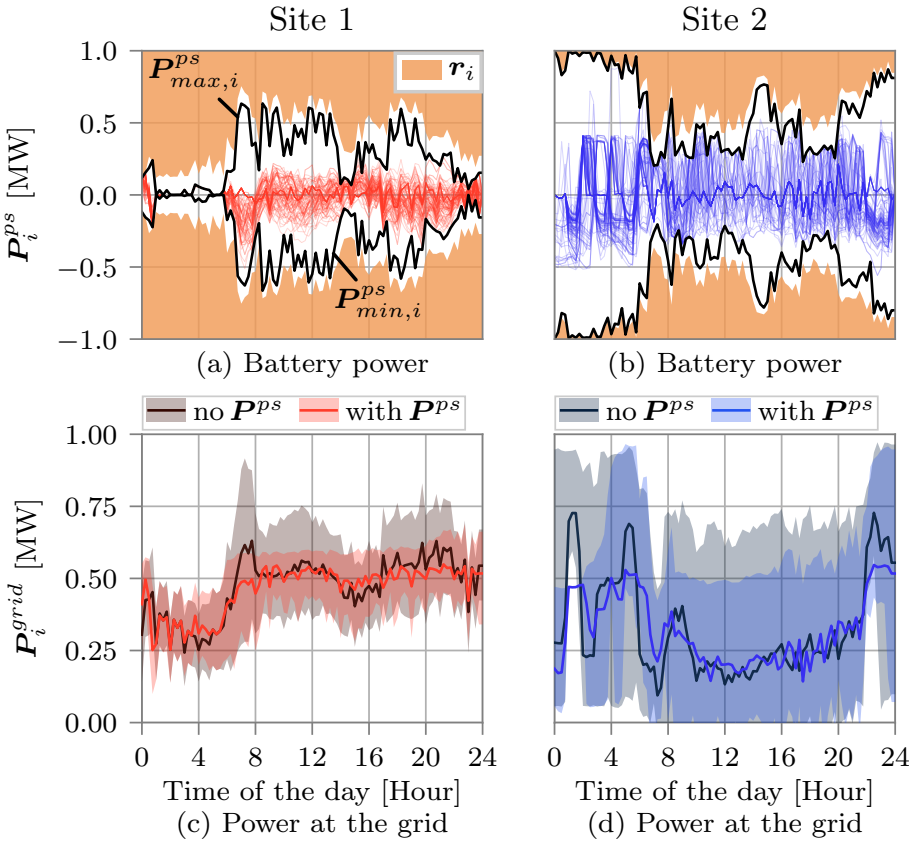

Figure 5.4: Aggregating two batteries at two sites performing peak shaving and frequency control. Each line in (a) & (b) shows the battery peak shaving power for a specific scenario, while (c) & (d) show the average (solid lines) and the 5th - 95th percentiles (shaded areas) of the grid power with and without the peak shaving from (a) & (b). The coloured area in (a) & (b) is the FCR capacity $\boldsymbol{r}_i$ of each site, which aggregated forms a constant capacity of 0.88 MW.

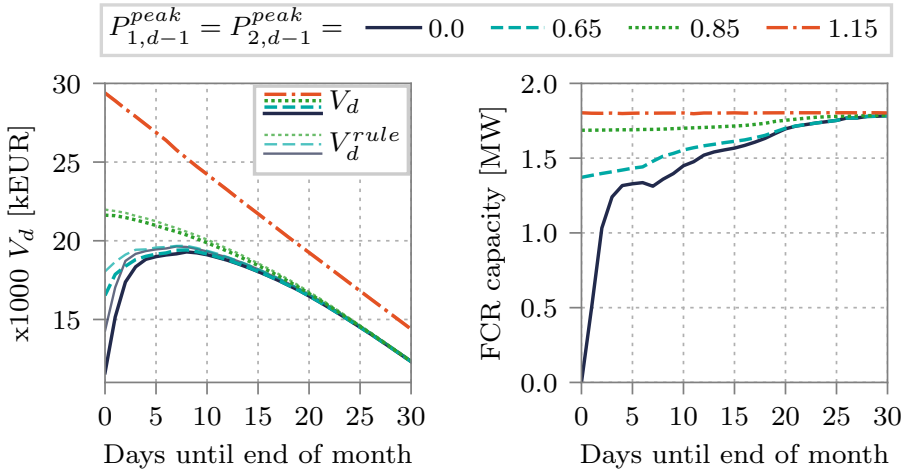

(a) Value function V_d of the optimisation (5.18) and V_d^{rule} of the rule-based controller (Alg. 2).

(b) Combined FCR capacity r_d of the two batteries at the two sites.

Figure 5.5: Evolution of (a) the value function and (b) FCR capacity r_d in function of the days left until the end of the month, for various peak powers $P^{peak}_{i,d-1}$ observed up to that day (here equal at the two sites: $P^{peak}_{1,d-1} = P^{peak}_{2,d-1}$).

sites. Figure 5.5b shows the evolution of the corresponding aggregated FCR capacity r_d, also from the last to the first day of the month.

Analysing both figures, we can draw some insightful conclusions. From Figure 5.5b, it turns out that a higher value of $P^{peak}_{i,d-1}$ results in a higher FCR capacity. In case a high value of $P^{peak}_{i,d-1}$ has been observed, there is a low probability that the consumption profile will be even higher and therefore, a larger share of the battery will be allocated for FCR. At a very high power peak $P^{peak}_{i,d-1} = 1.15$, the batteries will provide their maximum FCR capacity (1.80 MW) over the entire month. The linear decrease of the value function V_d in Figure 5.5a is thus solely due to the accumulation of FCR revenues.

Even in case $P^{peak}_{i,d-1}$ is low, the FCR capacity increases when more days remain until the end of the peak shaving period (one month). The longer the remaining period, the higher the probability on a high consumption peak which cannot be shaved successfully by the battery. Therefore, it is better not to lose the potential value from FCR and already use a major part of the battery for FCR. The value function of a low $P^{peak}_{i,d-1}$ will then decrease due to the FCR revenues, at almost the same rate as the value function of a high $P^{peak}_{i,d-1}$. When the remaining

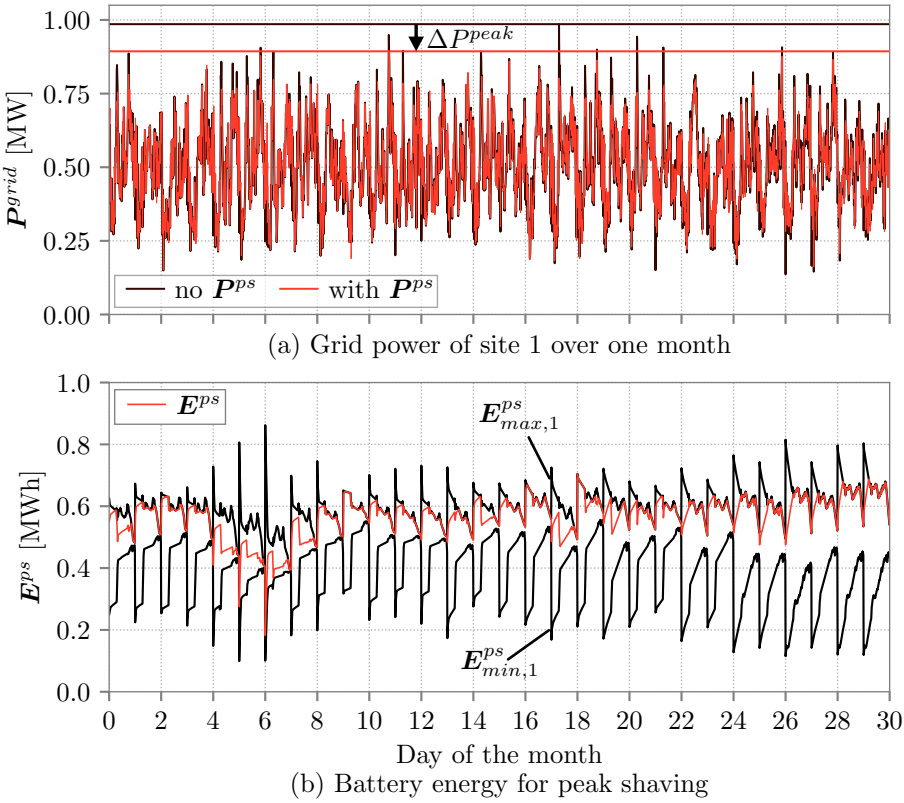

Figure 5.6: Example of peak shaving during one month at site 1. Figure (a) shows that, with the peak shaving power of the battery, the site is able to reduce its peak power with 110 kW. Figure (b) shows the corresponding actual $\boldsymbol{E}^{ps}$ and available $\boldsymbol{E}^{ps}_{max} - \boldsymbol{E}^{ps}_{min}$ energy content of the battery for peak shaving.

period shortens and $P^{peak}_{i,d-1}$ has been rather low, there is less probability a high peak will occur in the remaining period, and the FCR capacity will be reduced as a larger share of the battery will be assigned for peak shaving trying to maintaining $P^{peak}_{i,d-1}$ low. The value function decreases as the probability of a low peak over the entire month increases. Figure 5.6b, showing the peak shaving boundaries $(E_{max,ps}, E_{min,ps})$ over an entire month corresponding to the consumption profile of Figure 5.6a, also depicts this evolution. From the second half of the month, less capacity is used for FCR while the available energy for peak shaving becomes larger, trying to maintain the peak consumption at the level seen so far.

Finally, we note that the value functions V_d^{rule} of the rule-base peak shaving controller in Figure 5.5a are very close to the value functions V^d from the optimisation. Except when there are few days remaining and $P_{i,d-1}^{peak}$ is low, a state which does not occur in practice, the difference becomes larger. Hence, we can conclude that using perfect hindsight in the second stage of the stochastic optimisation is in practice a good approximation to the actual rule-based peak shaving controller.

5.4.3 Monthly Costs and Revenues

The performance of the entire control scheme can be evaluated in Table 5.1, which compares various costs components of the two sites for various cases: without batteries, with batteries performing peak shaving only, batteries performing FCR only and batteries combining FCR with peak shaving. The table gives the average of various consumption and frequency scenarios of one month. The "Peak Power" column gives the expected peak consumption power during one month of the two sites combined, while the "Average FCR Capacity" shows the averaged FCR capacity over the entire month and the "Total Net Profits" is the difference of the peak costs in the "Without Batteries" scenario and the peak and electricity costs minus the FCR revenues of the other scenarios.

Scenario	Peak Power [MW]	Peak Costs [k€]	Average FCR Capacity [MW]	FCR Revenues [k€]	Elec. Costs [€]	Total Net Profits [k€]
Without Batteries	1.91	24.9	–	–	–	–
Only Peak Shaving	1.35	17.5	–	–	197	7.2
Only FCR	2.09	27.3	1.80	15.6	118	13.1
FCR & Peak Shaving Combined	**1.96**	**25.5**	**1.76**	**15.2**	**177**	**14.4**

Table 5.1: Expected Monthly Costs and Revenues of the Two Sites With and Without Batteries.

When only performing peak shaving, the batteries are able to reduce the power peak with 560 kW, which results in a decrease of peak power costs of 7200 €.

When only performing frequency control, the batteries together provide the maximum FCR capacity of 1.80 MW during the entire month, which gives a revenue of 15 600 €. However, this also leads to an increase in peak power to 2.09 MW, reducing the net profits to 13 100 €. However, when combining FCR and peak shaving using the proposed methodology, the batteries are able to maintain the peak power at 1.96 MW, while still providing 1.76 MW of FCR capacity on average, resulting in a net profit of 14 400 €/month. In all scenarios, the additional electricity costs C^{elec} of the batteries are negligible.

5.5 Conclusion

In this paper, we have proposed a novel stochastic optimisation and control framework that is able to optimally combine peak shaving and frequency control objectives with a battery system installed behind the meter. The framework also allows to aggregate frequency control capacity of multiple batteries at different sites, thereby leveraging potential synergies.

In a case study on two 1 MW, 1 MWh batteries at two industrial sites, we show that combining peak shaving with frequency control using the proposed optimisation framework leads to an expected monthly profit of 14 400 €, which is two times the profit in case they would only perform peak shaving and around 10 % more than only performing frequency control.

Chapter 6

Impact of Distribution Grid Constraints on Low-Voltage Grid Connected Flexibility

---

Grid-Constrained Distributed Optimization for Frequency Control with Low-Voltage Flexibility

Jonas Engels, Bert Claessens and Geert Deconinck

Published in IEEE Transactions on Smart Grid, vol. 11, no. 1, pp. 612-622, January 2020

The first author is the main author of the article. The contributions of the first author include the literature review, the development of the distribution optimisation framework and the algorithm to construct the circle constraints, the execution and analysis of the case study, and the writing of the article.

©2019 IEEE. Reprinted, with permission.

Abstract:

Providing frequency control services with flexible assets connected to the low-voltage distribution grid, amongst which residential battery storage or electrical hot water boilers, can lead to congestion problems and voltage issues in the distribution grid. In order to mitigate these problems, a new regulation has been put in place in Belgium, imposing a specific constraint: in any circle with a radius of 100 m, there can be at maximum 10 connection points providing frequency control at any time. This paper presents an impact analysis and a coordination strategy of a flexibility service provider (FSP) that operates a pool of assets and is exposed to this new regulatory constraint. Results show that at 5 % participation, only 90 % of total control capacity can be used, with a large difference between neighbourhoods with different population densities. A distributed optimization framework to coordinate the assets arises naturally, in which the assets are able to keep their local cost functions private and only have to communicate with neighbouring assets that are geographically close, and with the FSP. Analysis of the proposed distributed optimization algorithm shows a clear trade-off between optimality gap, owing to the mixed-integer nature of the problem, and iterations to convergence.

6.1 Introduction

In recent years, ancillary services markets in Europe have been opening up for third party participants and non-conventional energy resources, such as battery storage or industrial demand response. The primary frequency control or frequency containment reserve market [24], where one is able to sell power capacity for primary frequency control to the transmission system operator, is one of the markets that have seen an increased participation of these new, flexible energy resources. This evolution has also fuelled interest in using flexibility from flexible residential energy resources such as domestic hot water heaters, which are connected to the low-voltage distribution grid.

As these assets are not able to participate in the FCR market by themselves, a new party, the flexibility service provider (FSP) is needed that facilitates the access of these assets to the FCR market, both in a technical and in an administrative way. The flexible FCR capacity of each of these assets is an order of magnitude smaller than the bid granularity in the FCR markets (e.g. 1 MW in Belgium [184]). Therefore, the FSP will have to put various flexibility assets together in a pool large enough to participate in the FCR market. Thereby, the FSP has to make sure that its pool of assets can provide a constant FCR capacity

for the duration of the bid (e.g. one week in Germany on the international Regelleistung bidding platform [26]).

As these new, flexible energy resources are connected to the distribution grid rather than directly to the transmission grid, the distribution system operator also becomes a stakeholder. The DSO has to make sure that the distribution grid remains within its operational constraints when these assets perform the FCR service. This is challenging, as the distribution grid has historically not been designed for these kinds of demand response actions.

In [143], it is shown that when some of these assets are located in the same area and are activated synchronously, which is usually the case when providing FCR, this can lead to congestion problems in the low-voltage distribution grid. Congestion in the distribution grid occurs when the transfer of active power over the grid exceeds the transfer capability of the grid, which is limited by the operational grid constraints: voltage limits, thermal limits of cables and transformers, the interface with the TSO and protection equipment [41].

Performing a detailed grid study on the impact of using each of these assets for FCR is too time-consuming, costly and requires detailed grid information, which is often not available. Therefore, various solutions to distribution grid congestion have been proposed in the literature, such as voltage regulation with active and reactive power control [25, 185, 186]. A local voltage droop controller is presented in [144], which is shown to be effective in avoiding distribution grid constraint violations while having very limited impact on the performance of the service to be delivered.

However, straightforward power curtailment cannot be applied to the FCR service, as this would result in non-delivery of the service to the TSO and hence into penalties for the FSP. Controlling the reactive power output of the grid-connected inverters could also reduce voltage issues [187]. However, this results in increased resistive losses as injecting additional reactive power increases the current through the cables [186]. An optimal control minimizing these losses is rather complex and requires additional control logic to be installed [187].

As these methods have their drawbacks, the DSO is looking at new regulations that are easily enforceable to avoid distribution grid problems with assets providing FCR.

The remainder of the paper is organized as follows: Section 6.2 explains the new 2018 Belgian regulation on providing FCR with low-voltage grid connected assets and motivates the distributed optimization architecture proposed in this paper. Section 6.3 describes an algorithm to construct the relevant constraints imposed by these new regulation. Section 6.4 then formulates the central optimization problem and the distributed optimization algorithm for an FSP

that is exposed to this regulation. Section 6.5 evaluates the impact of the new regulation and the performance of the distributed optimization. Finally, the paper is concluded in Section 6.6.

6.2 FCR with Low-Voltage Connected Assets in Belgium

Recently, the Belgian federation of electrical and gas network operators, Synergrid [188], has proposed a standard agreement contract between DSOs and FSPs that want to exploit flexibility on the low-voltage distribution grid for FCR services [189]. The agreement presents some constraints by which the FSP should comply in order to prevent congestion issues in the distribution grid when using the flexibility for FCR. The proposed constraints in the document are easily enforceable and do not require complicated assessments such as a detailed power flow calculation.

The two constraints imposed by Synergrid in the agreement contract are the following:

1. The maximum flexible power capacity used for FCR at one low-voltage connection point is 5 kW.
2. Within any circle with a radius of 100 m, there can be a maximum of 10 low-voltage connection points in the pool of the FSP providing flexibility for FCR at the same time.

The first constraint is straightforward and does not require further explanation. The second constraint is slightly more complicated and creates some room for optimization by the FSP. If, for instance, the FSP has 20 assets in its pool that are all located within a circle with radius of 100 m, the FSP can choose which of the 20 assets should provide the FCR capacity at each moment in time. It would then be beneficial to select the assets that can provide the *cheapest* FCR capacity at each moment in time. Besides, when assets are located in multiple circles it is not straightforward to select which assets should deliver FCR at minimal costs, as each circle imposes its constraint and all of them should be respected.

To find the cheapest FCR capacity, one has to define the cost of providing FCR capacity with a flexibility asset. This cost can include both the actual marginal cost of providing the flexibility (e.g. degradation cost of a battery providing frequency control) and the opportunity costs of using the same flexibility for

other purposes (e.g. using the battery to store locally generated PV energy). Optimizing in this way can lead to increased revenues for all parties, as synergies exist by combining flexibility for different objectives such as frequency control and electricity tariff optimization [111, 190].

6.2.1 A Distributed Optimization Framework for the FSP

As the flexible capacity from one asset connected to the distribution grid is usually rather small (and explicitly limited to 5 kW by the first constraint of Synergrid), there need to be a large number of assets in the pool of an FSP. This also means that, in case the entire optimization is performed centrally by the FSP, it can quickly become intractable due to the high number of variables and constraints [191].

A well-studied approach to mitigate this intractability is to distribute the optimization problem amongst the various assets in the FSP pool. This has the advantage that each asset only has to solve a small, local optimization problem. Besides, the assets can implement their constraints and cost functions locally, keeping this information private from the other assets and from the FSP, which is favourable from a confidentiality point of view [192]. Finally, a distributed optimization architecture arises naturally here, as the second constraint imposed by Synergrid, limiting the number of active assets in each circle of 100 m, results in a multitude of constraints, each including only neighbouring assets which are geographically close together.

In the literature, various architectures of distributed demand response aggregation have been proposed. A non-iterative, distributed approach is presented in [193], in which the assets calculate their local costs in a distributed way for each possible value of the dual variables. However, this works only in case the problem is completely decomposable in time, which is not the case here. Dual decomposition is used in [194] to aggregate demand response resources while maintaining user confidentiality. The alternating direction method of multipliers (ADMM), comparable to the distributed method proposed in this paper, is used in [195] to optimize electrical vehicle charging while taking into account maximum power constraints of the grid.

Figure 6.1 shows the distributed optimization architecture proposed in this paper, tailored to the problem of the FSP providing FCR while respecting the Synergrid constraints. Each asset performs a local optimization, maximizing their FCR revenues while taking into account their local costs and constraints. The assets share *circle constraints* with neighbouring assets that are within 200 m distance, corresponding to the circles in Synergrid's second constraint and illustrated by the red circles in the figure.

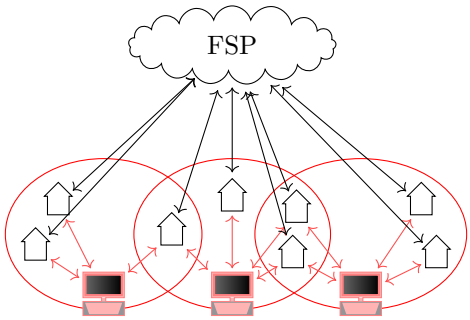

Figure 6.1: Proposed distributed optimization architecture. Each house represent a local flexibility asset and is constraint by circles with a radius of 100 m, here drawn in red. The assets communicate with the FSP and with circle constraint agents, represented by the red computers.

As the assets do not know nor can control the FCR capacity of the neighbouring assets, they cannot enforce the Synergrid's second constraint in the local optimization. Therefore, each circle constraint is assigned a *circle constraint agent*, illustrated by the red computers in Figure 6.1, that ensures there are not more than 10 assets delivering FCR at the same inside the particular circle. As one asset can be constrained by multiple circle constraints and each circle is managed by only one circle constraint agent, an asset communicates with all circle constraint agents of all circles it belongs to. In this way, it is ensured the asset respects all circle constraints they belong to. The assets also communicate with the FSP, which coordinates the assets to make sure the sum of the local FCR capacities is constant over the duration of the bidding period.

With this architecture, no entity has a global view on the central optimization problem, which is distributed amongst all relevant entities, each solving only a small, local part of the problem.

A peer-to-peer architecture, such as presented in [196], can also be achieved with the distributed optimization algorithm proposed in this paper. In such a peer-to-peer architecture, each asset would have a local implementation of all circle constraint agents of the circles constraining the asset. This eliminates the need for circle constraint agents as distinct entities, as each agent would already be implemented locally in the assets constrained by the respective circle. Instead of communicating with the circle constraint agents, an asset will then only have to communicate with neighbouring assets with which it shares a circle constraint, which are at maximum 200 m away.

Transforming the communication with the FSP into a peer-to-peer architecture,

thereby eliminating the FSP as a singly point of failure, is a bit more challenging, but can be achieved following the approaches presented in [196, 197]. In this case, copies of the calculation performed by the FSP have to be implemented locally in some or in all nodes. These nodes can then take the role of the FSP, coordinating the assets towards a constant FCR capacity for the duration of the bid. To avoid communication between all nodes (all-to-all communication) at every iteration, peer-to-peer communication can be achieved with a gossiping algorithm [196] or the distributed ADMM (D-ADMM) [197].

The distributed or the peer-to-peer architecture fits perfectly with recently proposed device-to-device communication architectures [198] and the internet of things (IoT) paradigm [199]. Low power wide area networks (LPWAN) [200] seem to be ideal candidates for this type of communication, as they have low hardware cost, low power consumption and a range largely surpassing the required 200 m.

The main contributions of this paper can be summarized as follows:

- We propose an algorithm to determine all relevant circles according to the new regulatory requirement from Synergrid, which is, to the best of our knowledge, the first time distribution grid constraints are explicitly imposed on demand response flexibility.
- We analyse the impact of these constraints on the total amount of FCR capacity that can be offered with a pool of assets connected to the distribution grid, using real data from a DSO.
- We describe the mixed-integer optimization problem of an FSP operating a pool of low-voltage grid connected assets providing FCR and present the use of a distributed optimization to solve the problem in a scalable way while keeping costs and constraints of the participating assets confidential.

6.3 Construction of Circle Constraints

To be able to implement the optimization problem of the FSP as a mathematical program, we have to translate Synergrid's second constraint into a closed mathematical expression. Therefore, we have to be able to find all circles with a radius of 100 m that contain at least one connection point. Below, we explain how we can find these circles.

We assume the geographical location of all assets or points $\mathcal{I} = \{1, \ldots, n_{\mathcal{I}}\}$ in the FSP pool is given by their two-dimensional coordinates $\boldsymbol{x}_i = (x_i^0, x_i^1)$, $i \in \mathcal{I}$ in a two-dimensional Cartesian coordinate system, such that a vector $\boldsymbol{x}_i : \|\boldsymbol{x}_i\|_2^2 = 1$

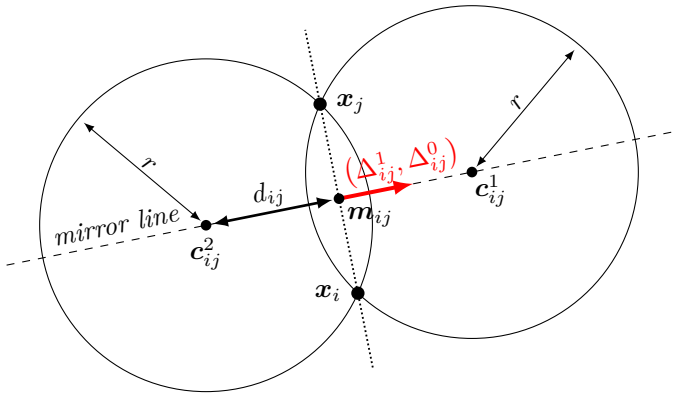

Figure 6.2: Illustration of equations (6.2) for the construction of the two unique circles with radius r passing through points $\boldsymbol{x}_i$ and $\boldsymbol{x}_j$.

has a length of 1 meter. In practice, both the DSO and the FSP should know the geographical location of the participating assets, as the connection points are part of the distribution grid, and the FSP should have a bilateral contract with the owner of the asset allowing the FSP to use the asset for FCR services.

The goal is to find all sets of points $\mathcal{C}_s \subset \mathcal{I}$, of which the smallest circle containing all points in the set has a radius r smaller than or equal to 100 m, and which is not a subset of any other such set of points:

$$\mathcal{C}_s = \{i \in \mathcal{I} \mid \exists \boldsymbol{c} \in \mathbb{R}^2 : \forall i, \|\boldsymbol{x}_i - \boldsymbol{c}\|_2 \leq 100\} \tag{6.1}$$

$$\text{and} \quad \mathcal{C}_s \nsubseteq \mathcal{C}_{s'}, s' = \{1, \ldots, s-1, s+1, \ldots n_{\mathcal{S}}\},$$

with $n_{\mathcal{S}}$ the total number of sets $\mathcal{C}_s$. The last requirement avoids adding trivial sets of points: for instance, if there is a circle with radius $r \leq 100$ m containing points $\{1, 2, 3\}$, then there are also circles with radii $r \leq 100$ m containing only points $\{1, 2\}$, $\{2, 3\}$ and $\{1, 3\}$. However, the constraints that would be imposed by these last three sets of points are already incorporated by the constraint defined by the set $\{1, 2, 3\}$. Hence, the smaller sets can be discarded.

A naive construction methodology for $\mathcal{C}_s$ would be to check the smallest circumscribed circle of all possible combinations of points. However, this would quickly become intractable for a rather limited number of points $n_{\mathcal{I}}$, as the number of possible combinations increases exponentially with $O(2^{n_{\mathcal{I}}})$.

To overcome this, we have developed Algorithm 3, which has complexity $O(n_{\mathcal{I}}^4)$. The algorithm is based on the idea that the smallest circumscribed circle of a set of points has at least two points on the boundary of that circle [201]. Thus,

by finding all circles with radius 100 m that have at least two points on their boundary, one obtains all circles to be considered when creating the sets $\mathcal{C}_s$.

Given a radius r and two distinct points $\boldsymbol{x}_i, \boldsymbol{x}_j$, one can define two unique circles with centre points $\boldsymbol{c}_{ij}^1, \boldsymbol{c}_{ij}^2$ as illustrated by Figure 6.2. These centre points can be found using the following equations, resulting from the relations defined in Figure 6.2,:

$$d_{ij} = \sqrt{r^2 - \left(\frac{\|\boldsymbol{x}_i - \boldsymbol{x}_j\|_2}{2}\right)^2}, \tag{6.2a}$$

$$\Delta_{ij}^0 = \frac{x_i^0 - x_j^0}{\|\boldsymbol{x}_i - \boldsymbol{x}_j\|_2}, \quad \Delta_{ij}^1 = \frac{-(x_i^1 - x_j^1)}{\|\boldsymbol{x}_i - \boldsymbol{x}_j\|_2}, \tag{6.2b}$$

$$\boldsymbol{c}_{ij}^1 = \left(\frac{x_i^0 + x_j^0}{2} + d_{ij}\Delta_{ij}^1, \frac{x_i^1 + x_j^1}{2} + d_{ij}\Delta_{ij}^0\right), \tag{6.2c}$$

$$\boldsymbol{c}_{ij}^2 = \left(\frac{x_i^0 + x_j^0}{2} - d_{ij}\Delta_{ij}^1, \frac{x_i^1 + x_j^1}{2} - d_{ij}\Delta_{ij}^0\right). \tag{6.2d}$$

Here, d_{ij} gives the distance between the centre points and the midpoint m_{ij} between $\boldsymbol{x}_i, \boldsymbol{x}_j$ along the *mirror line*, the line with all points at equal distance from both points $\boldsymbol{x}_i, \boldsymbol{x}_j$. The direction of the mirror line is given by the normalized vector $\left(\Delta_{ij}^1, \Delta_{ij}^0\right)$. The centre points are then found by starting from the midpoint $\boldsymbol{m}_{ij} = \left((x_i^0 + x_j^0)/2, (x_i^1 + x_j^1)/2\right)$ between $\boldsymbol{x}_i, \boldsymbol{x}_j$ and going with distance d_{ij} along the mirror line in the positive and the negative direction, as elaborated in equations (6.2c) and (6.2d).

Algorithm 3 shows how to construct the set $\mathcal{S} = \{\mathcal{C}_1, \ldots, \mathcal{C}_{n_S}\}$ containing all sets $\mathcal{C}_s$ defined by (6.1). The iteration over every asset in step 1 creates the local set $\mathcal{S}_i = \{\mathcal{C}_s \in \mathcal{S} | i \in \mathcal{C}_s\}$ containing the circle sets $\mathcal{C}_s$ in which asset i is contained. By executing this iteration in parallel at every asset i, the algorithm can be executed in a fully distributed fashion.

The iterations in step 3 finds then all neighbouring points j that are less than or equal to 200 m apart from each other, as points that are farther from each other can never be in the same circle with radius 100 m. This limits the combinations to be considered at each point i to the points that are in the neighbourhood of i, speeding up up the algorithm significantly.

Step 8 calculates the centre points of the two circles with radius 100 m determined by points i, j. Then, steps 9 and 10 determine all points from $\mathcal{I}$ that are enclosed

Algorithm 3 Construction of sets within circles of $r \leq 100\,\mathrm{m}$

1: **for each** point $i \in \mathcal{I}$, **do** (in parallel)
2: $\quad \mathcal{S}_i \leftarrow \emptyset$
3: $\quad \mathcal{I}_i \leftarrow \{j \in \mathcal{I} \mid \|\boldsymbol{x}_i - \boldsymbol{x}_j\|_2 \leq 200\}$
4: $\quad$ **if** $\mathcal{I}_i = \emptyset$ **then**
5: $\quad\quad \mathcal{S}_i \leftarrow \{i\}$
6: $\quad$ **else**
7: $\quad\quad$ **for each** $j \in \mathcal{I}_i$, **do**
8: $\quad\quad\quad$ Calculate c^1_{ij}, c^2_{ij} from $\boldsymbol{x}_i$ and $\boldsymbol{x}_j$ using (6.2).
9: $\quad\quad\quad \mathcal{C}^1 \leftarrow \{n \in \mathcal{I}_i \mid \|\boldsymbol{x}_n - \boldsymbol{c}^1_{ij}\| \leq 100\}$
10: $\quad\quad\quad \mathcal{C}^2 \leftarrow \{n \in \mathcal{I}_i \mid \|\boldsymbol{x}_n - \boldsymbol{c}^2_{ij}\| \leq 100\}$
11: $\quad\quad\quad$ **for each** $\mathcal{C}_s \in \mathcal{S}_i$, **do**
12: $\quad\quad\quad\quad$ **if** $\mathcal{C}_s \subset \mathcal{C}^1$ or $\mathcal{C}_s \subset \mathcal{C}^2$ **then**
13: $\quad\quad\quad\quad\quad \mathcal{S}_i \leftarrow \mathcal{S}_i \setminus \mathcal{C}_s$
14: $\quad\quad\quad$ **if** $\mathcal{C}^1 \nsubseteq \mathcal{C}_s, \forall \mathcal{C}_s \in \mathcal{S}_i$ **then**
15: $\quad\quad\quad\quad \mathcal{S}_i \leftarrow \mathcal{S}_i \cup \mathcal{C}^1$
16: $\quad\quad\quad$ **if** $\mathcal{C}^2 \nsubseteq \mathcal{C}_s, \forall \mathcal{C}_s \in \mathcal{S}_i$ **then**
17: $\quad\quad\quad\quad \mathcal{S}_i \leftarrow \mathcal{S}_i \cup \mathcal{C}^2$
18: $\mathcal{S} = \bigcup_{i \in \mathcal{I}} \mathcal{S}_i$

by these circles. This gives two potential sets of points $\mathcal{C}^1, \mathcal{C}^2$, for which it has to be checked if there does not already exist a set $\mathcal{C}_s \in \mathcal{S}_i$ that is a subset of $\mathcal{C}^1$ or $\mathcal{C}^2$, in which case $\mathcal{C}_s$ is removed from $\mathcal{S}_i$. Finally, if the sets $\mathcal{C}^1, \mathcal{C}^2$ are not in itself a subset of any $\mathcal{C}_s \in \mathcal{S}_i$, they are added to $\mathcal{S}_i$. These last two operations are performed to eliminate trivial sets, explained above. Finally, In step 18, the set $\mathcal{S} = \{\mathcal{C}_1, \ldots, \mathcal{C}_{n_\mathcal{S}}\}$ is created by taking the union over all subsets $\mathcal{S}_i$. However, when using the distributed optimization algorithm presented further this step is not required as in the local optimization problem (6.6) each asset i only needs the information of the subset $\mathcal{S}_i$.

An example of the results of the algorithm, applied to a neighbourhood in the city of Breda, is given in Figure 6.3. As one can see, the closer the points are together, the more circles can be drawn and thus more constraints have to be applied.

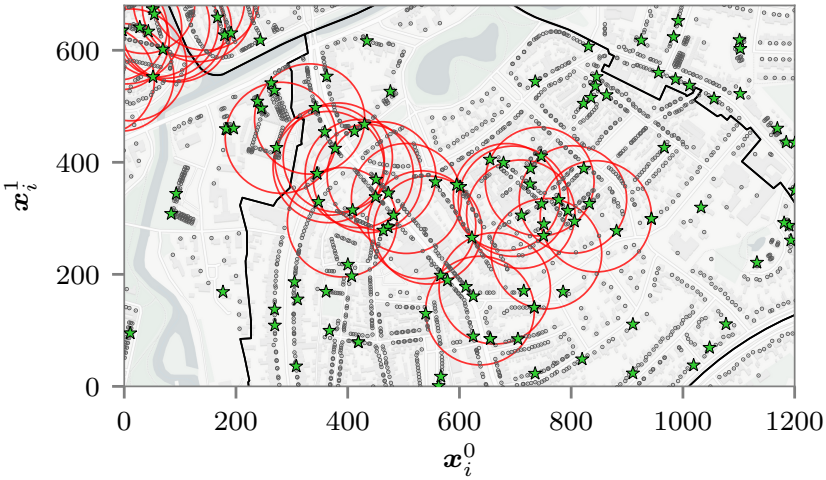

Figure 6.3: Example of the circles with more than 10 assets ($|\mathcal{C}_s| > 10$) in the *Zandberg* neighbourhood in the city of Breda. The black dots are all the connection points in the neighbourhood, obtained from [202], while the green stars denote the randomly selected connection points participating in the pool of the FSP, corresponding to 5 % of all connection points. Map data © OpenStreetMap contributors

6.4 Distributed Optimization of a Pool of Assets

This section first formulates the centralized optimization to be performed by an FSP that wants to sell FCR capacity to the TSO over the duration of one bidding period $n_{\mathcal{T}}$ with a pool of flexible assets connected to the distribution grid. Subsequently, this section elaborates the proposed distributed optimization algorithm, solving the problem according to the distributed architecture presented in Figure 6.1.

6.4.1 Central Optimization Problem

The objective of the optimization problem to be performed by the FSP is to maximize revenues from selling FCR capacity p_F provided by a pool of assets, minus the costs of using these asset for primary frequency control.

In European FCR markets, the FSP only gets paid a capacity fee (and no activation fee) when providing FCR to the TSO [26]. Therefore, the revenues for providing FCR are given by $c_F p_F n_{\mathcal{T}}$, with c_F the unit price to provide FCR per time step $t \in \mathcal{T} = \{1, \ldots, n_{\mathcal{T}}\}$, $n_{\mathcal{T}}$ the number of time steps in the bidding period, and p_F the aggregated FCR capacity the FSP is able to sell to the TSO. As the FCR price c_F and the amount of FCR capacity sold on the market p_F should be constant over the entire bidding period [184], c_F and p_F do not depend on the time t.

We define $\boldsymbol{p}_i = (p_{i,0}, \ldots, p_{i,n_{\mathcal{T}}})^T$ as the vector containing the FCR capacities in kW provided by asset i at every time step t of the bidding period. As the FSP sells the aggregate of these local FCR capacities to the TSO, the sum of the local FCR capacities over all assets should equal to the total FCR capacity sold p_F for every time step: $\sum_{i \in \mathcal{I}} p_{i,t} = p_F, \forall t \in \mathcal{T}$.

We define also $c_i : \mathbb{R}^{n_{\mathcal{T}}} \mapsto \mathbb{R} \cup \{+\infty\}$ as the local cost $c_i(\boldsymbol{p}_i)$ of asset i to provide the FCR capacity vector $\boldsymbol{p}_i$. As explained in Section II, this cost function can include both the actual marginal cost of controlling the asset and the opportunity costs of using the flexibility for other purposes. Such a cost function can also be viewed as the negative of a utility function, used in previous work [193, 203]. We allow $c_i(\boldsymbol{p}_i)$ to take on the value $+\infty$ when the point $\boldsymbol{p}_i$ is infeasible for the asset (e.g. a 2 kW battery cannot provide 5 kW frequency control capacity). To ensure a global optimum can be found, we assume $c_i(\boldsymbol{p}_i)$ to be convex.

The complete optimization problem to be solved by the FSP can then be formulated as a mixed-integer optimization program:

$$\min_{\boldsymbol{p}_i, \boldsymbol{z}_i, p_F} \quad \sum_{i \in \mathcal{I}} c_i(\boldsymbol{p}_i) - c_F p_F n_{\mathcal{T}} \tag{6.3a}$$

$$\text{s.t.} \quad 0 \leq p_{i,t} \leq 5 z_{i,t}, \qquad \forall t \in \mathcal{T}, \forall i \in \mathcal{I}, \tag{6.3b}$$

$$\sum_{i \in \mathcal{I}} p_{i,t} = p_F, \qquad \forall t \in \mathcal{T}, \tag{6.3c}$$

$$\sum_{i \in \mathcal{C}_s} z_{i,t} \leq 10, \qquad \forall t \in \mathcal{T}, \forall \mathcal{C}_s \in \mathcal{S}, \tag{6.3d}$$

$$\boldsymbol{z}_i \in \{0, 1\}^{n_{\mathcal{T}}}, \quad \forall i \in \mathcal{I}. \tag{6.3e}$$

Here $\boldsymbol{z}_i = (z_{i,0}, \ldots, z_{i,n_{\mathcal{T}}})^T$ is a vector of binary variables $z_{i,t}$ which gives 1 if asset i is providing FCR capacity at time step t and 0 otherwise. Constraint (6.3b) represents the first constraint of Synergrid, limiting the FCR capacity to 5 kW in case the asset is delivering FCR capacity (i.e. $z_{i,t} = 1$).

Constraint (6.3c) represents the requirement that the sum of the local FCR capacities should equal the total FCR capacity the FSP sells to the TSO, at each time step. Constraint (6.3d) represents the requirement to have maximum 10 assets providing FCR capacity in each circle of 100 m. Finally, (6.3e) constraints $\boldsymbol{z}_i$ to a binary variable of dimension $n_{\mathcal{T}}$.

Problem (6.3) is a mixed-integer optimization with a convex continuous relaxation, for which various solution methods exists that are able to find the global optimum, e.g. branch-and-bound [204], the extended cutting plane method [205] or the branch-and-cut method [206].

However, as this problem contains $n_{\mathcal{T}} n_{\mathcal{I}}$ binary variables, the complexity increases quickly with a growing number of assets. Therefore, we create a distributed version of the optimization problem (6.3), in which the assets only have to communicate with the FSP and the applicable circle constraint agents (or with their local neighbours in a peer-to-peer architecture, as explained in Section 6.2.1).

When participating in the FCR market, the FSP has to bid in the FCR capacity p_F at a certain capacity price c_{FCR}. The TSO then selects the cheapest bids in merit order, until the required FCR capacity is reached. As the market is a pay-as-bid market, the FSP only gets paid his bid price c_{FCR} and not the clearing price [26]. The FSP will thus first have to decide on the price c_F, which should be high enough to obtain as much revenues as possible, but not too high as then the bid might not be accepted. With the bid price c_F decided, the FSP can use (6.3) to optimize the FCR capacity of its pool of assets.

6.4.2 Distributed Optimization

One can identify three parts in problem (6.3): a local optimization to maximize the local FCR revenues minus the local costs; the global problem of the FSP, who tries to obtain a constant FCR capacity from all assets over the bidding period $n_{\mathcal{T}}$; and the local circle constraints imposed by Synergrid.

These three parts give a natural way to distribute the optimization problem into three subproblems. The first subproblem is the local optimization per asset to maximize $f_i(\boldsymbol{p}_i^f, \boldsymbol{z}_i^f)$, the local FCR revenues minus the local cost, equal to the objective (6.3a) constrained to (6.3b). The second subproblem is the optimization performed by the FSP, minimizing $h(\boldsymbol{p}_{i\in\mathcal{I}}^h)$, the indicator function

corresponding to (6.3c):

$$h(\boldsymbol{p}^h_{i\in\mathcal{I}}) = \begin{cases} 0, & \text{if } \exists p_F : \sum_{i\in\mathcal{I}} p^h_{i,t} = p_F, \forall t \in \mathcal{T}. \\ +\infty, & \text{otherwise.} \end{cases}$$

The third subproblem is an optimization per circle constraint s, minimizing $g_s\left(\boldsymbol{z}^{g_s}_{i\in\mathcal{C}_s}\right), s = 1, \dots n_{\mathcal{S}}$, with g_s the indicator function of one constraint from (6.3d) - (6.3e) (i.e. with only the set $\mathcal{C}_s$ corresponding to circle constraint s).

To distribute the optimization problem, we use the alternating direction method of multipliers (ADMM) because of its superior convergence properties [207] while being able to keep the cost functions local. However, as (6.3) is a mixed-integer problem and hence non-convex, ADMM nor other comparable distributed algorithms are guaranteed to converge to the global optimum [208]. Nevertheless, we observe in Section 6.5 that the proposed distributed algorithm is able to converge to a suboptimal but feasible point in a finite number of iterations.

To be able to distribute the problem using the ADMM methodology, each subproblem needs its own copy of the optimization variables $\boldsymbol{p}_i, \boldsymbol{z}_i$. Therefore, in the notation above and in what follows, we used the superscript ^{f} to denote the variables used in the local optimization of $f_i(\boldsymbol{p}^f_i, \boldsymbol{z}^f_i)$, the superscript ^{h} to denote the variables used in the optimization of $h(\boldsymbol{p}^h_{i\in\mathcal{I}})$ performed by the FSP and the superscript ^{g_s} to denote the variables used in the optimization of $g_s\left(\boldsymbol{z}^{g_s}_{i\in\mathcal{C}_s}\right)$ performed by the circle constraint agent s managing the circle constraint $\mathcal{C}_s$. This notation allows us to rewrite problem (6.3) as a consensus problem over the three subproblems:

$$\min_{\substack{(\boldsymbol{p}^f_i, \boldsymbol{z}^f_i, \boldsymbol{p}^{g_s}_i, \\ \boldsymbol{z}^{g_s}_i, \boldsymbol{p}^h_i)_{i\in\mathcal{I}}}} \quad \sum_{i\in\mathcal{I}} f_i(\boldsymbol{p}^f_i, \boldsymbol{z}^f_i) + \sum_{\mathcal{C}_s\in\mathcal{S}} g_s\left(\boldsymbol{z}^{g_s}_{i\in\mathcal{C}_s}\right) + h\left(\boldsymbol{p}^h_{i\in\mathcal{I}}\right)$$

$$\text{s.t.} \qquad \boldsymbol{z}^f_i = \boldsymbol{z}^{g_s}_i, \quad \forall i \in \mathcal{C}_s, \quad s = 1, \dots, n_{\mathcal{S}}, \tag{6.4a}$$

$$\boldsymbol{p}^f_i = \boldsymbol{p}^h_i, \quad \forall i \in \mathcal{I}. \tag{6.4b}$$

Of every local binary vector $\boldsymbol{z}^f_i$, there is one copy per circle constraint $\boldsymbol{z}^{g_s}_i$ applicable to asset i amongst which consensus has to be formed. The same holds for the local FCR capacity vector $\boldsymbol{p}^f_i$, of which there is a copy in the FSP objective $\boldsymbol{p}^h_i$.

To distribute (6.4) using ADMM, one has to form the *augmented Lagrangian* $\mathcal{L}_p$ of (6.4):

$$\begin{aligned}\mathcal{L}_p = &\sum_{i\in\mathcal{I}} f_i(\boldsymbol{p}_i^f, \boldsymbol{z}_i^f) + \sum_{\mathcal{C}_s\in\mathcal{S}} g_s\left(\boldsymbol{z}_{i\in\mathcal{C}_s}^{g_s}\right) + h\left(\boldsymbol{p}_{i\in\mathcal{I}}^h\right) \\ &+ \sum_{\mathcal{C}_s\in\mathcal{S}}\sum_{i\in\mathcal{C}_s}(\rho_F/2)\|\boldsymbol{z}_i^f - \boldsymbol{z}_i^{g_s} + \boldsymbol{u}_i^{g_s}\|_2^2 \\ &+ \sum_{i\in\mathcal{I}}(\rho_c/2)\|\boldsymbol{p}_i^f - \boldsymbol{p}_i^h + \boldsymbol{u}_i^h\|_2^2.\end{aligned} \tag{6.5}$$

To keep the notation concise, we have used the scaled form of the augmented Lagrangian [207], with $\boldsymbol{u}_i^{g_s}$ and $\boldsymbol{u}_i^h$ the scaled dual variables corresponding to (6.4a) and (6.4b) respectively and $\rho_F, \rho_c > 0$ the augmented Lagrangian parameters for the FSP constraint and the circle constraint, respectively.

Note that this expression is slightly different from the traditional augmented Lagrangian, that only employs one value for rho: $\rho = \rho_F = \rho_c$. However, by allowing $\rho_F \neq \rho_c$, we are able to fine-tune the ADMM convergence as we are able to steer the convergence of the primal or dual residuals of the circle and the FSP constraints separately.

The proposed distributed optimization algorithm, shown in full in Algorithm 4, consists of the alternating partial minimization of the augmented Lagrangian (6.5). First, an optimization is performed by the local agents minimizing f_i, followed by the circle constraint agents minimizing g_s and the FSP minimizing h. We will now discuss the three subproblems in detail.

Local Optimization

In the first step of each iteration k, (step 8 or 10 in Algorithm 4), the augmented Lagragian is minimized for each asset $i \in \mathcal{I}$ over the FCR capacity $\boldsymbol{p}_i^f$ and binary $\boldsymbol{z}_i^f$ variables, while keeping the other variables constant. The local optimization,

Algorithm 4 Distributed ADMM optimization

$\boldsymbol{z}_i^{g_s}, \boldsymbol{u}_i^{g_s} \leftarrow 0, \quad \forall i \in \mathcal{C}_s, s = 1, \ldots, n_{\mathcal{S}}.$
$\boldsymbol{p}_i^h, \boldsymbol{u}_i^h \leftarrow 0, \quad \forall i \in \mathcal{I}.$
$k \leftarrow 0.$
while $\exists \mathcal{C}_s \in \mathcal{S}, t \in \mathcal{T} : \sum_{i \in \mathcal{C}_s} z_{i,t}^f > 10, z_{i,t}^f \in \{0,1\}$
  and $\| \sum_{i \in \mathcal{I}} (\boldsymbol{p}_i^f - \boldsymbol{p}_i^h) \| > \alpha \| \sum_{i \in \mathcal{I}} \boldsymbol{p}_i^f \|$ **do**
  for each $i \in \mathcal{I}$ **do** (in parallel)
    if $(k \mod k_{IP}) = 0$ **then**
      $\boldsymbol{p}_i^f, \boldsymbol{z}_i^f \leftarrow \hat{\boldsymbol{p}}_i^f, \hat{\boldsymbol{z}}_i^f,$ using (6.6) with $z_{i,t}^f \in \{0,1\}$.
    else
      $\boldsymbol{p}_i^f, \boldsymbol{z}_i^f \leftarrow \hat{\boldsymbol{p}}_i^f, \hat{\boldsymbol{z}}_i^f,$ using (6.6).
    Send $\boldsymbol{z}_i^f$ to all circle constraint agents $s : \mathcal{C}_s \in \mathcal{S}_i$
    and $\boldsymbol{p}_i^f$ to the FSP.
  for each $\mathcal{C}_s \in \mathcal{S}$ **do** (in parallel)
    $\boldsymbol{z}_i^{g_s} \leftarrow \hat{\boldsymbol{z}}_i^{g_s}, \quad \forall i \in \mathcal{C}_s,$ using (6.7).
    $\boldsymbol{u}_i^{g_s} \leftarrow \boldsymbol{u}_i^{g_s} + \boldsymbol{p}_i^f - \boldsymbol{z}_i^{g_s}, \quad \forall i \in \mathcal{C}_s.$
    Send $\boldsymbol{z}_i^{g_s}, \boldsymbol{u}_i^{g_s}$ to all assets $i \in \mathcal{C}_s$.
  $\boldsymbol{p}_i^h \leftarrow \hat{\boldsymbol{p}}_i^h, \quad \forall i \in \mathcal{I},$ using (6.8).
  $\boldsymbol{u}_i^h \leftarrow \boldsymbol{u}_i^h + \boldsymbol{p}_i^f - \boldsymbol{p}_i^h, \quad \forall i \in \mathcal{I}.$
  Send $\boldsymbol{p}_i^h, \boldsymbol{u}_i^h$ to all assets $i \in \mathcal{I}$.
  $k \leftarrow k + 1.$

to be executed in parallel at each asset i, can then be formulated as:

$$\hat{\boldsymbol{p}}_i^f, \hat{\boldsymbol{z}}_i^f = \underset{\boldsymbol{p}_i^f, \boldsymbol{z}_i^f}{\arg\min} \quad c_i(\boldsymbol{p}_i^f) + \sum_{\mathcal{C}_s \in \mathcal{S}_i} \frac{\rho_F}{2} \|\boldsymbol{z}_i^f - \boldsymbol{z}_i^{g_s} + \boldsymbol{u}_i^{g_s}\|_2^2$$

$$+ \frac{\rho_c}{2} \|\boldsymbol{p}_i^f - \boldsymbol{p}_i^h + \boldsymbol{u}_i^h\|_2^2 - c_{FCR} \sum_{t \in \mathcal{T}} p_{i,t}^f \tag{6.6a}$$

$$\text{s.t.} \qquad 0 \leq p_{i,t}^f \leq 5 z_{i,t}^f, \quad \forall t \in \mathcal{T}, \tag{6.6b}$$

$$\boldsymbol{z}_i^f \in [0,1]^{n_{\mathcal{T}}}. \tag{6.6c}$$

This optimization problem incorporates the local optimization f_i, given by the part of the objective (6.3a) applicable to asset i constrained to (6.3b), together with the quadratic penalty terms of the augmented Lagragian (6.5) which are applicable to asset i. As this optimization only considers the variables of asset i and does not need variables of other assets, it succeeds in keeping all information about cost and local constraints private.

In (6.6), we have relaxed the binary constraint (6.3e) to be continuous, thereby avoiding oscillatory behaviour between this binary variable $z_{i,t}^f$ and the binary variables from (6.7), $z_{i,t}^{g_s}$. However, with $z_{i,t}^f$ continuous, the local asset i does not know if it actually can provide any FCR capacity. Therefore, every k_{IP} iterations, problem (6.6) is solved with $z_{i,t}^{g_s}$ constrained to an integer variable (step 8).

When asset i finishes its local optimization, in step 11, the FCR capacity variables $\hat{\boldsymbol{p}}_i^f$ are sent to the FSP for the optimization of h. The binary variables $\hat{\boldsymbol{z}}_i^f$ are sent to the circle constraint agents $s : \mathcal{C}_s \in \mathcal{S}_i$ of all circle constraints of which asset i is part of.

As shown in steps 1-2 of algorithm 4, we initialize the algorithm by setting $\boldsymbol{z}_i^{g_s} = \boldsymbol{p}_i^h = 0$. However, with $\rho_F, \rho_c > 0$ this results in a couple of initial iterations needed to raise $\boldsymbol{p}_i^f$ from 0 towards their economical value. These initial iterations can be avoided by setting $\rho_F = \rho_c = 0$ in the first iteration, thereby *warm-starting* the algorithm, as this means solving the optimization problem (6.3) without applying constraints (6.3c), (6.3d). This immediately results in using all assets at maximum FCR capacity $p_{i,t}^f = 5$ if this is economically interesting, i.e. if $c_{FCR} \sum_{t \in \mathcal{T}} p_{i,t} > c_i(\boldsymbol{p}_i)$.

Circle Constraint Optimization

Having received all locally optimized binary variables $\boldsymbol{z}_i^f, i \in \mathcal{C}_s$, in step 13 each circle constraint agent s optimizes (6.5) over its copy of these variables $\boldsymbol{z}_{i \in \mathcal{C}_s}^{g_s}$, to respect the circle constraints (6.3d)-(6.3e), corresponding to the partial optimization of the augmented Lagrangian (6.5). This optimization is also separable and can thus be executed for every circle constraint s in parallel. The optimization problem of one such circle constraint agent s results in a quadratic mixed-integer program:

$$\begin{aligned} \hat{\boldsymbol{z}}_{i \in \mathcal{C}_s}^{g_s} = \underset{\boldsymbol{z}_{i \in \mathcal{C}_s}^{g_s}}{\arg\min} \quad & \sum_{i \in \mathcal{C}_s} (\rho_c/2) \|\boldsymbol{z}_i^f - \boldsymbol{z}_i^{g_s} + \boldsymbol{u}_i^{g_s}\|_2^2 \\ \text{s.t.} \quad & \sum_{i \in \mathcal{C}_s} z_{i,t}^{g_s} \leq 10, \qquad \forall t \in \mathcal{T}, \\ & \boldsymbol{z}_i^{g_s} \in \{0,1\}^{n_\mathcal{T}}, \quad \forall i \in \mathcal{C}_s. \end{aligned} \tag{6.7}$$

Note that this problem is actually the Euclidean projection of $(\boldsymbol{z}_i^f + \boldsymbol{u}_i^{g_s})$ on the feasible set defined by constraints (6.3d)-(6.3e).

As (6.7) is a quadratic mixed-integer problem, it can be hard to solve. However, as there is no coupling in time, the problem can be separated into $n_{\mathcal{T}}$ distinct subproblems, each containing only one binary variable $z_{i,t}^t$, which can be solved very efficiently.

Having obtained the optimal $\hat{\boldsymbol{z}}_i^{g_s}$, the scaled dual variables of each point of each circle constraint $\boldsymbol{u}_i^{g_s}$ are updated in step 14. Both updates are sent back to the corresponding assets i in step 15 for use in the next iteration $k+1$.

FSP Optimization

The FSP tries to obtain a constant FCR capacity p_F from all assets over the bidding period $n_{\mathcal{T}}$. At iteration k, the FSP gathers all locally optimized variables $\boldsymbol{p}_i^f$ from all assets $i \in \mathcal{I}$ and minimizes the augmented Lagrangian (6.5) over its copy of the local FCR capacity variables $\boldsymbol{p}_i^h, i \in \mathcal{I}$:

$$\begin{aligned} \hat{\boldsymbol{p}}_{i\in\mathcal{I}}^h = \underset{p_F, \boldsymbol{p}_{i\in\mathcal{I}}^h}{\arg\min} \quad & \sum_{i\in\mathcal{I}} (\rho_F/2) \|\boldsymbol{p}_i^f - \boldsymbol{p}_i^h + \boldsymbol{u}_i^h\|_2^2 \\ \text{s.t.} \quad & \sum_{i\in\mathcal{I}} p_{i,t}^h = p_F, \quad \forall t \in \mathcal{T}. \end{aligned} \tag{6.8}$$

This problem is independent of (6.7), and can thus be executed in parallel to (6.7).

As with the circle constraints, when having obtained the optimal $\boldsymbol{p}_i^h$, the scaled dual variables $\boldsymbol{u}_i^h$ are updated in step 17. Finally, in step 18, both $\boldsymbol{p}_i^h$ and $\boldsymbol{u}_i^h$ are sent back to the corresponding assets i.

When asset i has received both $\boldsymbol{p}_i^h, \boldsymbol{u}_i^h$ from the FSP and $\boldsymbol{z}_i^{g_s}, \boldsymbol{u}_i^{g_s}$ from all circle constraint agents $s : \mathcal{C}_s \in \mathcal{S}_i$, it can start its next iteration $k+1$ by solving (6.6) with the updated parameters $\boldsymbol{p}_i^h, \boldsymbol{u}_i^h, \boldsymbol{z}_i^{g_s}, \boldsymbol{u}_i^{g_s}$, until convergence is reached.

The algorithm converges when the local variables $\boldsymbol{p}_i^f, \boldsymbol{z}_i^f$ reach a feasible operating point, as denoted by the while-conditions in steps 4 and 5. The condition in step 4 evaluates the circle constraints (6.3d) with $z_{i,t}^f$ binary, and can thus only be checked every k_{IP} iterations. The condition in step 5 evaluates if the total local FCR capacity $\sum_{i\in\mathcal{I}} p_{i,t}^f$ is close enough to the aggregated FCR capacity $p_F = \sum_{i\in\mathcal{I}} p_{i,t}^h$, with α a parameter denoting the relative error between the norm of the difference $\sum_{i\in\mathcal{I}} (\boldsymbol{p}_i^f - \boldsymbol{p}_i^h)$ over every time step t, relative to the norm of the total local FCR capacity $\sum_{i\in\mathcal{I}} \boldsymbol{p}_i^f$.

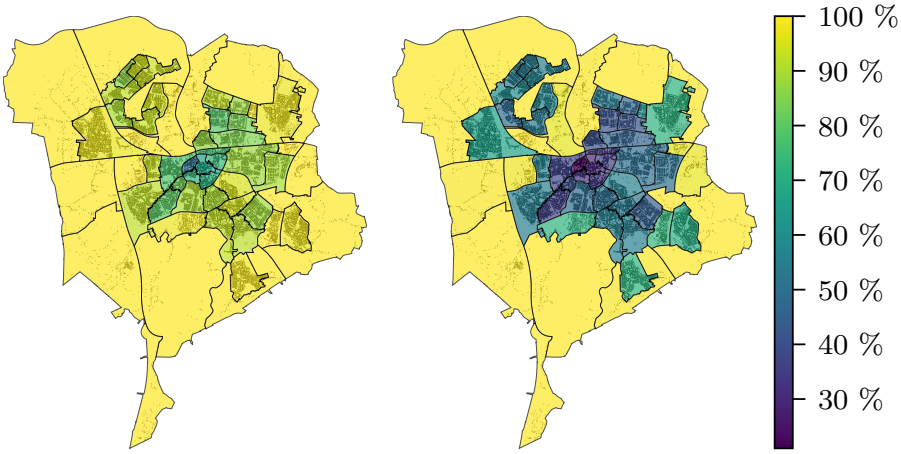

(a) 5% Participation (b) 15% Participation

Figure 6.4: Usable proportion of total available LV grid connected FCR capacity in different neighbourhoods in the city of Breda, taking into account the circle constraints imposed by Synergrid, in case 5% and 15% of all LV connection points are able to participate in FCR.

6.5 Case Study: Distributed Assets in Breda

In this section, we evaluate the impact of the circle constraints on the portfolio capacity an FSP can provide with low-voltage connected, distributed assets providing FCR and the performance of the proposed distributed ADMM algorithm.

We present a case study using actual data of the low-voltage connection points in the city of Breda, a middle-sized municipality in the South of the Netherlands with 183 765 inhabitants [209] and 86 868 low voltage (LV) connection points. The geographic location of the connection points in the municipality is provided by Enexis, the local distribution grid operator, with an accuracy up to 1 m and can be freely accessed online [202]. We used the municipality of Breda as a case study rather than a Belgian municipality as accurate data on the location of LV connection points was not available for a Belgian municipality.

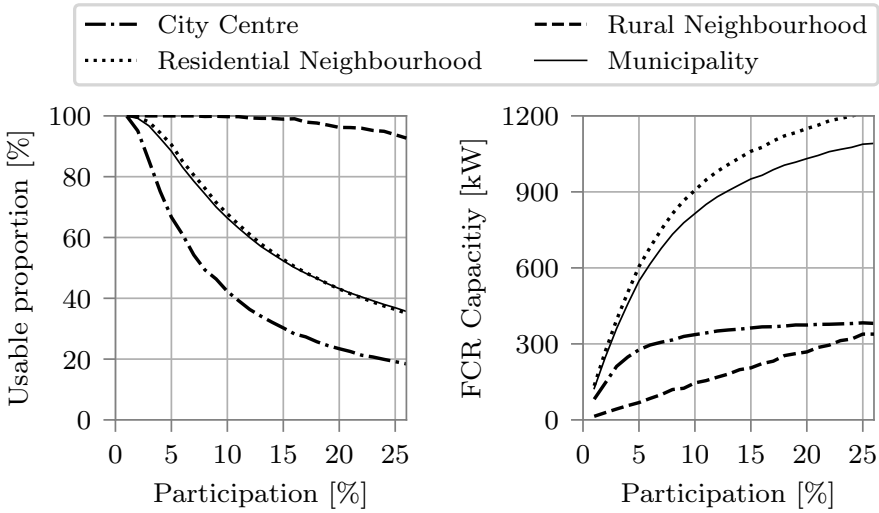

(a) Usable proportion of total available FCR capacity.

(b) Total FCR capacity.

Figure 6.5: (a) Usable proportion of total available FCR capacity and (b) total FCR capacity in function of the participation rate in the averaged city centre, residential, rural neighbourhood and of the entire municipality.

6.5.1 Impact of Circle Constraints on Usable FCR Capacity

The circle constraints imposed by Synergrid will reduce the amount of FCR capacity that can be used by the FSP. Figure 6.4 shows the maximal proportion of the total available FCR capacity that can be used in an FSP pool per neighbourhood in Breda, taking into account the circle constraints as imposed by Synergrid. Figure 6.4a gives the results for a participation rate of 5 %, meaning that 5 % of all available LV connection points are able to provide FCR capacity, while Figure 6.4b gives the results for a participation rate of 15 %. In the figure, a neighbourhood with a value of 100 % indicates that all available FCR capacity, and thus all participating assets, can be used in the FSP pool, while a value of e.g. 70 % indicates that only up to 70 % of the available FCR capacity or participating assets can be used for FCR, in order to comply with the circle constraints imposed by Synergrid. We select the location of the participating assets randomly from the available connection points according to a uniform distribution, so that the total number of participating assets equals the participation rate.

For this calculation, we assumed that every participating connection point is

able to provide at least 5 kW of FCR capacity and selected the participating connection point randomly from all LV connection points in Breda. We calculated the maximum amount of FCR capacity in an FSP pool can by solving (6.3) with $\forall i : c_i(\boldsymbol{p}_i) = 0$ and $c_{FCR} = 1$, for which we used Gurobi [163]. To eliminate the effect of randomness in the location of the assets, Figure 6.4 shows the Monte Carlo average of ten such simulations.

From Figure 6.4, it is clear that there exists a large spatial difference in reduction of FCR capacity: at 5 % participation, mainly in the city centre there is already a substantial amount of reduction of the usable FCR capacity. At 15 % participation, the reduction of the usable FCR in the city centre becomes very strong and also in more suburban neighbourhoods there is a considerable amount of reduction observable. On the other hand, in the more rural, outer neighbourhoods, up to 100 % of available FCR capacity can still be used.

Figure 6.5a quantifies this spacial difference, showing the usable proportion of available FCR capacity in function of the degree of participation for the three types of neighbourhoods identified previously: rural, residential (suburban) and the city centre. The neighbourhoods in the city centre show the biggest decrease between 2 % and 10 % participation, while rural neighbourhoods only start to decrease their usable proportion after 15 % participation, at a much slower rate.

However, this slower reduction in rural neighbourhoods does not automatically translate into a higher total FCR capacity, as the number of connection points in a rural neighbourhood is much lower than in a residential neighbourhood. This can be seen in Figure 6.5b, which shows the total FCR capacity of each type of neighbourhood. While FCR capacity increases linearly with the participation rate in rural neighbourhoods, the capacity is still much lower than in a residential neighbourhood, as there are many more connection points. In the city centre, the increase in total FCR capacity levels off at around 5 −10 % participation, indicating that any additional FCR assets deployed in the city centre beyond this level of participation will not increase the total FCR capacity of the pool of the FSP.

6.5.2 Performance of the Distributed Optimization Algorithm

This section discusses the performance of the proposed distributed optimization algorithm. To limit the simulation time, we limit simulate only the *Zandberg* neighbourhood in Breda (shown in Figure 6.3), a typical residential neighbourhood.

We simulate $n_{\mathcal{T}} = 24$ time steps, each corresponding to one hour of a day. To keep the optimization problems efficiently solvable, we assume the local cost

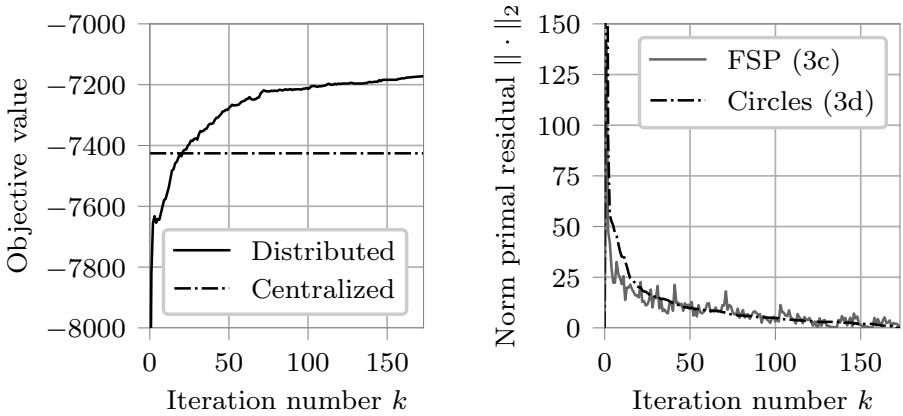

(a) Objective value (6.3a) of the distributed and centralized optimization.

(b) Euclidean norms of the primal residuals of circle constraints (6.3d) and the FSP constraint (6.3c).

Figure 6.6: Evolution of the objective value (a) and primal residuals of the distributed constraints (b) using the proposed distributed optimization, in function of the iteration number k.

of providing FCR capacity $c_i(\boldsymbol{p}_i)$ is a linear function of the frequency control capacity: $c_i(\boldsymbol{p}_i) = \tilde{\boldsymbol{c}}_i^T \boldsymbol{p}_i$, with $\tilde{\boldsymbol{c}}_i = (\tilde{c}_{i,0}, \ldots, \tilde{c}_{i,n_\mathcal{T}})^T$. As the goal is to obtain an idea of the performance of the algorithm, rather than calculating the actual monetary value of the objective, we choose $\tilde{c}_{i,t}$ from a uniform distribution between 0 and 1 for each time step t and asset i. The price of FCR capacity is chosen to be $c_{FCR} = 0.8$, as primary frequency control is usually one of the most valuable services for flexibility [133]. Choosing $c_{FCR} = 0.8$, means that in 20 % of the cases the local cost for FCR capacity will still be higher than what one can gain from FCR capacity during that time step. To compare the performance of the distributed optimization algorithm, we also solve problem (6.3) in a centralized fashion towards a global optimal point, using the Gurobi solver [163].

Finally, in Algorithm 4, we set $k_{IP} = 10$ and $\alpha = 0.005$.

Convergence

Figure 6.6a the evolution of the objective value when simulating the distributed algorithm with $\rho_F = 0.25$ and $\rho_c = 0.3$, for 10 % participation in function of the iteration number k. The figure also shows the global optimum of

the centralized solver. As expected, rather than to the global optimum, the distributed optimization converges to a suboptimal solution which is 3.4 % from the global optimum.

Figure 6.6b shows the evolution of the Euclidean norm of the primal residuals of constraints (6.3d) and (6.3c), the two constraints that have been distributed. One can see that both norms decrease rapidly in the beginning, but convergence slows down when the algorithm advances. For this scenario, the algorithm converges to a feasible point in 173 iterations.

Comparing Figure 6.6a with Figure 6.6b, one can observe that the low objective value in the beginning is possible due to the high value of the primal residual of constraints (6.3c) and (6.3d). When the distributed optimization advances, the solution is forced towards a more feasible solution, thereby increasing the objective value and decreasing the primal residuals. The values of ρ_c and ρ_F determine how fast the primal residuals are forced towards zero.

Impact of ρ_c

Figure 6.7 shows the relative optimality gap of the distributed optimization algorithm versus the number of iterations until convergence towards a feasible point, for values of ρ_c ranging between 0.1 and 2.0 and $\rho_F = 0.25$. The relative optimality gap is defined as the difference between the objective value of the converged distributed optimization algorithm and the global optimum found by the centralized solver, divided by this global optimum. To account for the randomness in the location of the assets and the local costs $c_{i,t}$, we ran the distributed optimization algorithm for eight randomly drawn scenarios. Each marker type in Figure 6.7 represents one scenario with 10 % participation with the continuous black line the average of the eight scenarios. As can be seen, there is a clear trade-off between the optimality gap and the number of iterations needed for convergence, which can be tuned by varying the parameter ρ_c.

Increasing ρ_c results in quicker convergence towards a feasible point as more weight is put on the penalty terms in the augmented Lagrangian (6.5), but the algorithm also gets stuck quicker on a suboptimal integer solution. A smaller ρ_c on the other hand encourages exploration of other integer solutions, but also requires more iterations to reach a feasible point.

As ρ_c only impacts convergence of the circle constraints (6.3d), an analogue reasoning can be followed for ρ_F and the convergence of the FSP constraint (6.3c). However, as the circle constraints are much more restricting, we found that the impact of ρ_F is much less than that of ρ_c.

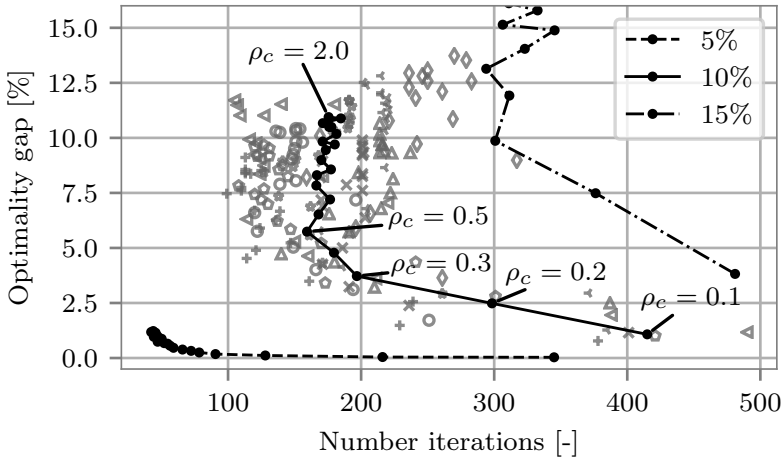

Figure 6.7: Optimality gap versus number of iterations until convergence for various values of ρ_c, at 10 % participation. Each marker type represents a different randomly drawn scenario, ran for ρ_c ranging between 0.1 and 2.0 and $\rho_F = 0.25$. The black line is the average of all scenarios, with each black dot corresponding to one value of ρ_c. The dashed lines are the averages at 5 % and 15 % participation.

Figure 6.7 also shows the averages of eight randomly drawn scenarios with 5 % participation and five scenarios with 15 % participation. These show a clear trend: as the number of participating assets decreases, both the optimality gap and the number of iterations needed for convergence decrease as well, and vice versa. However, the trade-off between iterations and optimality gap remains visible for all participation degrees.

Although the optimality gap increases with a higher participation, this will not cancel out the additional revenues resulting from a larger aggregate FCR capacity p_F that comes with a higher participation, as indicated by Table 6.1. The table shows the global optimum found with a centralized solver and the objective value of the distributed algorithm with $\rho_c = 0.3$ after convergence, averaged over all simulated scenarios. As one can see, although the optimality gap increases with increasing participation, the objective value of the distributed optimization still decreases (which means an increase in revenues) due to a larger amount of FCR capacity that can be valorized.

Finally, Figure 6.8 compares the execution time of the distributed algorithm with a centralized solver, in function of the number of assets $n_{\mathcal{I}}$ in the simulation.

	Participation [%]		
	5	10	15
Objective (6.3a) global optimum	-4201	-7451	-9464
Objective (6.3a) distributed optimization	-4194	-7175	-8532
Optimality gap distributed optimization	0.18%	3.2%	9.9%

Table 6.1: Average Optimality Gap and Objective Value (6.3a), Solved to a Global Optimum with a Centralized Solver and with the Distributed Optimization Algorithm with $\rho_c = 0.3$.

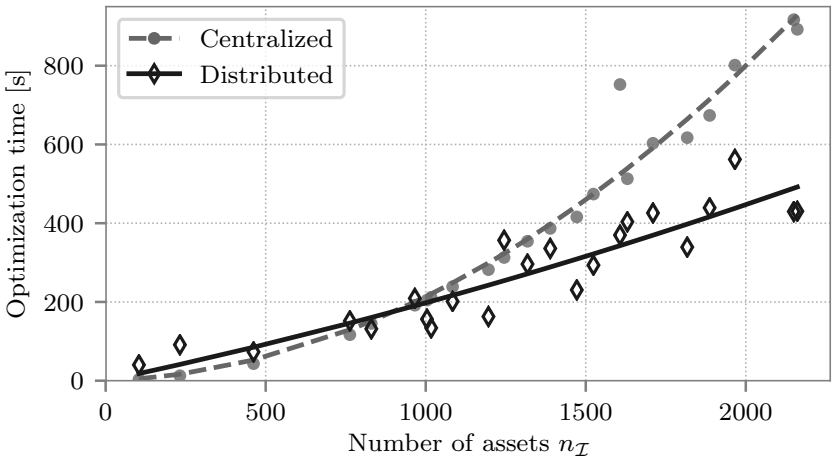

Figure 6.8: Optimisation time in function of the number of assets when solving the problem centralized, using cvxpy [210] and Gurobi [163] and with the distributed optimization algorithm with $\rho_c = 0.3$ and a participation of 10 %.

The results are obtained by including an increasing number of neighbourhoods, each with a participation of 10 %, into the simulation. The time needed for the centralized solver increases rapidly with the number of nodes, while the time for the distributed solver increases at a slower rate, owing to the parallelization of the local optimization (6.6) and of the circle constraint optimization (6.7). The figure clearly shows that, as from about 1000 assets, the distributed optimization becomes faster than a centralized solver.

In [211], another heuristic is proposed for ADMM applied to a mixed-integer unit commitment problem: first solving the continuous relaxed problem, and then

switching to the integer problem. However, solving the continuous relaxed problem already consumes a lot of iterations, and we found that a same optimality gap can be achieved with fewer iterations by choosing an appropriate value of ρ_c.

6.6 Conclusion

In this paper, we presented the problem of an FSP operating a pool of low-voltage connected flexibility resources to optimally provide FCR, while being compliant with the 2018 Belgian regulatory constraints at the distribution grid level.

We showed that these new regulatory constraints have a considerable impact on the total FCR capacity that can be monetized, however the impact varies strongly between neighbourhoods with different population densities.

We elaborated the mixed-integer problem of an FSP when operating such a pool of low-voltage grid connected assets and have proposed a distributed optimization algorithm that solves the problem in a tractable way while maintaining confidentiality of costs and the constraints of the local participants. A performance assessment of the distributed optimization shows a trade-off between the number of iterations needed for convergence towards a feasible point and the optimality gap. We showed that the distributed optimization converges quicker than a centralized solver when the number of participating assets increases above 1000.

Future work includes comparison of the proposed distributed ADMM with other distributed algorithms, such as the dual ascent method or column generation and an assessment on how the optimality gap could be decreased. Finally, it would be interesting to assess to what extent the new regulations are able to mitigate problems in the low-voltage distribution grid.

Chapter 7

General Conclusions and Future Work

This dissertation studies the use of battery energy storage systems in the electricity grid and electricity markets. The main contributions of the work include:

- An overview of the different applications battery storage systems can be used for.
- An in-depth techno-economic analysis, involving the optimised sizing and control of battery storage providing primary frequency control.
- Optimised controllers that allow behind-the-meter battery storage systems to combine primary frequency control with self-consumption or peak shaving and thereby increase value.
- An analysis of the impact of distribution grid constraints on the aggregated primary frequency control flexibility from low-voltage grid connected assets.

The section below summarises the answers this dissertation provides to the research questions posed in Section 1.3, and is followed by a general conclusion of the dissertation. Finally some suggestions for future work are given.

7.1 Answers to the Research Questions

1. For which applications can battery storage systems be used in today's market conditions?

(a) Which of these applications are relevant for third party battery owners and operators?

(b) What is the value of a battery in each of these applications and which application can be expected to deliver the most value?

Chapter 2 answers these research questions and describes the various applications BESSs can be used for in the European power grid and electricity markets. The chapter classifies the applications into three groups: ancillary services offered to grid operators, wholesale electricity market applications and applications for the end-consumer.

As TSOs have started to procure ancillary services for load-frequency control from non-conventional energy resources, providing these ancillary services have been of interest for BESS investors and operators. Especially providing FCR has been the purpose of many utility-scale battery projects, as batteries can respond very fast and the service requires the least amount of energy capacity.

The chapter also provides a quantitative estimation of the value of the different applications per MWh of energy capacity of a 1 C BESS. Our analysis shows that FCR is the application which can provide the highest value, due to the rather limited energy content needed and a liquid market with a relatively high remuneration. There is a high potential value in arbitraging on short-term (intraday) wholesale markets and imbalance markets. However, achieving this value requires perfect hindsight knowledge of the market prices, so that the practically achievable value lies a lot lower. It is expected that an increase of renewable generation will lead to an increase in volatility on short-term electricity markets, further increasing the potential revenues for arbitraging on these markets. Positive business cases for BESS used by grid operators to provide congestion management and grid investment deferral exist, but markets to procure this service from third party battery operators are still in a pilot phase.

Self-consumption and peak shaving are two consumer applications which can be provided by behind-the-meter battery storage and can create a considerable value for the consumer. The actual value of these application depends on the consumption profile, the size of the BESS and the electricity tariff structure faced by the consumer. However, at current market prices, only FCR and aFRR are able to pay back a BESS at an investment cost of 500 €/kWh.

2. What is the value of a battery storage system delivering frequency control reserves?

(a) How to optimise the battery control over its lifetime, while taking the details of battery dynamics and degradation into account?

(b) What is the optimal size of a battery delivering frequency control?

These research questions are dealt with in Chapter 3. The chapter proposes a novel holistic optimisation framework for the investment analysis, sizing and control design of a battery energy storage system used for frequency control. As a battery energy storage system has a limited energy content, a recharge controller is needed to ensure the battery is never empty nor full, as this would mean the symmetric frequency control capacity is not available any more. In the chapter, we optimised a parametrised recharge controller to ensure the battery is always able to delivery the service, while minimising degradation and electricity cost. Since the grid frequency is stochastic, we formulated the problem as a stochastic optimisation problem. We adopted a global evolutionary optimisation algorithm, which allowed us to use a more detailed battery and degradation model of which a closed mathematical expression is not readily available. Via a thorough analysis, we were able to decrease the amount of data needed, reducing the execution time while keeping the approximation error within predefined limits.

As a case study, the optimisation framework is applied to the German FCR market, considering all relevant regulations and using real frequency data. The results show that a positive business case for a BESS providing FCR is possible. To provide 1 MW of FCR capacity, a battery storage system rated at 1.6 MW/1.6 MWh has the highest net present value and can provide FCR for 10.8 years, after which it is degraded to 80 % state of health. The degradation is mainly due to calender degradation, as most of the cycles when doing FCR are with low DoD, which have limited impact on degradation.

3. How can a battery storage system combine multiple applications?

(a) How to design a controller that optimally combines multiple applications?

(b) Does the value of the battery storage increases by combining multiple applications?

The combination of multiple applications with a battery storage system is addressed in Chapters 4 and 5, which study how to take advantage of behind-

the-meter battery storage systems for frequency control together with self-consumption or peak shaving, respectively.

The chapters propose a battery controller which allows to combine multiple applications and is the result of a stochastic optimisation problem, performing the trade-off between the expected value of both applications and so maximising total value. To ensure the required frequency control capacity is continuously available, we employed a linear recharging controller which we integrated into the optimisation problem using robust optimisation as a safe, tractable approximation to the probabilistic constraints, allowing to ensure the risk on unavailability is below a predefined value while keeping the problem efficiently solvable. To combine frequency control with peak shaving, we extended this controller with a dynamic programming framework which allowed us to combine the daily decision making in the frequency control markets with the longer-term objective of peak shaving.

Case study results from both chapters show that there are synergies when combining frequency control with self-consumption or peak shaving and more value can be created by combining the applications than by using the battery for one application only. The controllers resulting from the proposed optimisations allow to reserve more energy and battery power for self-consumption at moments when expected production is high, or for peak shaving when a peak is expected in the consumption profile. The combination of FCR with self-consumption allows to increase the revenues of the battery with 35 % compared to performing frequency control only, and times 2.5 compared to self-consumption only. Besides an increase in revenues, the ability to use a BESS for multiple applications also presents a hedge against changing market conditions in one of the applications.

The dynamic program developed to combine frequency control with peak shaving shows that the optimal frequency control capacity varies with the consumption peak observed so far. Finally, results show that additional value can be obtained by aggregating FCR capacity from multiple batteries installed at different sites while they perform peak shaving locally at each site. In a case study we show that aggregating two batteries in this way doubles revenues compared to using the batteries for peak shaving only, and increases revenues with 10 % compared to using them for FCR only.

4. What is the impact of distribution grid constraints on flexibility from battery storage?

This research question is treated in Chapter 6. In 2018, a new Belgian regulation became into force, limiting the flexible capacity connected to the low-voltage distribution grid that can be used for frequency control. The chapter analyses

the impact of this new distribution grid constraint on the total frequency control capacity that can be used by an aggregator. As the regulation considers how close the flexible assets are located together, there is a larger impact on the flexibility from neighbourhoods with a high population density, such as city centres, than from rural neighbourhoods. For instance, if 5 % of the households participate in demand response flexibility, only around 70 % of totally available frequency control capacity can be used in city centres, but still 100 % of totally available frequency control capacity in more rural neighbourhoods, and 90 % on average. Although it is unrealistic that 5 % of all households will provide frequency control capacity, as the frequency control market volume is simply not large enough, the presented analysis can be applicable for certain areas, such as newly build neighbourhoods, that have a higher density in flexibility from e.g. battery storage.

To deal with the distribution grid constraints and maximise the frequency control capacity, the chapter proposes the use of a scalable distributed optimisation algorithm to aggregate frequency control capacity, which allows the assets to keep their cost functions private and only have to communicate with neighbouring assets that are geographically close, and with the flexibility service provider or aggregator.

7.2 General Conclusions

As more intermittent renewable generation is being installed into the electricity grid, the need for flexibility to balance the grid increases as well. However, traditional flexible assets such as gas-fired power are not climate-neutral and are being pushed out of the market by renewable generation that have a lower marginal cost. Decreasing prices of battery cells are making batteries a promising option for energy storage and flexibility in the electricity grid. Nevertheless, the return of investment in battery storage remains low and uncertain, holding back a widespread rollout of battery energy storage in the power grid.

Battery storage can deliver a number of different services to different stakeholders in the electricity grid. This dissertation analyses and compares the value of multiple battery storage applications and shows that frequency containment reserve brings the most value for battery storage as the remuneration is relatively high and the required energy for activation is rather low. The value for battery storage in automatic frequency restoration reserve is also considerably high, mainly due to the high activation payments, and both ancillary services for load-frequency control and are able to pay back the investment in a BESS at an investment cost of 500 €/kWh. In theory, there is more value in battery storage

providing arbitrage in short-term (intraday) wholesale and balancing markets. However, as one does not have perfect hindsight knowledge of the market prices, the practical achievable value lies lower and is dependable on the quality of the market price forecaster that one is able to develop.

When providing frequency containment reserve, a battery energy storage system needs a recharge controller, ensuring the battery is never empty nor full, as this would mean the symmetric reserve capacity is not available any more. This dissertation provides a way to optimise such a recharge controller, minimising degradation of the battery while complying with regulatory constraints. Using such an optimised controller and taking into account a detailed degradation model, we have shown that battery energy storage delivering frequency containment reserves in the German market can indeed be profitable for certain sizes of battery systems and if market prices do not decline too much.

Combining applications is another way to increase value from battery energy storage. This is especially interesting for behind-the-meter battery storage, where additional value can be created by providing ancillary services on top of the local service the battery provides to the consumer where the battery is installed. In this dissertation, we have studied how to combine frequency control with self-consumption or with peak shaving. We have developed controllers that allow to optimally combine these applications, maximising the value from the battery. We show that synergies between the services exists, i.e. more value can be obtained from combining the applications than by using the battery storage for one application only. Besides, we have shown that value can be increased even further when aggregating frequency control capacity of multiple battery storage systems installed at multiple sites, when used simultaneously for peak shaving at these sites. The ability to use a BESS for multiple applications does not only lead to increased revenues, but also presents a hedge against changing market conditions for one of the applications.

Most of the behind-the-meter battery storage will be connected to the distribution grid. Therefore, when aggregating the flexibility from these battery storage systems to be used on wholesale markets or to offer ancillary services to the TSO, it is important to take into account distribution grid constraints. By analysing the impact of a new regulatory constraint that has the objective to prevent congestion of the distribution grid caused by flexible assets in Belgium, we show that such distribution grid constraints indeed have a limiting effect on total aggregated flexible capacity, especially in areas where the density of flexible assets is high.

Recommendations for Policy Makers and Regulators

Currently, providing load-frequency control as ancillary service to the transmission grid operators is one of the most important applications for battery storage. Due to their limited energy content, battery energy storage systems delivering frequency control reserves have to be controlled differently than traditional power assets, as they have to manage their state of charge. Despite regulations from the European Commission that have the objective to come to more integrated European ancillary services markets with harmonised products, the product details often still differ between various European countries and rules on state of charge management are not always clear. A clear, unambiguous regulatory framework that establishes harmonised ancillary services products and lays down the rules on state of charge management would therefore help to take away uncertainty towards investors, to create a level playing field for all assets, with or without a limited energy content, and so stimulate the development of energy storage in the grid. Together with the design of liquid and transparent ancillary services markets that have a low bid size granularity, regulators and grid operators have some important tools to advance the development of energy storage and stimulate innovation in the power grid.

Energy costs of battery storage providing FCR in Germany are low and therefore do not represent a considerable cost. However, this is due to regulations that exempt stand-alone battery storage of many grid costs and levies which are typically charged to electricity consumers. When these electricity consumption taxes and levies are not exempted, these levies and taxes are effectively double charged if the stored energy is not used on the same premises. The levies are charged once when consuming electricity from the grid to charge the battery, and later again by the end consumer who uses the electricity discharged by the battery. This can present a large burden for energy storage when providing ancillary services or wholesale market arbitrage. A novel directive of the European Parliament on the electricity market already states that battery storage cannot be subject to such double charges, including grid tariffs, when providing flexibility services to grid operators [212]. A quick implementation of this directive by member states will boost profitability as it decreases the cost of using battery storage flexibility in the grid.

Currently, distribution grid constraints for aggregators are either non-existing or are rather basic. For instance, the regulatory constraint studied in this dissertation is simple to enforce, but it is not clear if it is the most efficient way to avoid distribution grid problems. Using a more accurate representation of distribution grid constraints, for instance by taking specific time periods or actual grid load into account, will allow for more flexibility at places in the grid where there is still some headroom, and restrain the use of flexibility only at

places and times where there are real problems.

7.3 Future Work

In today's battery storage market, there is a rather clear separation between the battery storage system manufacturer, which designs and produces the battery energy storage system as a final product, and the battery system operator, who operates the battery storage system and tries to create value with it by using the battery storage system for a certain application, as described in this dissertation. While the manufacturer has a deep understanding of the dynamics and the components of the battery system, typically not all this information is shared with the battery operator, which can therefore only optimise the operation of the battery system using a simplified battery model. This issue becomes especially apparent when considering battery degradation. A battery storage system manufacturer typically warrants the remaining energy capacity of a battery system in function of some simplified parameters, like total throughput. However, using such a simplified metric in warranties does not represent reality and a battery operator who uses this metric to optimise its operational control strategy will therefore obtain a sub-optimal control strategy which lead to a conservative operation of the battery storage system.

An integrated design of both the battery system and the operational controller, taking the end-use application, the dynamics and degradation into account, can clearly bring additional value. However, such an integrated design can quickly become very complex due to the large amount of parameters. Useful future work will therefore consist of creating integrated design methods for the operational control and system design of battery storage systems.

To achieve this, more research is needed into accurate, yet practically usable degradation models for battery storage systems. Current research on battery degradation is focussed on degradation of a single cell, when stored at a constant SoC or cycled with a constant depth of discharge. However, these conditions do not represent the actual operation of a battery system and it is still largely unclear how exactly battery storage systems degrade when used in actual applications.

Most degradation models assume the battery cell reaches its end of life when the remaining energy capacity is at 80 % of initial energy capacity. Nevertheless, such a battery cell still has 80 % of energy capacity remaining, and there is no physical reason to stop using cell after this threshold. The same holds for second life batteries, e.g. from electric vehicles. While the remaining capacity of a battery might be too low for electric vehicles, it could still be used for energy

storage in the grid, at a much lower capital cost than new battery storage systems. However, the current understanding of degraded and second life batteries is rather limited and more research can stimulate the use of degraded and second life batteries for energy storage.

In this dissertation, we have paid much attention to controllers that are implementable in practice, e.g. by avoiding the use of any hindsight knowledge, and using real data where this was available. Nevertheless, relevant future work consists of the practical validation of the performance of the developed controllers on actual battery systems installed in a real-life setting.

Aggregating battery storage systems with other types of flexibility such as demand response from industrial processes or residential consumption can lead additional value. For instance, when the other flexible assets have a larger or even unlimited energy content, they can help to overcome the energy capacity requirements of applications which require a long activation time. Therefore, promising future work consists of researching which types of assets have the most potential to be aggregated with battery storage systems and developing control strategies to deliver the required services with multiple assets while respecting the constraints of each asset.

Finally, interesting future research is on the integration of distribution grid constraints in market clearing algorithms, both in wholesale markets and in ancillary services markets. Besides, flexibility can also be used to relieve distribution grid congestion problems and support de DSO in operating the distribution grid. Therefore, promising future work consist of using flexibility to offer localised ancillary services to the DSO, possibly via a *microgrid* concept, where battery storage is shared in a neighbourhood to relieve distribution grid congestion at the point where the neighbourhood is connected to the rest of the distribution grid.

Appendix A

Rainflow Counting Algorithm

The rainflow counting algorithm used in (3.2) starts from all the local extrema ν_i of the vector $\boldsymbol{SoC}$ and is shown below:

Algorithm A.1 Rainflow Counting Algorithm [99]

1: Let $\boldsymbol{\nu} = (\nu_1, \nu_2, \ldots, \nu_{n_\nu})$ be a vector containing the local extrema of $\boldsymbol{SoC} \in \mathbb{R}^{n_t}$.
2: $s \leftarrow 1, i \leftarrow 3, i_c \leftarrow 0, Q_0 \leftarrow 0$.
3: **while** $i \leq n_\nu$ **do**
4: **while** $i - s < 2$ **do**
5: $i \leftarrow i + 1$.
6: $\Delta_1 \leftarrow |\nu_{i-2} - \nu_{i-1}|, \Delta_2 \leftarrow |\nu_{i-1} - \nu_i|$.
7: **if** $\Delta_2 \geq \Delta_1$ **then**
8: **if** $i - 2 = s$ **then**
9: Store $|\nu_{i-2} - \nu_{i-1}|$ as a half cycle:
10: $i_c \leftarrow i_c + 1$, $SoC^{cyc}_{av,i_c} \leftarrow (\nu_{i-2} + \nu_{i-1})/2$, $DoD_{i_c} \leftarrow \Delta_1$, $Q_{i_c} \leftarrow Q_{i_c-1} + \Delta_1 C/2$.
11: Remove ν_{i-2} from $\boldsymbol{\nu}$, re-index and set $s \leftarrow s + 1, i \leftarrow i - 1$.
12: **else**
13: Store $|\nu_{i-2} - \nu_{i-1}|$ as a full cycle:
14: $i_c \leftarrow i_c + 1$, $SoC^{cyc}_{av,i_c} \leftarrow (\nu_{i-2} + \nu_{i-1})/2$, $DoD_{i_c} \leftarrow \Delta_1$, $Q_{i_c} \leftarrow Q_{i_c-1} + \Delta_1 C$.
15: Remove ν_{i-2} and ν_{i-1} from $\boldsymbol{\nu}$, re-index and set $i \leftarrow i - 2$.
16: **else**
17: $i \leftarrow i + 1$.
18: Store all remaining differences $|\nu_{i-1} - \nu_i|$ in $\boldsymbol{\nu}$ as a half cycle, according to step 10.

Bibliography

[1] United Nations. Climate Change. [Online]. Available: www.un.org/en/sections/issues-depth/climate-change/ [Accessed 2019-10-03].

[2] Earth Science Communications Team - NASA. Responding to Climate Change. [Online]. Available: climate.nasa.gov/solutions/adaptation-mitigation/ [Accessed 2019-10-03].

[3] United Nations Treaty Collection, Chapter XXVII 7. d, "Paris agreement (adopted 12 dec. 2016 and entered into force 4 nov. 2016)."

[4] European Environment Agency. Total greenhouse gas emission trends and projections. [Online]. Available: www.eea.europa.eu/data-and-maps/indicators/greenhouse-gas-emission-trends-6/assessment-2 [Accessed 2019-10-03].

[5] D. Steinberg, D. Bielen, J. Eichman, K. Eurek, J. Logan, T. Mai, C. McMillan, A. Parker, L. Vimmerstedt, and E. Wilson, "Electrification and decarbonization: Exploring us energy use and greenhouse gas emissions in scenarios with widespread electrification and power sector decarbonization," National Renewable Energy Lab.(NREL), Golden, CO (United States), Tech. Rep., 2017.

[6] European Commission. 2030 climate & energy framework. [Online]. Available: ec.europa.eu/clima/policies/strategies/2030_en [Accessed 2019-10-03].

[7] European Commission. 2050 long-term strategy. [Online]. Available: ec.europa.eu/clima/policies/strategies/2050_en [Accessed 2019-10-03].

[8] B. Shen, G. Ghatikar, Z. Lei, J. Li, G. Wikler, and P. Martin, "The role of regulatory reforms, market changes, and technology development to make demand response a viable resource in meeting energy challenges," *Applied Energy*, vol. 130, pp. 814 – 823, 2014. doi: 10.1016/j.apenergy.2013.12.069

[9] P. Tielens and D. Van Hertem, "The relevance of inertia in power systems," *Renewable and Sustainable Energy Reviews*, vol. 55, pp. 999 – 1009, 2016. doi: 10.1016/j.rser.2015.11.016

[10] H. Höschle, C. De Jonghe, D. Six, and R. Belmans, "Capacity remuneration mechanisms and the transition to low-carbon power systems," in *2015 12th International Conference on the European Energy Market (EEM)*, May 2015. doi: 10.1109/EEM.2015.7216647 pp. 1–5.

[11] N. Kittner, F. Lill, and D. M. Kammen, "Energy storage deployment and innovation for the clean energy transition," *Nature Energy*, vol. 2, no. 9, p. 17125, 2017. doi: 10.1038/nenergy.2017.125

[12] B. Nykvist and M. Nilsson, "Rapidly falling costs of battery packs for electric vehicles," *Nature climate change*, vol. 5, no. 4, p. 329, 2015. doi: 10.1038/nclimate2564

[13] A. Stephan, B. Battke, M. Beuse, J. H. Clausdeinken, and T. S. Schmidt, "Limiting the public cost of stationary battery deployment by combining applications," *Nature Energy*, vol. 1, no. 7, p. 16079, 2016. doi: 10.1038/nenergy.2016.79

[14] G. Fitzgerald, J. Mandel, J. Morris, and H. Touati, "The economics of battery energy storage: How multi-use, customer-sited batteries deliver the most services and value to customers and the grid," *Rocky Mountain Institute*, p. p6, 2015.

[15] P. Hardy and A. Pinto-Bello, "EU Market Monitor for Demand Side Flexibility 2019," smartEn - Smart Energy Europe, Delta-EE, Tech. Rep., November 2019. [Online]. Available: www.smarten.eu/wp-content/uploads/2019/11/EU_Market_Monitor_2019_short_final.pdf [Accessed 03-12-2019].

[16] "Battery Storage to Drive the Power System Transition," BATSTORM H2020 project, Tech. Rep., September 2018. [Online]. Available: ec.europa.eu/energy/en/topics/technology-and-innovation/energy-storage/batteries#batstorm-project [Accessed 03-12-2019].

[17] A. Poullikkas, "A comparative overview of large-scale battery systems for electricity storage," *Renewable and Sustainable Energy Reviews*, vol. 27, pp. 778 – 788, 2013. doi: 10.1016/j.rser.2013.07.017

[18] K. Imran and I. Kockar, "A technical comparison of wholesale electricity markets in north america and europe," *Electric Power Systems Research*, vol. 108, pp. 59 – 67, 2014. doi: 10.1016/j.epsr.2013.10.016

[19] Q. Wang, C. Zhang, Y. Ding, G. Xydis, J. Wang, and J. Østergaard, "Review of real-time electricity markets for integrating distributed energy resources and demand response," *Applied Energy*, vol. 138, pp. 695 – 706, 2015. doi: 10.1016/j.apenergy.2014.10.048

[20] D. Newbery, G. Strbac, and I. Viehoff, "The benefits of integrating european electricity markets," *Energy Policy*, vol. 94, pp. 253 – 263, 2016. doi: 10.1016/j.enpol.2016.03.047

[21] European Commission, "Commission Regulation (EU) 2017/1485 of 2 August 2017 establishing a guideline on electricity transmission system operation."

[22] European Commission, "Commission regulation (eu) 2017/2195 of 23 november 2017 establishing a guideline on electricity balancing."

[23] ENTSO-E. Glossary. [Online]. Available: docstore.entsoe.eu/data/data-portal/glossary [Accessed 24-06-2019].

[24] ENTSO-E, "Network Code on Load-Frequency Control and Reserves," Tech. Rep., 2013. [Online]. Available: www.entsoe.eu/fileadmin/user_upload/_library/resources/LCFR/130628-NC_LFCR-Issue1.pdf

[25] J. Tant, F. Geth, D. Six, P. Tant, and J. Driesen, "Multiobjective battery storage to improve pv integration in residential distribution grids," *IEEE Transactions on Sustainable Energy*, vol. 4, no. 1, pp. 182–191, Jan 2013. doi: 10.1109/TSTE.2012.2211387

[26] Deutsche ÜNB. Regelleistung, Internetplattform zur Vergabe von Regelleistung. [Online]. Available: www.regelleistung.net/

[27] Elia, "General framework for frequency containment reserve service by non-CIPU resources 2019-2021," Jan 2019. [Online]. Available: www.elia.be/~/media/files/Elia/Suppliers/Purchasing%20categories/GFA%20FCR%20NonCIPU%20201901%20VFINAL.pdf

[28] Deutsche ÜNB, "Eckpunkte und Freiheitsgrade bei Erbringung von Primärregelleistung," Tech. Rep., Apr. 2014. [Online]. Available: www.regelleistung.net/ext/download/eckpunktePRL

[29] Deutsche ÜNB, "Anforderungen an die Speicherkapazität bei Batterien für die Primärregelleistung," Tech. Rep., Sep. 2015. [Online]. Available: www.regelleistung.net/ext/download/anforderungBatterien

[30] J. Kopiske, S. Spieker, and G. Tsatsaronis, "Value of power plant flexibility in power systems with high shares of variable renewables: A scenario

outlook for germany 2035," *Energy*, vol. 137, pp. 823 – 833, 2017. doi: 10.1016/j.energy.2017.04.138

[31] NERC, "Balancing and frequency control - a technical document prepared by the nerc resources subcommittee," NERC - North American Electric Reliability Corporation, Tech. Rep., January 2011.

[32] 50Hertz, Amprion, TenneT, TransnetBW, "Präqualifikationsverfahren für Regelreserveanbieter in Deutschland - 23.05.2019," Tech. Rep., 2019. [Online]. Available: www.regelleistung.net/ext/download/PQ_Bedingungen_FCR_aFRR_mFRR

[33] Elia, "R2 Non-CIPU. description and conclusions of the pilot project. assessment of implications of transfer of energy." Tech. Rep., Dec 2017. [Online]. Available: www.elia.be/~/media/files/Elia/users-group/Working-Group-Balancing/20171221_R2-non-CIPU-Report.pdf

[34] C. Olk, D. U. Sauer, and M. Merten, "Bidding strategy for a battery storage in the german secondary balancing power market," *Journal of Energy Storage*, vol. 21, pp. 787 – 800, 2019. doi: 10.1016/j.est.2019.01.019

[35] ENTSO-E WGAS. Survey on ancillary services procurement, balancing market design 2018. [Online]. Available: entsoe.eu/publications/market-reports/#survey-on-ancillary-services-procurement-and-electricity-balancing-market-design [Accessed 2019-03-20].

[36] "Challenges and Opportunities for the Nordic Power System," Statnett, Fingrid, Energinet.dk, Svenska Kraftnät, Tech. Rep., Augustus 2016. [Online]. Available: www.fingrid.fi/globalassets/dokumentit/fi/yhtio/tki-toiminta/report-challenges-and-opportunities-for-the-nordic-power-system.pdf

[37] F. M. Gonzalez-Longatt and S. M. Alhejaj, "Enabling inertial response in utility-scale battery energy storage system," in *2016 IEEE Innovative Smart Grid Technologies - Asia (ISGT-Asia)*, Nov 2016. doi: 10.1109/ISGT-Asia.2016.7796453. ISSN 2378-8542 pp. 605–610.

[38] R. Eriksson, N. Modig, and K. Elkington, "Synthetic inertia versus fast frequency response: a definition," *IET Renewable Power Generation*, vol. 12, no. 5, pp. 507–514, 2018. doi: 10.1049/iet-rpg.2017.0370

[39] "Need for synthetic inertia (SI) for frequency regualation," ENTSO-E, Tech. Rep., January 2018. [Online]. Available: docstore.entsoe.eu/Documents/Network%20codes%20documents/NC%20RfG/IGD_Need_for_Synthetic_Inertia_final.pdf [Accessed 18-12-2019].

[40] Imperial Irrigation District (IID). IID demonstrates battery's emergency black start capability. [Online]. Available: www.iid.com/Home/Components/News/News/557/30?backlist=%2F [Accessed 27-06-2019].

[41] P. Bach Andersen, J. Hu, and K. Heussen, "Coordination strategies for distribution grid congestion management in a multi-actor, multi-objective setting," in *2012 3rd IEEE PES Innovative Smart Grid Technologies Europe (ISGT Europe)*, Oct 2012. doi: 10.1109/ISGTEurope.2012.6465853. ISSN 2165-4816 pp. 1–8.

[42] H. P. Knops, L. J. de Vries, and R. A. Hakvoort, "Congestion management in the european electricity system: an evaluation of the alternatives," *Journal of Network Industries*, no. 3, pp. 311–351, 2001.

[43] K. Spiliotis, S. Claeys, A. R. Gutierrez, and J. Driesen, "Utilizing local energy storage for congestion management and investment deferral in distribution networks," in *2016 13th International Conference on the European Energy Market (EEM)*, June 2016. doi: 10.1109/EEM.2016.7521198. ISSN 2165-4093 pp. 1–5.

[44] A. Ramos, C. D. Jonghe, V. Gómez, and R. Belmans, "Realizing the smart grid's potential: Defining local markets for flexibility," *Utilities Policy*, vol. 40, pp. 26 – 35, 2016. doi: 10.1016/j.jup.2016.03.006

[45] Centrica. Cornwall local energy market. [Online]. Available: www.centrica.com/innovation/cornwall-local-energy-market [Accessed 2019-12-18].

[46] L. Hirth, I. Schlecht, C. Maurer, and B. Terteegen, "Cost- or market-based? Future redispatch procurement in Germany," Commissioned by the Federal Ministry for Economic Affairs and Energy Germany, Tech. Rep., October 2019. [Online]. Available: www.bmwi.de/Redaktion/EN/Publikationen/Studien/future-redispatch-procurement-in-germany.pdf?___blob=publicationFile&v=2 [Accessed 19-12-2019].

[47] D. I. Chatzigiannis, G. A. Dourbois, P. N. Biskas, and A. G. Bakirtzis, "European day-ahead electricity market clearing model," *Electric Power Systems Research*, vol. 140, pp. 225 – 239, 2016. doi: 10.1016/j.epsr.2016.06.019

[48] Epex Spot SE - Belpex. Product specifications. [Online]. Available: www.belpex.be/about-us/contact/ [Accessed 2019-07-12].

[49] Epex Spot SE. Epex Spot introduces curtailable blocks and loop blocks on all Day-Ahead markets. [Online]. Available: www.epexspot.com/en/press-media/press/details/Press/show_detail/40116 [Accessed 10-10-2019].

[50] ENTSO-E. ENTSO-E Transparency Platform. [Online]. Available: transparency.entsoe.eu/ [Accessed 2019-08-27].

[51] D. Keles, J. Scelle, F. Paraschiv, and W. Fichtner, "Extended forecast methods for day-ahead electricity spot prices applying artificial neural networks," *Applied Energy*, vol. 162, pp. 218 – 230, 2016. doi: 10.1016/j.apenergy.2015.09.087

[52] K. Neuhoff, N. Ritter, A. Salah-Abou-El-Enien, and P. Vassilopoulos, "Intraday markets for power: Discretizing the continuous trading?" *DIW Berlin Discussion Paper*, vol. 1544, Jan. 2016. doi: 10.2139/ssrn.2723902

[53] T. Gomez, I. Herrero, P. Rodilla, R. Escobar, S. Lanza, I. de la Fuente, M. L. Llorens, and P. Junco, "European union electricity markets: Current practice and future view," *IEEE Power and Energy Magazine*, vol. 17, no. 1, pp. 20–31, Jan 2019. doi: 10.1109/MPE.2018.2871739

[54] Epex Spot SE. Intraday market with delivery on the German TSO zone. [Online]. Available: www.epexspot.com/en/product-info/intradaycontinuous/germany [Accessed 29-01-2018].

[55] Epex Spot SE. [Online]. Available: www.epexspot.com [Accessed 2019-09-02].

[56] A. Mesbah, "Stochastic model predictive control: An overview and perspectives for future research," *IEEE Control Systems Magazine*, vol. 36, no. 6, pp. 30–44, Dec 2016. doi: 10.1109/MCS.2016.2602087

[57] I. Richardson, M. Thomson, D. Infield, and C. Clifford, "Domestic electricity use: A high-resolution energy demand model," *Energy and Buildings*, vol. 42, no. 10, pp. 1878–1887, 2010. doi: 10.1016/j.enbuild.2010.05.023

[58] J. M. Bright, C. J. Smith, P. G. Taylor, and R. Crook, "Stochastic generation of synthetic minutely irradiance time series derived from mean hourly weather observation data," *Solar Energy*, vol. 115, pp. 229–242, 2015. doi: 10.1016/j.solener.2015.02.032

[59] BDEW. Strompreis für Haushalte. [Online]. Available: www.bdew.de/service/daten-und-grafiken/strompreis-fuer-haushalte/ [Accessed 2019-09-04].

[60] Bundesnetzagentur. EEG-Registerdaten un -Fördersätze. [Online]. Available: www.bundesnetzagentur.de/DE/Sachgebiete/ElektrizitaetundGas/Unternehmen_Institutionen/ErneuerbareEnergien/ZahlenDatenInformationen/EEG_Registerdaten/EEG_Registerdaten_node.html/ [Accessed 2019-09-04].

[61] A. Picciariello, J. Reneses, P. Frias, and L. Söder, "Distributed generation and distribution pricing: Why do we need new tariff design methodologies?" *Electric Power Systems Research*, vol. 119, pp. 370–376, feb 2015. doi: 10.1016/j.epsr.2014.10.021

[62] Bundesrepublik Deutschland, Bundesrechtsverordnung. (2015, Jul.) Stromnetzentgeltverordnung (StromNEV). [Online]. Available: www.gesetze-im-internet.de/stromnev/

[63] Journal officiel de la République Française, "Décret n°2016-141 du 11 février relatif au statut d'électro-intensif et à la réduction TURPE ." [Online]. Available: www.legifrance.gouv.fr/affichTexte.do;jsessionid=3DA5A16655A37CDAF6706146DFFA9E1D.tpdila16v_3?cidTexte=JORFTEXT000032036397&dateTexte=20160212

[64] Westnetz. Netzentgelte Strom. [Online]. Available: iam.westnetz.de/ueber-westnetz/unser-netz/netzentgelte-strom/ [Accessed 2019-09-05].

[65] Y. Wang and L. Li, "Time-of-use electricity pricing for industrial customers: A survey of u.s. utilities," *Applied Energy*, vol. 149, pp. 89 – 103, 2015. doi: 10.1016/j.apenergy.2015.03.118

[66] J. Stöckl, P. Jonke, B. Bletterie, and S. Kadam, "Power quality improvement strategies for battery storage systems with low-voltage grid support," in *2017 19th European Conference on Power Electronics and Applications (EPE'17 ECCE Europe)*, Sep. 2017. doi: 10.23919/EPE17ECCEEurope.2017.8099053

[67] R. Dharavath, I. J. Raglend, and A. Manmohan, "Implementation of solar pv — battery storage with dvr for power quality improvement," in *2017 Innovations in Power and Advanced Computing Technologies (i-PACT)*, April 2017. doi: 10.1109/IPACT.2017.8245134 pp. 1–5.

[68] J. Stuyts, "Implementation of unbalance compensation using grid-supporting converters," Ph.D. dissertation, KU Leuven, 2018.

[69] R. Green and N. Vasilakos, "Market behaviour with large amounts of intermittent generation," *Energy Policy*, vol. 38, no. 7, pp. 3211 – 3220, 2010. doi: 10.1016/j.enpol.2009.07.038

[70] T. Rintamäki, A. S. Siddiqui, and A. Salo, "Does renewable energy generation decrease the volatility of electricity prices? an analysis of denmark and germany," *Energy Economics*, vol. 62, pp. 270 – 282, 2017. doi: 10.1016/j.eneco.2016.12.019

[71] D. Greenwood, K. Lim, C. Patsios, P. Lyons, Y. Lim, and P. Taylor, "Frequency response services designed for energy storage," *Applied Energy*, vol. 203, pp. 115 – 127, 2017. doi: 10.1016/j.apenergy.2017.06.046

[72] R. Lee, S. Homan, N. M. Dowell, and S. Brown, "A closed-loop analysis of grid scale battery systems providing frequency response and reserve services in a variable inertia grid," *Applied Energy*, vol. 236, pp. 961 – 972, 2019. doi: 10.1016/j.apenergy.2018.12.044

[73] R. Hollinger, L. M. Diazgranados, C. Wittwer, and B. Engel, "Optimal provision of primary frequency control with battery systems by exploiting all degrees of freedom within regulation," *Energy Procedia*, vol. 99, pp. 204 – 214, 2016. doi: 10.1016/j.egypro.2016.10.111

[74] D. I. Stroe, V. Knap, M. Swierczynski, A. I. Stroe, and R. Teodorescu, "Operation of a grid-connected lithium-ion battery energy storage system for primary frequency regulation: A battery lifetime perspective," *IEEE Transactions on Industry Applications*, vol. 53, no. 1, pp. 430–438, Jan 2017. doi: 10.1109/TIA.2016.2616319

[75] T. Thien, D. Schweer, D. vom Stein, A. Moser, and D. U. Sauer, "Real-world operating strategy and sensitivity analysis of frequency containment reserve provision with battery energy storage systems in the german market," *Journal of Energy Storage*, vol. 13, pp. 143 – 163, 2017. doi: 10.1016/j.est.2017.06.012

[76] Y. J. A. Zhang, C. Zhao, W. Tang, and S. H. Low, "Profit-maximizing planning and control of battery energy storage systems for primary frequency control," *IEEE Transactions on Smart Grid*, vol. 9, no. 2, pp. 712–723, March 2018. doi: 10.1109/TSG.2016.2562672

[77] B. Cheng and W. B. Powell, "Co-optimizing battery storage for the frequency regulation and energy arbitrage using multi-scale dynamic programming," *IEEE Transactions on Smart Grid*, vol. 9, no. 3, pp. 1997–2005, May 2018. doi: 10.1109/TSG.2016.2605141

[78] Y. Shi, B. Xu, Y. Tan, D. Kirschen, and B. Zhang, "Optimal battery control under cycle aging mechanisms in pay for performance settings," *IEEE Transactions on Automatic Control*, vol. 64, no. 6, pp. 2324–2339, June 2019. doi: 10.1109/TAC.2018.2867507

[79] F. M. Gatta, A. Geri, R. Lamedica, S. author, M. Maccioni, F. Palone, M. Rebolini, and A. Ruvio, "Application of a lifepo4 battery energy storage system to primary frequency control: Simulations and experimental results," *Energies (2016)*, vol. 9, no. 11. doi: 10.3390/en9110887

[80] M. Kazemi and H. Zareipour, "Long-term scheduling of battery storage systems in energy and regulation markets considering battery's lifespan," *IEEE Transactions on Smart Grid*, vol. 9, no. 6, pp. 6840–6849, Nov 2018. doi: 10.1109/TSG.2017.2724919

[81] S. Melo, U. Brand, T. Vogt, J. Telle, F. Schuldt, and K. Maydell, "Primary frequency control provided by hybrid battery storage and power-to-heat system," *Applied Energy*, vol. 233-234, pp. 220 – 231, 2019. doi: 10.1016/j.apenergy.2018.09.177

[82] B. Lian, A. Sims, D. Yu, C. Wang, and R. W. Dunn, "Optimizing lifepo4 battery energy storage systems for frequency response in the uk system," *IEEE Transactions on Sustainable Energy*, vol. 8, no. 1, pp. 385–394, Jan 2017. doi: 10.1109/TSTE.2016.2600274

[83] L. Johnston, F. Díaz-González, O. Gomis-Bellmunt, C. Corchero-García, and M. Cruz-Zambrano, "Methodology for the economic optimisation of energy storage systems for frequency support in wind power plants," *Applied Energy*, vol. 137, pp. 660 – 669, 2015. doi: 10.1016/j.apenergy.2014.09.031

[84] J. Fleer, S. Zurmühlen, J. Meyer, J. Badeda, P. Stenzel, J.-F. Hake, and D. U. Sauer, "Techno-economic evaluation of battery energy storage systems on the primary control reserve market under consideration of price trends and bidding strategies," *Journal of Energy Storage*, vol. 17, pp. 345 – 356, 2018. doi: 10.1016/j.est.2018.03.008

[85] R. L. Fares, J. P. Meyers, and M. E. Webber, "A dynamic model-based estimate of the value of a vanadium redox flow battery for frequency regulation in texas," *Applied Energy*, vol. 113, pp. 189 – 198, 2014. doi: 10.1016/j.apenergy.2013.07.025

[86] C. Betzin, H. Wolfschmidt, and M. Luther, "Electrical operation behavior and energy efficiency of battery systems in a virtual storage power plant for primary control reserve," *International Journal of Electrical Power & Energy Systems*, vol. 97, pp. 138 – 145, 2018. doi: 10.1016/j.ijepes.2017.10.038

[87] T. F. Fuller, M. Doyle, and J. Newman, "Simulation and optimization of the dual lithium ion insertion cell," *Journal of the Electrochemical Society*, vol. 141, no. 1, pp. 1–10, 1994. doi: 10.1149/1.2054684

[88] M. R. Jongerden and B. R. Haverkort, "Which battery model to use?" *IET software*, vol. 3, no. 6, pp. 445–457, 2009. doi: 10.1049/iet-sen.2009.0001

[89] X. Hu, S. Li, and H. Peng, "A comparative study of equivalent circuit models for Li-ion batteries," *Journal of Power Sources*, vol. 198, pp. 359–367, jan 2012. doi: 10.1016/j.jpowsour.2011.10.013

[90] K. Li and K. J. Tseng, "Energy efficiency of lithium-ion battery used as energy storage devices in micro-grid," in *IECON 2015 - 41st Annual Conference of the IEEE Industrial Electronics Society*. IEEE, nov 2015. doi: 10.1109/IECON.2015.7392923 pp. 005 235–005 240.

[91] *Datasheet Cell Type UR18650E*, Panasonic/Sanyo. [Online]. Available: www.master-instruments.com.au/file/62415/1/Sanyo-UR18650E.pdf

[92] M. Ecker, N. Nieto, S. Käbitz, J. Schmalstieg, H. Blanke, A. Warnecke, and D. U. Sauer, "Calendar and cycle life study of Li(NiMnCo)O_2-based 18650 lithium-ion batteries," *Journal of Power Sources*, vol. 248, pp. 839–851, feb 2014. doi: 10.1016/j.jpowsour.2013.09.143

[93] J. Schmalstieg, S. Käbitz, M. Ecker, and D. U. Sauer, "A holistic aging model for Li(NiMnCo)O_2 based 18650 lithium-ion batteries," *Journal of Power Sources*, vol. 257, pp. 325–334, jul 2014. doi: 10.1016/j.jpowsour.2014.02.012

[94] E. P. Roth, "Thermal abuse performance of MOLI, panasonic and sanyo 18650 Li-ion cells," Sandia National Laboratories, Tech. Rep., 2005. [Online]. Available: prod.sandia.gov/techlib-noauth/access-control.cgi/2004/046721.pdf

[95] J. Vetter, P. Novák, M. Wagner, C. Veit, K.-C. Möller, J. Besenhard, M. Winter, M. Wohlfahrt-Mehrens, C. Vogler, and A. Hammouche, "Ageing mechanisms in lithium-ion batteries," *Journal of Power Sources*, vol. 147, no. 1-2, pp. 269–281, sep 2005. doi: 10.1016/j.jpowsour.2005.01.006

[96] A. Barré, B. Deguilhem, S. Grolleau, M. Gérard, F. Suard, and D. Riu, "A review on lithium-ion battery ageing mechanisms and estimations for automotive applications," *Journal of Power Sources*, vol. 241, pp. 680–689, nov 2013. doi: 10.1016/j.jpowsour.2013.05.040

[97] R. Darling and J. Newman, "Modeling side reactions in composite $Li_yMn_2O_4$ electrodes," *Journal of The Electrochemical Society*, vol. 145, no. 3, pp. 990–998, 1998. doi: 10.1149/1.1838376

[98] G. Ning, R. E. White, and B. N. Popov, "A generalized cycle life model of rechargeable Li-ion batteries," *Electrochimica Acta*, vol. 51, no. 10, pp. 2012–2022, feb 2006. doi: 10.1016/j.electacta.2005.06.033

[99] "ASTM E1049 - 85(2017), Standard Practices for Cycle Counting in Fatigue Analysis," ASTM International, West Conshohocken, PA, Standard, 2017.

[100] G. He, Q. Chen, C. Kang, P. Pinson, and Q. Xia, "Optimal bidding strategy of battery storage in power markets considering performance-based regulation and battery cycle life," *IEEE Transactions on Smart Grid*, vol. 7, no. 5, pp. 2359–2367, 2016. doi: 10.1109/TSG.2015.2424314

[101] B. Xu, A. Oudalov, A. Ulbig, G. Andersson, and D. S. Kirschen, "Modeling of lithium-ion battery degradation for cell life assessment," *IEEE Transactions on Smart Grid*, vol. 9, no. 2, pp. 1131–1140, March 2018. doi: 10.1109/TSG.2016.2578950

[102] SMA, "Efficiency and derating. Sunny Boy / Sunny Boy Storage / Sunny Tripower / Sunny Mini Central / Sunny Highpower," SMA, Tech. Rep. WirkungDerat-TI-en-43, April 2017. [Online]. Available: files.sma.de/dl/1348/WirkungDerat-TI-en-47.pdf [Accessed 20-12-2019].

[103] F. M. Gatta, A. Geri, S. Lauria, M. Maccioni, and F. Palone, "Battery energy storage efficiency calculation including auxiliary losses: Technology comparison and operating strategies," *IEEE PowerTech 2015, Eindhoven.*, 2015. doi: 10.1109/PTC.2015.7232464

[104] M. Doyle and J. Newman, "Analysis of capacity–rate data for Lithium batteries using simplified models of the discharge process," *Journal of Applied Electrochemistry*, vol. 27, no. 7, pp. 846–856, Jul 1997. doi: 10.1023/A:1018481030499

[105] W. Peukert, "Über die Abhängigkeit der Kapazität von der Entladestromstärke bei Bleiakkumulatoren," *Elektrotechnische Zeitschrift*, vol. 20, pp. 20–21, 1897.

[106] D. Doerffel and S. A. Sharkh, "A critical review of using the peukert equation for determining the remaining capacity of lead-acid and lithium-ion batteries," *Journal of Power Sources*, vol. 155, no. 2, pp. 395 – 400, 2006. doi: 10.1016/j.jpowsour.2005.04.030

[107] A. Oudalov, D. Chartouni, and C. Ohler, "Optimizing a Battery Energy Storage System for Primary Frequency Control," *IEEE Transactions on Power Systems*, vol. 22, no. 3, pp. 1259–1266, 2007. doi: 10.1109/TPWRS.2007.901459

[108] M. Delfanti, D. Falabretti, M. Merlo, and G. Monfredini, "Distributed Generation Integration in the Electric Grid: Energy Storage System for Frequency Control," *Journal of Applied Mathematics*, vol. 2014, pp. 1–13, 2014. doi: 10.1155/2014/198427

[109] T. Borsche, A. Ulbig, M. Koller, and G. Andersson, "Power and energy capacity requirements of storages providing frequency control reserves," in *2013 IEEE Power & Energy Society General Meeting*. IEEE, 2013. doi: 10.1109/PESMG.2013.6672843

[110] O. Mégel, J. L. Mathieu, and G. Andersson, "Maximizing the potential of energy storage to provide fast frequency control," in *IEEE PES ISGT Europe 2013*. IEEE, Oct. 2013. doi: 10.1109/ISGTEurope.2013.6695380 pp. 1–5.

[111] J. Engels, B. Claessens, and G. Deconinck, "Combined stochastic optimization of frequency control and self-consumption with a battery," *IEEE Transactions on Smart Grid*, vol. 10, no. 2, pp. 1971–1981, Mar. 2019. doi: 10.1109/TSG.2017.2785040

[112] D. P. Bertsekas, D. P. Bertsekas, D. P. Bertsekas, and D. P. Bertsekas, *Dynamic programming and optimal control*. Athena scientific Belmont, MA, 2005, vol. 1, no. 3.

[113] A. Shapiro and A. Philpott, "A tutorial on stochastic programming," *Manuscript*, pp. 1–35, 2007. [Online]. Available: www2.isye.gatech.edu/people/faculty/Alex_Shapiro/TutorialSP.pdf

[114] W.-K. Mak, D. P. Morton, and R. Wood, "Monte Carlo bounding techniques for determining solution quality in stochastic programs," *Operations Research Letters*, vol. 24, no. 1-2, pp. 47–56, Feb. 1999. doi: 10.1016/S0167-6377(98)00054-6

[115] G. Calafiore and M. Campi, "The Scenario Approach to Robust Control Design," *IEEE Transactions on Automatic Control*, vol. 51, no. 5, pp. 742–753, May 2006. doi: 10.1109/TAC.2006.875041

[116] V. N. Vapnik, *Statistical learning theory*, ser. Adaptive and learning systems for signal processing, communications, and control. New York (N.Y.): Wiley, 1998. ISBN 0471030031

[117] M. Vidyasagar, "Randomized algorithms for robust controller synthesis using statistical learning theory," *Automatica*, vol. 37, no. 10, pp. 1515 – 1528, 2001. doi: 10.1016/S0005-1098(01)00122-4

[118] S. Grammatico, X. Zhang, K. Margellos, P. Goulart, and J. Lygeros, "A scenario approach for non-convex control design," *IEEE Transactions on Automatic Control*, vol. 61, no. 2, pp. 334–345, Feb 2016. doi: 10.1109/TAC.2015.2433591

[119] V. N. Vapnik and A. Y. Chervonenkis, "On the uniform convergence of relative frequencies of events to their probabilities," *Theory of Probability & Its Applications*, vol. 16, no. 2, pp. 264–280, 1971. doi: 10.1137/1116025

[120] A. Shapiro and A. Dentcheva, Darinka Ruszczyński, *Lectures on Stochastic Programming*. Siam, 2014. ISBN 9781611973426

[121] R. Storn and K. Price, "Differential evolution – a simple and efficient heuristic for global optimization over continuous spaces," *Journal of Global Optimization*, vol. 11, no. 4, pp. 341–359, Dec 1997. doi: 10.1023/A:1008202821328

[122] Bundesrepublik Deutschland, Bundesgesetz. (2005, Jun.) Gesetz über die Elektrizitäts- und Gasversorgung (Energiewirtschaftsgesetz — EnWG). [Online]. Available: www.gesetze-im-internet.de/enwg_2005/

[123] Bundesrepublik Deutschland, Bundesgesetz. (1990, Mar.) Stromsteuergesetz (StromStG). [Online]. Available: www.gesetze-im-internet.de/stromstg/

[124] Bundesrepublik Deutschland, Bundesgesetz, Einspruchsgesetz. (2017, Jul.) Gesetz für den Ausbau erneuerbarer Energien (Erneuerbare-Energien-Gesetz — EEG2017). [Online]. Available: www.gesetze-im-internet.de/eeg_2014/

[125] Bundesrepublik Deutschland, Bundesgesetz. (2016, Jan.) Gesetz für die Erhaltung, die Modernisierung und den Ausbau der Kraft-Wärme-Kopplung (Kraft-Wärme-Kopplungsgesetz — KWKG). [Online]. Available: www.gesetze-im-internet.de/kwkg_2016/

[126] Bundesrepublik Deutschland, Bundesgesetz. (1992, Jan.) Stromnetzentgeltverordnung (StromNEV). [Online]. Available: www.gesetze-im-internet.de/kav/

[127] Bundesrepublik Deutschland, Bundesrechtsverordnung. (2016, Aug.) Verordnung zu abschaltbaren Lasten (AblaV). [Online]. Available: www.gesetze-im-internet.de/ablav_2016/

[128] J. Fleer, S. Zurmühlen, J. Meyer, J. Badeda, P. Stenzel, J.-F. Hake, and D. U. Sauer, "Price development and bidding strategies for battery energy storage systems on the primary control reserve market," *Energy Procedia*, vol. 135, pp. 143 – 157, 2017. doi: 10.1016/j.egypro.2017.09.497

[129] Directorate-General for Economic and Financial Affairs (DG ECFIN) - European Commission. Economic forecast for Germany. [Online]. Available: ec.europa.eu/info/business-economy-euro/economic-performance-and-

forecasts/economic-performance-country/germany/economic-forecast-germany_en [Accessed 03-07-2018].

[130] Speichermonitoring, "Wissenschaftliches Mess- und Evaluierungsprogramm Solarstromspeicher 2.0 - Jahresberich 2017," 2017. [Online]. Available: www.speichermonitoring.de/fileadmin/user_upload/Speichermonitoring_Jahresbericht_2017_ISEA_RWTH_Aachen.pdf

[131] G. Mulder, D. Six, B. Claessens, T. Broes, N. Omar, and J. V. Mierlo, "The dimensioning of PV-battery systems depending on the incentive and selling price conditions," *Applied Energy*, vol. 111, pp. 1126–1135, 2013. doi: 10.1016/j.apenergy.2013.03.059

[132] V. Knap, S. K. Chaudhary, D. I. Stroe, M. Swierczynski, B. I. Craciun, and R. Teodorescu, "Sizing of an energy storage system for grid inertial response and primary frequency reserve," *IEEE Transactions on Power Systems*, vol. 31, no. 5, pp. 3447–3456, 2016. doi: 10.1109/TPWRS.2015.2503565

[133] A. Oudalov, D. Chartouni, C. Ohler, and G. Linhofer, "Value analysis of battery energy storage applications in power systems," in *2006 IEEE PES Power Systems Conference and Exposition*, Oct 2006. doi: 10.1109/PSCE.2006.296284 pp. 2206–2211.

[134] J. Fleer and P. Stenzel, "Impact analysis of different operation strategies for battery energy storage systems providing primary control reserve," *Journal of Energy Storage*, vol. 72, no. 2015, p. 19, 2016. doi: 10.1016/j.est.2016.02.003

[135] CAISO. (2012) Non-generator resource (ngr) and regulation energy management (rem) overview - phase 1. [Online]. Available: www.caiso.com/Documents/NGR-REMOverview.pdf

[136] Y. Xiao, Q. Su, F. S. S. Bresler, R. Carroll, J. R. Schmitt, and M. Olaleye, in *2014 IEEE PES General Meeting | Conference Exposition*, July.

[137] T. Borsche, A. Ulbig, and G. Andersson, "A new frequency control reserve framework based on energy-constrained units," in *2014 Power Systems Computation Conference.* IEEE, aug 2014. doi: 10.1109/PSCC.2014.7038111

[138] C. Jin, N. Lu, S. Lu, Y. Makarov, and R. a. Dougal, "Coordinated control algorithm for hybrid energy storage systems," in *2011 IEEE Power and Energy Society General Meeting.* IEEE, jul 2011. doi: 10.1109/PES.2011.6039893

[139] C. Brivio, S. Mandelli, and M. Merlo, "Battery energy storage system for primary control reserve and energy arbitrage," *Sustainable Energy, Grids and Networks*, vol. 6, pp. 152–165, jun 2016. doi: 10.1016/j.segan.2016.03.004

[140] O. Mégel, J. L. Mathieu, and G. Andersson, "Scheduling distributed energy storage units to provide multiple services under forecast error," *International Journal of Electrical Power and Energy Systems*, vol. 72, pp. 48–57, 2015. doi: 10.1016/j.ijepes.2015.02.010

[141] F. Braam, L. M. Diazgranados, R. Hollinger, B. Engel, G. Bopp, and T. Erge, "Distributed solar battery systems providing primary control reserve," *IET Renewable Power Generation*, vol. 10, no. 1, pp. 63–70, 2016. doi: 10.1049/iet-rpg.2015.0147

[142] Y. Shi, B. Xu, D. Wang, and B. Zhang, "Using battery storage for peak shaving and frequency regulation: Joint optimization for superlinear gains," *IEEE Transactions on Power Systems*, vol. 33, no. 3, pp. 2882–2894, May 2018. doi: 10.1109/TPWRS.2017.2749512

[143] A. Shahsavari, A. Sadeghi-Mobarakeh, E. Stewart, E. Cortez, L. Alvarez, F. Megala, and H. Mohsenian-Rad, *IEEE Transactions on Smart Grid.*

[144] G. Deconinck, K. D. Craemer, and B. Claessens, "Combining market-based control with distribution grid constraints when coordinating electric vehicle charging," *Engineering*, vol. 1, no. 4, pp. 453 – 465, 2015. doi: 10.15302/J-ENG-2015095

[145] Photovoltaikforum. (2016) Regelleistungsmodell von Caterva: Für jedes Kilowatt Regelleistung 150 bis 160 Euro im Jahr. [Online]. Available: www.photovoltaikforum.com/magazin/praxis/regelleistungsmodell-von-caterva-fuer-jedes-kilowatt-regelleistung-150-bis-160-euro-im-jahr-4765/

[146] Sonnen. (2017) sonnen-Messkonzept zur mehrfache Nutzung von Batteriespeichern für den FNN-Hinweis vorgeschlagen. [Online]. Available: www.sonnenbatterie.de/de/sonnen-messkonzept-zur-mehrfache-nutzung-von-batteriespeichern-fuer-den-fnn-hinweis-vorgeschlagen/

[147] E. Vrettos, F. Oldewurtel, and G. Andersson, "Robust Energy-Constrained Frequency Reserves from Aggregations of Commercial Buildings," *IEEE Transactions on Power Systems*, vol. 31, no. 6, pp. 4272–4285, 2016. doi: 10.1109/TPWRS.2015.2511541

[148] A. Ben-Tal, L. El Ghaoui, and A. Nemirovski, *Robust Optimization.* Princeton University Press, 2009. ISBN 9780691143682

[149] P. J. Goulart, E. C. Kerrigan, and J. M. Maciejowski, "Optimization over state feedback policies for robust control with constraints," *Automatica*, vol. 42, no. 4, pp. 523–533, Apr. 2006. doi: 10.1016/j.automatica.2005.08.023

[150] J. W. Rombouts and J. Gheerardyn, "Portfolio managed, demand-side response system," U.S. Patent 9 471 080, Oct. 18, 2016.

[151] M. Dyer and L. Stougie, "Computational complexity of stochastic programming problems," *Mathematical Programming*, vol. 106, no. 3, pp. 423–432, May 2006. doi: 10.1007/s10107-005-0597-0

[152] A. Charnes and W. W. Cooper, "Chance-Constrained Programming," *Management Science*, vol. 6, no. 1, pp. 73–79, Oct. 1959. doi: 10.1287/mnsc.6.1.73

[153] K. Margellos, P. Goulart, and J. Lygeros, "On the road between robust optimization and the scenario approach for chance constrained optimization problems," *IEEE Transactions on Automatic Control*, vol. 59, no. 8, pp. 2258–2263, 2014. doi: 10.1109/TAC.2014.2303232

[154] A. Nemirovski, "On safe tractable approximations of chance constraints," *European Journal of Operational Research*, vol. 219, no. 3, pp. 707–718, 2012. doi: 10.1016/j.ejor.2011.11.006

[155] R. T. Rockafellar and S. Uryasev, "Optimization of conditional value-at-risk," *The Journal of Risk*, vol. 2, no. 3, pp. 21–41, 2000. doi: 10.21314/JOR.2000.038

[156] D. Bertsimas, D. Pachamanova, and M. Sim, "Robust linear optimization under general norms," *Operations Research Letters*, vol. 32, no. 6, pp. 510–516, Nov. 2004. doi: 10.1016/j.orl.2003.12.007

[157] X. Chen, M. Sim, and P. Sun, "A Robust Optimization Perspective on Stochastic Programming," *Operations Research*, vol. 55, no. 6, pp. 1058–1071, 2007. doi: doi:10.1287/opre.1070.0441

[158] W. Chen, M. Sim, J. Sun, and C.-P. Teo, "From CVaR to Uncertainty Set: Implications in Joint Chance-Constrained Optimization," *Operations Research*, vol. 58, no. 2, pp. 470–485, 2010. doi: 10.1287/opre.1090.0712

[159] W. Chen and M. Sim, "Goal-Driven Optimization," *Operations Research*, vol. 57, no. 2, pp. 342–357, Apr. 2009. doi: 10.1287/opre.1080.0570

[160] A. Kessy, A. Lewin, and K. Strimmer, "Optimal whitening and decorrelation," *The American Statistician*, vol. 72, no. 4, pp. 309–314, 2018. doi: 10.1080/00031305.2016.1277159

[161] J. Dupačová, N. Gröwe-Kuska, and W. Römisch, "Scenario reduction in stochastic programming," *Mathematical Programming*, vol. 95, no. 3, pp. 493–511, Mar. 2003. doi: 10.1007/s10107-002-0331-0

[162] J. Löfberg, "YALMIP : A Toolbox for Modeling and Optimization in MATLAB," in *Proceedings of the CACSD Conference*, Taipei, Taiwan, 2004.

[163] Gurobi Optimization Inc., "Gurobi optimizer reference manual," 2012. [Online]. Available: www.gurobi.com

[164] BDEW. Energiedaten - Durchschnittlicher Strompreis für Haushalte 2016. [Online]. Available: www.bdew.de/internet.nsf/id/DE_Energiedaten#cat/Daten%2FGrafiken%5CEnergie%20allgemein%5CEnergiedaten%5C3.%20Stromversorgung/3-15-strompreis-fuer-haushalte-de

[165] Bundesnetzagentur, "Photovoltaikanlagen - Datenmeldungen und EEG-Vergütungssätze."

[166] A. Malhotra, B. Battke, M. Beuse, A. Stephan, and T. Schmidt, "Use cases for stationary battery technologies: A review of the literature and existing projects," *Renewable and Sustainable Energy Reviews*, vol. 56, pp. 705 – 721, 2016. doi: 10.1016/j.rser.2015.11.085

[167] D. Wu, M. Kintner-Meyer, Tao Yang, and P. Balducci, "Economic analysis and optimal sizing for behind-the-meter battery storage," in *2016 IEEE Power and Energy Society General Meeting (PESGM)*, July 2016. doi: 10.1109/PESGM.2016.7741210. ISSN 1944-9933 pp. 1–5.

[168] "TSOs' proposal for the establishment of common and harmonised rules and processes for the exchange and procurement of balancing capacity for Frequency Containment Reserves (FCR) (...)." ENTSO-E, Tech. Rep., Oktober 2018.

[169] R. Passey, N. Haghdadi, A. Bruce, and I. MacGill, "Designing more cost reflective electricity network tariffs with demand charges," *Energy Policy*, vol. 109, no. July, pp. 642–649, 2017. doi: 10.1016/j.enpol.2017.07.045

[170] Bayernwerk. Netzentgelte §17 und 27 abs. 1 stromnev. [Online]. Available: www.bayernwerk-netz.de/de/bayernwerk-netz-gmbh/netzinformation/netzentgelte/netzentgelte-strom.html [Accessed 2019-05-17].

[171] J. Leadbetter and L. Swan, "Battery storage system for residential electricity peak demand shaving," *Energy and Buildings*, vol. 55, pp. 685 – 692, 2012. doi: 10.1016/j.enbuild.2012.09.035

[172] M. Koller, T. Borsche, A. Ulbig, and G. Andersson, "Review of grid applications with the Zurich 1MW battery energy storage system," *Electric Power Systems Research*, vol. 120, pp. 128–135, Mar. 2015. doi: 10.1016/j.epsr.2014.06.023

[173] B. P. Bhattarai, K. S. Myers, and J. W. Bush, "Reducing demand charges and onsite generation variability using behind-the-meter energy storage," in *2016 IEEE Conference on Technologies for Sustainability (SusTech)*, Oct 2016. doi: 10.1109/SusTech.2016.7897156 pp. 140–146.

[174] A. Oudalov, R. Cherkaoui, and A. Beguin, "Sizing and optimal operation of battery energy storage system for peak shaving application," in *2007 IEEE Lausanne Power Tech*, July 2007. doi: 10.1109/PCT.2007.4538388 pp. 621–625.

[175] G. Piero Schiapparelli, S. Massucco, E. Namor, F. Sossan, R. Cherkaoui, and M. Paolone, "Quantification of primary frequency control provision from battery energy storage systems connected to active distribution networks," in *2018 Power Systems Computation Conference (PSCC)*, June 2018. doi: 10.23919/PSCC.2018.8442554 pp. 1–7.

[176] F. Braeuer, J. Rominger, R. McKenna, and W. Fichtner, "Battery storage systems: An economic model-based analysis of parallel revenue streams and general implications for industry," *Applied Energy*, vol. 239, pp. 1424 – 1440, 2019. doi: 10.1016/j.apenergy.2019.01.050

[177] R. Moreno, R. Moreira, and G. Strbac, "A MILP model for optimising multi-service portfolios of distributed energy storage," *Applied Energy*, vol. 137, pp. 554 – 566, 2015. doi: 10.1016/j.apenergy.2014.08.080

[178] H. Heitsch and W. Römisch, "Scenario Reduction Algorithms in Stochastic Programming," *Computational Optimization and Applications*, vol. 24, no. 2/3, pp. 187–206, 2003. doi: 10.1023/A:1021805924152

[179] S. T. Rachev and W. Römisch, "Quantitative stability in stochastic programming: The method of probability metrics," *Mathematics of Operations Research*, vol. 27, no. 4, pp. 792–818, 2002. doi: 10.1287/moor.27.4.792.304

[180] J. M. Morales, S. Pineda, A. J. Conejo, and M. Carrion, "Scenario reduction for futures market trading in electricity markets," *IEEE Transactions on Power Systems*, vol. 24, no. 2, pp. 878–888, May 2009. doi: 10.1109/TPWRS.2009.2016072

[181] D. P. Bertsekas, *Dynamic programming and optimal control: approximate dynamic programming*, 4th ed. Athena scientific Belmont, MA, 2012, vol. 2.

[182] C. Cervellera, A. Wen, and V. C. Chen, "Neural network and regression spline value function approximations for stochastic dynamic programming," *Computers & operations research*, vol. 34, no. 1, pp. 70–90, 2007.

[183] V. C. Chen, "Application of orthogonal arrays and mars to inventory forecasting stochastic dynamic programs," *Computational statistics & data analysis*, vol. 30, no. 3, pp. 317–341, 1999.

[184] Elia, "General framework for frequency containment reserve service by non-CIPU resources," 2017. [Online]. Available: www.elia.be/~/media/files/Elia/Products-and-services/ancillary%20services/purchase%20of%20ancillary%20services/General-Framework-R1-Non-CIPU-2015_2018_version-May-2017.pdf

[185] R. D'hulst and E. Peeters, "Distributed voltage control strategies in a LV distribution network," in *International Conference on Renewable Energies and Power Quality (ICREPQ10), Granada (Spain), 23rd to 25th March*, vol. 2010, 2010.

[186] E. Demirok, P. C. González, K. H. B. Frederiksen, D. Sera, P. Rodriguez, and R. Teodorescu, "Local reactive power control methods for overvoltage prevention of distributed solar inverters in low-voltage grids," *IEEE Journal of Photovoltaics*, vol. 1, no. 2, pp. 174–182, Oct 2011. doi: 10.1109/JPHOTOV.2011.2174821

[187] S. Deshmukh, B. Natarajan, and A. Pahwa, "Voltage/var control in distribution networks via reactive power injection through distributed generators," *IEEE Transactions on Smart Grid*, vol. 3, no. 3, pp. 1226–1234, Sep. 2012. doi: 10.1109/TSG.2012.2196528

[188] Synergrid. Synergrid. [Online]. Available: www.Synergrid.be/ [Accessed 2018-06-13].

[189] Synergrid, "Overeenkomst tussen de DNB en de dienstverlener van flexibiliteit in het kader van de levering van R1 aan Elia door het gebruik van flexibiliteit bij distributienetgebruikers op het laagspanningsdistributienet," Tech. Rep., May 2018.

[190] G. Litjens, E. Worrell, and W. van Sark, "Economic benefits of combining self-consumption enhancement with frequency restoration reserves provision by photovoltaic-battery systems," *Applied Energy*, vol. 223, pp. 172 – 187, 2018. doi: 10.1016/j.apenergy.2018.04.018

[191] A. C. Chapman, G. Verbič, and D. J. Hill, "Algorithmic and strategic aspects to integrating demand-side aggregation and energy management methods," *IEEE Transactions on Smart Grid*, vol. 7, no. 6, pp. 2748–2760, Nov 2016. doi: 10.1109/TSG.2016.2516559

[192] S. Mhanna, A. C. Chapman, and G. Verbič, "A fast distributed algorithm for large-scale demand response aggregation," *IEEE Transactions on Smart Grid*, vol. 7, no. 4, pp. 2094–2107, July 2016. doi: 10.1109/TSG.2016.2536740

[193] S. Weckx, R. D'Hulst, B. Claessens, and J. Driesen, "Multiagent charging of electric vehicles respecting distribution transformer loading and voltage limits," *IEEE Transactions on Smart Grid*, vol. 5, no. 6, pp. 2857–2867, Nov 2014. doi: 10.1109/TSG.2014.2345886

[194] N. Gatsis and G. B. Giannakis, "Decomposition algorithms for market clearing with large-scale demand response," *IEEE Transactions on Smart Grid*, vol. 4, no. 4, pp. 1976–1987, Dec 2013. doi: 10.1109/TSG.2013.2258179

[195] C. K. Wen, J. C. Chen, J. H. Teng, and P. Ting, "Decentralized plug-in electric vehicle charging selection algorithm in power systems," *IEEE Transactions on Smart Grid*, vol. 3, no. 4, pp. 1779–1789, Dec 2012. doi: 10.1109/TSG.2012.2217761

[196] J. Engels, H. Almasalma, and G. Deconinck, "A distributed gossip-based voltage control algorithm for peer-to-peer microgrids," in *2016 IEEE International Conference on Smart Grid Communications (SmartGridComm)*, Nov 2016. doi: 10.1109/SmartGridComm.2016.7778789

[197] J. F. C. Mota, J. M. F. Xavier, P. M. Q. Aguiar, and M. Püschel, "D-ADMM: a communication-efficient distributed algorithm for separable optimization," *IEEE Transactions on Signal Processing*, vol. 61, no. 10, pp. 2718–2723, May 2013. doi: 10.1109/TSP.2013.2254478

[198] P. Gandotra, R. K. Jha, and S. Jain, "A survey on device-to-device (d2d) communication: Architecture and security issues," *Journal of Network and Computer Applications*, vol. 78, pp. 9 – 29, 2017. doi: 10.1016/j.jnca.2016.11.002

[199] A. Al-Fuqaha, M. Guizani, M. Mohammadi, M. Aledhari, and M. Ayyash, "Internet of things: A survey on enabling technologies, protocols, and applications," *IEEE Communications Surveys Tutorials*, vol. 17, no. 4, pp. 2347–2376, jun 2015. doi: 10.1109/COMST.2015.2444095

[200] U. Raza, P. Kulkarni, and M. Sooriyabandara, "Low power wide area networks: An overview," *IEEE Communications Surveys Tutorials*, vol. 19, no. 2, pp. 855–873, jan 2017. doi: 10.1109/COMST.2017.2652320

[201] H. W. Jung, "Über den kleinsten kreis, der eine ebene figur einschließt." *Journal für die reine und angewandte Mathematik*, vol. 137, pp. 310–313, 1910.

[202] Enexis Netbeheer. Open data. [Online]. Available: www.enexis.nl/over-ons/documenten-en-publicaties/open-data [Accessed 2018-06-13].

[203] P. Samadi, H. Mohsenian-Rad, R. Schober, and V. W. S. Wong, "Advanced demand side management for the future smart grid using mechanism design," *IEEE Transactions on Smart Grid*, vol. 3, no. 3, pp. 1170–1180, Sep. 2012. doi: 10.1109/TSG.2012.2203341

[204] O. K. Gupta and A. Ravindran, "Branch and bound experiments in convex nonlinear integer programming," *Management Science*, vol. 31, no. 12, pp. 1533–1546, 1985. doi: 10.1287/mnsc.31.12.1533

[205] T. Westerlund and F. Pettersson, "An extended cutting plane method for solving convex minlp problems," *Computers & Chemical Engineering*, vol. 19, pp. 131 – 136, 1995. doi: 10.1016/0098-1354(95)87027-X

[206] R. A. Stubbs and S. Mehrotra, "A branch-and-cut method for 0-1 mixed convex programming," *Mathematical Programming*, vol. 86, no. 3, pp. 515–532, Dec 1999. doi: 10.1007/s101070050103

[207] S. Boyd, N. Parikh, E. Chu, B. Peleato, and J. Eckstein, "Distributed optimization and statistical learning via the alternating direction method of multipliers," *Foundations and Trends® in Machine Learning*, vol. 3, no. 1, pp. 1–122, 2011. doi: 10.1561/2200000016

[208] J. Eckstein and D. P. Bertsekas, "On the Douglas–Rachford splitting method and the proximal point algorithm for maximal monotone operators," *Mathematical Programming*, vol. 55, no. 1, pp. 293–318, Apr 1992. doi: 10.1007/BF01581204

[209] Bevolkingsontwikkeling; regio per maand [Population growth; region per month]. CBS Statline. [Online]. Available: opendata.cbs.nl/statline/#/CBS/nl/dataset/37230ned/table?ts=1528880736628 [Accessed 2018-06-13].

[210] S. Diamond and S. Boyd, "CVXPY: A Python-embedded modeling language for convex optimization," *Journal of Machine Learning Research*, vol. 17, no. 83, pp. 1–5, 2016.

[211] M. J. Feizollahi, M. Costley, S. Ahmed, and S. Grijalva, "Large-scale decentralized unit commitment," *International Journal of Electrical Power & Energy Systems*, vol. 73, pp. 97 – 106, 2015. doi: 10.1016/j.ijepes.2015.04.009

[212] Directive (EU) 2019/944 of the European Parliament and of the Council of 5 June 2019 on common rules for the internal market for electricity and amending Directive 2012/27/EU. [Online]. Available: data.europa.eu/eli/dir/2019/944/oj [Accessed 2019-12-24].

Curriculum Vitae

Jonas Engels

Born on 4th August, 1990 in Lier, Belgium.

2002 - 2008	Secondary School, Sciences-Mathematics (8h), Sint-Gummaruscollege Lier, Belgium.
2009 - 2012	Bachelor of Engineering: Mechanical & Electrical Engineering, KU Leuven, Belgium. Graduated Cum Laude.
Fall 2012	Erasmus Program, KTH Royal Institute of Technology, Stockholm, Sweden.
2012 - 2014	Master of Engineering: Energy, KU Leuven, Belgium. Graduated Magna Cum Laude.
2014 - 2015	Business Consultant, Sia Partners, Brussels, Belgium.
2015 - 2019	Ph.D. in Engineering Science, Department of Electrical Engineering, KU Leuven, Belgium.
2016 - ...	Researcher, REstore / Centrica Business Solutions Belgium.

List of Publications

Status on 1 January, 2020.

Articles in Peer-Reviewed Journals

1. **Engels J.**, Claessens B., Deconinck G. (2019). Optimal Combination of Frequency Control and Peak Shaving with Battery Storage Systems. IEEE Transactions on Smart Grid (Early Access), December 2019.

2. **Engels J.**, Claessens B., Deconinck G. (2019). Grid-Constrained Distributed Optimization for Frequency Control with Low-Voltage Flexibility. IEEE Transactions on Smart Grid, vol. 11, no. 1, pp. 612-622, Jan 2020.

3. **Engels J.**, Claessens B., Deconinck G. (2019). Techno-economic analysis and optimal control of battery storage for frequency control services, applied to the German market. Applied Energy 242, pp. 1036-1049. May 2019.

4. **Engels J.**, Claessens B., Deconinck G. (2017). Combined Stochastic Optimization of Frequency Control and Self-Consumption with a Battery. IEEE Transactions on Smart Grid, vol. 10, no. 2, pp. 1971-1987, March 2019.

Patents

1. Claessens B., **Engels J.**, Peeters S., Rombouts J.W., (2018) Self-Organizing Demand-Response System. US16/157,431. Pending.

International Conferences

1. Almasalma H., **Engels J.** and Deconinck G. (2017). Dual-decomposition-based peer-to-peer voltage control for distribution networks. CIRED, vol. 2017, no. 1, pp. 1718-1721, Glasgow, 12-15 June 2017.

2. **Engels J.**, Almasalma H., Deconinck G. (2016). A Distributed Gossip-based Voltage Control Algorithm for Peer-to-Peer Microgrids. IEEE International Conference on Smart Grid Communications (SmartGrid-Comm), pp. 376-381, Sydney, 6-9 November 2016.

3. Almasalma H., **Engels J.**, Deconinck G. (2016). Peer-to-Peer Control of Microgrids. 8th IEEE Benelux Young researchers symposium in Electrical Power Engineering, Eindhoven, 12-13 May 2016.

4. Van Stiphout A., **Engels J.**, Guldentops D., Deconinck G. (2015). Quantifying the Flexibility of Residential Electricity Demand in 2050: a Bottom-Up Approach. IEEE Powertech, Eindhoven, 29 June - 2 July 2015.

FACULTY OF ENGINEERING SCIENCE
DEPARTMENT OF ELECTRICAL ENGINEERING
DIV. ELECTA
Kasteelpark Arenberg 10 box 2445
B-3001 Leuven
jonas.engels@kuleuven.be
www.esat.kuleuven.be/electa